Division of Research & Innovation

Investigation of Flange Failures in Falsework Cap and Sill Beams

Recommendations for the Design of Beams and Posts in Bridge Falsework

Final Report

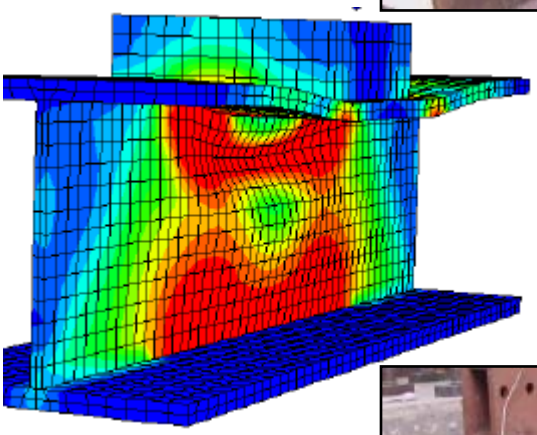

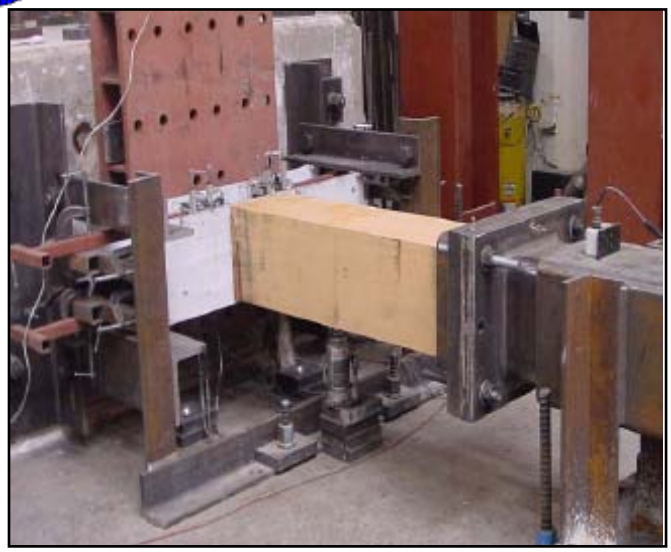

Report CA06-0629
December 2008

Investigation of Flange Failures in Falsework Cap and Sill Beams

Recommendations for the Design of Beams and Posts in Bridge Falsework

Final Report

Report No. CA06-0629

December 2008

Prepared By:

Department of Civil & Environmental Engineering
University of Nevada
Reno, NV 89557

Prepared For:

California Department of Transportation
Engineering Services Center
1801 30th Street
Sacramento, CA 95816

California Department of Transportation
Division of Research and Innovation, MS-83
1227 O Street
Sacramento, CA 95814

DISCLAIMER STATEMENT

This document is disseminated in the interest of information exchange. The contents of this report reflect the views of the authors who are responsible for the facts and accuracy of the data presented herein. The contents do not necessarily reflect the official views or policies of the State of California or the Federal Highway Administration. This publication does not constitute a standard, specification or regulation. This report does not constitute an endorsement by the Department of any product described herein.

STATE OF CALIFORNIA DEPARTMENT OF TRANSPORTATION

TECHNICAL REPORT DOCUMENTATION PAGE

TR0003 (REV. 10/98)

1. REPORT NUMBER	2. GOVERNMENT ASSOCIATION NUMBER	3. RECIPIENT'S CATALOG NUMBER
CA06-0629		

4. TITLE AND SUBTITLE	5. REPORT DATE
Investigation of Flange Failures in Falsework Cap and Sill Beams: Recommendations for the Design of Beams and Posts in Bridge Falsework.	December, 2008
	6. PERFORMING ORGANIZATION CODE

7. AUTHOR(S)	8. PERFORMING ORGANIZATION REPORT NO.
Lyle Carden, Ahmad Itani, Gokhan Pekcan	UNR / CCEER 05-11

9. PERFORMING ORGANIZATION NAME AND ADDRESS	10. WORK UNIT NUMBER
Department of Civil & Environmental Engineering University of Nevada Reno, NV 89557-0152	11. CONTRACT OR GRANT NUMBER DRI Research Task No. 0629 Contract No. 59A0445

12. SPONSORING AGENCY AND ADDRESS	13. TYPE OF REPORT AND PERIOD COVERED
California Department of Transportation Engineering Services Center 1801 30th Street Sacramento, CA 95816 California Department of Transportation Division of Research and Innovation, MS-83 1227 O Street Sacramento, CA 95814	Final Report 14. SPONSORING AGENCY CODE 913

15. SUPPLEMENTAL NOTES

This report may also be referenced as report UNR / CCEER 05-11 published by the University of Nevada, Reno.

16. ABSTRACT

Recent field observations in bridge falsework identified potential deficiencies in the design of falsework resulting in localized bending in sill and cap beam flanges and lateral buckling in other beams. Possible limits states associated with the bearing of timber and steel posts on cap and sill beams are investigated in this report. The critical limit states are related to flange bending, post crushing or yielding, web yielding, web crippling, lateral web buckling and corbel crushing. Different methods are investigated for predicting the capacity of the flange. The first assumes a uniform stress distribution resulting in bending of the flange. This is adequate for timber posts, but not as accurate at the second more elaborate method which accounts for an interaction between flange bending and post compression strength, found to be effective for timber posts. The third method uses an effective bearing area of the post, which is more effective with steel posts. For beams with relatively thick webs, such as those typically used in bridge falsework, the web was found to have a greater capacity than the flange and posts. The critical web limit state was web yielding (referred to as web crippling in the Caltrans Falsework manual) with variations of existing equations found to be appropriate for predicting the capacity. Web crippling (as defined by ASCE) is found to generally not govern the design, particularly when two sill beams are stacked on top of each other. Blocking may be used to increase the flange bending and web yielding capacity, although lateral bracing or stiffeners are recommended to increase lateral buckling capacity. Design equations are presented in allowable stress design format for the consideration of the critical limit states in a falsework bent. These are compared to current Caltrans design practice and other relevant specifications. Two design examples are also provided to demonstrate the application of these equations, one using timber posts and a second using steel posts.
.

17. KEY WORDS	18. DISTRIBUTION STATEMENT
Bridge Falsework, Falsework Beam Design, Flange Failure, Bottom Flange Bending, Buckling, Cap Beam Bending, Cap Beam Shear, Design Equation	No restrictions. This document is available to the public through the National Technical Information Service, Springfield, VA 22161

19. SECURITY CLASSIFICATION (of this report)	20. NUMBER OF PAGES	21. PRICE
Unclassified	170 Pages	

Report No. CCEER 05-11

Recommendations for the Design of Beams and Posts in Bridge Falsework

Lyle P. Carden
Ahmad M. Itani
Gokhan Pekcan

Center for Civil Engineering Earthquake Research
University of Nevada, Reno

January, 2006

Technical Report Documentation Page

1. Report No.	2. Government Accession No.	3. Recipient's Catalog No.

4. Title and Subtitle	5. Report Date
Investigation of Flange Failures in Falsework Cap and Sill Beam Recommendations for the Design of Beams and Posts in Bridge Falsework	January 20, 2006 6. Performing Organization Code
7. Author(s)	8. Performing Organization Report No.
Lyle Carden, Ahmad Itani, Gokhan Pekcan	UNR / CCEER 05-11
9. Performing Organization Name and Address Department of Civil and Environmental Engineering University of Nevada Reno, Nevada 89557-0152	10. Work Unit No. (TRAIS) 11. Contract or Grant No.
12. Sponsoring Agency Name and Address California Department of Transportation Engineering Service Center 1801 30th St., West Building MS 9-2/5i Sacramento, California 95816	13. Type of Report and Period Covered Final Report 14. Sponsoring Agency Code

15. Supplementary Notes

Prepared in cooperation with the State of California Department of Transportation.

16. Abstract

Recent field observations in bridge falsework identified potential deficiencies in the design of falsework resulting in localized bending in sill and cap beam flanges and lateral buckling in other beams. Possible limits states associated with the bearing of timber and steel posts on cap and sill beams are investigated in this report. The critical limit states are related to flange bending, post crushing or yielding, web yielding, web crippling, lateral web buckling and corbel crushing. Different methods are investigated for predicting the capacity of the flange. The first assumes a uniform stress distribution resulting in bending of the flange. This is adequate for timber posts, but not as accurate at the second more elaborate method which accounts for an interaction between flange bending and post compression strength, found to be effective for timber posts. The third method uses an effective bearing area of the post, which is more effective with steel posts. For beams with relatively thick webs, such as those typically used in bridge falsework, the web was found to have a greater capacity than the flange and posts. The critical web limit state was web yielding (refered to as web crippling in the Caltrans Falsework manual) with variations of existing equations found to be appropriate for predicting the capacity. Web crippling (as defined by ASCE) is found to generally not govern the design. Lateral web buckling may govern the design, particularly when two sill beams are stacked on top of each other. Blocking may be used to increase the flange bending and web yielding capacity, although lateral bracing or stiffeners are recommended to increase lateral buckling capacity. Design equations are presented in allowable stress design format for the consideration of the critical limit states in a falsework bent. These are compared to current Caltrans design practice and other relevant specifications. Two design examples are also provided to demonstrate the application of these equations, one using timber posts and a second using steel posts.

17. Key Words	18. Distribution Statement
bottom flange bending, buckling, cap beam, cap beam bending, cap beam shear, design equation, falsework, falsework beams, falsework design, flange buckling, flange failure, flange-post interaction, lateral buckling, patch loads, post yielding, posts, sill beam, steel posts, timber blocking timber corbels, timber posts, top flange bending, University of Nevada, web buckling, web crippling, web yielding	Unlimited

19. Security Classification (of this report)	20. Security Classification (of this page)	21. No. of Pages	22. Price
Unclassified	Unclassified	166 Pages	

ABSTRACT

Recent field observations in bridge falsework identified potential deficiencies in the design of falsework resulting in localized bending in sill and cap beam flanges and lateral buckling in other beams. Possible limits states associated with the bearing of timber and steel posts on cap and sill beams are investigated in this report. The critical limit states are related to flange bending, post crushing or yielding, web yielding, web crippling, lateral web buckling and corbel crushing. Different methods are investigated for predicting the capacity of the flange. The first assumes a uniform stress distribution resulting in bending of the flange. This is adequate for timber posts, but not as accurate at the second more elaborate method which accounts for an interaction between flange bending and post compression strength, found to be effective for timber posts. The third method uses an effective bearing area of the post, which is more effective with steel posts. For beams with relatively thick webs, such as those typically used in bridge falsework, the web was found to have a greater capacity than the flange and posts. The critical web limit state was web yielding (refered to as web crippling in the Caltrans Falsework manual) with variations of existing equations found to be appropriate for predicting the capacity. Web crippling (as defined by ASCE) is found to generally not govern the design. Lateral web buckling may govern the design, particularly when two sill beams are stacked on top of each other. Blocking may be used to increase the flange bending and web yielding capacity, although lateral bracing or stiffeners are recommended to increase lateral buckling capacity. Design equations are presented in allowable stress design format for the consideration of the critical limit states in a falsework bent. These are compared to current Caltrans design practice and other relevant specifications. Two design examples are also provided to demonstrate the application of these equations, one using timber posts and a second using steel posts.

ACKNOWLEDGEMENTS

The authors would like to extend their gr atitude to the California Department of Transportation for funding of this study under contract number 59A0445, with special thanks to John Lammers and Peter Lee for their assistance and direction. They would also like the thank the laboratory manager , Patrick Laplace and and de velopment technician, Paul Lucas for their assistan ce. T o the under graduate assi stants, Michael Schreiber and Mathew Ethridge, thank you also for your tireless efforts.

TABLE OF CONTENTS

SECTION	PAGE
ABSTRACT	**I**
ACKNOWLEDGEMENTS	**III**
TABLE OF CONTENTS	**V**
LIST OF FIGURES	**IX**
LIST OF TABLES	**XIII**
LIST OF SYMBOLS	**XV**
1 INTRODUCTION	**1**
2 EXPERIMENTS ON FALSEWORK COMPONENTS AND SUB-ASSEMBLIES	**5**
2.1 Overview	5
2.2 Setup of Sub-assembly Experiments on Beams with Posts and Corbels	5
2.3 Coupon Tests	6
2.4 Component Experiments	9
2.4.1 Timber Posts	9
2.4.2 Timber Corbels	11
2.4.3 Timber Blocking	12
2.4.4 Steel Post	12
2.5 Sub-assembly Experiments on Beams with Posts and Corbels	15
2.5.1 Overview	15
2.5.2 Beams with Resulting in Post-Flange Bending and Post Crushing	15
2.5.3 Beams with Timber Posts and Timber Corbels Resulting in Corbel Crushing	20
2.5.4 Beams with Steel Posts and Three Timber Corbels Resulting in Corbel Crushing and Post Yielding	22
2.5.5 Beams with Rigid Patch Loads and No Corbels Resulting in Web Yielding	23
2.6 Comparison of Failure Load with Load where Flaking is Observed	26
3 FINITE ELEMENT ANALYSIS OF FALSEWORK BEAMS	**51**
3.1 Overview	51
3.2 Properties of the Finite Element Models	51
3.3 Comparisons between the Experimental and Finite Element Results	55
3.3.1 Overview	55
3.3.2 Post-flange Bending - Post Crushing Capacity	55
3.3.3 Corbel-flange Bending - Corbel Crushing	56
3.3.4 Web Yielding and Lateral Buckling	58
3.4 Other Finite Element Analysis Results	61
3.4.1 Other Configurations not Considered Experimentally	61
3.4.2 Prevention of Lateral Buckling	62
3.4.3 Effect of Eccentricity	62

4 PREDICTION OF THE FLANGE BENDING, POST AND CORBEL CAPACITIES 65
4.1 Overview 65
4.2 Post-flange Bending Limit State 65
4.3 Post Compression Strength in the Flange-Post Connection Region 68
4.4 Interaction between Flange Bending and Post Compression Limit States 69
4.5 Effective Post Bearing Area for Calculating Flange-Post Capacity 69
4.6 Corbel-flange Bending Limit State 70
4.7 Corbel Strength 72
4.8 Strength of Blocking 73
4.9 Comparison of Calculated Strengths with Finite Element Analysis 73
4.9.1 Capacity of Post-flange and Post for the Concentrically Loaded Unblocked Beams 73
4.9.2 Effect of Eccentricity and Blocking on the Capacity of the Post-flange and Post 76
4.9.3 Capacity of the Corbel-flange and Corbels 79
4.10 Comparison of Calculated Limit States with Experimental Results 81

5 PREDICTION OF THE WEB YIELDING, CRIPPLING AND LATERAL BUCKLING CAPACITY 85
5.1 Overview 85
5.2 Web Yielding and Crippling 85
5.3 Web Buckling 86
5.4 Strength of Blocking 87
5.5 Comparison of Calculated Strengths with Finite Element Analysis 88
5.5.1 Localized Capacity of Web for Braced Beams 88
5.5.2 Lateral Web Buckling Capacity 91
5.6 Comparison of Calculated Strengths with Finite Element Analysis 93

6 PROPOSED DESIGN OF FALSEWORK BEAMS AND POSTS FOR GRAVITY LOADS 95
6.1 Overview 95
6.2 Design of Critical Members and Connections for Gravity Loads 95
6.2.1 Cap Beam Members for Flexure and Shear 95
6.2.2 Lateral Web Buckling in a Cap Beam 95
6.2.3 Web Yielding in a Cap Beam 96
6.2.4 Post-flange Bending in a Cap Beam with a Timber Post 97
6.2.4.1 Method 1 - Simplified Method 97
6.2.4.2 Method 2 - Interaction Method 97
6.2.5 Localized Yielding of a Steel Post from Bearing of the Cap Beam 98
6.2.6 Timber Post Design 99
6.2.7 Steel Post Design 101
6.2.8 Localized Yielding of a Steel Post due to Bearing onto a Sill Beam 103
6.2.9 Flange Bending-Post Crushing in a Sill Beam with a Timber Post 103
6.2.10 Web Yielding in a Sill Beam 103
6.2.11 Lateral Web Buckling in a Sill Beam 103
6.2.12 Corbel-flange Bending in a Sill Beam 103
6.2.13 Corbel Capacity 104
6.3 Comparison of Different Limit States in Beams and Posts 104
6.3.1 Comparison using Actual Strengths 104
6.3.2 Comparison using Allowable Stresses based Current Caltrans Provisions 106

6.3.3 Comparison using Allowable Stresses based Recommended Provisions 107

7 DESIGN EXAMPLES 109
7.1 Overview 109
7.2 Design of Falsework with Timber Posts 109
7.2.1 Loads 109
7.2.2 Cap Beam Bending 109
7.2.3 Cap Beam Shear 111
7.2.4 Lateral Web Buckling in the Cap Beam 111
7.2.5 Web Yielding in the Cap Beam 112
7.2.6 Localized Flange Bending in the Flange-Post Joint Region in the Cap Beam 112
7.2.7 Post Compression Strength 113
7.2.8 Flange-post Interaction, Web Yielding and Web Buckling in the Sill Beam 113
7.2.9 Corbel-flange Bending in Sill Beam 113
7.2.10 Corbels 114
7.3 Design of Falsework with Steel Posts 114
7.3.1 Loads 114
7.3.2 Cap Beam Bending 114
7.3.3 Cap Beam Shear 116
7.3.4 Lateral Web Buckling in the Cap Beam 116
7.3.5 Web Yielding in the Cap Beam 117
7.3.6 Localized Post Yielding in the Cap Beam 117
7.3.7 Post Compression Strength 118
7.3.8 Flange-post Interaction, Web Yielding and Web Buckling in the Sill Beam 118
7.3.9 Corbel-flange Bending in Sill Beam 119
7.3.10 Corbels 119

8 SUMMARY, CONCLUSIONS AND RECOMMENDATIONS 121
8.1 Summary and Conclusions 121
8.2 Recommendations 122

REFERENCES 125

APPENDIX 1 PREDICTION OF THE FLANGE BENDING, POST AND CORBEL CAPACITIES USING LOAD AND RESISTANCE FACTOR DESIGN 127

APPENDIX 2 GENERAL LAYOUT AND TYPICAL CROSS SECTIONS OF BRIDGE FALSEWORK FOR THE ARCH ROAD STAGE 4 BRIDGE 129

LIST OF FIGURES

FIGURE	HEADING	PAGE
FIGURE 1-1	Bridge Falsework for the Petaluma River Bridge at the intersection of California State Routes 101 and 116	1
FIGURE 1-2	Bridge Falsework for Railroad Avenue Overcrossing at Pittsburg, California	2
FIGURE 1-3	Localized flange bending failure in sill beam (J. Lammers, Caltrans, Personal communication)	3
FIGURE 1-4	Instability of sill beam resulting in lateral deformation of web (J. Lammers, Caltrans, Personal communication)	3
FIGURE 2-1	Sub-assembly setup with actuator, timber post, steel beam, restraints and corbels	6
FIGURE 2-2	Typical experimental setup for beam with timber post and corbels	7
FIGURE 2-3	Sub-assembly setup without timber corbels	8
FIGURE 2-4	Sub-assembly setup without a post or timber corbels	8
FIGURE 2-5	Component experiment on 4 foot long 12x12 in. Timber Post	10
FIGURE 2-6	Actuator force vs slider displacement for different post component experiments	10
FIGURE 2-7	Stiffness vs slider displacement for post component experiment (Post 1)	12
FIGURE 2-8	Component experiment on 4 foot long 12x12 in. timber corbel	13
FIGURE 2-9	Actuator force vs slider displacement for timber corbel	13
FIGURE 2-10	Component experiment on blocking in load frame	14
FIGURE 2-11	Actuator force vs actuator displacement for three timber block component experiments	14
FIGURE 2-12	Component experiment on 4 ft. long 18 in. diameter steel post	16
FIGURE 2-13	Actuator force vs slider displacement for timber corbel	16
FIGURE 2-14	Actuator force vs slider displacement for 1253TPNBSCRE0 - Beam 18	27
FIGURE 2-15	Flange bending and post deformation observed during loading of 1253TPNBSCRE0 - Beam 18	27
FIGURE 2-16	Strain gages on beam close to where flaking of lime paint is first observed	28
FIGURE 2-17	Actuator force vs strain in two strain gages located close to the yield line location in 1253TPNBSCRE0 - Beam 18	28
FIGURE 2-18	Actuator force vs slider displacement for 1253TPBSCRE0 - Beam 19	29
FIGURE 2-19	Actuator force vs slider displacement for 1253TPNBSCRE12 - Beam 16	29
FIGURE 2-20	Actuator force vs slider displacement for 1253TPBSCRE12 - Beam 17	30
FIGURE 2-21	Actuator force vs slider displacement for 1253TPNBSCRE6 - Beam 14	30
FIGURE 2-22	Actuator force vs strain in four strain gages located close to the yield line locations in 1253TPNBSCRE6 - Beam 14	31
FIGURE 2-23	Actuator force vs slider displacement for 1253TPBSCRE6 - Beam 15	31
FIGURE 2-24	Actuator force vs slider displacement for 1473TPNBSCRE0 - Beam 20	32
FIGURE 2-25	Actuator force vs slider displacement for 1473TPBSCRE0 - Beam 21	32
FIGURE 2-26	Actuator force vs slider displacement for 1473TPNBSCRE6 - Beam 27	33
FIGURE 2-27	Actuator force vs slider displacement for 1473TPBSCRE0 - Beam 25	33
FIGURE 2-28	Actuator force vs slider displacement for 1490TPNBSCRE0 - Beam 22	34
FIGURE 2-29	Actuator force vs slider displacement for 1490TPBSCRE0 - Beam 23	34
FIGURE 2-30	Actuator force vs slider displacement for 1490TPNBSCRE0 - Beam 24	35
FIGURE 2-31	Actuator force vs slider displacement for 1253TPNBTCRE0 - Beam 12	35
FIGURE 2-32	Corbel-flange bending, corbel crushing and post crushing after the completion of 1253TPNBTCRE0 - Beam 12	36
FIGURE 2-33	Actuator force vs slider displacement for 1253TPBTCRE0 - Beam 13	36
FIGURE 2-34	Actuator force vs slider displacement for 1490TPNBTCRE0 - Beam 1	37
FIGURE 2-35	Actuator force vs slider displacement for 1490TPNBTCRE6 - Beam 4	37
FIGURE 2-36	Actuator force vs slider displacement for 1490SPNBTCRE0 - Beam 2	38
FIGURE 2-37	Onset of yielding and buckling in the steel post for 1490SPNBTCRE0 - Beam 2	38

FIGURE 2-38 Actuator force vs slider displacement for 1490SPNBTCRE6 - Beam 3 39
FIGURE 2-39 Actuator force vs slider displacement for 1253NPNBNCRE0 - Beam 10 39
FIGURE 2-40 Post-elastic buckling/crippling of the web in 1253NPNBNCRE0 - Beam 10 40
FIGURE 2-41 Actuator force vs slider displacement for 1253NPNBNCRE6 - Beam 11 40
FIGURE 2-42 Actuator force vs slider displacement for 1473NPNBNCRE0 - Beam 9 41
FIGURE 2-43 Actuator force vs slider displacement for 1473NPNBNCRE6 - Beam 8 41
FIGURE 2-44 Actuator force vs slider displacement for 1490NPNBNCRE0 - Beam 6 42
FIGURE 2-45 Actuator force vs slider displacement for 1490NPNBNCRE6 - Beam 7 42
FIGURE 2-46 Actuator force vs slider displacement for 1473TPNBNCNRE0 - Beam 29 43
FIGURE 2-47 Actuator force vs slider displacement for 1473TPBNCNRE0 - Beam 30 43
FIGURE 2-48 Failure of post during experiment on unrestrained beam 1473TPNBNCNRE6 - Beam 31 44
FIGURE 2-49 Actuator force vs slider displacement for 1473TPNBNCNRE6 - Beam 31 44
FIGURE 2-50 Actuator force vs slider displacement for 1473TPBNCNRE6 - Beam 32 45
FIGURE 2-51 Actuator force vs slider displacement for 1490TPNBNCNRE0 - Beam 26 45
FIGURE 2-52 Lateral Buckling of 1490TPNBNCNRE0 - Beam 26 46
FIGURE 2-53 Actuator force vs slider displacement for 1490TPBNCNRE0 - Beam 28 46
FIGURE 2-54 Actuator force vs slider displacement for 1490NPNBNCNRE0 - Beam 5 47
FIGURE 2-55 Comparison of observed load when flaking occurred with calculated failure load from experiments with post-flange-post failure 48
FIGURE 2-56 Comparison of observed load when flaking occurred with calculated failure load from experiments with flange-corbel failure 48
FIGURE 2-57 Comparison of observed load when flaking occurred with calculated failure load from experiments with web yielding failure 49
FIGURE 3-1 Finite element models for a) a timber post and beam, b) a steel post and beam, c) a beam with a rigid patch load and d) long double stacked beam and post 52
FIGURE 3-2 Force-displacement curve for a finite element model of a timber post compared to the experimental data 53
FIGURE 3-3 Force-displacement curve for a finite element model of a timber block compared to the experimental data 54
FIGURE 3-4 Force-displacement curve for a finite element model of a timber corbel compared to the component experimental 54
FIGURE 3-5 Force-displacement curve for finite element model of HP12x53 beam and timber post exhibiting flange bending and post crushing 57
FIGURE 3-6 Force-displacement curve for finite element model of HP12x53 beam and timber post with blocking exhibiting flange bending and post crushing 57
FIGURE 3-7 Failure load from finite element analysis compared with experimental failure load for beams exhibiting flange-post failure 58
FIGURE 3-8 Force-displacement curve for finite element model of HP12x53 beam with corbels and posts exhibiting corbel-flange bending and corbel crushing 59
FIGURE 3-9 Failure load from finite element analysis compared with experimental failure load for beams exhibiting flange-corbel failure 59
FIGURE 3-10 Force-displacement curve for the FE model of the HP12x53 beam with a concentric rigid patch load exhibiting web yielding and post-elastic buckling/crippling 60
FIGURE 3-11 Force-displacement curve for the finite element model of the unrestrained W14x90 beam with a timber post resulting in lateral web buckling 60
FIGURE 3-12 Failure load from finite element analysis compared with experimental failure load for beams exhibiting web yielding and lateral buckling 61
FIGURE 3-13 Finite element model of beam with stiffener to prevent lateral buckling 62
FIGURE 3-14 Failure load of beams with different eccentricities between the beam and post 63
FIGURE 4-1 Yield line pattern on beams for a post patch load assuming a uniform stress distribution in the post 66

FIGURE 4-2 Cross section of a beam for a patch load assuming a triangular stress distribution in the post 68
FIGURE 4-3 Effective area of a) timber post and b) steel post for calculation of ultimate post load 70
FIGURE 4-4 Yield line pattern on corbel-flange of sill beam due to reaction from the corbels 71
FIGURE 4-5 Comparison of flange bending capacity with failure load from the finite element models for different beams 74
FIGURE 4-6 Comparison of post capacity for a short length of post with failure load from the finite element models for different beams 74
FIGURE 4-7 Calculated flange-post capacity a) using the minimum of the flange bending strength with β=11 and post strength and b) using the interaction equation between flange bending strength with β=18 and post strength, compared to failure load from the finite element models for different beams 75
FIGURE 4-8 Comparison of calculated flange-post capacity using effective post bearing area with failure load from the finite element models for different beams 77
FIGURE 4-9 Comparison of calculated flange-timber post capacity using interaction equation with finite element failure load for beams with blocking and eccentricities 77
FIGURE 4-10 Comparison of calculated flange-timber post capacity using minimum of flange (β=11) and post strength with finite element failure load for beams with blocking and eccentricities 78
FIGURE 4-11 Comparison of calculated steel post capacity using effective yielding area with finite element failure load for beams with blocking and eccentricities 79
FIGURE 4-12 Comparison of calculated corbel capacity with finite element failure load for beams with corbel failures 80
FIGURE 4-13 Comparison of calculated flange-timber post capacity using interaction equation with finite element failure load for beams with blocking and eccentricities 82
FIGURE 4-14 Comparison of calculated flange-timber post capacity using minimum of flange capacity (β=11) and post capacity with finite element failure load for beams with blocking and eccentricities 83
FIGURE 4-15 Comparison of calculated corbel capacity with experimental failure load for beams with and without eccentricities 83
FIGURE 5-1 Effective web yielding region for a) timber post and b) steel post 86
FIGURE 5-2 Calculated web yielding, and crippling capacity versus finite element failure load for concentrically load, unblocked beams 89
FIGURE 5-3 Calculated web yielding capacity (α=2) versus finite element failure load for different beams with blocking and eccentricities 89
FIGURE 5-4 Calculated web yielding capacity (α=5) versus finite element failure load for different beams with blocking and eccentricities 90
FIGURE 5-5 Calculated web crippling capacity versus finite element failure load for different beams with blocking and eccentricities 90
FIGURE 5-6 Calculated lateral web buckling capacity versus finite element failure load for 10 ft. long beams without blocking or eccentricities 92
FIGURE 5-7 Comparison of calculated ultimate load using web yielding and lateral web buckling equations with the experimental failure load 92
FIGURE 6-1 Column stability factor, C_p, for 12 x 12 in. Number 2 Douglas Fir posts of different lengths (AFPA 2001) 100
FIGURE 6-2 Allowable stress vs post length for 12 x 12 in. Number 2 Douglas Fir timber posts based on the NDS specifications and Caltrans Falsework Manual 100
FIGURE 6-3 Allowable stress vs post length for 18 in. diameter 3/8 in. thick round hollow steel post based on the AISC specifications and Caltrans Falsework Manual 102
FIGURE 7-1 Portion of a falsework bent with timber post identifying critical limits states 110
FIGURE 7-2 Portion of a falsework bent with steel post identifying critical limits states 115

LIST OF TABLES

TABLE	HEADING	PAGE
TABLE 2-1	Combinations of beams, posts, corbels, blocking and eccentricities used i experiments	9
TABLE 2-2	Summary of results from coupon tests	9
TABLE 4-1	β_1 values for beams assuming uniform and triangular stress distributions and 11.5 in. square patch load	67
TABLE 4-2	β_2 values for beams assuming uniform stress distributions, 11.5 in. wide corbels and a spacing between corbels of 24 in.	72
TABLE 6-1	Comparison of calculated ultimate beam, post and corbel loads based on actual strengths from experiments (kip)	105
TABLE 6-2	Comparison of calculated allowable beam, post and corbel loads based on original Caltrans allowable stresses (kip)	106
TABLE 6-3	Comparison of calculated allowable beam-post loads based on recommended strengths from experiments (kip)	107

LIST OF SYMBOLS

A_b	Cross sectional area of blocking
A_{bg}	Bearing area
A_p	Cross sectional area of post
A_w	Area of web
b_c	Width of corbel
b_f	Width of flange
b_{feff}	Effective outstanding flange width
b_p	Width of post
b_{peff}	Effective post width outside web region
c	Factor for timber type
C_p	Column stability factor
d	Depth of beam
d_p	Depth of post
E	Elastic modulus
f_b	Applied bending stress
f_{bg}	Applied bearing stress
f_{cw}	Applied stress in web
f_{cp}	Applied stress in post
f_v	Applied shear stress
F_b	Allowable bending stress
F_c'	Nominal or allowable compressive stress
F_c^*	Allowable compressive stress in post without modification for column stability
$F_{c\perp}'$	Nominal or allowable compressive stress perpendicular to the grain
F_{cb}'	Allowable stress in blocking
F_{cE}	Euler buckling load as applied to timber post
F_{cf}	Allowable effective stress in flange
F_{cp}	Allowable stress in steel post
F_{cp}'	Allowable stress in timber post
F_{cpb}	Allowable stress in steel post accounting for blocking
F_{cr}	Critical stress

F_{cw}	Allowable compressive stress in web
F_{cwb}	Allowable compressive stress in web accounting for blocking
F_e	Euler buckling load
F_{gf}	Allowable effective bearing stress
F_v	Allowable shear stress
F_{yf}	Minimum specified yield strength of flange
F_{yp}	Minimum specified yield strength of post
F_{yw}	Minimum specified yield strength of web
h	Clear height of web between flanges less the fillet radius
k	Distance from outer face of flange to toe of web
k_1	Distance from center of web to edge of fillet in beam
K	Effective length factor
K_{cE}	Timber compression stability constant
l_e	Effective length of post
l_{eff}	Effective length of web
L	Length of beam or post
M	Maximum applied bending moment
N	Length of bearing
p	Applied distributed load
P	Applied axial load
P_b	Axial load capacity of blocking
P_u	Axial load capacity of blocking
r	Radius of gyration
R	Applied load
R_c	Bearing capacity of corbel
R_{f1}	Flange load capacity due to a post patch load
R_{f2}	Flange load capacity due to a patch load from corbels
R_n	Nominal load capacity
R_p	Localized load capacity of post
R_w	Web load capacity
R_u	Ultimate applied load
s_c	Center to center spacing of outermost corbels in a corbel group
t_{ep}	Thickness of end plate of steel post

t_f	Flange thickness
t_p	Wall thickness of steel post
t_w	Thickness of web
w	Applied distributed load
W	Weight
V	Applied shear force
Z	Plastic section modulus
α	Stress gradient factor
β_1	Flange bending factor due to a post load
β_2	Flange bending factor due to a corbel load
γ	Blocking effectiveness factor
λ	Time effect factor (load duration factor)
ϕ	Resistance factor
ϕ_b	Resistance factor for bending
ϕ_c	Resistance factor for compression
θ	Angle of yield line

SECTION 1
INTRODUCTION

Falsework is used in the construction of cast-in-place box girder bridges, found extensively on the west coast of the United States. Falsework is defined at the temporary structure that supports the main structure during construction, in contrast to formwork, which consists of the temporary components used to provide the desired shape to a structure. Construction falsework in bridges typically consists of: timber or concrete foundations pads; timber corbels, sand jacks and wedges; steel sill beams; timber or round hollow steel posts; steel cap beams, timber or steel stringer beams and timber joists. These are stabilized for lateral loads using a series of timber or cable braces. An example of these components with steel posts and stringer beams is shown in Figure 1-1, while a another example with timber posts is shown in Figure 1-2.

Historically failure of falsework has occurred due to a number of causes, from events that result in overload of the falsework, to inadequate design and checking of the falsework (Hadipriono 1986) Generally these failures can be prevented by proper execution of an established design procedure and appropriate construction management. However, recent field observations highlighted possible design deficiencies in the type of falsework shown in Figures 1-1 and 1-2. In some cases localized flange bending was observed at the interface between the cap and sill beams and posts, as illustrated in Figure 1-3. While local

FIGURE 1-1 Bridge Falsework for the Petaluma River Bridge at the intersection of California State Routes 101 and 116

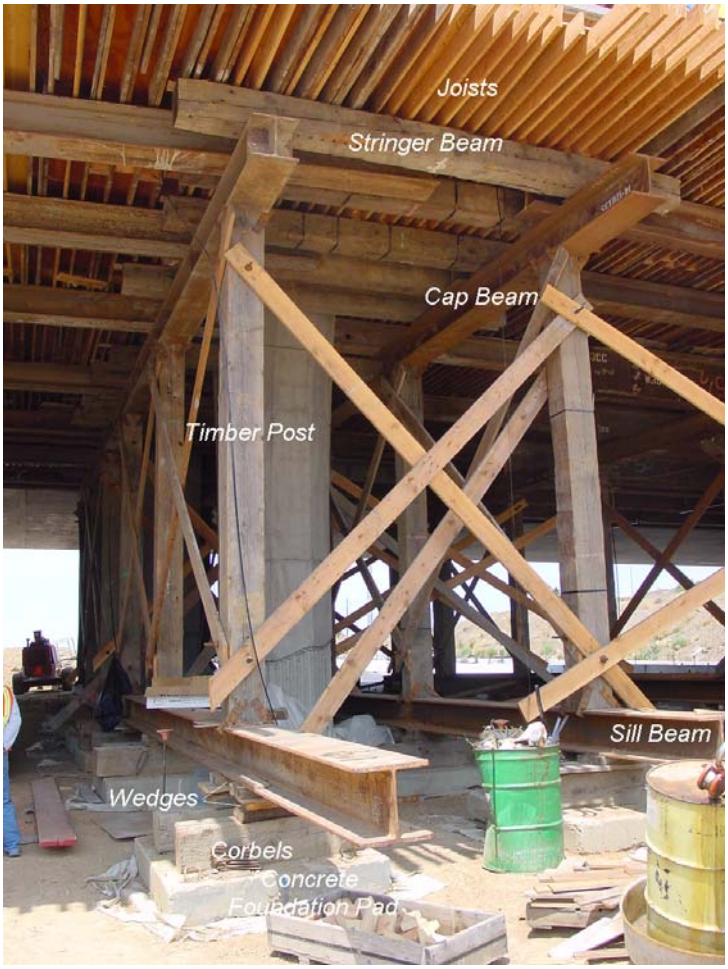

FIGURE 1-2 Bridge Falsework for Railroad Avenue Overcrossing at Pittsburg, California

web yielding of the beam may be checked during design, there is no available method for checking the flange bending capacity required to resist the effects of a flexible patch loading from a timber or steel post. In another example of falsework failure, lateral instability of a beam is observed through deformation of an unrestrained web, as shown in Figure 1-4. Sill and cap beams are generally not braced and not stiffened, thus the potential for lateral instability is much greater than for beams in other typical applications. Thus the stability of the beams should be considered in design, although there is currently no rational method for such consideration.

The AISC LRFD specifications for structural steel buildings (AISC 2005) allows for the calculation of flange bending capacity in beam column joints. The ultimate load in the column flange assumes that a tensile line load is applied to the column flange from the beam flange (Graham et al. 1959). A yield line pattern in the column flange and a uniform stress distribution from the beam flange is then assumed in order to calculate the ultimate capacity of the flange. However, this equation is very conservative if applied to flange bending from compressive patch loading as the region of flange available to resist the load

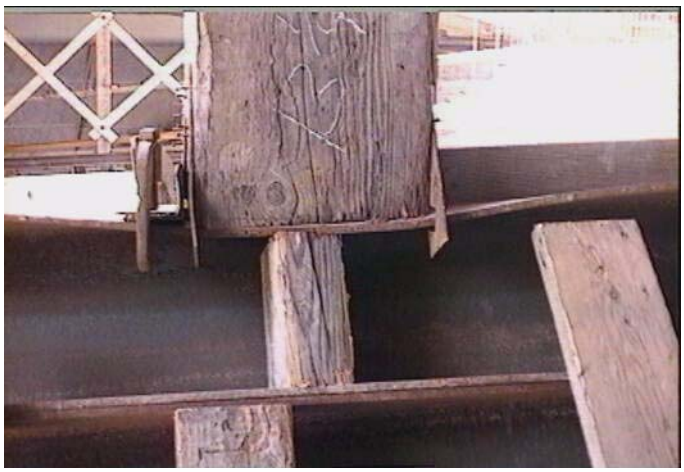

FIGURE 1-3 Localized flange bending failure in sill beam (J. Lammers, Caltrans, Personal communication)

FIGURE 1-4 Instability of sill beam resulting in lateral deformation of web (J. Lammers, Caltrans, Personal communication)

is much g reater for a patch load than a li ne load and a compression load allows lar ge stresses around the web. Past studies on the effect of patch loading (Roberts and Rockey 1979, Roberts and Markovic 1983, Elgaaly 1983, Roberts and Newark 1997, Graciano and Edlund 2003) have generally assumed rigi d patch loads which ha ve not resulted in flange bending other than that required for deformation of th e web. A rigid patch load is defined as one where the patc h load does not deform resu lting in a redistribution of stresses if the loaded member de forms. This is in contra st to a flexible patch loa d which deforms as the loaded member deforms resu lting in a more cons tant distribution of stresses. The case of a flex ible patch load provided by a timber post has not been considered and, therefore, there is no method for predicting the resulting capacity of the beam flange.

The effect of patch loading on the web of beams or columns has been considered by a number of researchers. As a result there are two limit states considered for the localized loading of a beam web, local web yielding that governs for stocky webs, summarized by Galambos (1976), and web crippling that governs for more slender webs, as summarized by Elgaaly (1983). Chen and Newlin (1973) developed an expression for the localized buckling of beam webs for an equal and opposite concentrated load applied to both edges of the web, based on classic plate buckling theory (Timoshenko and Gere 1961). As with the equation developed for flange bending, this equation is expected to be conservative for an applied patch loading, where the area of web involved in resisting the load is considerably greater than for concentrated loads. The buckling equation developed by Chen and Newlin (1973) also assumes that both flanges are restrained from lateral deformation. If there are no stiffeners at any location along a beam, then it may be possible for buckling of the web with lateral deformation of one of the flanges.

Thus, in development of design criteria for unstiffened beams used in bridge falsework, further study is required to investigate the effect of patch loads from timber and steel posts on bending of the beam flanges, yielding or crushing of the posts, and yielding, crippling or lateral buckling of the web.

The objectives of this study are to:

- Experimentally investigate the flange bending capacity of typical falsework beams subjected to patch loading from timber and steel posts.
- Experimentally investigate the localized critical web limit states in falsework beams for timber and steel post loads.
- Experimentally investigate global instability of the web without the use of stiffeners and lateral bracing.
- Determine effectiveness of blocking in increasing the flange and web capacities.
- Determine the impact of accidential eccentricity between the centroid of a timber or steel posts and centroid of the beams.
- Compare the current design equations and allowable stresses in the Caltrans Falsework Manual with other current design specifications.
- Provide recommendations for changes to the current design procedure to prevent future failures of falsework beams.

The scope of this study is limited to experiments on subassemblies of timber or steel post and beam joint regions. Finite element analyses are used to investigate the longer beams and posts for critical cases. Several typical size falsework beams are considered experimentally with a larger range of beams used in finite element analyses. The focus of this study is on the critical components in falsework with the stability of falsework systems not considered.

SECTION 2
EXPERIMENTS ON FALSEWORK COMPONENTS AND SUB-ASSEMBLIES

2.1 Overview

A series of component experiments were performed on short lengths of typical timber posts, timber corbels and steel posts used in bridge falsework. Sub-assembly experiments were also performed with timber and steel posts bearing onto short beam segments using beams with sizes like those typically used in bridge falsework. In some cases corbels were also placed under the beam. The set-up and results from each of the component and subassembly experiments are outlined below.

2.2 Setup of Sub-assembly Experiments on Beams with Posts and Corbels

A series of experiments were performed to study the different limit states in a beam-post connection region. A typical setup with a 48 in. long 12x12 in. timber post, 48 in. long steel beam and 48 in. long 12x12 in. timber corbels centered 24 in. apart behind the beam, is shown in Figure 2-1. The configuration and dimensions of a typical experiment with a timber post and corbels are shown in Figure 2-2. The actual vertically orientated falsework was orientated horizontally to facilitate loading during experiments. The post-flange is consisted to be the flange adjoining the post while the corbel-flange is the flange bearing against the timber or steel corbels, as for a sill beam in typical falsework. A cap beam would be similar, although only the post-flange need be considered as there are no corbels.

The flanges were restrained at the ends of the 48 in. long beam segments by a steel frame, as shown in the figure, preventing lateral instability of the beams for studying the localized flange and post limit states. Loads were applied to the end of the 48 in. long posts through a slider, to limit lateral deformation at the end of the post, in turn attached to a displacement controlled hydraulic actuator. Three different beam sections were used, including ASTM A572Gr50 HP12x53 and HP14x73 beams, and ASTM A992 W14x90 beams. Number 2 Douglas Fir 12 x 12 in. timber members were used for the posts and corbels, while an 18 in. diameter $^{3}/_{8}$ in. thick round hollow steel section with a $^{1}/_{2}$ in. thick base plate was also used to simulate a steel post in two experiments. In these experiments an additional corbel was placed directly in line with the centroid of the columns. In some experiments the timber corbels were replaced with steel plates as shown in Figure 2-3 in order to eliminate the effect of the corbels from the system. In other experiments, that focused on web yielding and crippling, a rigid 12 x 12 in. steel plate was used instead of a post, as shown in Figure 2-4. Some experiments also used 6 x 8 in. Number 2 Douglas Fir timber blocking, placed between the flanges on both sides of the web. This blocking is sometimes used in falsework in an attempt to increase the flange and web capacity of the beams and was investigated to determine its effectiveness. In some cases an eccentricity

FIGURE 2-1 Sub-assembly setup with actuator, timber post, steel beam, restraints and corbels

was employed between the centroid of the beam and post, equal to $^1/_{12}$th of the beam flange width or $^1/_6$th of the flange width. The final variation in the experiments was the removal of the lateral restraints, in which case the beams were supported by connecting one flange to the steel bracket behind the beam. The removal of restraints allowed the other flange to deflect laterally on application of loading from a post. This is to simulate lateral buckling of an unrestrained, unbraced beam.

The combination of beam sizes, with and without corbels, with and without blocking, with and without eccentricities and with different types of posts is described in Table 2-1. The highlighted regions refer to combinations that were used in experiments and the numbers refer to the order of the experiments. In addition to the subassembly experiments described in this table, component experiments were performed on timber posts, corbels a steel post along with coupon tests on samples from the steel beams to better understand the material and component behavior of the various elements, as described below.

2.3 Coupon Tests

Eight coupons were cut from the flange and web of four beams after experiments were completed in order to determine the material properties of the steel in the beams. The results from the coupon tests are given in Table 2-2. The average yield stress is 53.3 ksi,

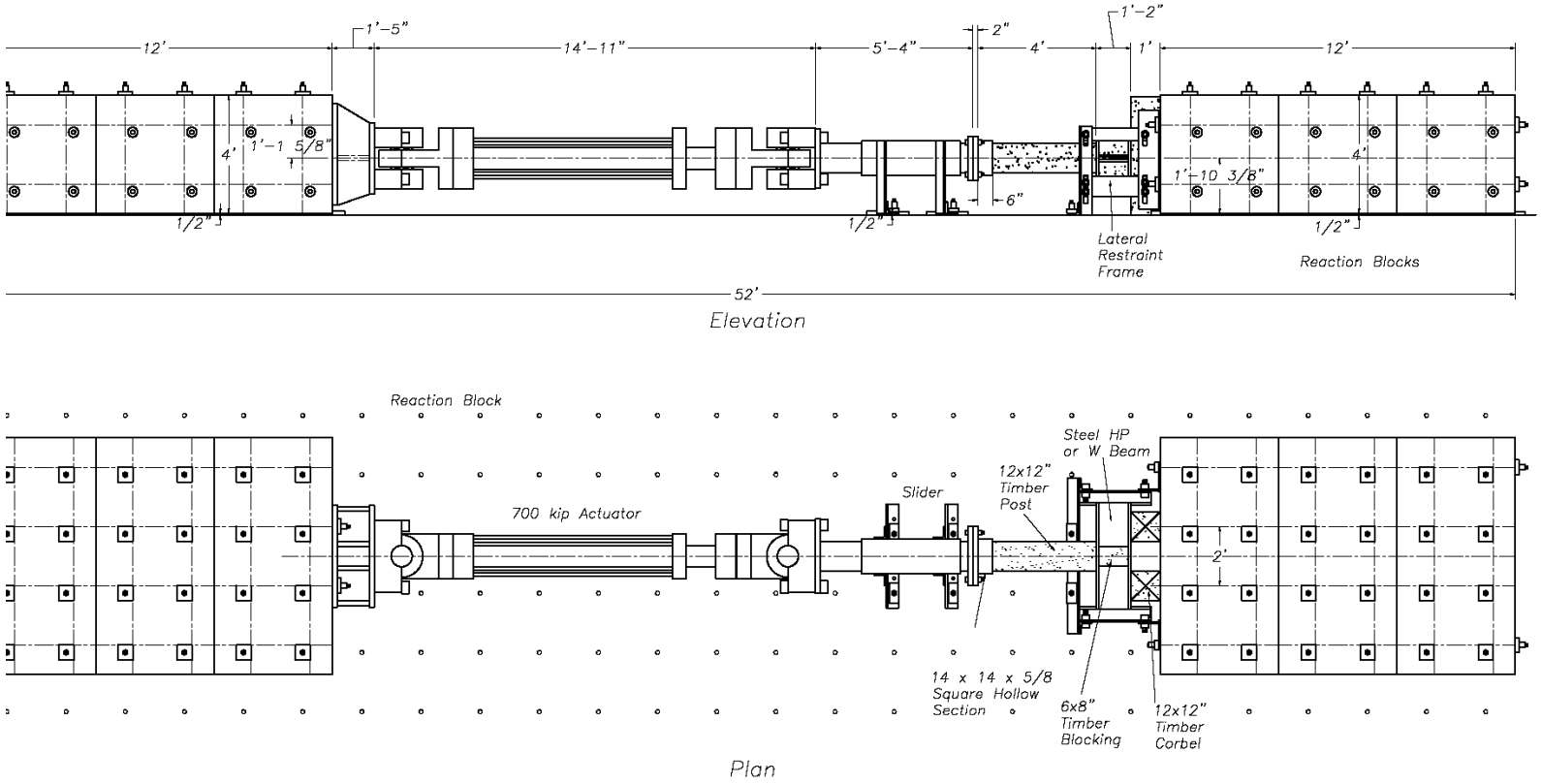

FIGURE 2-2 Typical experimental setup for beam with timber post and corbels

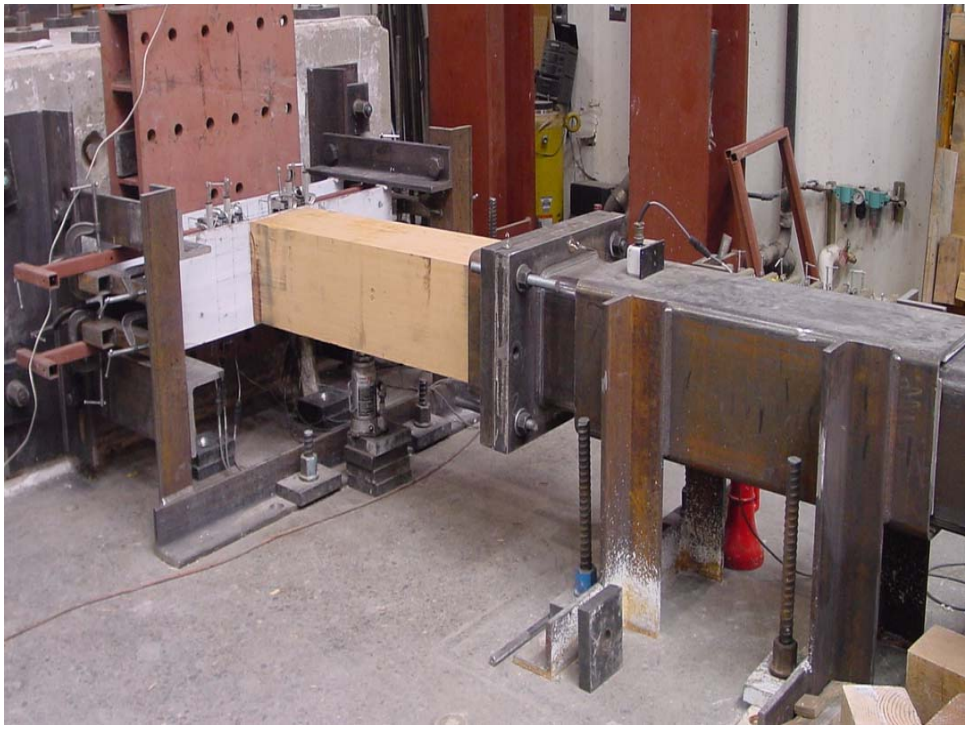

FIGURE 2-3 Sub-assembly setup without timber corbels

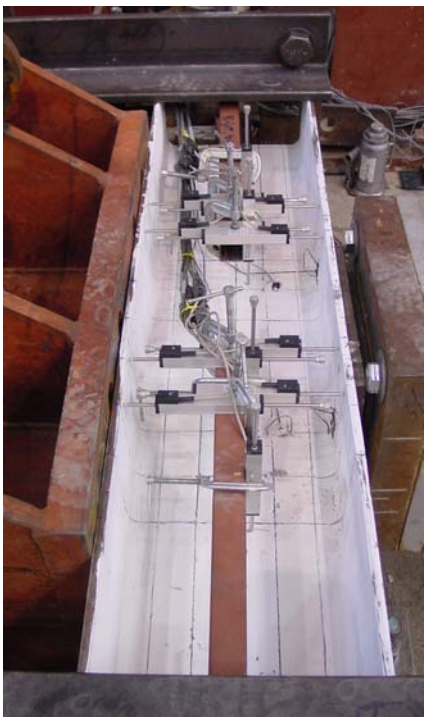

FIGURE 2-4 Sub-assembly setup without a post or timber corbels

TABLE 2-1 Combinations of beams, posts, corbels, blocking and eccentricities used i experiments

Section		HP12x53			HP14x73			W14x90					
Post Type		None	Timber	Timber	None	Timber	Timber	None	Timber	Timber	Steel	Timber	None
Corbels		None	2 Timber	2 Steel[4]	None	2 Steel	2 Steel[4]	None	2 Timber	2 Steel[4]	3 Timber	2 Steel[4]	None
Lateral Restraint		Yes	Yes	Yes	Yes	Yes	No	Yes	Yes	Yes	Yes	No	No
Nominal Eccentricity = 0	No Blocking	Beam #10	Beam #12	Beam #18	Beam #9	Beam #20	Beam #29	Beam #6	Beam #1	Beam #22	Beam #2	Beam #26	Beam #5
	Blocking		Beam #13[3]	Beam #19		Beam #21	Beam #30			Beam #23		Beam #28	
Nominal Eccentricity = $b_f/12$	No Blocking			Beam #16									
	Blocking			Beam #17									
Nominal Eccentricity = $b_f/6$	No Blocking	Beam #11		Beam #14	Beam #8	Beam #27	Beam #31	Beam #7	Beam #4	Beam #24	Beam #3		
	Blocking			Beam #15		Beam #25	Beam #32						

Notes:
1. Highlighted areas show combinations of beams and other factors that have were used in experiments
2. All beams shown in this above matrix are 4' long
3. This experiment had timber corbels but also steel plates between the beam and the corbels to minimize stress concentrations in the corbels
4. Steel plates were used in place of timber corbels.

TABLE 2-2 Summary of results from coupon tests

Section	Coupon Location	Yield Stress (ksi)	Ultimate Stress (ksi)	Ultimate Strain (%)	Elastic Modulus (ksi)
HP12x53	Flange	55.7	76.4	31.6%	28200
	Web	54.3	75.7	30.9%	29000
HP14x73	Flange	49.4	68.3	32.5%	34100
	Web	50.9	72.2	33.0%	35800
W14x90 - 1	Flange	52.5	71.0	36.7%	N/A
	Web	58.2	73.0	32.4%	30000
W14x90 - 2	Flange	51.4	69.5	38.5%	31800
	Web	54.3	72.0	30.7%	31800

with a range between 49.4 and 58.2, and is close to the expected stress for the A572 Gr. 50 steel and A992 steel of 55 ksi. It is greater than or appr oximately equal to the minimum specified stress of 50 ksi in all cases. The ultimate stress is around 20 to 40% higher than the yield stress. The ultimate strain varies between 30 to 39%. The elastic modulus varies between 28000 and 36000 ksi, within 25% of the design value of 29000 ksi.

2.4 Component Experiments

2.4.1 Timber Posts

Three, 4 foot long, Number 2, Douglas Fir, 12x12 in. timber posts were crushed as shown in Figure 2-5 to determine the compressive stre ngth of these posts parallel to the grain. The actuator force is plotted agains t the di splacement measu red at the end of the slider where it connects to the post in Figure 2-6 for the three posts. The figure shows that the stiffness for each pos t, indicated by the slope of the curves, is initial relatively small but

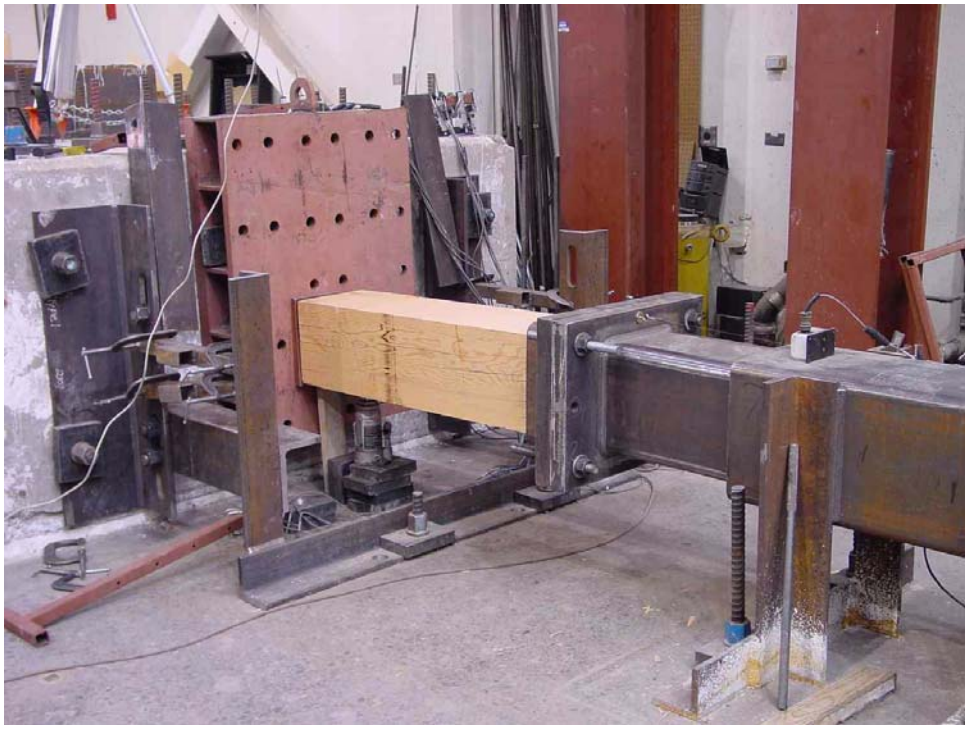

FIGURE 2-5 Component experiment on 4 foot long 12x12 in. Timber Post

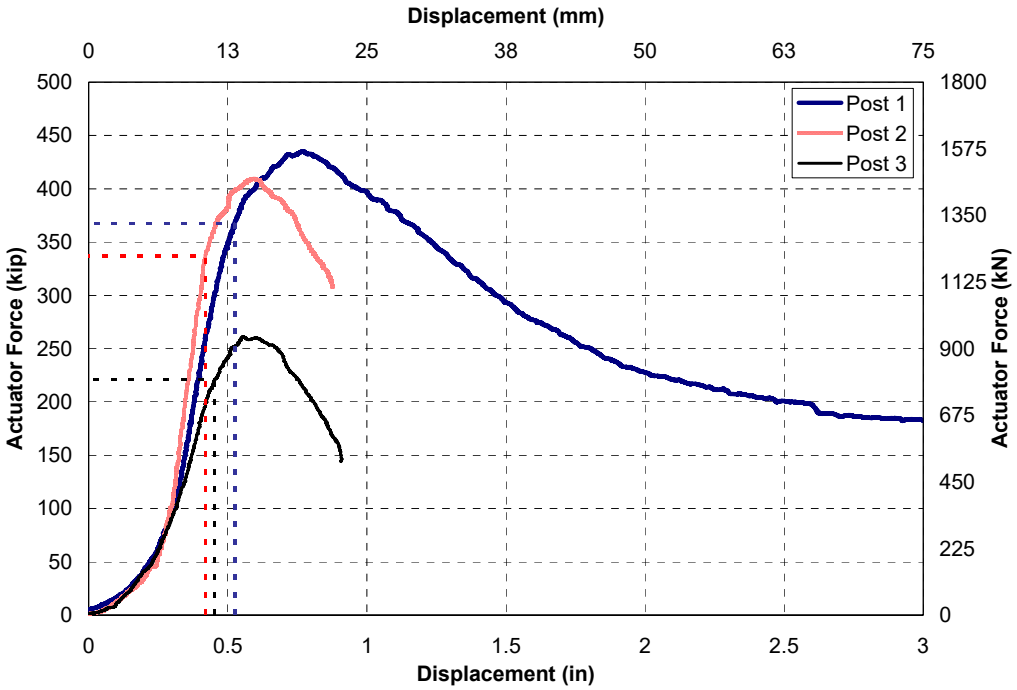

FIGURE 2-6 Actuator force vs slider displacement for different post component experiments

increases as any gaps between the ends of the post and adjacent reactions are closed. Once this happens the maximum stiffness is reached. As the load continues to increase the stiffness starts to drop again indicating the onset of crushing of the post. When the maximum load is reached, severe crushing and splitting of the post is observed. The maximum load in posts 1 and 2 is within 10% of each other, however the maximum load in post 3 is 30-40% less. This is indicative of the large variability possible in these posts particularly as they are Number 2 specimens thus splitting and imperfections are typically found in the members. The lower strength is also attributed to a lack of squareness, which was most pronounced at the end of this post, andresulted in stress concentrations in part of the post inducing premature failure of the post. This is a typical feature of falsework posts and therefore a conservative design of the post is required.

The failure load in each post and all other experiments was not defined as the maximum load, but at a load where the stiffness of the post dropped to 50% of its initial stiffness. The initial stiffness was defined from the force-displacement curve between 25 and 75% of the estimated failure load. This was used in order to define significant crushing or yielding and was generally with in 10 to 15% of the maximum applied force for each experiment where a reduction in force was observed after failure. In some experiments such as those where timber corbels crushed, as described in the following section, a reduction in force was not observed. Instead the force continued to increase up to large inelastic displacements. In this case a definition of failure load as above was necessary to define failure.

The stiffness of Post 1 is plotted against the slider displacement in Figure 2-7 with some averaging of the data used to smooth the stiffness. The initial stiffness for this post was estimated at 975 kip/in. The force in the post corresponding to where the load dropped to 50% of this initial stiffness was determined and defined as the failure load. The failure loads were 367, 337 and 221 kip respectively for the three timber post component experiments, as shown by the dashed lines in Figure 2 for each of the posts. The corresponding axial failure compression stresses were 2770, 2540 and 1670 psi based on 11.5 in square actual post dimensions.

2.4.2 Timber Corbels

A component experiment was performed on a 12x12 in. Number 2 Douglas Fir timber corbel, as shown in Figure 2-8. A 15 in. wide patch load was applied to the corbel, similar to the 14 to 15 in. wide flange of a typical falsework beam. The corbel was identical to the timber post except that the load was applied perpendicular to the grain. The failure load in the corbel was defined when the stiffness reduced to 50% of the initial stiffness using the same procedure as for the timber post. Unlike the timber post, however, the force-displacement curve in Figure 2-9 shows that once the failure load was reached the force did not drop but continued to increase as the timber in the corbel densified with increasing deformation. Thus failure of a corbel is likely to be less catastrophic than failure of the post as it continues to carry the load after failure. The failure load for the corbel was

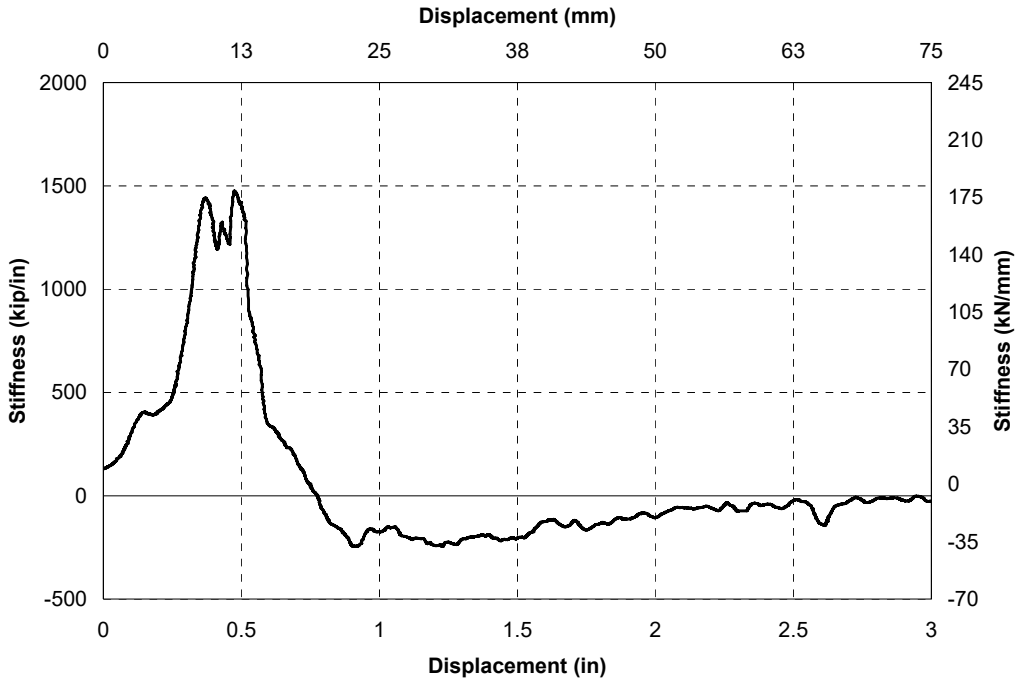

FIGURE 2-7 Stiffness vs slider displacement for post component experiment (Post 1)

calculated at 93 kip, correspondi ng to a failure bearing stre ss of 540 psi for the 1 1.5 in. wide member.

2.4.3 Timber Blocking

Component experiments, with axial loads applied using a lo ad frame as s hown in Figure 2-10, were performed on three timber blocks . The resulting force-displacement curves for the three blocks are shown in Figure 2-11. The failure load for the blocks was quite variable. The strength in the blocks was much higher than the nominal strength based on the NDS wood specifications (AFPA 1996) and, in one case, the force in the blocking reached the capacity of the actuator in the load frame. However , as the stif fness of the blocking just started to drop, the failure load was determined just before the experiment was terminated at 199 kip. The failure load s for the other two bl ocks were 159 and 133 kip respectively. The fail ure loads corresponded to st resses of 4820, 3850 and 3220 psi respectively based on 7.5 x 5.5 actual blocking dimensions.

2.4.4 Steel Post

A component experiment was also conducted on a 18 in. diameter $^{3}/_{8}$ in. thick A500 Grade B (42 ksi minimum specified yield stress) steel post, as shown in Figure 2-12. The base plate of the post was $^{1}/_{2}$ in thick A36 steel connected to the post using a $^{5}/_{16}$ in. fillet

FIGURE 2-8 Component experiment on 4 foot long 12x12 in. timber corbel

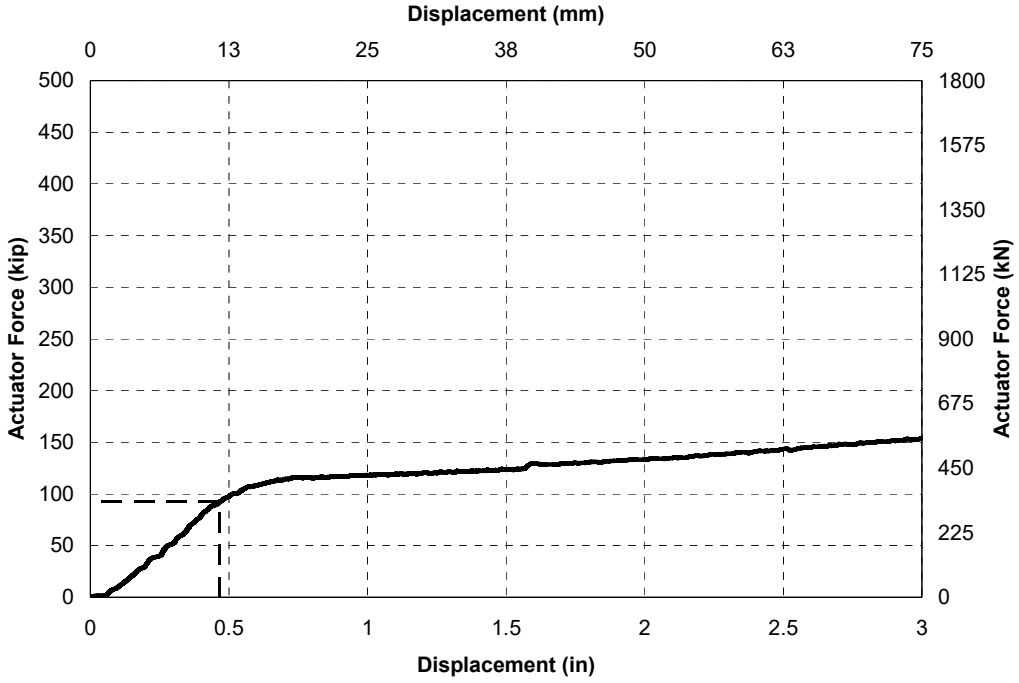

FIGURE 2-9 Actuator force vs slider displacement for timber corbel

FIGURE 2-10 Component experiment on blocking in load frame

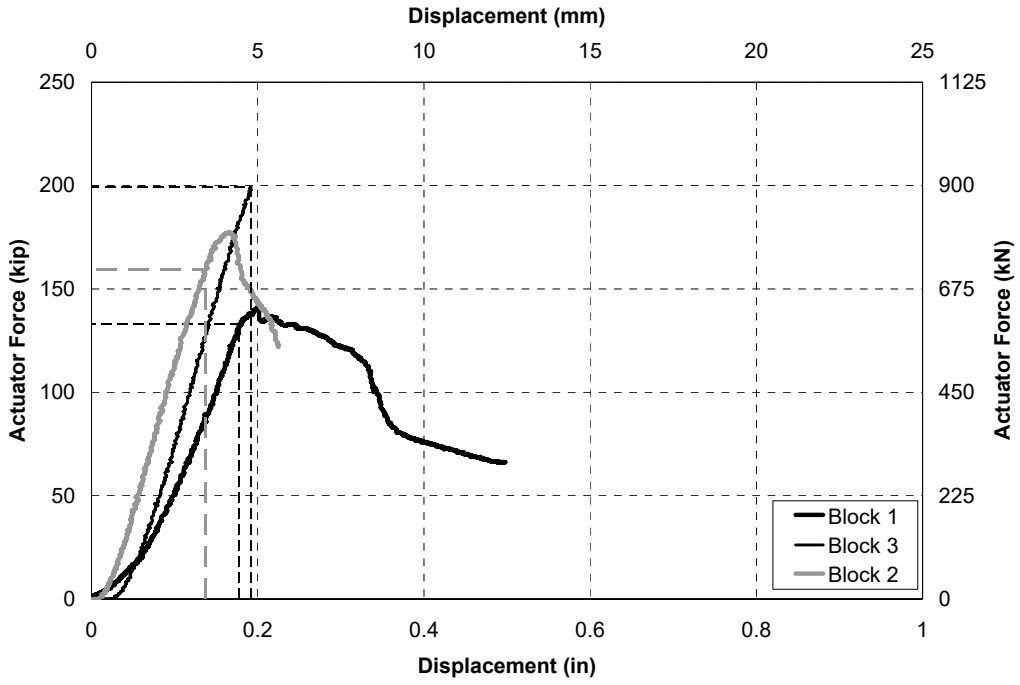

FIGURE 2-11 Actuator force vs actuator displacement for three timber block component experiments

weld. At the end attached to the slider a 1 $^1/_2$ in. thick plate was welded to the post. The failure load in the steel post was calculated at 811 kip as using the same definition for failure as for the timber posts and corbel. At around the failure load, the onset of yielding and buckling was observed in the post near the end with the $^1/_2$ in base plate. The force displacement curve in Figure 2-13 does not show a reduction in force after yielding of the post, although the post is at the upper capacity of the actuator, therefore the experiment had to be terminated once the onset of yielding was observed.

2.5 Sub-assembly Experiments on Beams with Posts and Corbels

2.5.1 Overview

The behavior of each of the sub-assembly experiments is described in this section. The experiments with steel corbels are first discussed which resulted in crushing or yielding of the timber or steel post respectively in conjunction with bending of the a post-flange of the beam. The next set of experiments discussed are the beams with corbels, which resulted in bending of the corbel-flange and crushing of the corbels. The third set of experiments considered are those without any posts or corbels which resulted in yielding and buckling of the web. The final set of experiments are those beams without any lateral restraints in some cases resulting in lateral web buckling. A summary of each experiment is given, along with actuator force versus slider displacement curves. Each beam is named based on: the section size; whether is has a timber, steel or no post; whether it has blocking or no blocking; the use of a timber, steel, or no corbel; whether or not it is restrained, and, what level of eccentricity it has between the post and beam. The number referring to the beam number in Table 2-1 is also given.

2.5.2 Beams with Resulting in Post-Flange Bending and Post Crushing

1253TPNBSCRE0 - Beam 18

This was one of the smallest section considered, loaded through a timber post, without blocking, with steel corbels, laterally restrained at the flanges and without any eccentricity between the beam and post. As an increasing load was applied axially through a timber post the stiffness of the force-displacement curve (Fig. 2-14) increased until it became constant at around 50 kip up to a force of approximately 240 kip. The initial stiffening of the system was typical for all of the experiments as the gaps between the different components closed. Flaking, indicative of plastic deformation, was observed in the post-flange close to the locations of the strain gauges at a force of around 210 kip. As the load increased the onset of post deformation around the web of the beam was observed as necessary to allow the post-flange to bend, as shown in Figure 2-15. The force-displacement curve started to flatten, as shown in Figure 2-14. The failure load, based on a 50% reduction in stiffness, was calculated at 237 kip therefore was around 13% greater than the load when flaking was first observed in this beam. The maximum load was

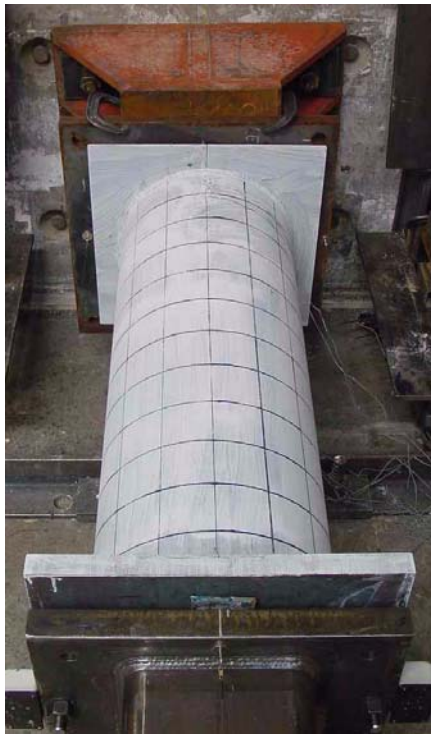

FIGURE 2-12 Component experiment on 4 ft. long 18 in. diameter steel post

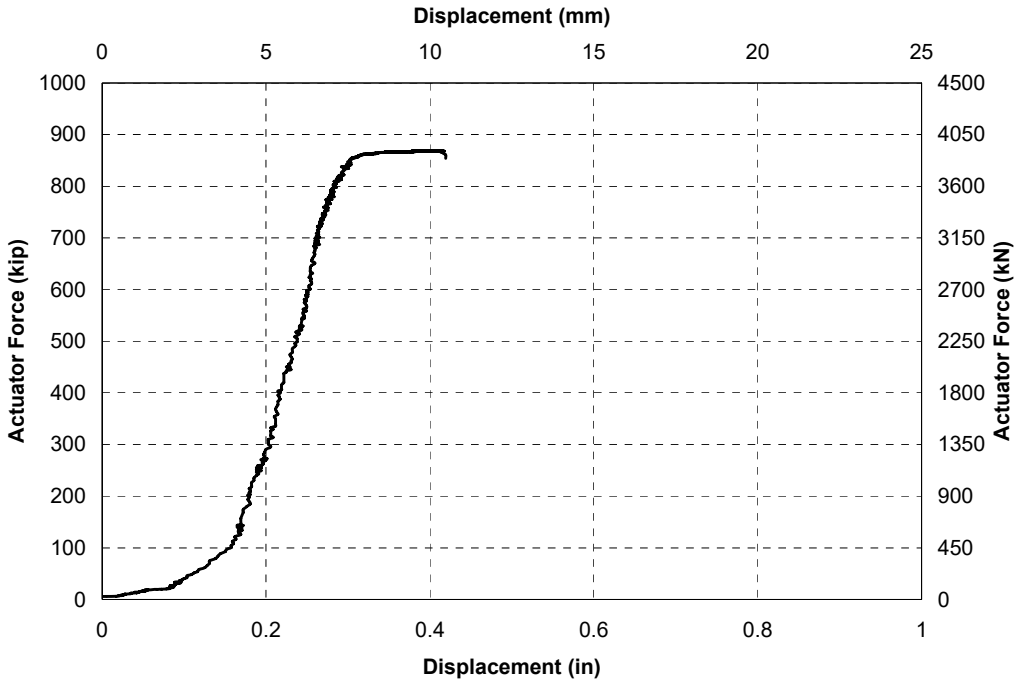

FIGURE 2-13 Actuator force vs slider displacement for timber corbel

reached at 243 kip at which point post crushing was observed. No corbel-flange yielding or web deformation was observed in this experiment.

Two strain gages located on the flange of this beam around where yielding was first observed, as shown in Figure 2-16, are plotted against the actuator force in Figure 2-17. One strain gage shows possible yielding due to flattening of the curve at around 205 kip, close the point where flaking was first observed. The second strain gage shows flattening at close to 230 kip, around where the failure load was calculated. Therefore the failure load is consistent with the observed inelastic behavior in the flange using these strain gages. Similar observations can be made for the other beams exhibiting flange bending when strain gages were located close to the observed yield lines.

1253TPBSCRE0 - Beam 19

This experiment was identical to the last except that blocking was used between the post- and corbel-flanges on both sides of the web. As the load was applied to the post the stiffness increased until the elastic stiffness was reached. Then the post started to deform around the web and flange as in the previous experiment corresponding to a reduction in stiffness (Fig. 2-18). Engagement of the blocking increased the failure load with onset of flaking on the post-flange observed at around 310 kip, although the calculated failure load was a little less at 289 kip. The maximum load was reached at 320 kip, which corresponded to flange bending and timber post failure. Slight bending was observed in the corbel-flange as well, though not enough to cause flaking. There was no observed web deformation.

1253TPNBSCRE12 - Beam 16

The loading was applied axially through timber post in this experiment with an eccentricity of $b_f/12$ (1.0 in.) between the post and unblocked beam. The force-displacement curve (Fig. 2-19) was similar to that for the concentrically loaded case although the stiffness was smaller, which could be due to different material properties as well as the eccentricity. The post deformed around the web of the beam as in the previous cases, with the effect of the eccentricity simply moving the deformation laterally in the post. Flaking in the post-flange was observed at around 200 kip and the failure load was calculated at 212 kip. The maximum force was observed at 225 kip, along with severe post deformation and further yielding of the post-flange. Therefore, although the failure and maximum loads were reduced by around 10%, there was not an appreciable change in response compared to the concentrically loaded case.

1253TPBSCRE12 - Beam 17

The same eccentricity as the previous case was imposed with blocking also used between the flanges. The observed response of the beam was similar to the previous blocked case. The force-displacement curve (Fig. 2-20) showed typical stiffening, followed by a period

of elastic response, followed by a reduction in stiffness due to post crushing. After an initial drop in load the force increased slightly then plateaued as the forces were redistributed through the post, although failure was considered to have occurred prior to this behavior. The failure load was calculated to be 284 kip. No flaking was observed in the flange until a force of 320 kip was reached. There was a small amount of bending prior to this, as a small gap observed between the blocking and the flange closed, but this was not sufficient to cause yielding. The load reached a maximum of 335 kip.

253TPNBSCRE6 - Beam 14

This unblocked beam had a larger eccentricity equal to $b_f/6$ (2.0 in.). The response (Fig. 2-21) was almost identical to the previously described unblocked case. The failure load was calculated to be 221 kip. At this point, bending of the post-flange and flaking was observed close to the location of the strain gauges. Figure 2-22 shows the strains in four gages on the post-flange of the beam located close to the yield lines, with two on each side of the web. These strain gages all show the onset of yielding at a force of between 210 to 220 kip. Despite the eccentricity the strain gages on both sides of the web show yielding at a similar force. The force reached a maximum of 230 kip before being reduced as complete post crushing was observed.

1253TPBSCRE6 - Beam 15

This eccentrically loaded blocked beam performed similarly to the previous case with blocking. Upon yielding of the beam and crushing of the post an immediate reduction in load was not observed (Fig. 2-23), instead the load plateaued. The failure load was calculated at 285 kip. At around 300 kip yielding of the post was observed with some inelastic bending in the post-flange observed at this time. The maximum load was reached after significant inelastic deformation at 335 kip, when the post completely crushed.

1473TPNBSCRE0 - Beam 20

This was the next size beam considered, loaded concentrically without blocking. The response (Fig. 2-24) was similar to that for the smaller beam, although the failure load was increased due to increased flange bending capacity, even though the post had a similar strength. The failure load was calculated to be 275 kip with a maximum load reached of 290 kip, whereupon the onset of bending in the post-flange was observed. Flaking was observed at around 290 kip. Crushing of the post and the flange appeared to occur almost simultaneously. No corbel-flange yielding was observed.

1473TPBSCRE0 - Beam 21

The same configuration as above was used for this beam with additional blocking between the flanges. At 340 kip the onset of flaking was observed in the post-flange, although it was limited as the blocking was activated. The failure load was calculated at 381 kip (Fig.

2-25). The maximum load was around 395 kip, after which the post failed. Relatively little bending was observed in the post-flange due to bloc king, but it wa s enough to be considered failure of the beam.

1473TPNBSCRE6 - Beam 27

This unblocked beam had an eccentricity between the beam and post of $b_f/6$ (1.2 in.). The failure load was calculated to be approximately 283 kip, thus very similar to the concentrically loaded beam. Bending in the post-flange was observed along with sudden post deformation at failure. No flaking was observed until after the maximum load wa s reached. The load dropped quickly after th e maximum load was reached, as shown in Figure 2-26.

1473TPBSCRE6 - Beam 25

The blocked, eccentrically loaded beam has a reduced strength compared to the concentrically loaded beam, although this could be lar gely due to a variation in post strength. The failure load was calculated to be 310 kip. The load-displacement curve (Fig. 2-27) peaked at around 320 kip and stayed rela tively constant over 0.4 inches of applied displacement. Some initial post-f lange flaking was observed as post deformation increased, but was limited once blocking was activated until well after the maximum load was reached. At large displacements, the timber block split, resulting in significant flange bending and an reduction in the load carrying capacity at this stage.

1490TPNBSCRE0 - Beam 22

This is the first of the W14x90 beams, concen trically loaded, without blocking. As with the other beam sizes flaking was observed in the post-flange, although at a higher load of around 300 kip due to the thicker flange. Th e failure load was cal culated to be 291 kip. The force peaked at 320 kip a nd stayed constant for about 0.2 inches of applied post displacement, after which is started to dr op, as shown in Figure 2-28. The failure was through a combination of flange bending and post crushing as for the previous beams.

1490TPBSCRE0 - Beam 23

With blocking, the response (Fig. 2-29) of the W14x90 beam was similar to the unblocked case. The failure load was calculated at 307 kip with a small amount of flaking around the block observed at around 325 kip. Bending of the post-fl ange diminished once the blocking became effective. The load rose to a maximum of 335 kip at which time failure was observed largely through crushing of the post. As in all previous experiments, no web yielding was observed.

1490TPNBSCRE6 - Beam 24

This eccentrically loaded, unblocked beam performed similarly to the concentrically loaded beam. The failure load was calculated at 293 kip. Flaking around the post-flange was observed at the same level of force. The load reached a maximum of approximately 300 kip (Fig. 2-30), at which point web yielding was observed. In this experiment the onset of web yielding was observed through flaking of the web at the maximum load, attributed to the eccentricity coupled with a relatively thin web compared to the flange thickness. Despite the web inelasticity, it did not significantly affect the performance of the beam.

Summary

In summary all beams loaded with timber posts resulted in some measure of post-flange deformation coupled with post deformation around the web of the beam and subsequent crushing. The failure load of the flange-post joint region appeared to be coupled to the thickness of the flange and strength of the post. Eccentricity had minimal effect on the response with some reduction in failure load observed, but typically no more than 10%. Blocking increased the failure load, with some flange deformation observed to engage the blocking, but an overall reduction in flange deformation resulted in an increase in the flange-post joint capacity.

2.5.3 Beams with Timber Posts and Timber Corbels Resulting in Corbel Crushing

1253TPNBTCRE0 - Beam 12

This set of beams had 2 timber corbels behind the corbel-flange of each beam. This was intended to simulate sill beams, although usually a sand jack, blocks and wedges would be used between the sill beam and corbel. For each beam in this section the load was applied axially through a timber post. In this beam, the load increased to around 100 kip then apparent inelastic deformation started to occur, as illustrated by Figure 2-31. This apparent yielding was attributed to crushing of the corbels as well as bending of the corbel-flange of the beam as shown in Figure 2-32 shown after the completion of the experiment. In this respect these experiments may not be quite like what would be observed in the field, as the sand jack and blocks may reduce the concentration of corbel deformation around the web of the beam, resulting in increased capacity in the corbels. The failure load was calculated at 131 kip, also corresponding to the observation of lime paint flaking on the corbel-flange of the beam. Unlike when post crushing was observed, the load continued to increase after the corbels started to crush, therefore this limit state is much less catastrophic than one involving post crushing. At 170 kip, there was significant cracking in the timber corbels. Soon after, the experiment was paused to remove some instruments then resumed. As the load reached 200 kip, bending in the post-flange was observed with flaking of the lime paint. At the maximum load of 240 kip, the post, post-flange, and corbel-flange all had significant deformation and yielding although the load

continued to increase. The experiment was terminated as the limit of instruments was reached.

1253TPBTCRE0 - Beam 13

In this experiment two 1 in. thick, 12 x 12 in. steel plates were used between the corbel-flange and each timber corbel to simulate to the presence of jacks and wedges. Blocking was also used between the beam flanges. The use of the plates at the corbels increased the failure load to 202 kip, compared to 131 kip for the previous beam. At the failure load, the onset of crushing in the corbels was observed. This is considered a more realistic representation of the actual conditions found in the field and corresponds to an average individual corbel failure load of 101 kip, within 9% of the 93 kip load measured during the component experiment. In this beam no corbel-flange bending was observed around the corbels. At a force of 260 kip, the onset of post crushing was observed and the load started to drop (Fig. 2-33).

1490TPNBTCRE0 - Beam 1

In this larger beam the configuration was similar to that for Beam 12. There were no steel plates between the corbel-flange and corbels, which resulted in corbel-flange bending in conjunction with corbel crushing. The failure load was calculated at 234 kip close to the point where corbel-flange bending and flaking of the lime paint was observed at around 240 kip. At this point the force-displacement curve started to flatten (Fig. 2-34). The experiment was held to make observations at this level allowing the force to drop due to creep in the system, although this was regained as soon as the loading was reapplied. At around 250 kip further bending of the corbel-flange was observed. The post-flange also exhibited some bending along with deformation of the post. This behavior continued until an ultimate load of 356 kip was reached at which point the end of the post crushed.

1490TPNBTCRE6 - Beam 4

This was the same as the previous experiment except for an eccentricity between the post and beam of $b_f/6$ (2.4 in.). This appeared to result in a more gradual transition between the elastic and inelastic deformation of the corbel. The failure load was calculated to be 190 kip, although Figure 2-35 shows that there was no clear transition to indicate inelastic behavior. At around 250 kip flaking of the lime paint on due to bending in the corbel-flange was observed. The post crushed shortly after, at a maximum load of 270 kip, with some post-flange bending also observed.

Summary

Corbel crushing typically occurred before post crushing and flange bending, although corbel crushing was not catastrophic and allowed an increase in forces leading to eventual complete failure due to post and post-flange failure. Allowing bending of the corbel-

flange reduced the corbel capacity, although this is conservative, as in the field the sand jacks and blocks between the beam and corbel are likely to reduce stress concentrations in the corbel.

2.5.4 Beams with Steel Posts and Three Timber Corbels Resulting in Corbel Crushing and Post Yielding

1490SPNBTCRE0 - Beam 2

In this section two beams were considered with steel posts. For the first beam the post load was applied concentrically to the beam. Three corbels were placed behind the beam, including one directly under where the load was applied and the other two centered 12 in. each side of the middle corbel. The force-displacement curve (Fig. 2-36) for this experiment was elastic (after initiating full contact of the various components) up to an observed load of around 250 kip. At this load, deformation of the corbels behind the beam began to be observed. The failure load was calculated at 292 kip as the stiffness decreased. Corbel-flange yielding was observed through flaking of the whitewash paint at 330 kip as the load continued to increase. At 400 kip corbel-flange yielding had progressed along the entire length of the beam. At 475 kip some deformation of the post-flange was observed with bending in the base plate of the steel post. Yielding of the post-flange though whitewash flaking was observed at this level. The onset of buckling of the end of the post in line with the beam flange was also observed, as shown in Figure 2-37. The ultimate load was reached at 520 kip at which time the corbels where unable to maintain the load, while significant buckling of the post was also observed.

1490SPNBTCRE6 - Beam 3

In this experiment the load was applied eccentrically to the beam through the steel post. The force-displacement response (Fig. 2-38) was almost identical to that for the concentrically loaded beam. The failure load was calculated to be 270 kip. At 340 kip, flaking was observed in the corbel-flange. Flaking stretched across the length of the beam at 400 kip. The onset of localized post yielding was apparent at around 425 kip on one side of the post. The force continued to increase up to a force of 525 kip. At the end of the experiment some localized web yielding was observed.

Summary

The strength of the steel posts appeared to the governed by localized yielding and crippling of the post where it bears onto the web of the beam. This is similar to yielding that may be observed in the web of beams when a concentrated load is applied to the beam. An eccentricity has little effect on the response of the post as it simply moves the yielding region to a new region of the post, still in line with the web of the beam. As the end of the steel post is rigid, no flange bending is observed until after yielding and crippling of the post is observed. The strength of the corbels in these experiments was

similar to those observed previously, with some reduction in strength due to bending of the corbel-flange.

2.5.5 Beams with Rigid Patch Loads and No Corbels Resulting in Web Yielding

1253NPNBNCRE0 - Beam 10

As the timber and steel posts failed before significant deformation was observed in the web of the beams, rigid patch loads from a steel plate were applied to a series of beams to investigate critical web limit states. All the beams in this series were laterally restrained to prevent lateral deformation of the post-flange. This beam, an HP12x53, was one of the smallest sections, although it has the same size web as the W14x90. The load was applied through the rigid 12 x 12 in. patch load as shown in Figure 2-4. The force-displacement curve for this beam is shown in Figure 2-39. At 240 kip, the onset of flaking in the web was observed, although the failure load was not calculated until the force reached 370 kip. The maximum load was reached at 380 kip. At the failure load significant yielding of the web was observed along with an onset of lateral deformation in the web. As the deformation increased beyond the maximum load and the load began to drop, the web started to buckle/ cripple as shown in Figure 2-40. As this deformation occurs after significant yielding was observed, it was considered post-elastic buckling/crippling. There was no evidence of flange bending or yielding until significant deformation occurred in the web and was consistent with that required to allow deformation of the web.

1253NPNBNCRE6 - Beam 11

This is almost identical to the previous beam except that the load was applied eccentrically. However, as the patch load was rigid, it was found the effect of the eccentricity was minimal. The failure load was calculated at 370 kip, identical to the previous beam. At the failure load, the onset of web yielding was observed. The first yielding was observed near the center of the web indicating an onset of web buckling. The maximum force was reached at 380 kip (Fig. 2-41) at which point buckling became evident.

1473NPNBNCRE0 - Beam 9

This was the next size larger beam with loading applied concentrically using the patch load as in the previous two beams. At 325 kip, the onset of web flaking was observed before it was observed that the upper lateral restraints were slipping resulting in a small lateral deformation of the post-flange. The experiment was paused to tighten the restraints then resumed. The failure load was calculated at 417 kip. The maximum load was reached at 440 kip (Fig. 2-42). This load was potentially reduced due to the small lateral deformation, although comparisons with the following beam do not suggest this was significant.

1473NPNBNCRE6 - Beam 8

Similar to the previous beam but with an eccentricity , the failure load was calculated at 419 kip, almost identical to the previous beam. The maximum force was reached at 480 kip (Fig. 2-43). W eb yielding followed by post-elastic cr ippling/buckling was observed as in previous experiments.

1490NPNBNCRE0 - Beam 6

This was a concentrically loaded W14x90 beam and its response followed the pattern of the previous beams. Even though the web was relatively thinner compared to the flange, post-elastic buckling/crippling was observed. At 410 kip the onset of web buckling was observed through flaking of the web, although th e failure load was cal culated at 457 kip. The force reached a maximum at 470 kip before going into a gradual decline as shown in Figure 2-44.

1490NPNBNCRE6 - Beam 7

As with the previous beams the eccentricity from the rigid patch lo ad resu lting in little change in response, in fact the loads in this beam were slightly larger than in the previous beam. At 430 kip, the onset of web flaking was observed. The failure load was observed at 510 kip. The maximum load was reached at 530 kip (Fig. 2-45).

Summary

Web de formation for the se beams where the flanges were late rally restrained to prevent lateral deformation of the fl ange were categorized by yiel ding followed by post-elastic buckling/crippling the web. Th e ef fect of eccentricity from the rigid patch load wa s negligible. The yielding of the web occurred at lar ger forces than post crus hing or yielding and flange bending obser ved in previous experiment s. B eams with No Lateral Restraints Resulting in Possible Lateral Web Buckling

1473TPNBSCNRE0 - Beam 29

As falsework is not typically braced or st iffened, a series of beams without lateral restraints were considered. For these beams the loads were applied concentrically though a timber post. As the load was applied to the beam the post-flange and end of the post started to deform. The failur e loa d was c alculated in th e beam due to post and flange deformation at 300 kip. At 310 kip, flaking of the lime paint was observed on the post-flange. A maximum load of 315 kip was reached at which point some flaking of the paint on the web was observed indi cating web bending. Despite some bending sudden lateral buckling was no observed. The load then dropped due to crushing of the post (Fig. 2-46). With n o latera l r estraints this beam esse ntially per formed the sa me a s the equiv alent restrained beam (Beam 20).

1473TPBSCNRE0 - Beam 30

This beam was the same as the previous except blocking was placed between the flanges. As a result it was expected that the load would be greater than in the previous beam, potentially inducing buckling in the beam. However, due to an apparently weak post, the failure load for this beam was calculated at 275 kip, less than for the previous experiment. After initial crushing of the post, the failure load was maintained and increased slightly up to a maximum of 300 kip at a large deformation until eventually dropping, as shown in Figure 2-47. No web deformation was observed.

1473TPNBSCNRE6 - Beam 31

The load was applied eccentrically to this unstiffened beam through a timber post. The load increased up to a calculated failure load of 332 kip, around when the post failed, as shown in Figure 2-48. After the maximum load of 340 kip was reached web yielding was observed due to the orientation of the failed post fragments. It also resulted in some flange bending. The force-displacement curve is shown in Figure 2-49.

1473TPBSCNRE6 - Beam 32

In this experiment the eccentrically loaded beam was also blocked. The failure load in this beam was again much less than expected due to another relatively weak post. The failure load was calculated at 190 kip. The maximum load was reached at 195 kip. Flange bending and post crushing were observed, but no web bending was seen until the post became more heavily damaged and the load was redistributed into the side of the flange (Fig. 2-50).

1490TPNBSCNRE0 - Beam 26

Although heavier than the previous four beams, this beam had a thinner web and thicker flange, therefore was more susceptible to lateral buckling of the web. The failure load was calculated to be 276 kip when there was a reduction in stiffness, although this appeared to be somewhat premature. The maximum load was reached at 310 kip at which point the post-flange suddenly deformed laterally through buckling of the web. This can be seen from the sudden drop in load in Figure 2-51. The deformed shape of this beam is shown in Figure 2-52. No bending in the flange was observed during the experiment.

1490TPBSCNRE0 - Beam 28

This beam had the same configuration as the last but included blocking between the flanges. As a result, buckling was not observed in this beam and failure occurred due to flange bending and post crushing at a load of 360 kip. The maximum force was reached at 420 kip. There was no buckling of the beam indicating that blocking may have been effective at increased the buckling capacity. As there was no buckling, Figure 2-53 shows that there was no sudden drop in load after failure as observed in the previous beam.

1490NPNBNCNRE0 - Beam 5

This beam was similar to the Beam 27 except that the load was applied though a rigid patch load instead of the flexible timber post. Despite being rigid the patch load had a small allowance for lateral deformation through tolerances in the slider. As a result lateral buckling was also observed in this beam. The failure load was calculated at 320 kip, close to the maximum load of 330 kip. In this beam the load did not drop as in the previous beam as the lateral deformation of the post was limited and thus did not allow a lateral deformation that resulted in a large reduction in the load. The force displacement curve for this beam is shown in Figure 2-54. This beam shows that the lateral buckling was not just limited to timber posts but is possible for other types of posts.

Summary

This section showed that the HP14x73 beams with thicker webs were not susceptible to lateral buckling, however the W14x90 beams with thinner webs were susceptible when no lateral bracing or stiffeners are used in falsework beams. The buckled mechanism is such that the entire length of the beam tends to deflect sideways unlike lateral torsional buckling in beams where part of the beam may buckle between braces through torsional as well as the lateral deformation of the flange. This limit state, where a long portion of the beam deflects laterally through buckling of the web is similar to that observed in falsework failure shown in Figure 1-4, therefore is a realistic limit state. Comparison of Beams 27 and 28 indicated that blocking was effective at reducing the propensity of a beam to buckle laterally. However, with limited data it is difficult to make conclusions about the effectiveness of blocking. As there is no positive connection between the blocking and the flanges, unlike with a welded stiffener or bracing, the effectiveness of the blocking is questionable. Consequently, bracing or stiffeners are recommended for beams that are susceptible to buckling.

2.6 Comparison of Failure Load with Load where Flaking is Observed

For each of the beams, the observed load when flaking occurred on the beam flange, with flaking typically located initially at the edge of the fillet between the flange and web under the post is compared with the failure load based on the change in stiffness as previously defined. Figure 2-55 shows a comparison of the observed flaking load with the calculated failure load for the beams which failed due to post-flange bending and timber post crushing. The vertical axis has the observed load divided by the calculated failure load, while the horizontal axis gives the calculated failure load. The different series represent different configurations, with and without blocking and with different eccentricities. The different points in each series represent the different size beams. With the steel posts, flaking was not observed in the beams until after the posts had already yielded and, thus,

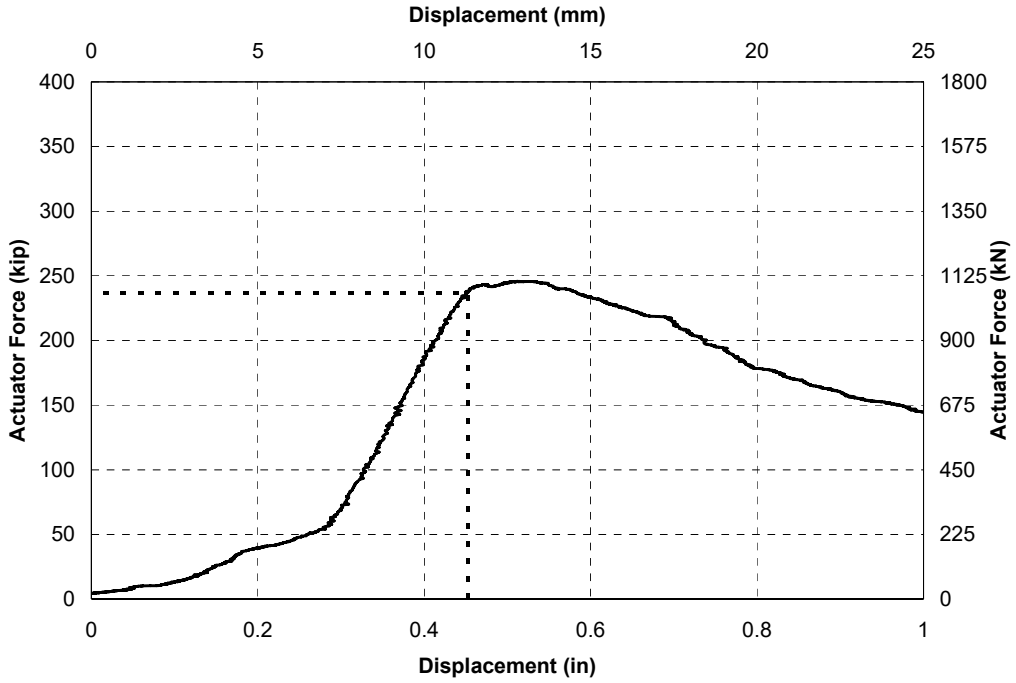

FIGURE 2-14 Actuator force vs slider displacement for 1253TPNBSCRE0 - Beam 18

FIGURE 2-15 Flange bending and post deformation observed during loading of 1253TPNBSCRE0 - Beam 18

FIGURE 2-16 Strain gages on beam close to where flaking of lime paint is first observed

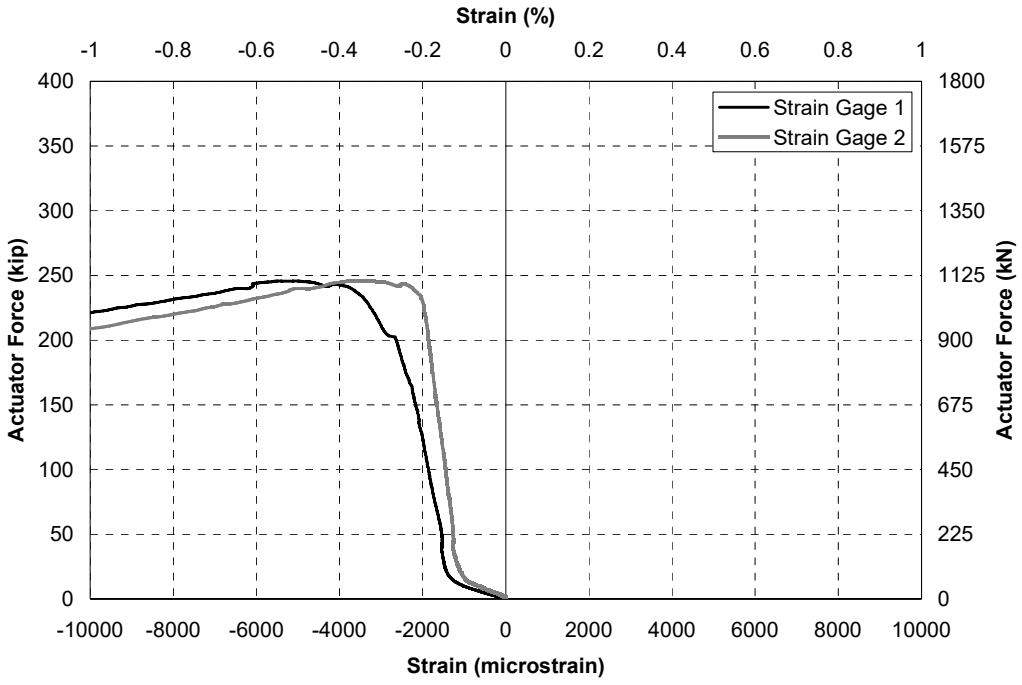

FIGURE 2-17 Actuator force vs strain in two strain gages located close to the yield line location in 1253TPNBSCRE0 - Beam 18

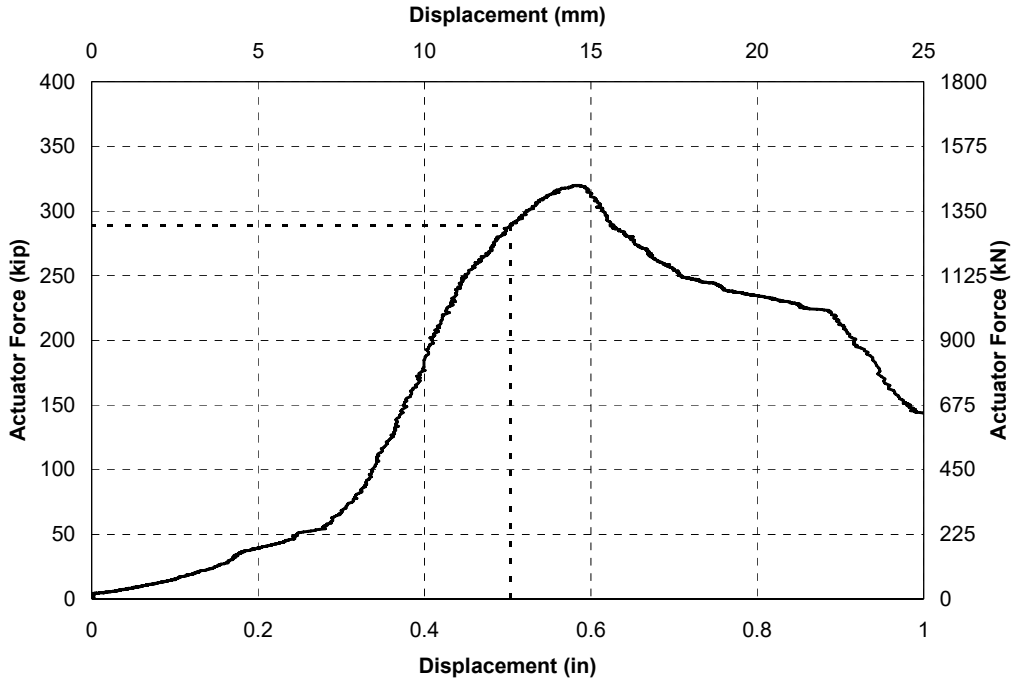

FIGURE 2-18 Actuator force vs slider displacement for 1253TPBSCRE0 - Beam 19

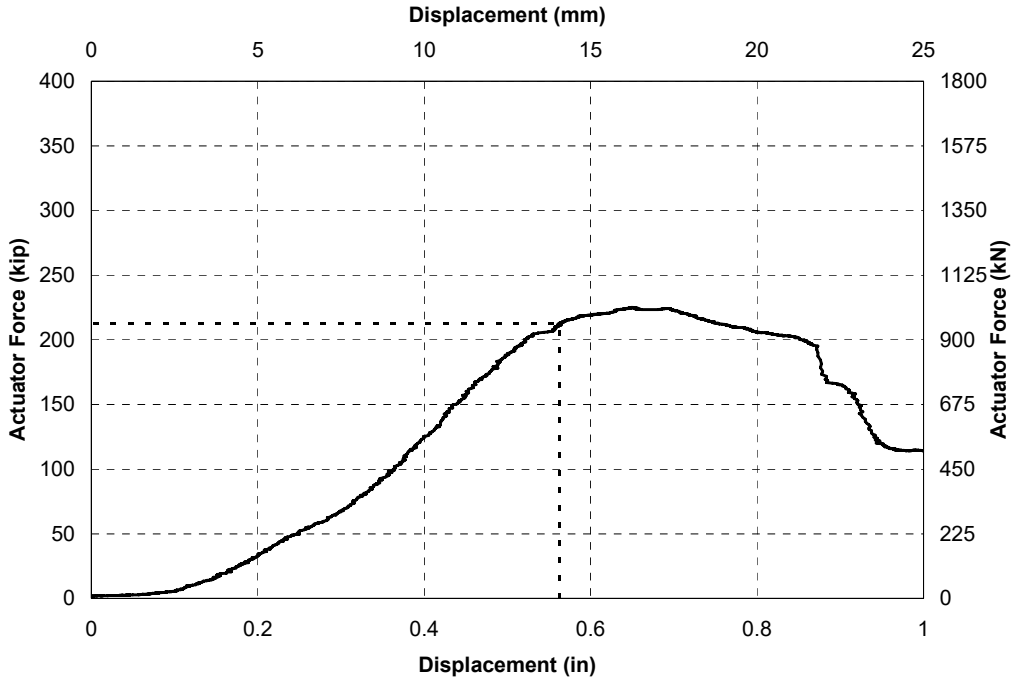

FIGURE 2-19 Actuator force vs slider displacement for 1253TPNBSCRE12 - Beam 16

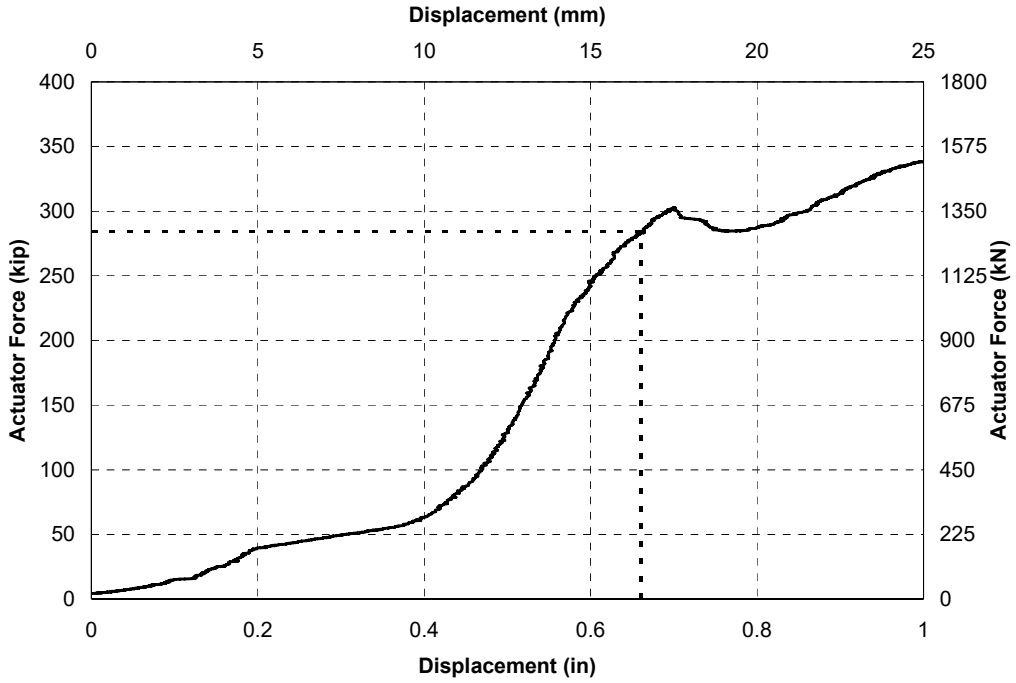

FIGURE 2-20 Actuator force vs slider displacement for 1253TPBSCRE12 - Beam 17

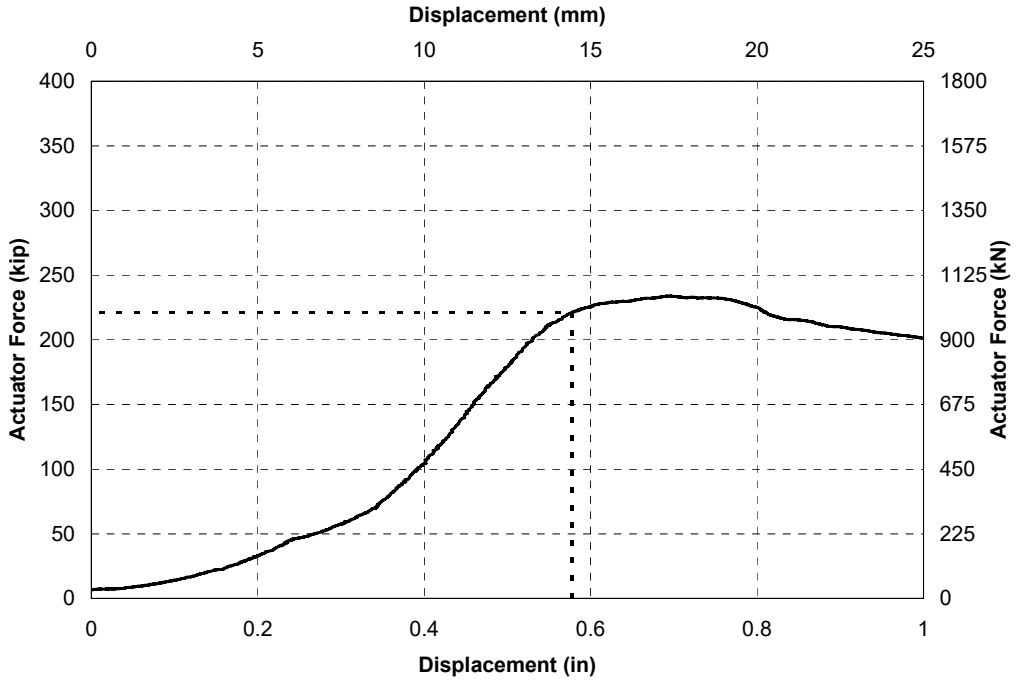

FIGURE 2-21 Actuator force vs slider displacement for 1253TPNBSCRE6 - Beam 14

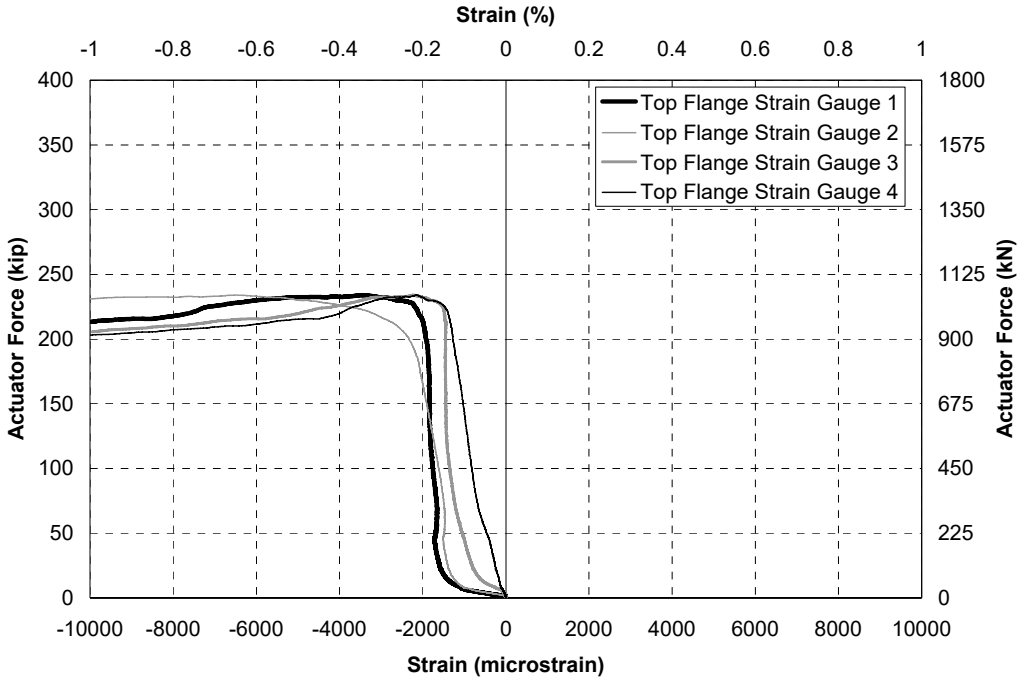

FIGURE 2-22 Actuator force vs strain in four strain gages located close to the yield line locations in 1253TPNBSCRE6 - Beam 14

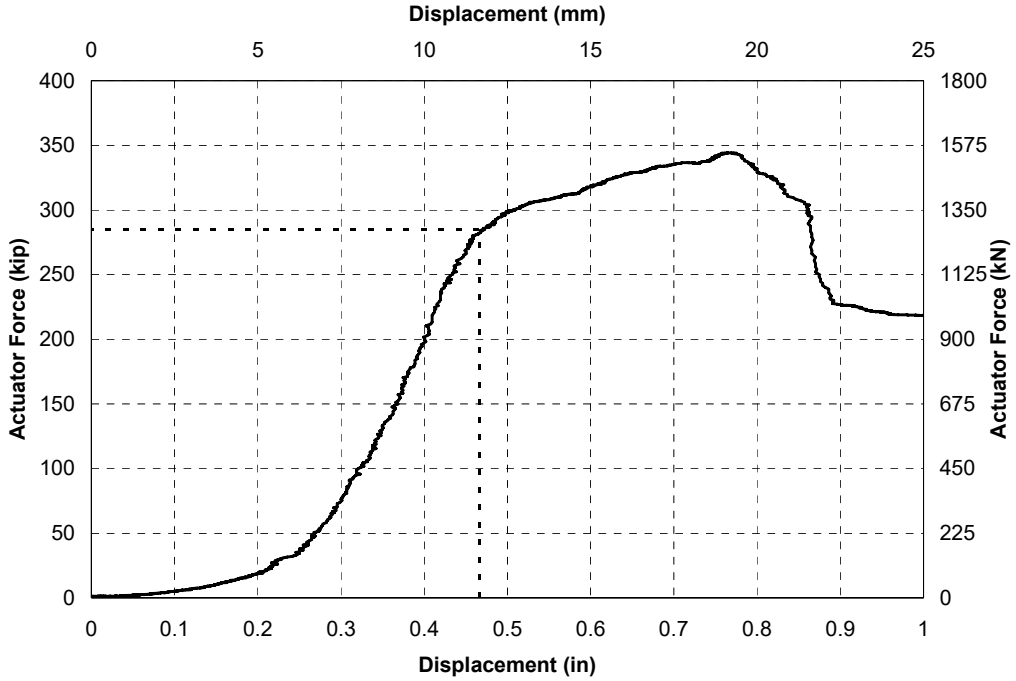

FIGURE 2-23 Actuator force vs slider displacement for 1253TPBSCRE6 - Beam 15

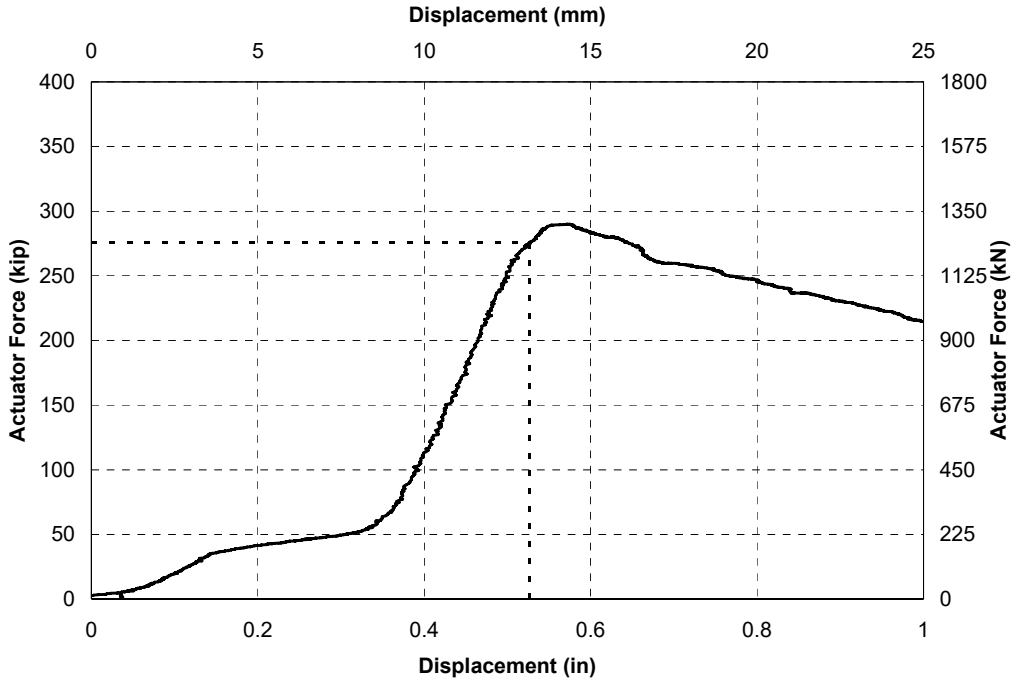

FIGURE 2-24 Actuator force vs slider displacement for 1473TPNBSCRE0 - Beam 20

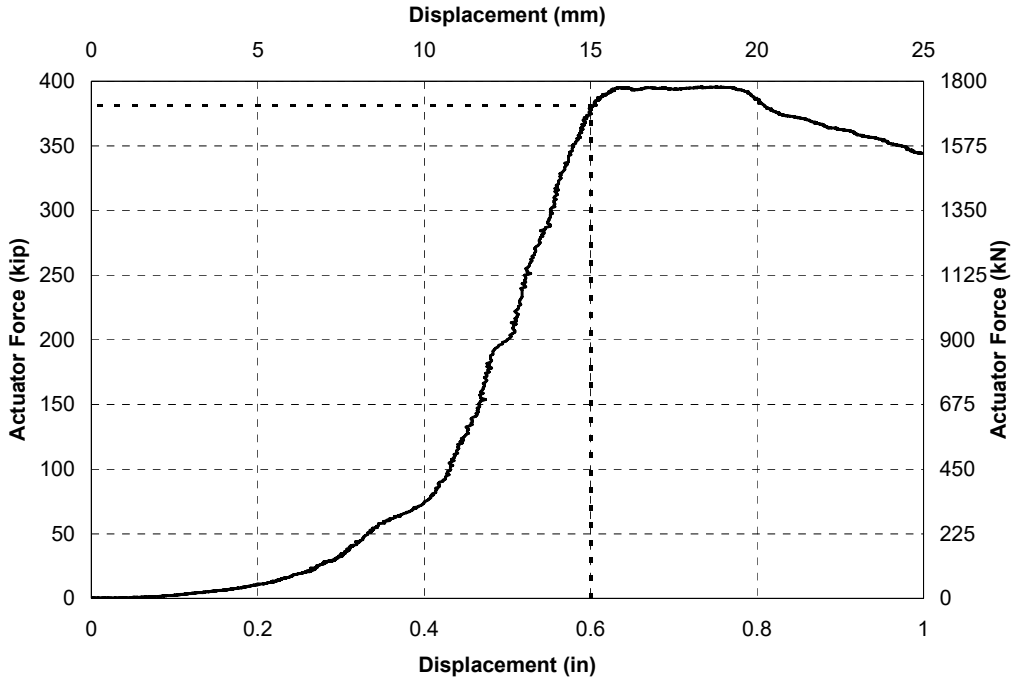

FIGURE 2-25 Actuator force vs slider displacement for 1473TPBSCRE0 - Beam 21

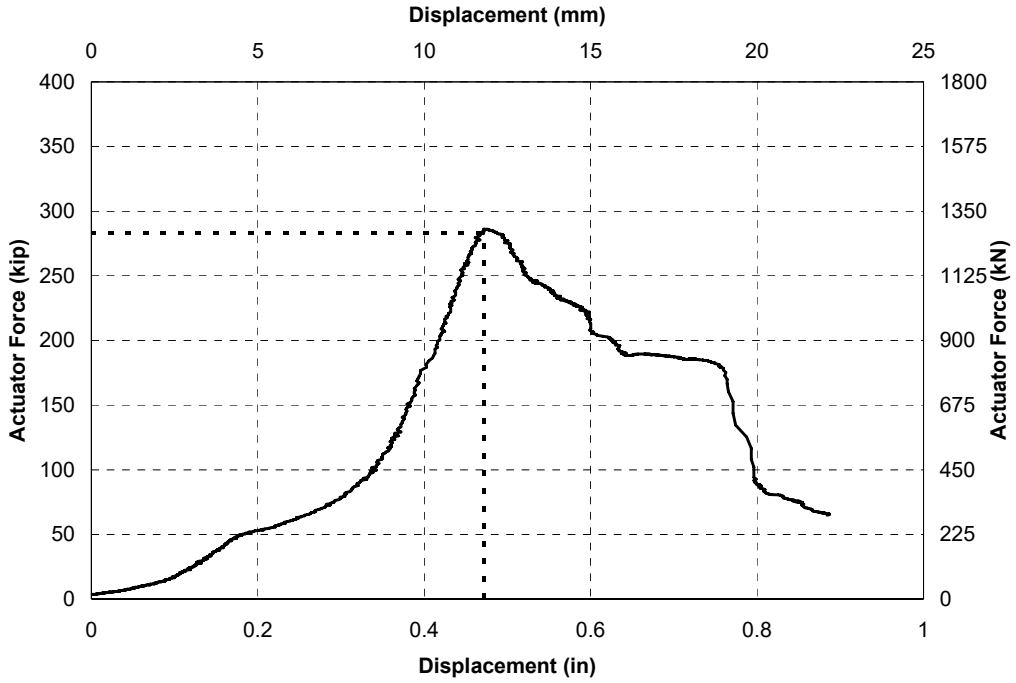

FIGURE 2-26 Actuator force vs slider displacement for 1473TPNBSCRE6 - Beam 27

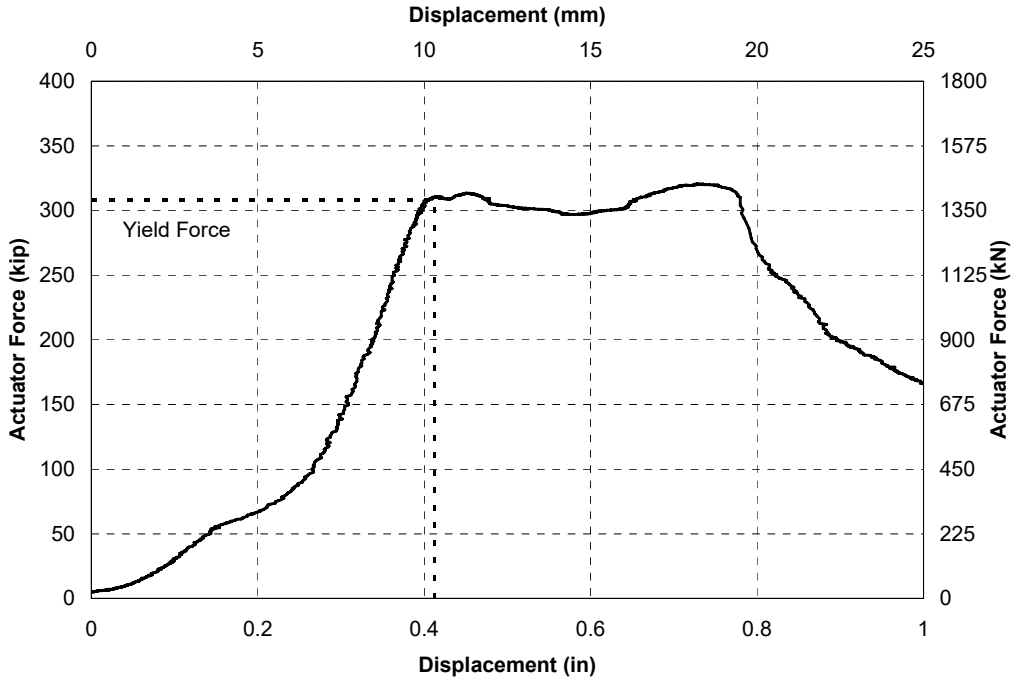

FIGURE 2-27 Actuator force vs slider displacement for 1473TPBSCRE0 - Beam 25

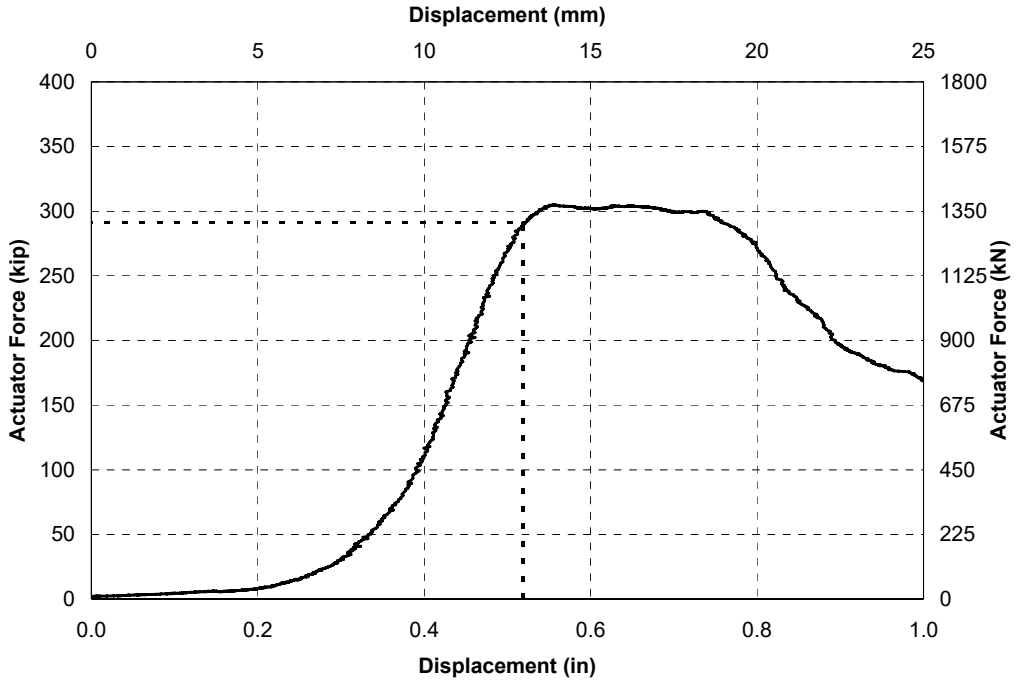

FIGURE 2-28 Actuator force vs slider displacement for 1490TPNBSCRE0 - Beam 22

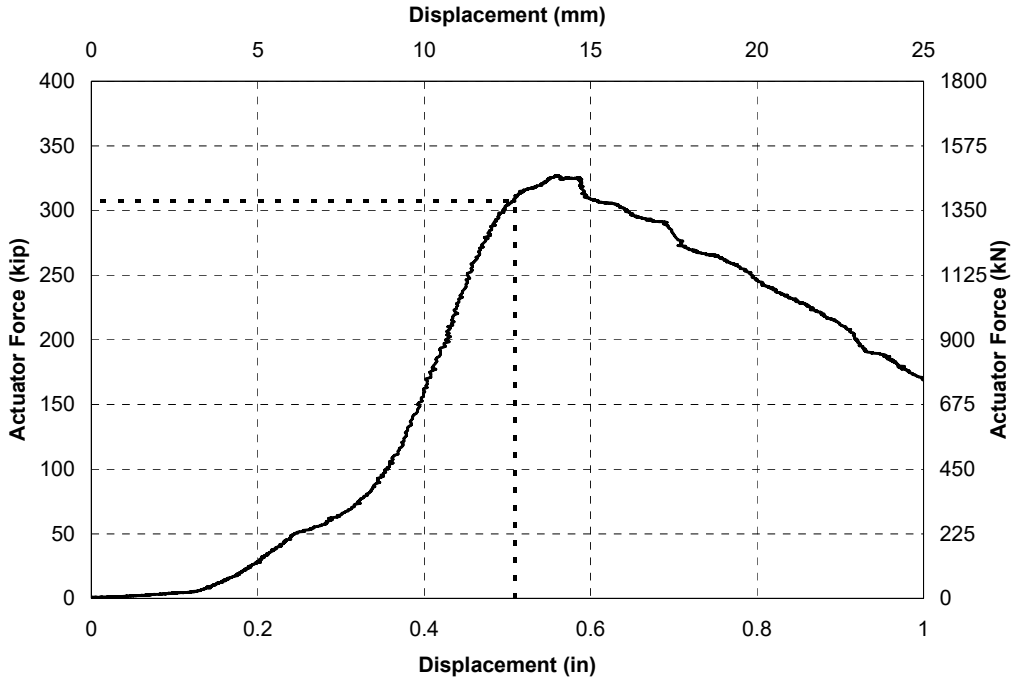

FIGURE 2-29 Actuator force vs slider displacement for 1490TPBSCRE0 - Beam 23

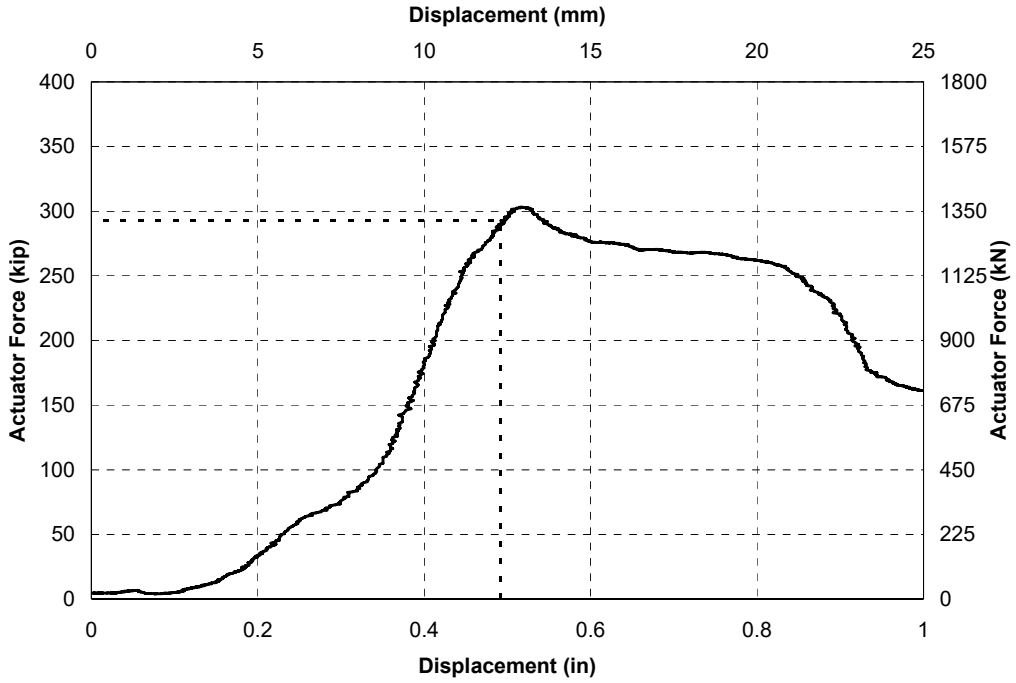

FIGURE 2-30 Actuator force vs slider displacement for 1490TPNBSCRE0 - Beam 24

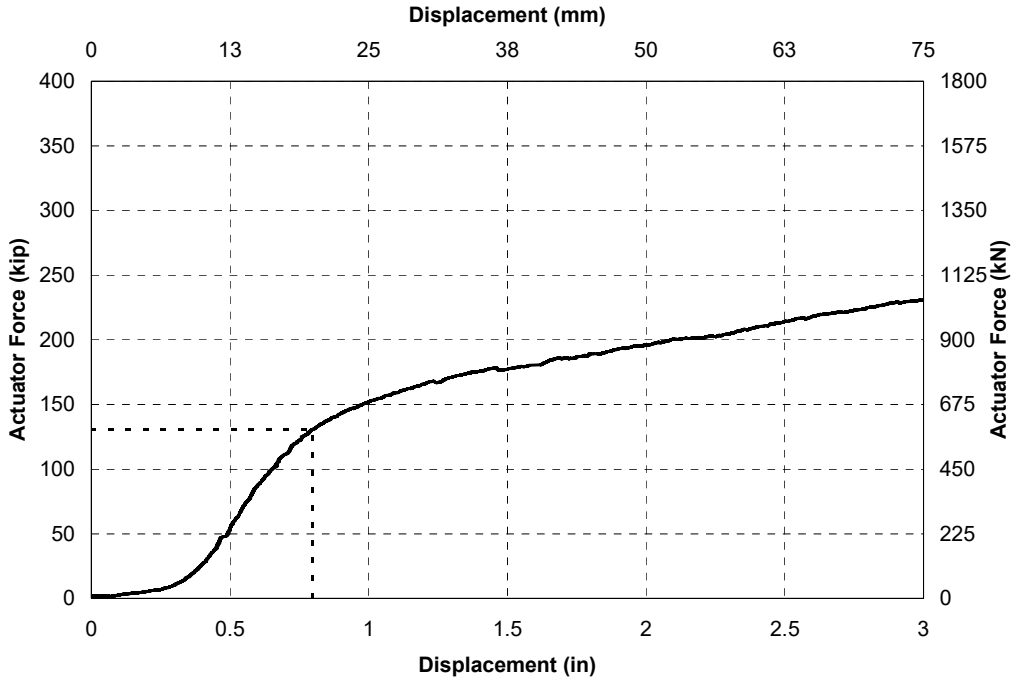

FIGURE 2-31 Actuator force vs slider displacement for 1253TPNBTCRE0 - Beam 12

FIGURE 2-32 Corbel-flange bending, corbel crushing and post crushing after the completion of 1253TPNBTCRE0 - Beam 12

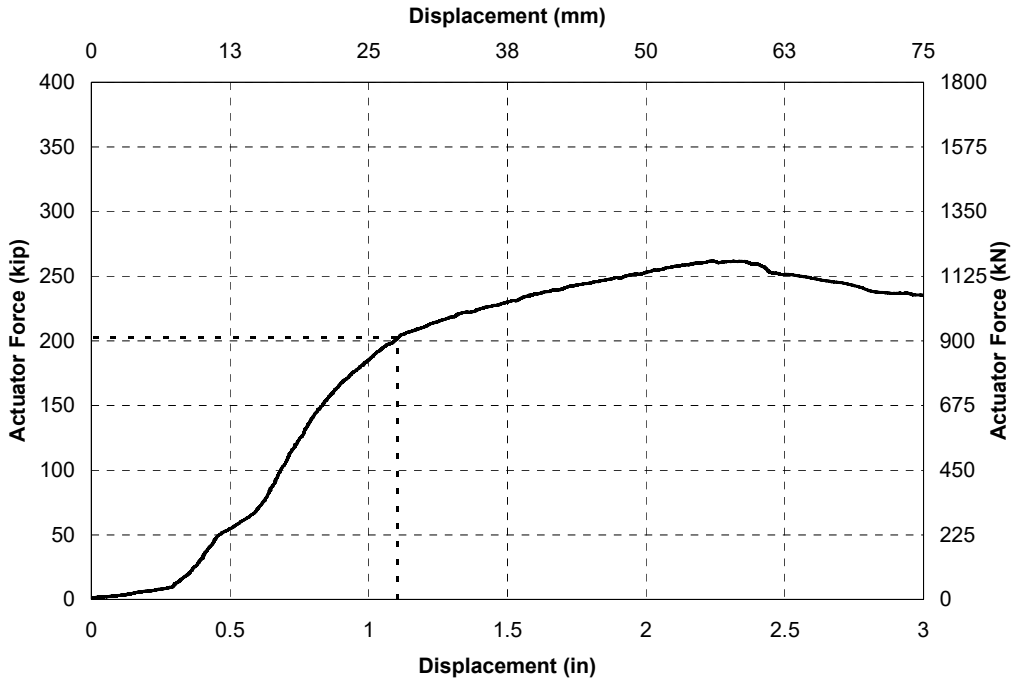

FIGURE 2-33 Actuator force vs slider displacement for 1253TPBTCRE0 - Beam 13

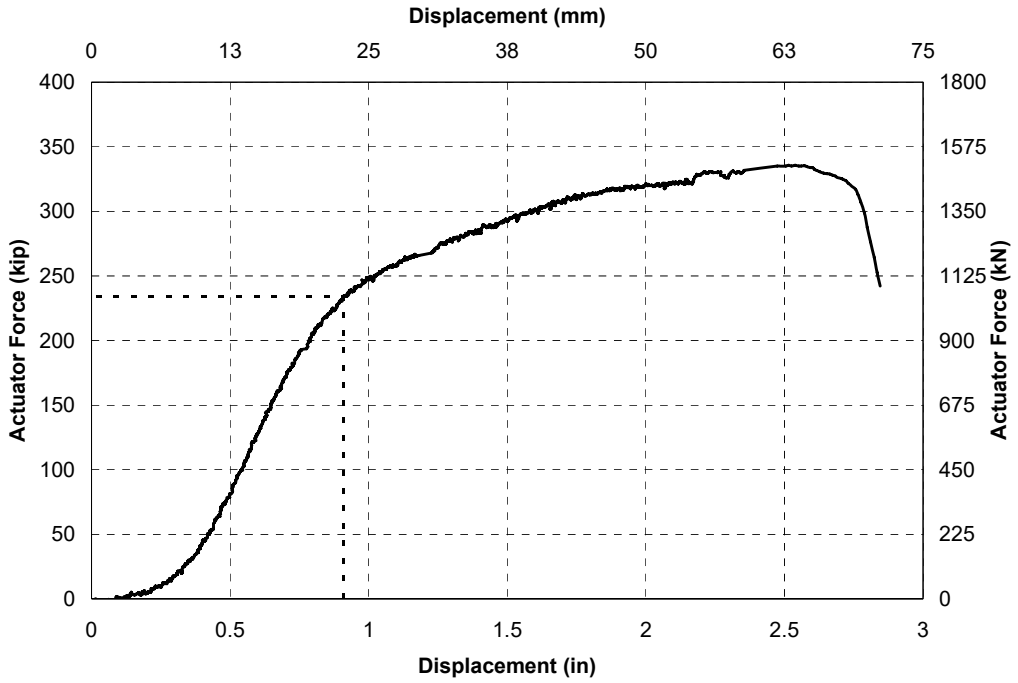

FIGURE 2-34 Actuator force vs slider displacement for 1490TPNBTCRE0 - Beam 1

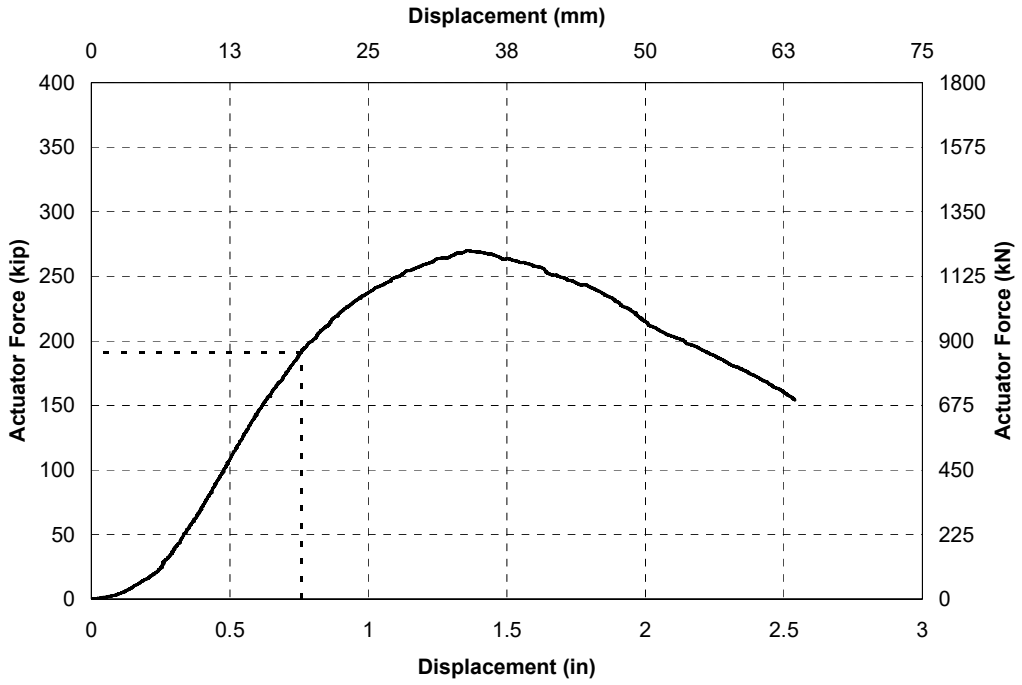

FIGURE 2-35 Actuator force vs slider displacement for 1490TPNBTCRE6 - Beam 4

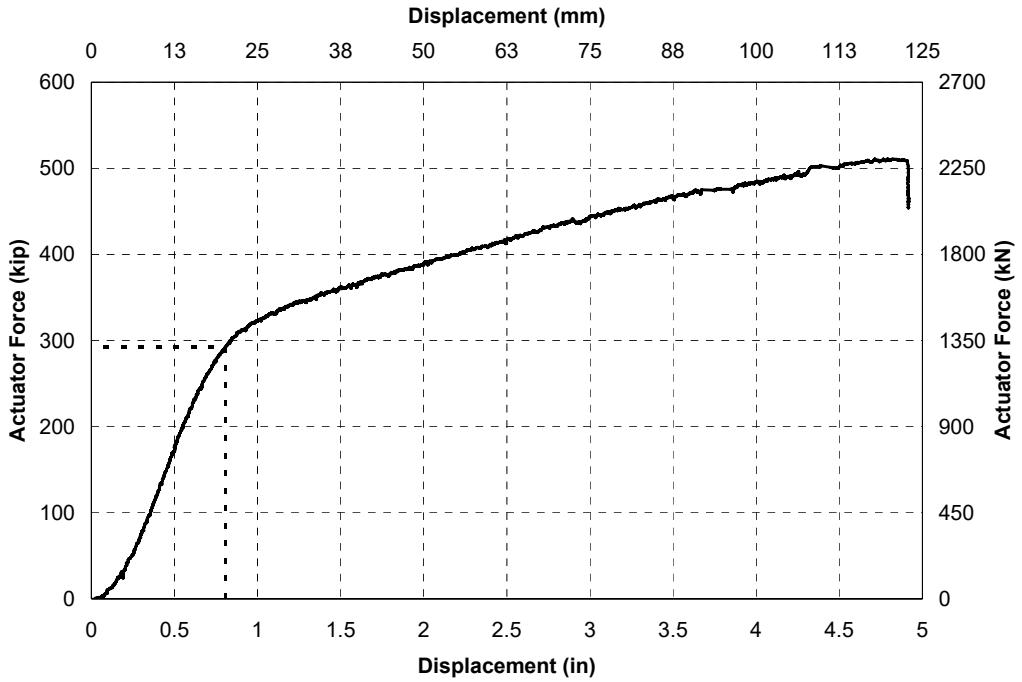

FIGURE 2-36 Actuator force vs slider displacement for 1490SPNBTCRE0 - Beam 2

FIGURE 2-37 Onset of yielding and buckling in the steel post for 1490SPNBTCRE0 - Beam 2

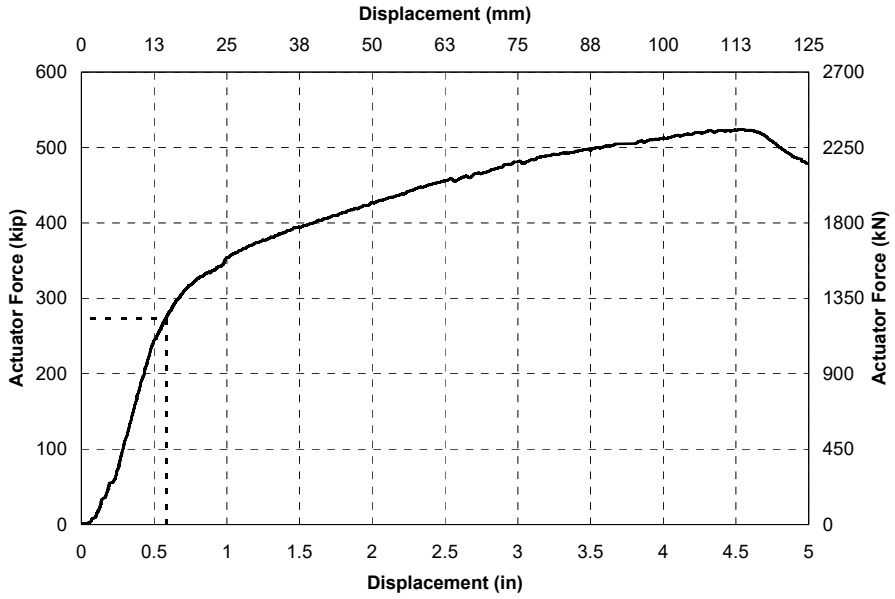

FIGURE 2-38 Actuator force vs slider displacement for 1490SPNBTCRE6 - Beam 3

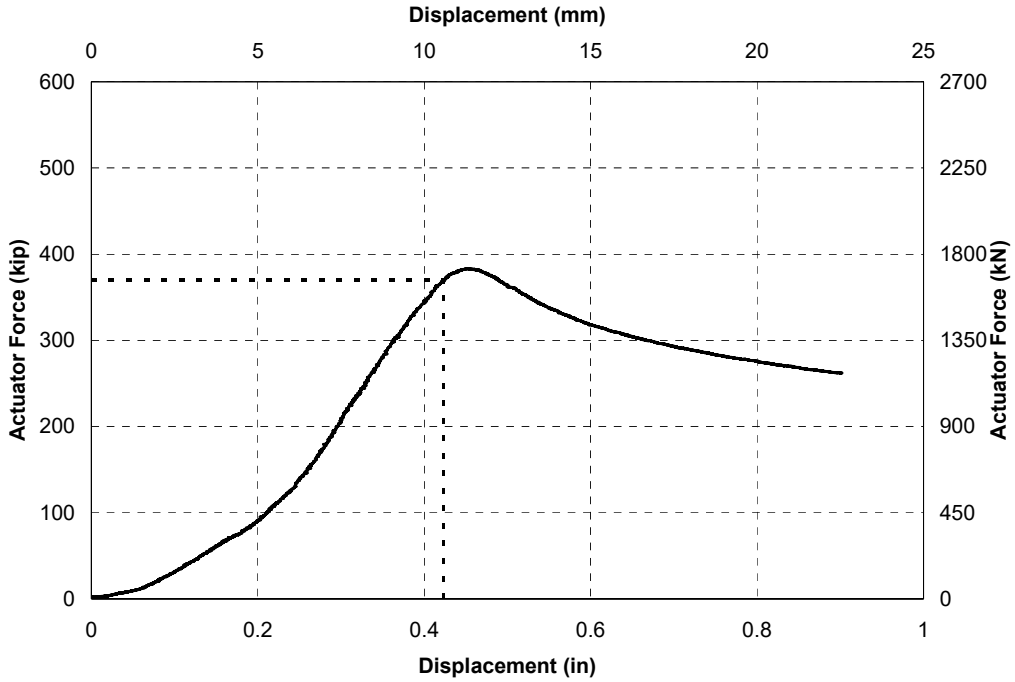

FIGURE 2-39 Actuator force vs slider displacement for 1253NPNBNCRE0 - Beam 10

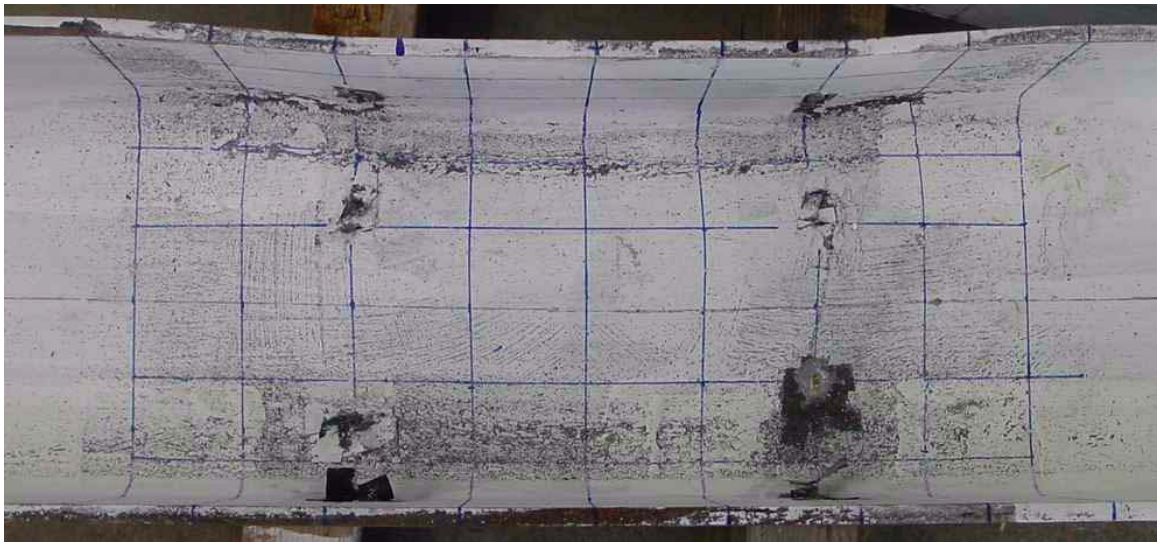

FIGURE 2-40 Post-elastic buckling/crippling of the web in 1253NPNBNCRE0 - Beam 10

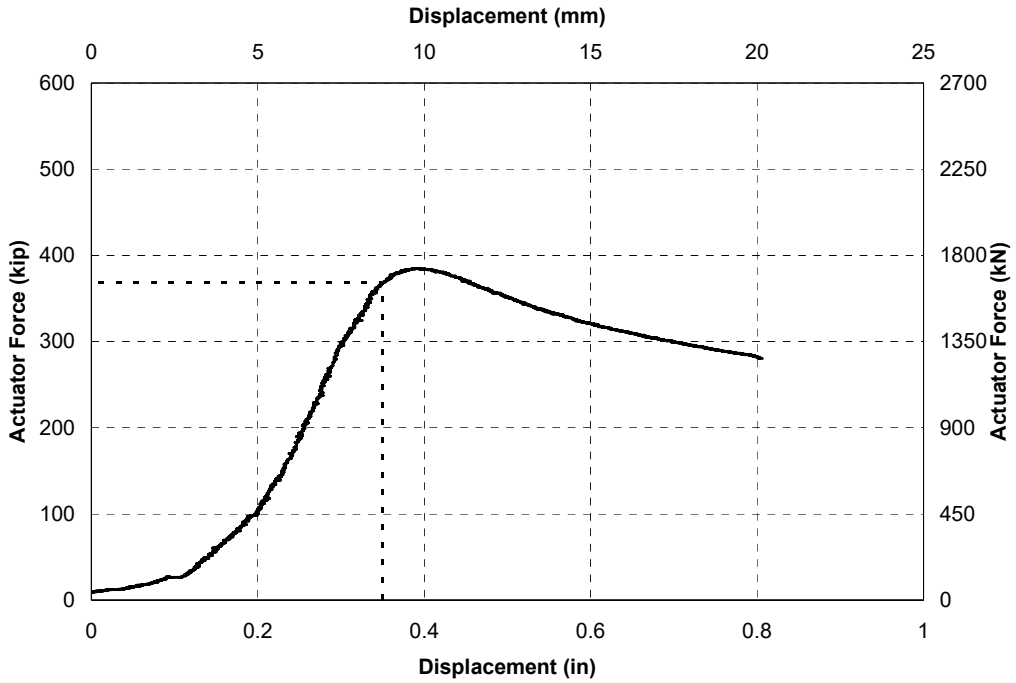

FIGURE 2-41 Actuator force vs slider displacement for 1253NPNBNCRE6 - Beam 11

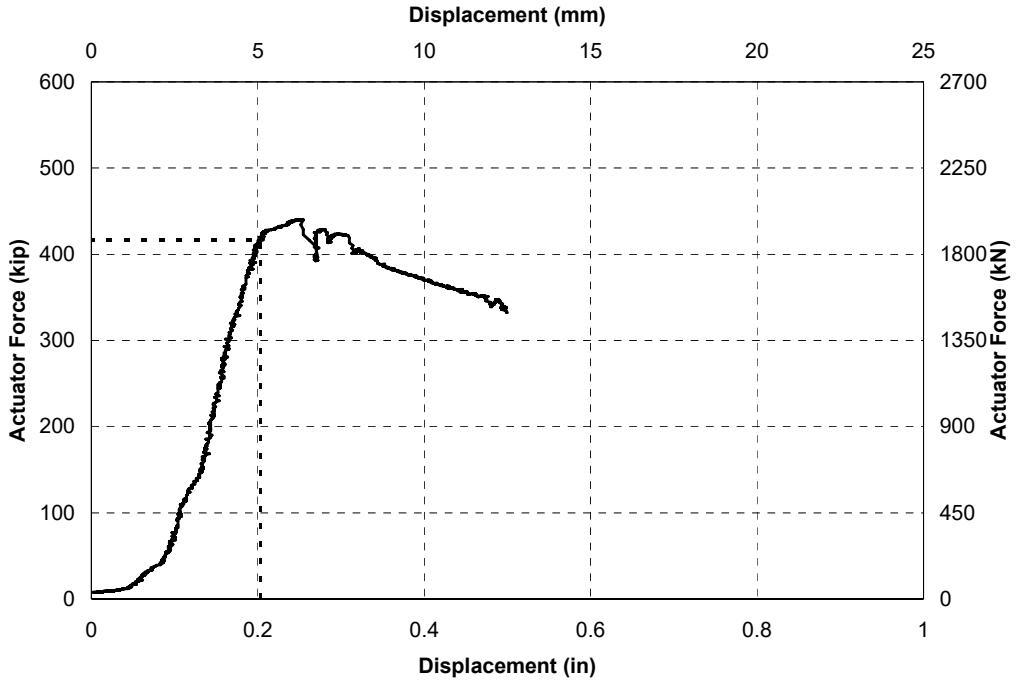

FIGURE 2-42 Actuator force vs slider displacement for 1473NPNBNCRE0 - Beam 9

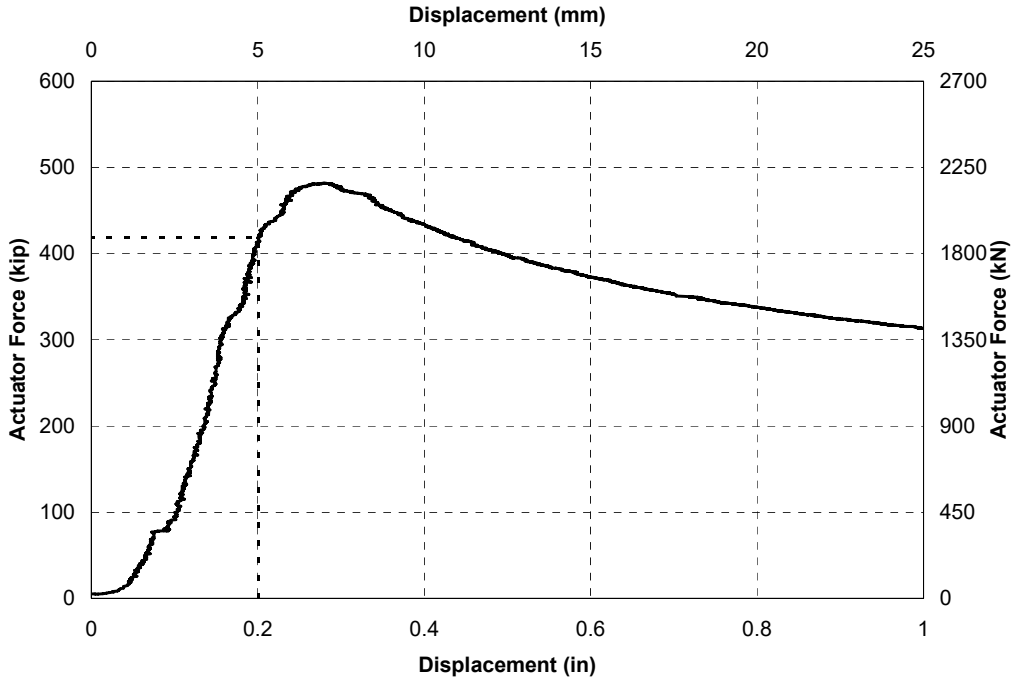

FIGURE 2-43 Actuator force vs slider displacement for 1473NPNBNCRE6 - Beam 8

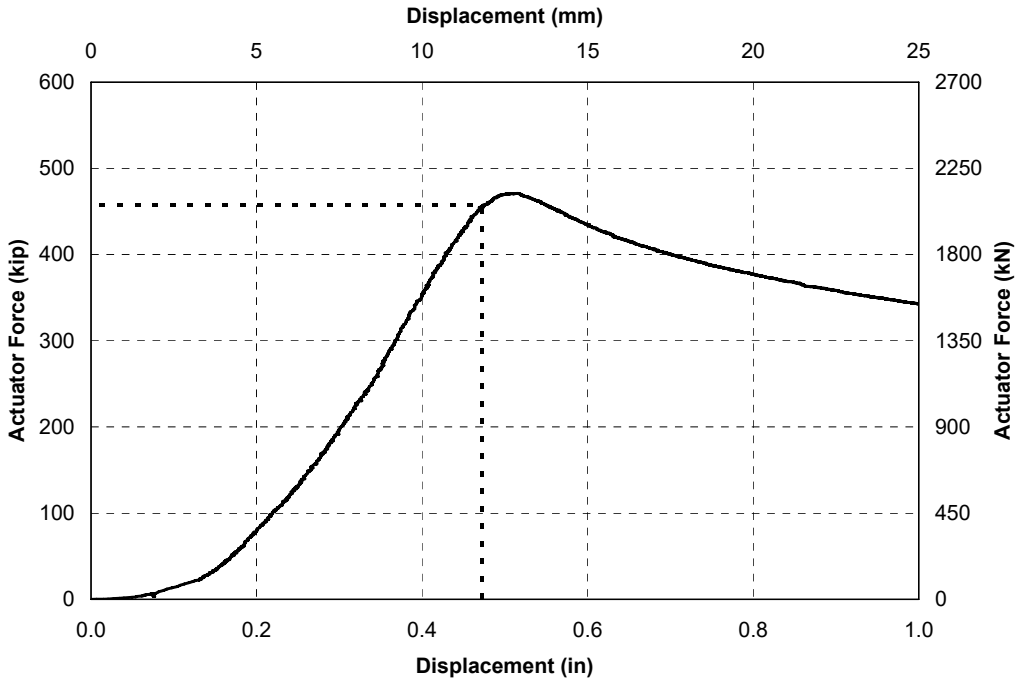

FIGURE 2-44 Actuator force vs slider displacement for 1490NPNBNCRE0 - Beam 6

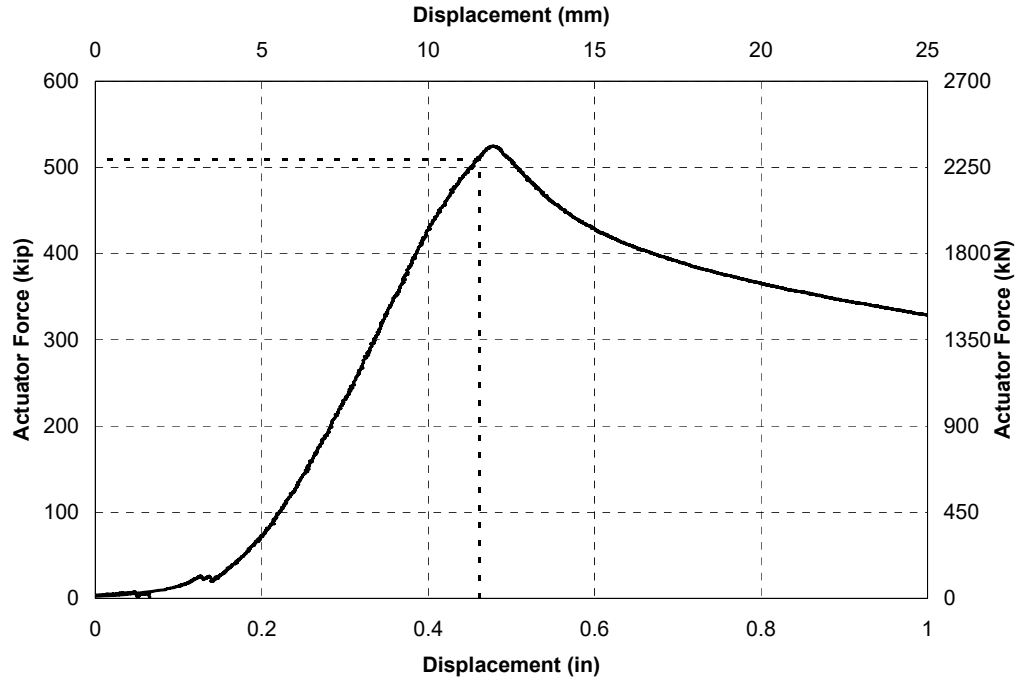

FIGURE 2-45 Actuator force vs slider displacement for 1490NPNBNCRE6 - Beam 7

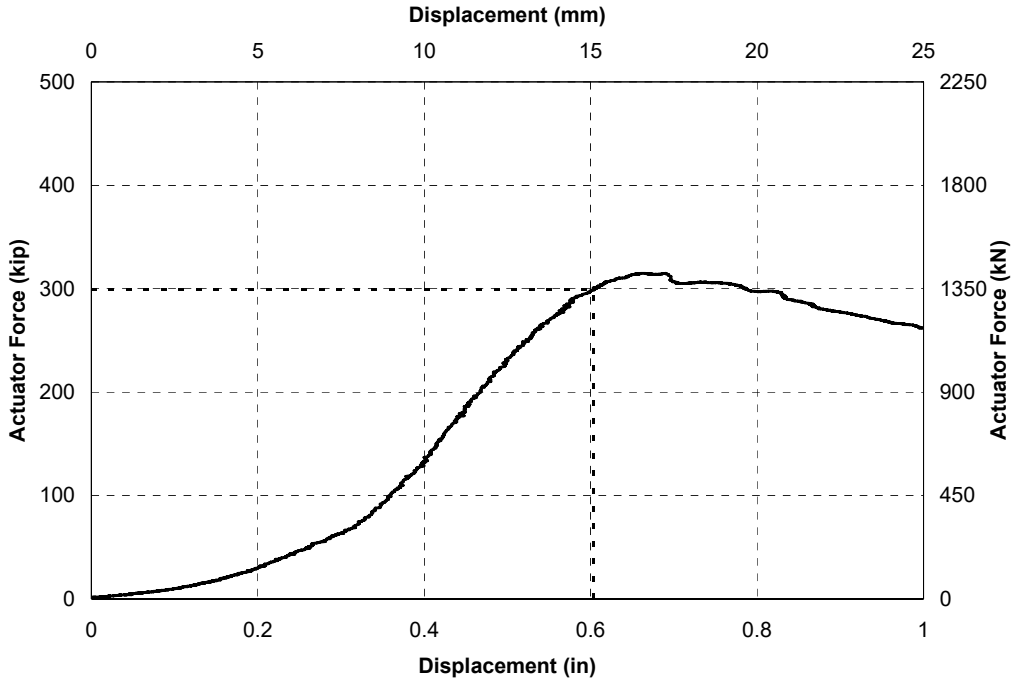

FIGURE 2-46 Actuator force vs slider displacement for 1473TPNBNCNRE0 - Beam 29

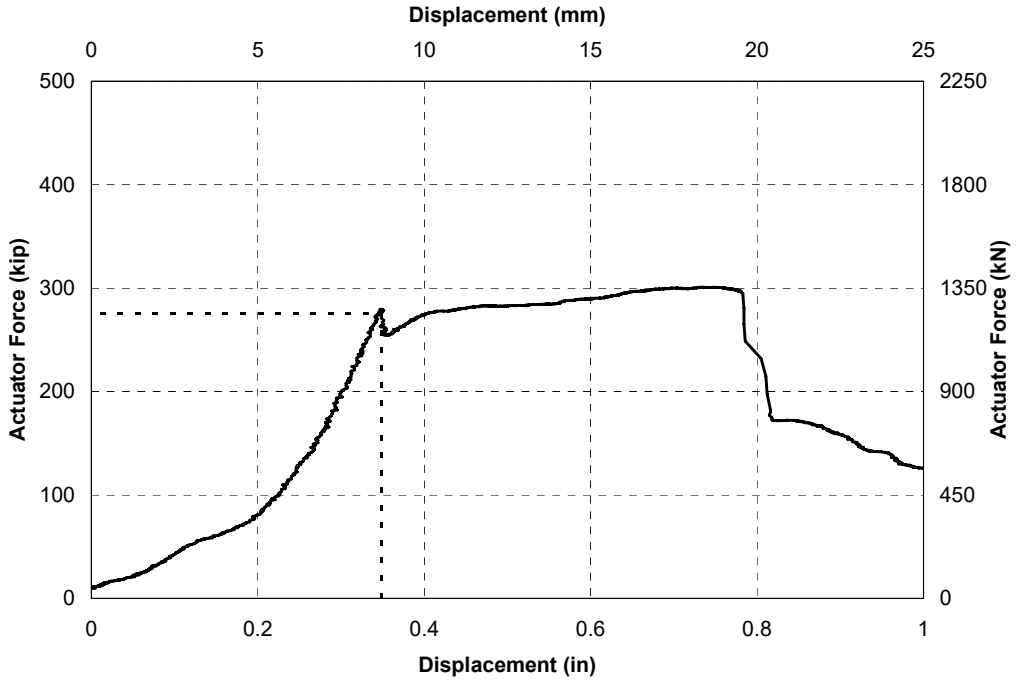

FIGURE 2-47 Actuator force vs slider displacement for 1473TPBNCNRE0 - Beam 30

FIGURE 2-48 Failure of post during experiment on unrestrained beam 1473TPNBNCNRE6 - Beam 31

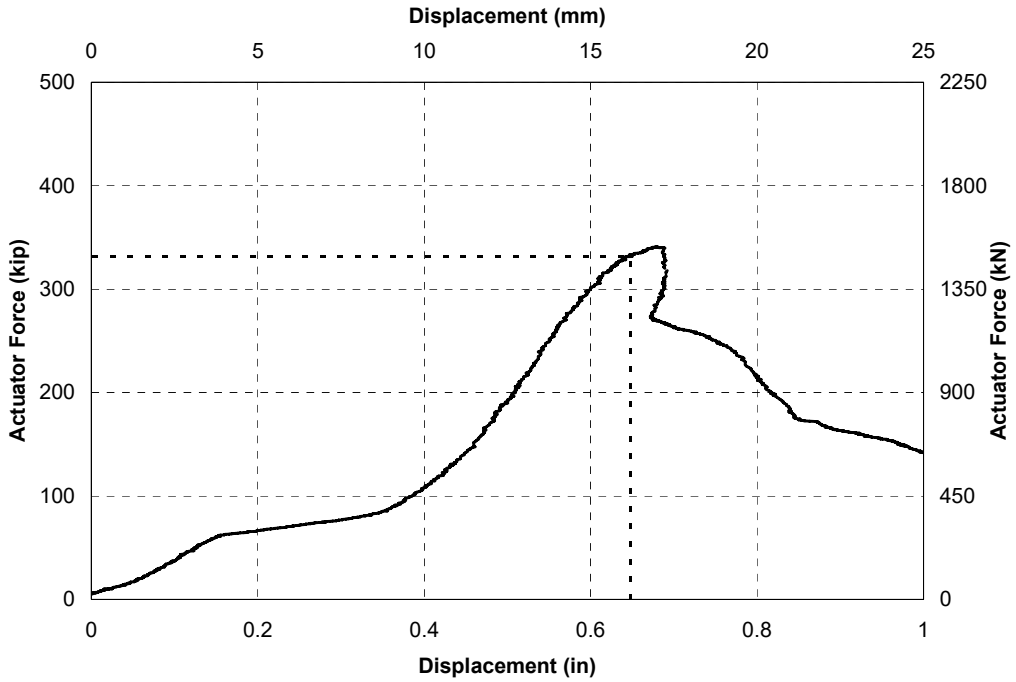

FIGURE 2-49 Actuator force vs slider displacement for 1473TPNBNCNRE6 - Beam 31

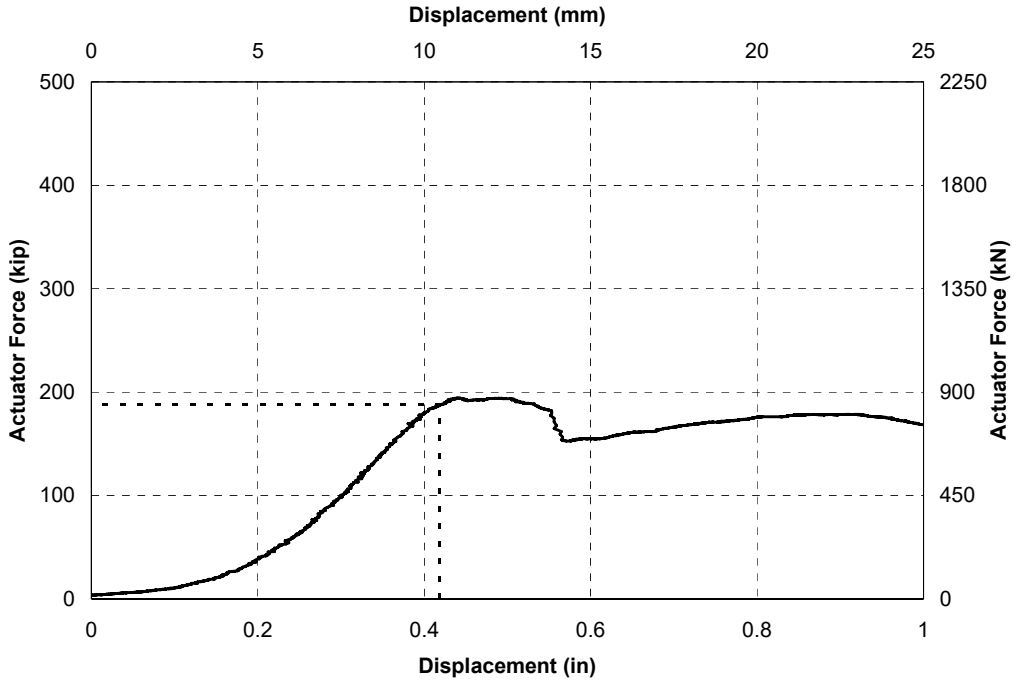

FIGURE 2-50 Actuator force vs slider displacement for 1473TPBNCNRE6 - Beam 32

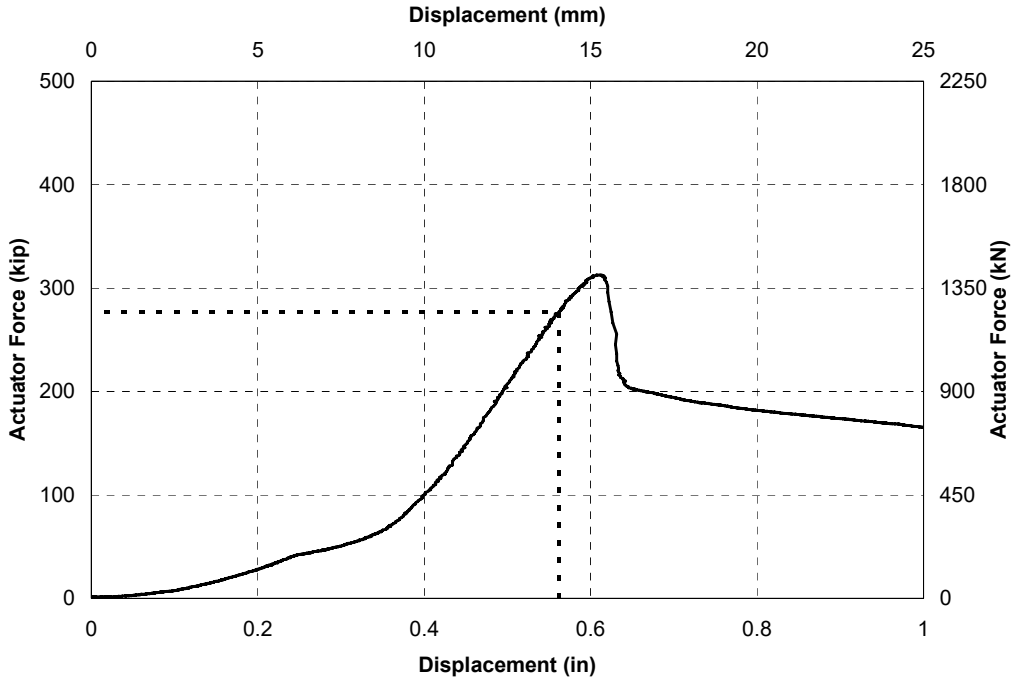

FIGURE 2-51 Actuator force vs slider displacement for 1490TPNBNCNRE0 - Beam 26

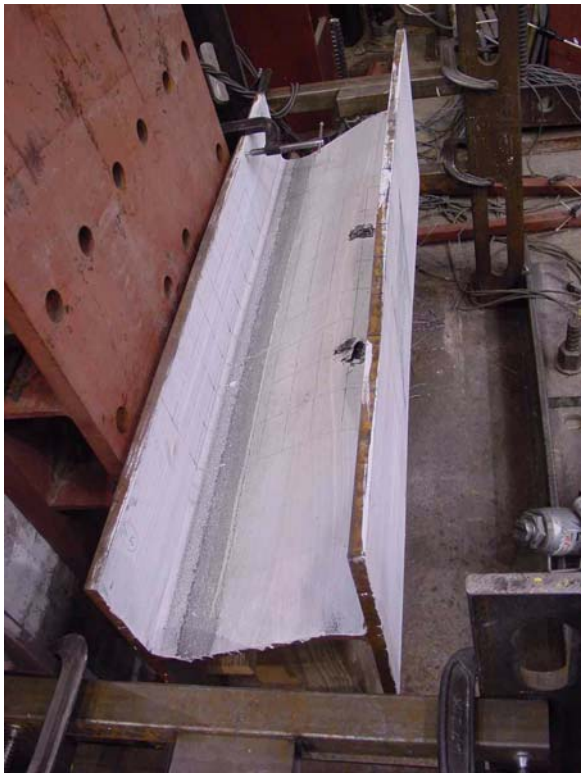

FIGURE 2-52 Lateral Buckling of 1490TPNBNCNRE0 - Beam 26

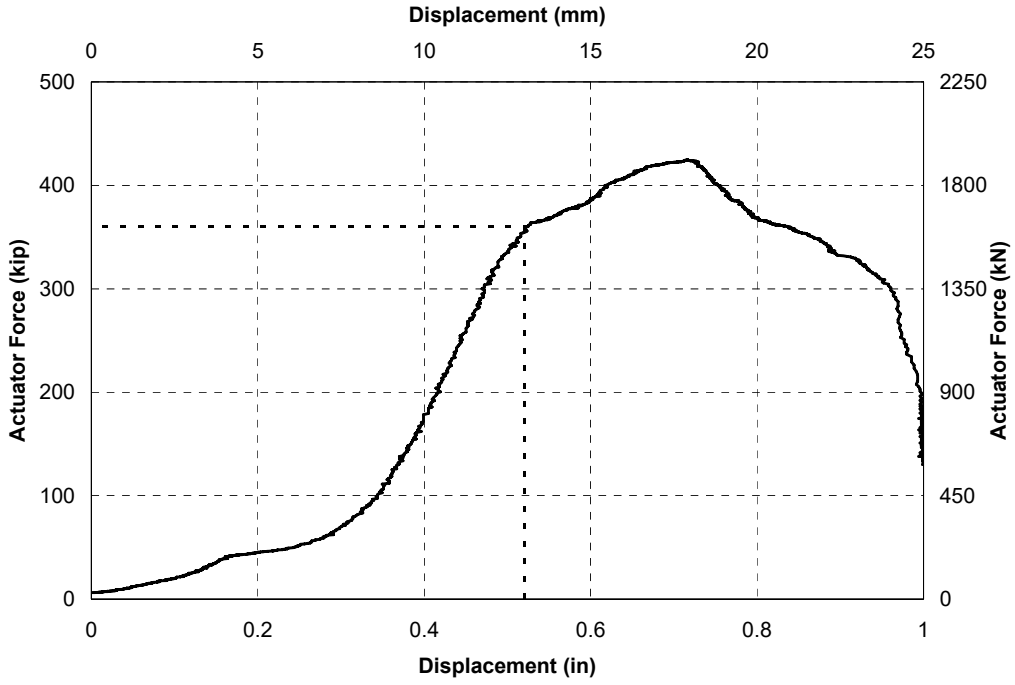

FIGURE 2-53 Actuator force vs slider displacement for 1490TPBNCNRE0 - Beam 28

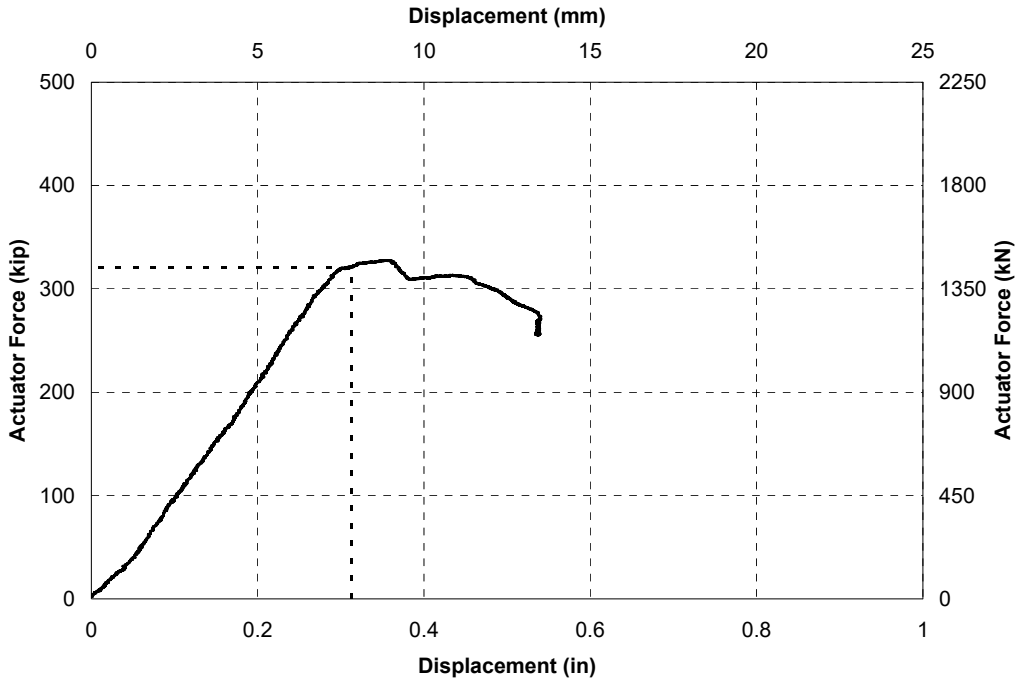

FIGURE 2-54 Actuator force vs slider displacement for 1490NPNBNCNRE0 - Beam 5

these are not included in the figure. There are only 12 points for 13 experiments with timber posts resulting post-flange bending failure as flaking was not observed at the appropriate time in one of the beams. Figure 2-55 shows that the observed flaking and calculated failure load is different by no more than 13% for each beam, with an average difference of 2%. The comparison therefore indicates that the estimated ultimate load, estimated based on a 50% reduction in stiffness, is similar to the load at which yielding is first observed and, thus, is an appropriately defined ultimate load.

A similar plot is shown for the beams that resulted in corbel-flange bending and corbel crushing in Figure 2-56. This figure shows that the estimated failure load tends to be conservative by around 10-20% compared to the load where flaking is observed except for the smallest beam. This is attributed to the corbel starting to crush before flange bending is observed. The definition of failure is still considered to be appropriate, although it is conservative with regards to observed inelastic behavior in the beam.

A comparison of the observed flaking load and estimated failure load for the restrained beams with rigid patch loading resulting in web yielding is shown in Figure 2-57. The observed flaking load is within 15% of the calculated failure load in all case with an average difference of 1%. Therefore, the definition of failure is also appropriate for the beams with web yielding and post-elastic crippling or buckling.

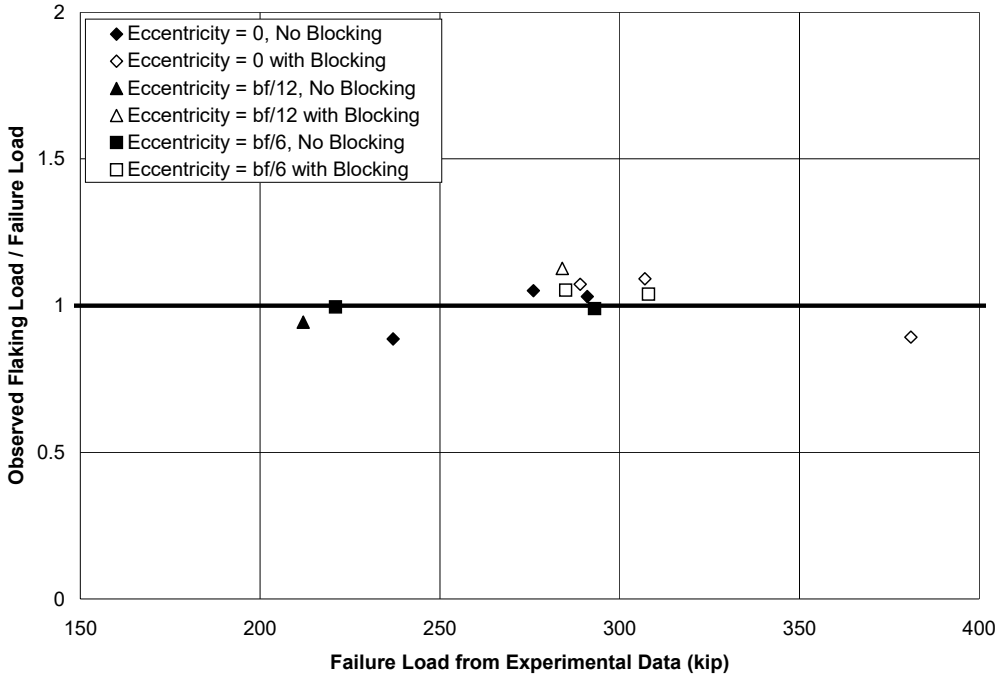

FIGURE 2-55 Comparison of observed load when flaking occurred with calculated failure load from experiments with post-flange-post failure

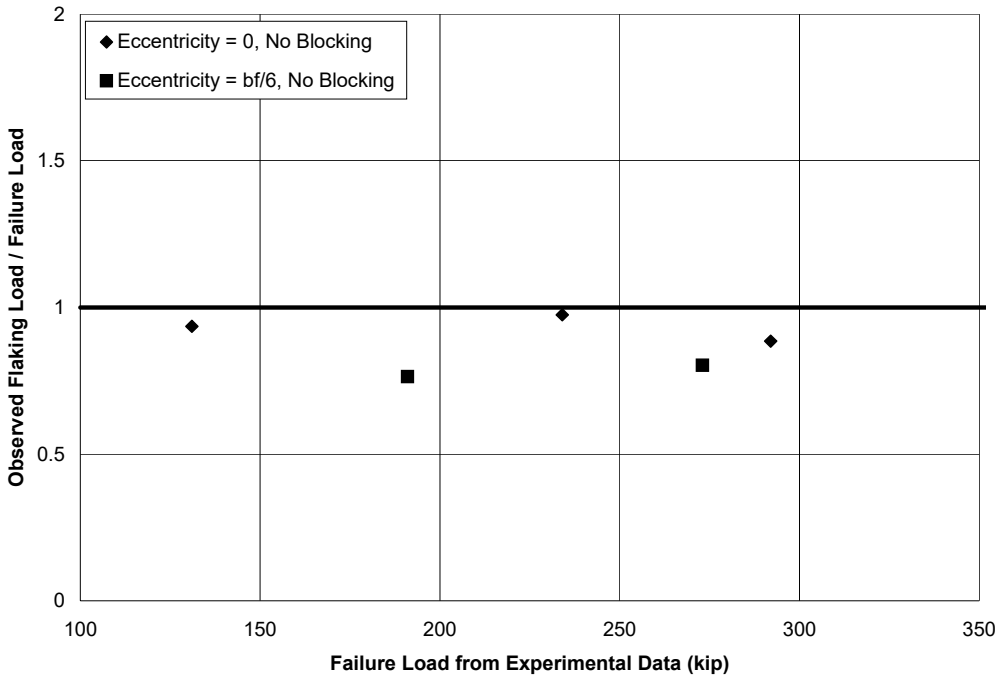

FIGURE 2-56 Comparison of observed load when flaking occurred with calculated failure load from experiments with flange-corbel failure

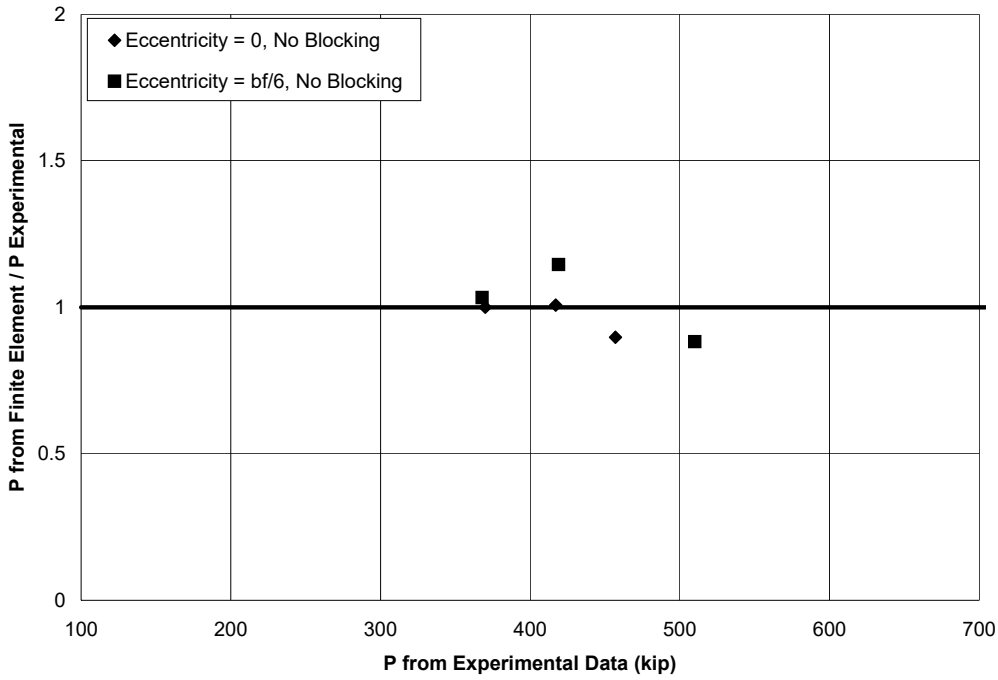

FIGURE 2-57 Comparison of observed load when flaking occurred with calculated failure load from experiments with web yielding failure

SECTION 3
FINITE ELEMENT ANALYSIS OF FALSEWORK BEAMS

3.1 Overview

In order to further investigate the critical failure modes of the falsework beams with posts and corbels, and expand the range of cases considered a series of finite element models were generated. The finite element models were calibrated to the experimental data for direct comparison of models with the experimental data. These models are then used to check design equations, without the impact of material variability and other experimental factors affecting the comparisons.

3.2 Properties of the Finite Element Models

There were four groups of finite element models. The first group used a 48 in. long post bearing against a 48 in. long section of beam to determine the localized flange bending capacity for a timber post patch load (Fig. 3-1a). The second group replaced the timber post with a section of 18 in. diameter, $^{3}/_{8}$ in. thick steel pipe and a $^{1}/_{2}$ in. base plate, which was assumed for use with the larger beams (Fig. 3-1b). In the third group, a rigid 12 x 12 in. patch load was modeled on top of the beam to determine critical localized web yielding and crippling limit states (Fig. 3-1c). In the final group a 10 ft. long single or double stacked beam was modeled with a 10 ft. long post, to study lateral web buckling (Fig. 3-1d). This length beam is considered a typical post spacing in bridge falsework. These figures show the post bearing down onto a sill beam, although the system could be inverted for the connection region between a post and cap beam.

HP12x53, HP14x73, HP12x89 and W14x90 beams were modeled with timber posts, like that shown in Figure 3-1a, and W14x90, HP14x117 and W14x120 beams are modeled with steel posts as shown in Figure 3-1b. These beams encompassed the range of typical beam sizes used as cap and sill beams in Falsework. As these typical falsework beams had relatively thick webs, they did not allow a full range of web deformation to occur including the type of deformation observed in beams with thinner webs. Thus a larger range of beams including a W12x26, W12x40, W12x53, W14x22, W14x30, W14x43, W14x61, W14x90, W14x132, HP12x53, HP14x73, HP14x89 and HP14x117 were considered with rigid patch loads.

The beams, posts and blocking were modeled with linear brick elements in ABAQUS (Hibbett et al. 2005), meshed typically as shown in Figure 3-1. The steel members were modeled with a plastic isotropic material using the expected yield strength of 55 ksi for the A572 Gr. 50 and A992 steel beams (almost equal to the 53.3 ksi average strength measured from coupon tests) and 46 ksi for the A500 Gr42 steel posts.

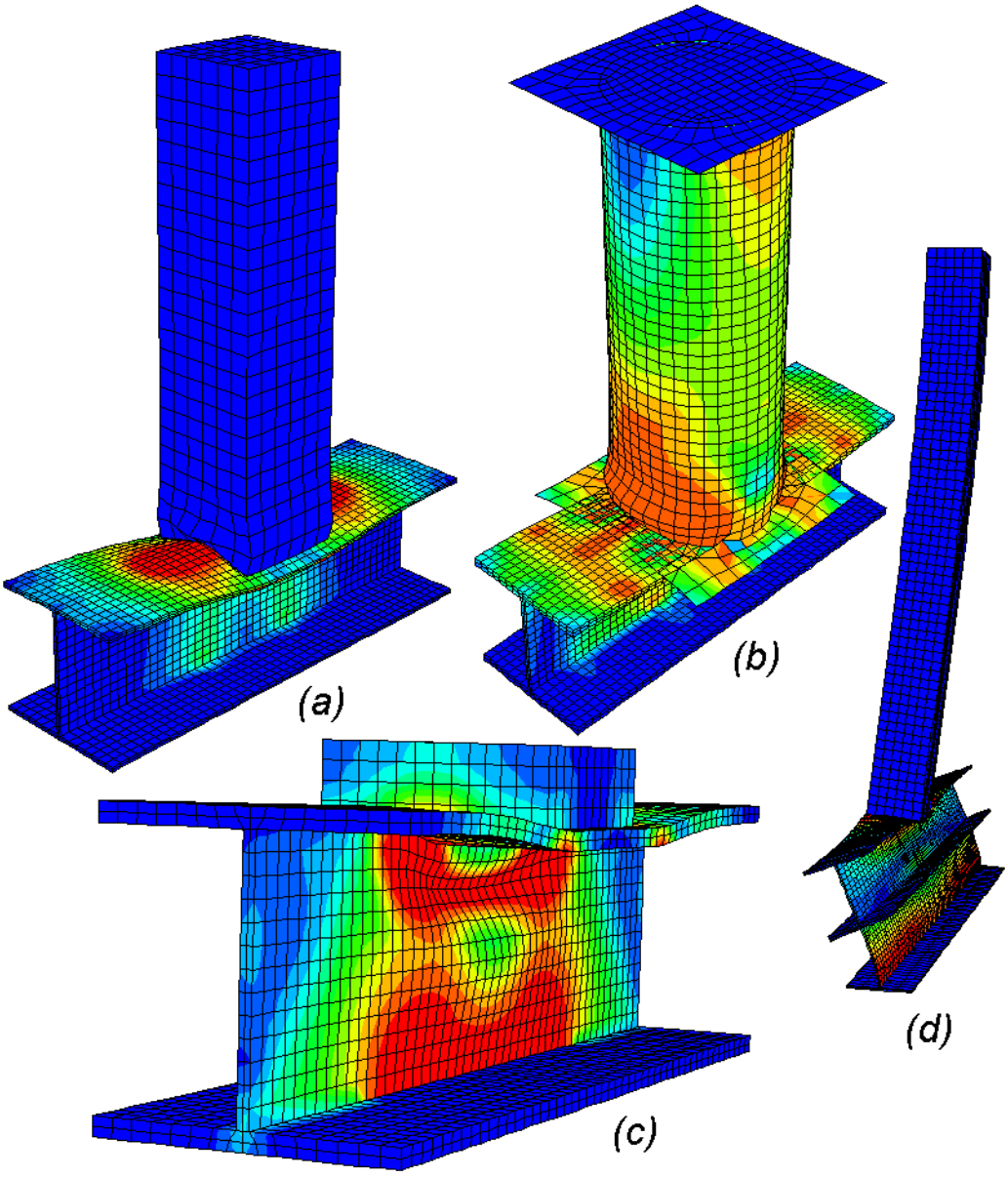

FIGURE 3-1 Finite element models for a) a timber post and beam, b) a steel post and beam, c) a beam with a rigid patch load and d) long double stacked beam and post

From the component experiments on Posts 1 and 2 for the 1 1.5 in. square Douglas Fir timber posts, the average calculated nominal post strength was 2.7 ksi. This was assumed as the yield stress in the fi nite element model and, in orde r to fit the force displacement curve, this was increased linearly by 20% up to 2 times the yield strain before being gradually reducing to zero at a strain of 10% to reflect the reduction in strength due to crushing. The elastic modulus was assumed to be 550 ksi, based on the average measured stiffness from experiments. On ly posts 1 and 2 were used to calibrate the finite element

models as Post 3 was considered atypical of the posts used during the sub-assembly experiments. A finite element model of a timber post similar to that shown in Figure 3-1a, but without any beams or other elements was used to compare with the experimental data. The resulting force displacement curve for the post is shown, along with the experimental data for Posts 1 and 2, in Figure 3-2. The stiffness and failure load is shown to compare well to the experimental data.

The 7.5 x 5.5 in. blocking elements were modeled with a 4.0 ksi yield stress and a 330 ksi elastic modulus, based on an average of the three component experiments. After yielding it was assumed the stress would drop to zero at a strain of 10%. The resulting force-displacement curve for the blocking is shown in Figure 3-3 compared to the experiments. It is shown to approximate an average response for the three blocks.

The 11.5 in. square corbels were modeled with and elasto-plastic model having an elastic modulus of 11 ksi and a yield stress of 0.39 ksi. The yield stress was determined from a modified bearing area and is different from the ultimate bearing strength for the corbels used in Section 4, but results in a better correlation with the finite element analysis. The resulting force displacement curve from a finite element model of the corbel compared to the component experiment is shown in Figure 3-4 for a 15 in. long rigid patch load on the corbel, similar to that used in the corbel experiment. The experimental data matches the initial stiffness yield and post-yield stiffness of the finite element model.

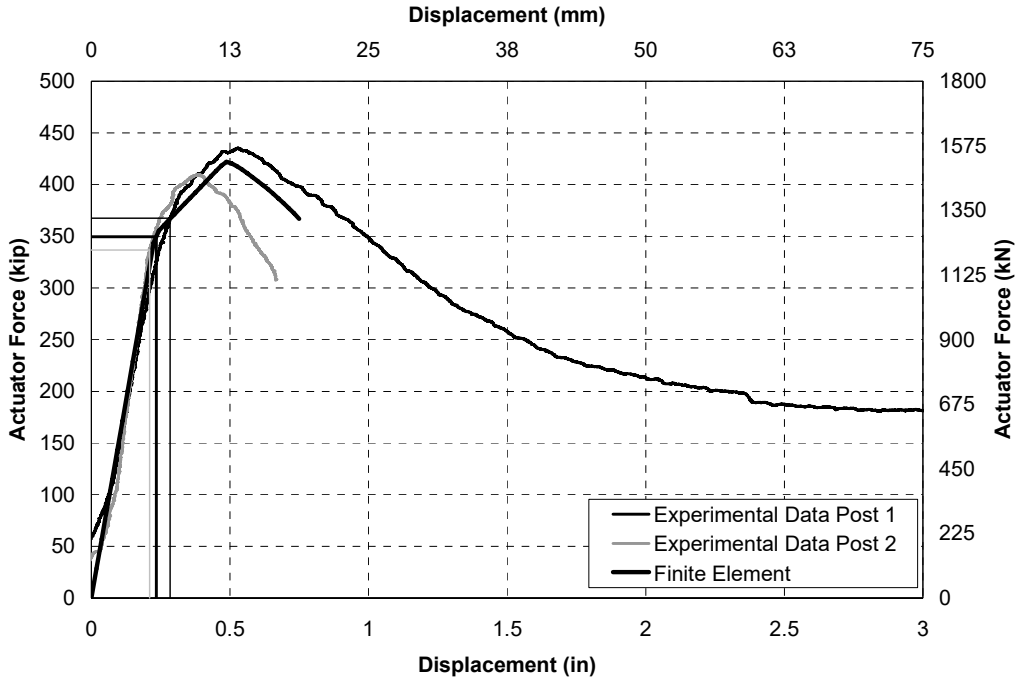

FIGURE 3-2 Force-displacement curve for a finite element model of a timber post compared to the experimental data

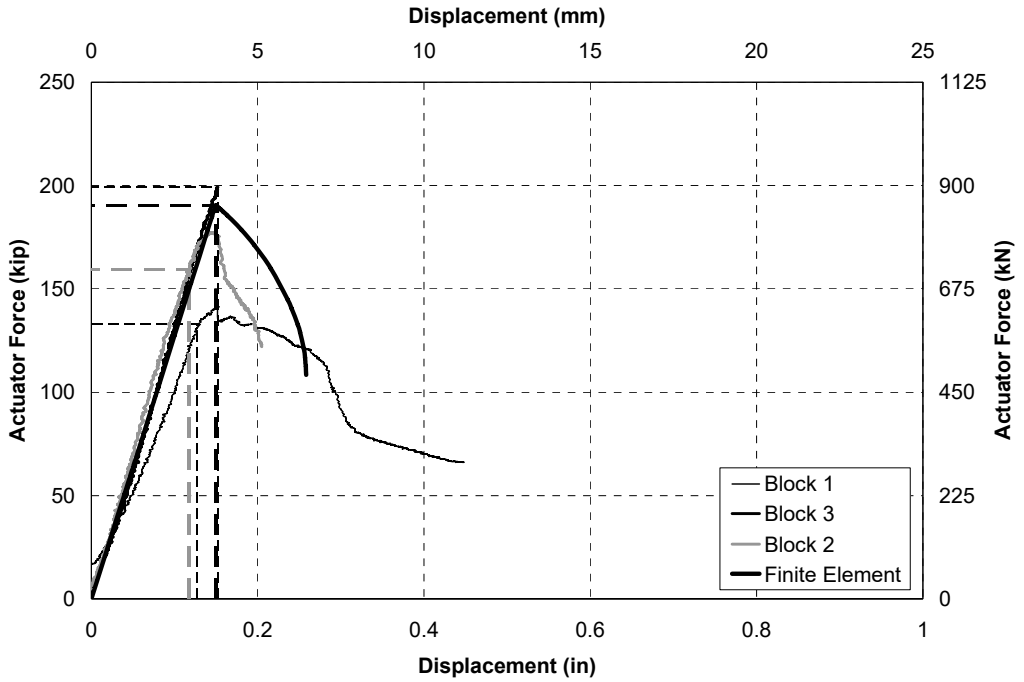

FIGURE 3-3 Force-displacement curve for a finite element model of a timber block compared to the experimental data

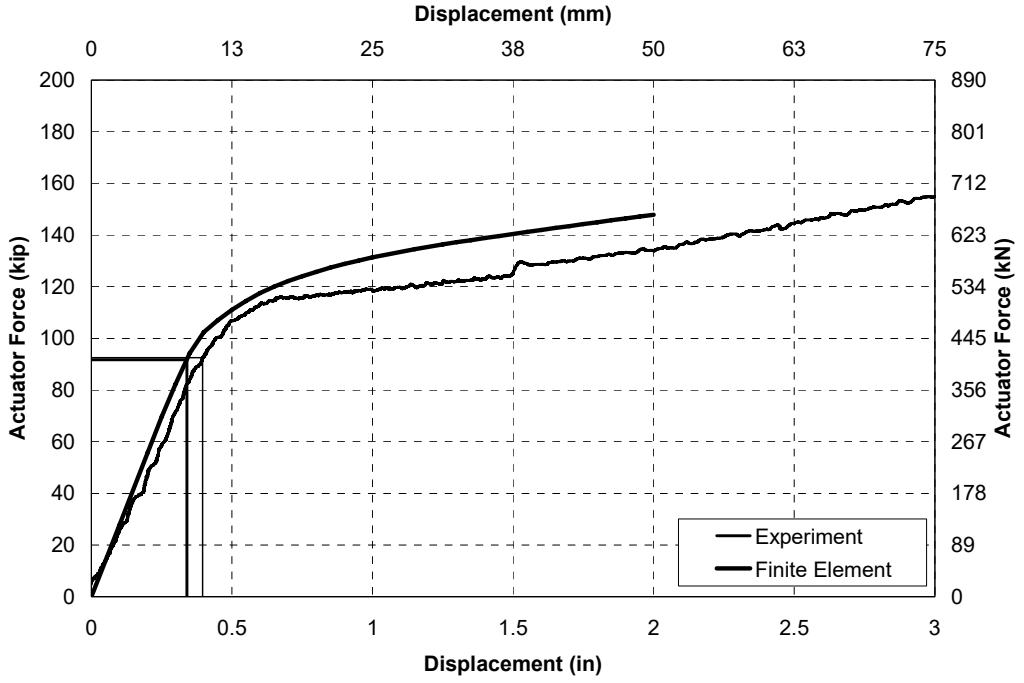

FIGURE 3-4 Force-displacement curve for a finite element model of a timber corbel compared to the component experimental

Loads were applied to the top of the post or patch load in displacement control. The interfaces between the beams and other components were modeled with contact surfaces. The nodes under the beams were completely restrained, while at the free end of the post the nodes were restrained to allow axial deformation only. Both flanges at the ends of the beam were also restrained to prevent out-of-plane deformation of the flanges except in the beams where the post-flange restraints were removed to investigate lateral web buckling.

For each configuration considered, the axial force in the post or force applied to the patch load is plotted against the axial displacement at the free end of the post or patch load. For each experiment the failure load is defined from the force displacement curve at a point where the tangential stiffness reduced to 50% of the initial stiffness, as in the experiments.

3.3 Comparisons between the Experimental and Finite Element Results

3.3.1 Overview

Comparisons between the experimental and finite element results are divided into three categories:

- Post-flange bending and post crushing or yielding;
- Corbel-flange bending with corbel crushing when timber corbels were used;
- Web yielding, crippling or lateral web buckling.

Each of these is discussed below.

3.3.2 Post-flange Bending - Post Crushing Capacity

A typical force-displacement curve for one of the beams exhibiting post-flange bending and post crushing the HP12x53 beam concentrically loaded with a timber post exhibiting failure by post-flange bending and post crushing is shown in Figure 3-5. The displacement in the experimental data is offset in order to have an extrapolation of the elastic stiffness through the origin, removing the observed stiffening that occurred as the gaps between the various components in the sub-assembly experiments were closed. The finite element curve matches the experimental data reasonably well. The initial stiffness close to that observed, although, as localized yielding occurred in the finite element model a reduction of stiffness occurred that began earlier than observed in this particular experiment. Consequently, the failure load was calculated to be 12% less in the finite element model than the experimental model. In the experiment the force in the system appeared to reduce more quickly than in the finite element model, suggesting that perhaps the post elastic stiffness of the post should be reduced. However, there is a relatively large variability in response between the different experiments, as observed in Section 2, with

other experiments exhibited a more gradual post-elastic reduction in forces. Furthermore, the response after calculation of the failure load is of mini mal consequence as the failure load is the critical factor in determining the performance of the various assemblies. Thus the post-elastic behavior is considered acceptable.

A similar figure is shown fo r the concentrically loaded HP12x53 with blocking between the flanges in Figure 3-6. In this case the failure load from the finite element model is 19% greater than the experiment al failure load. This could be attributed to a number of factors, such as the post or blocks in the experiment being stronger than assumed in the finite e lement model. Despit e this, the finite element res ponse, particularly in initial stiffness, compared reasonably well with the experimental response.

The failure load from the exp eriments is co mpared to the f ailure loa d f rom the finite element models in Figure 3-7. The figure s hows that for the dif ferent configurations exhibiting flange-post failure, the load from the finite el ement analysis is between 76% and 119% of the experimental load, with an average of 96%. It appeared that the strength of unblocked beams was conservatively pred icted by the finite element model, by an average of 14%, while the capacity of the blocked beams was over predicted by an average of 7%. This is cons istent with that observed by the force-displacement curve s (Figs. 3-5 and 3-6), suggest ing an over -prediction of th e blocking strength and under prediction of the post and beam strength. This va riability is attribute d pr imarily to the variability in the capacity of the dif ferent posts and blocking, which is lar gely unavoidable. Overall, ther e is good correlation between the experimental and finite element res ults. The beams wi th steel posts could not be compared directly to the experimental data as the fa ilure load was dominated by the corbel response in the experiments. However, the failure loads calculated from the finite element models were at around the loads where yielding was observed experimentally in the posts.

3.3.3 Corbel-flange Bending - Corbel Crushing

Finite element models for three beams with timber posts and two timber corbels, and two beams with stee l pos ts and three timber co rbels were compared to the exper imental results. A typical force-dis placement curve for one of th e beams exhibiting corbel-flange bending and corbel crushing when corbels were placed behind the beams is shown in Figure 3-8. This figure, for the con centrically loaded HP12x53 beam, shows good correlation between the finite element analysis and experimental data, after the removal of initial stiffening that occurred as the gaps closed between the vari ous components in the sub-assembly. Consequently , the failure load from the finite element model wa s calculated to be within 4% of that from the experiment. Th is is typical of other beams with corbels, although the finite element model tends to be more conservative for these other beams.

The failure load from the expe riments for all the be ams with corbe ls is c ompared to the failure load from the finite element models in Figure 3-9. The figur e sh ows that for the different configurations exhibi ting flange-corbel failure, the load from the finite element

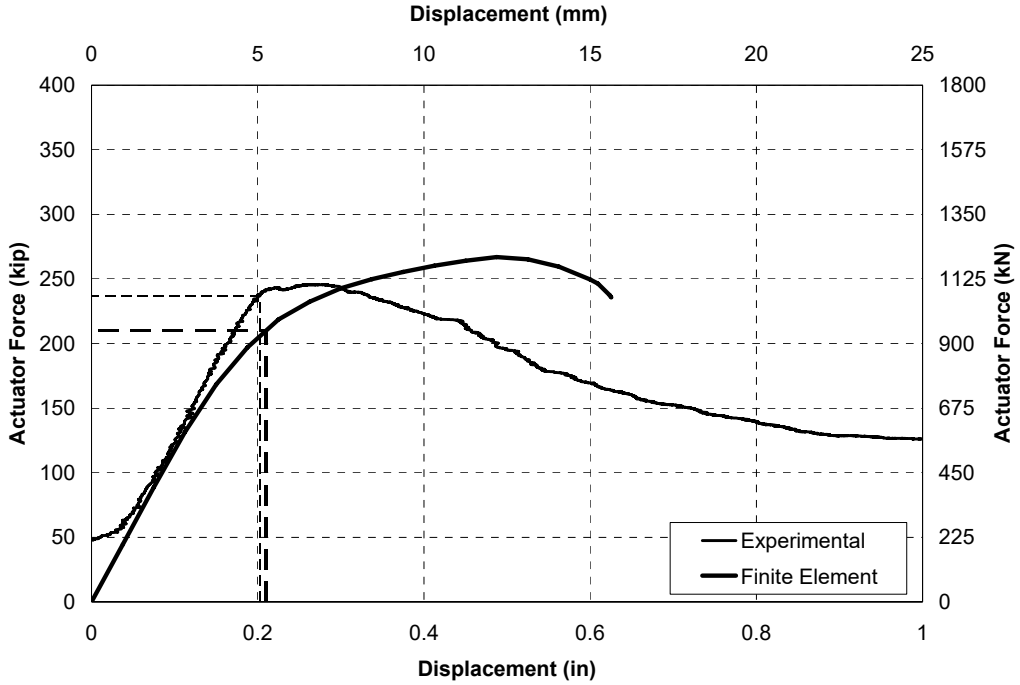

FIGURE 3-5 Force-displacement curve for finite element model of HP12x53 beam and timber post exhibiting flange bending and post crushing

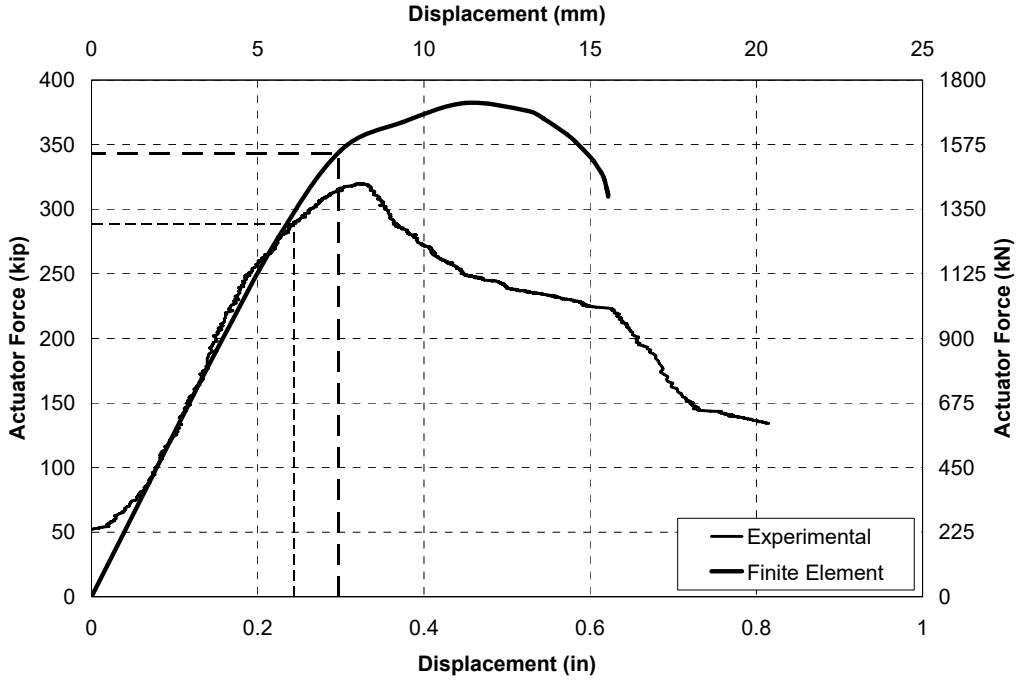

FIGURE 3-6 Force-displacement curve for finite element model of HP12x53 beam and timber post with blocking exhibiting flange bending and post crushing

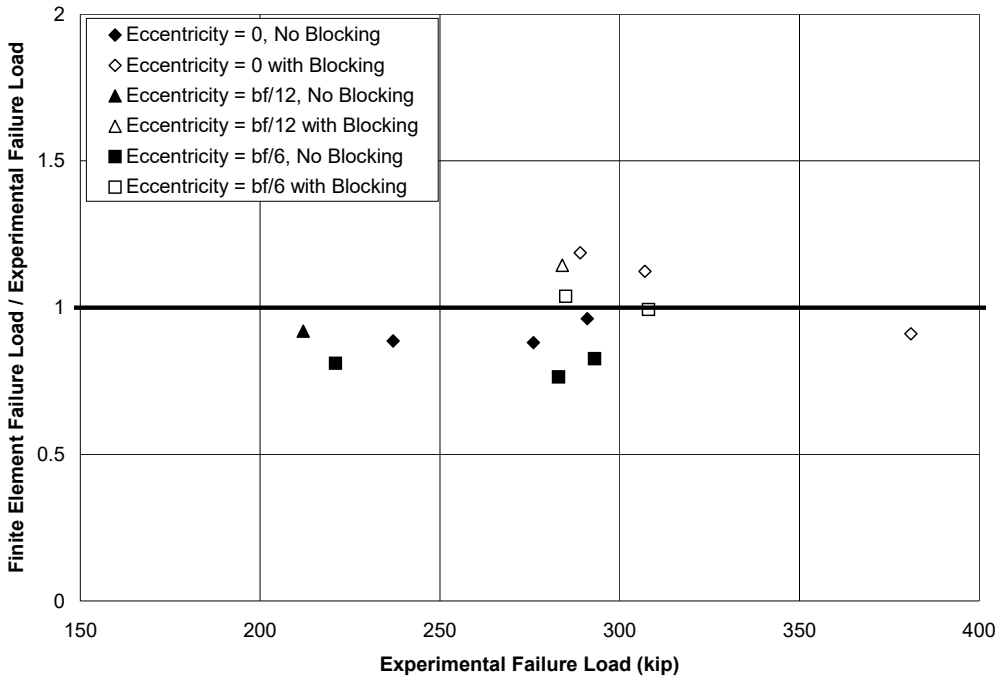

FIGURE 3-7 Failure load from finite element analysis compared with experimental failure load for beams exhibiting flange-post failure

analysis is between 76% and 104% of the experimental load, with an average of 87%. Thus the models were generally conservative, with the variation attributed to the difference in corbel strengths.

3.3.4 Web Yielding and Lateral Buckling

Finite element models for six different beams with rigid patch loads exhibiting web yielding followed by post-elastic crippling or buckling were compared to the experiments. The finite element and experimental force-displacement curves for the HP12x53 beam with a concentric rigid patch load are compared in Figure 3-10. This comparison shows that the shape of the force-displacement curves are similar, although the initial stiffness and maximum load reached in the finite element model is much greater than measured during experiments. The lower stiffness in the experiments is attributed to the slider and patch loading assembly which had some flexibility, that becomes much more apparent in this very rigid setup. Despite the error in elastic stiffness it does not greatly affect the yielding of the beam. The calculated failure load from the finite element model is within 5% of that from the experiment. Similar observations are made when comparing the other beams where web yielding occurred.

In addition to the web yielding cases, finite element models with timber posts and unrestrained post-flanges were developed to simulate lateral buckling for the two W14x90

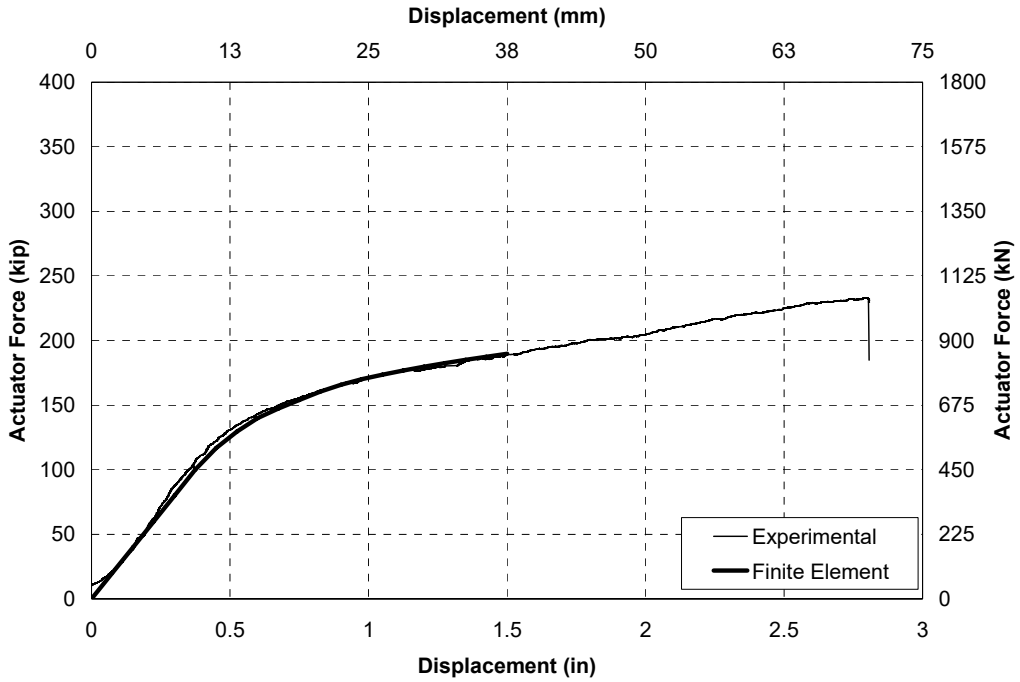

FIGURE 3-8 Force-displacement curve for finite element model of HP12x53 beam with corbels and posts exhibiting corbel-flange bending and corbel crushing

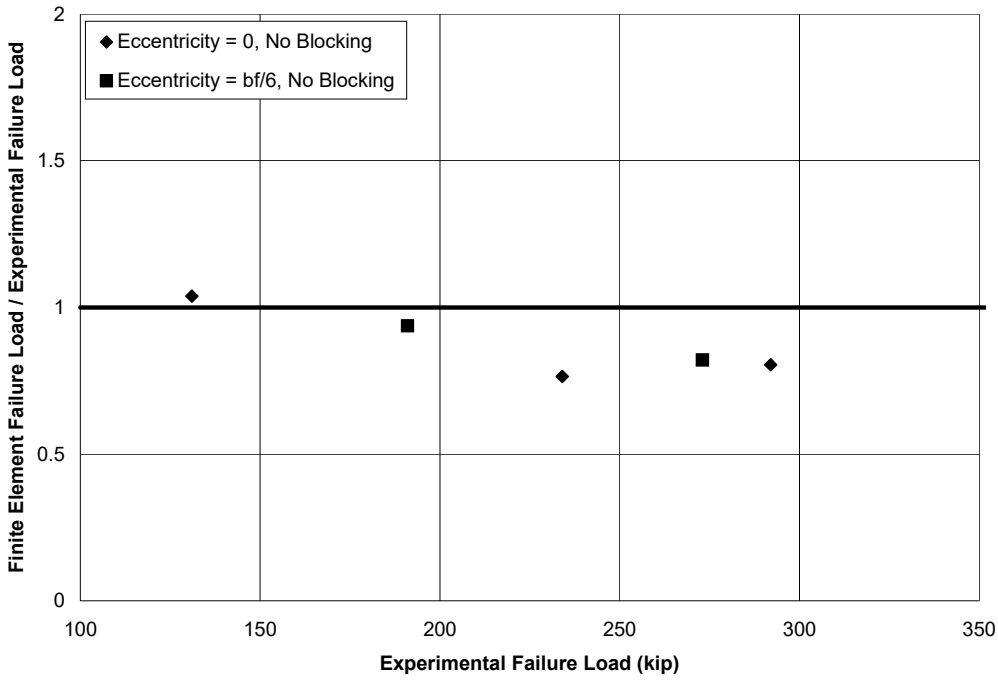

FIGURE 3-9 Failure load from finite element analysis compared with experimental failure load for beams exhibiting flange-corbel failure

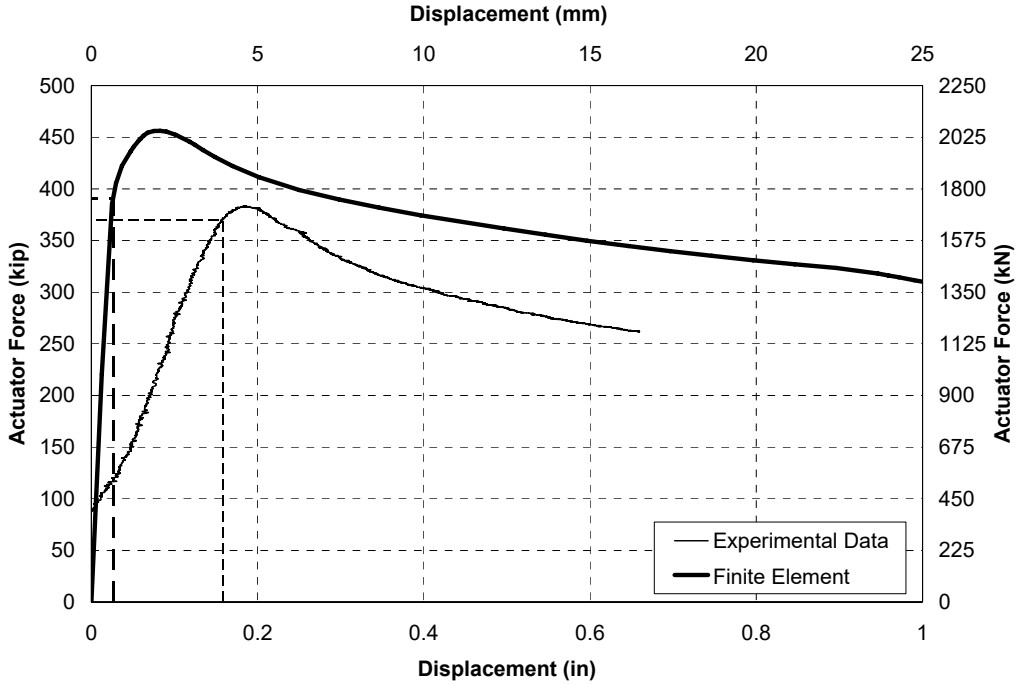

FIGURE 3-10 Force-displacement curve for the FE model of the HP12x53 beam with a concentric rigid patch load exhibiting web yielding and post-elastic buckling/crippling

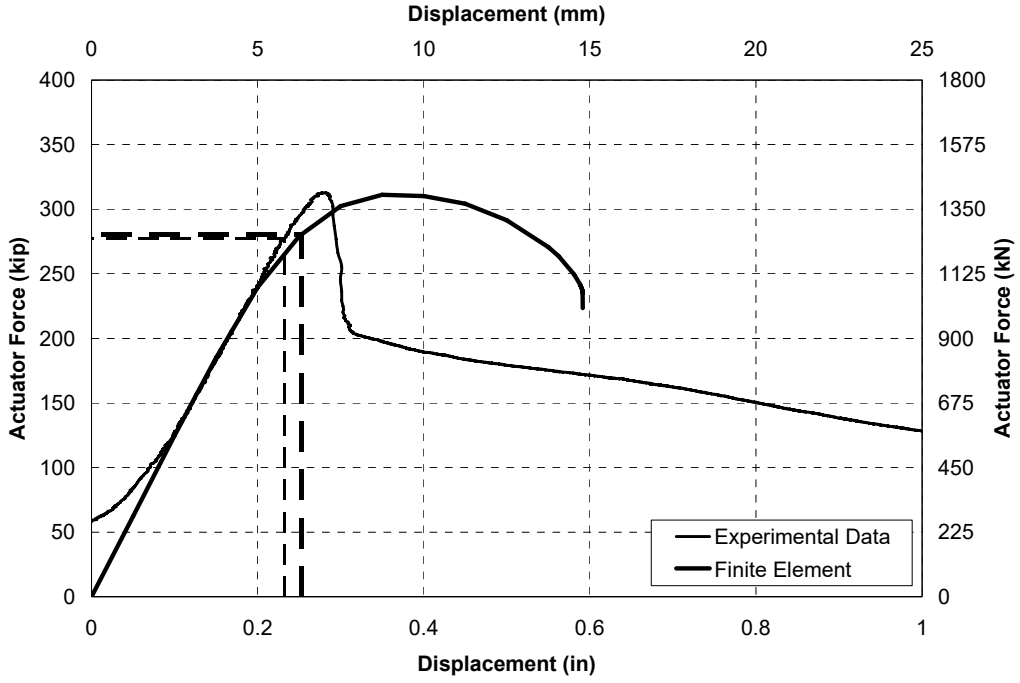

FIGURE 3-11 Force-displacement curve for the finite element model of the unrestrained W14x90 beam with a timber post resulting in lateral web buckling

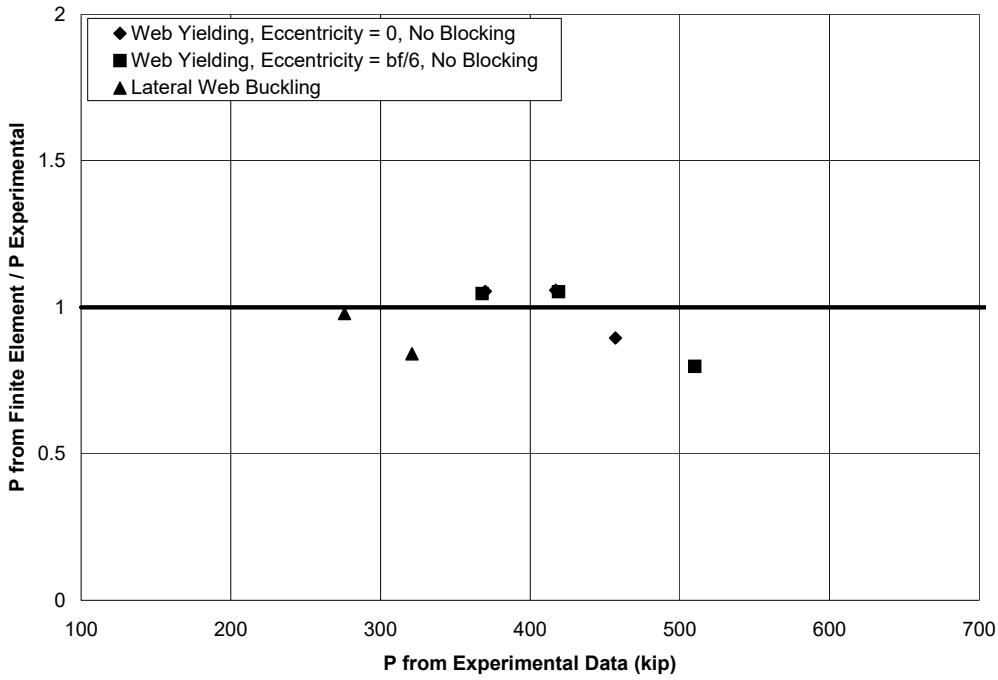

FIGURE 3-12 Failure load from finite element analysis compared with experimental failure load for beams exhibiting web yielding and lateral buckling

beams where this was observed. A typical force-displacement curve for one of these beams is shown in Figure 3-11. The drop in load is not as sudden in the finite element model as observed in the experiment, with a more gradual inelastic deformation observed. Despite this, the initial stiffness compares well and the maximum load and calculated failure loads compare to with 1% between the finite element analysis and experiment.

The failure load from the experiments for all the beams with web failures are shown in Figure 3-12. The figure shows that the load from the finite element analysis is between 80% and 106% of the experimental load, with an average of 97%. Thus the models compared well with the experimental results.

3.4 Other Finite Element Analysis Results

3.4.1 Other Configurations not Considered Experimentally

A larger range of beam sizes, combinations with timber and steel posts, blocking, beam and post lengths and restraints were considered with finite element models than considered in the experiments. The additional analyses are discussed more extensively when comparing the failure loads with calculated limit states in the following section.

3.4.2 Prevention of Lateral Buckling

Lateral torsional buckling cannot be prevente d by adding stif feners to a beam as the torsional deformation is stil l able to occur . However pure lateral buckling, where the deformation is due to bending in the web not torsion of the section, can be prevented by using web stif feners. When stif feners, wi th a th ickness e qual to the thickne ss o f the flange, are added to the beam directly under the post load location, as shown in Figure 3-13, no buckling of the beam is observed. This is due to an increase in the radius of gyration of the web which can be easily calculated.

Alternatively, lateral bracing could also be used to prevent the lateral buckling of the web. The advantage of using lateral bracing is that it will also prevent any torsional buckling modes in the beam, which may be allowed if the top of the beam and bottom of the beam are allowed to rotate due to inadequate stif fness in the supports. This limit state is not considered in this study as it requires investigation of a co mplete system. However, from the observed deformation in pa st falsework failures, some deformation of the web is observed with the beam instab ilities, therefore prevention of the web deformation will prevent instabilities in most cases.

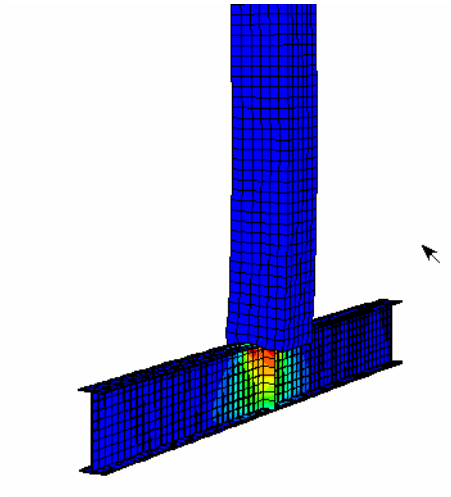

FIGURE 3-13 Finite element model of beam with stiffener to prevent lateral buckling

3.4.3 Effect of Eccentricity

The experimental data showed that eccentricity between the centroids of the flange and post equal to a maximum of $^1/_6$th of the flange width, result ed in some reduction in the flange-post capacity, typicall y around 10-15% when using a ti mber post. W ith a steel post, each eccentric cas e resulted in an al most iden tical f lange-post c apacity to the concentric case. To further study the effect of an eccentricity on the failure load, additional finite element analyses were performed. T en foot lengt hs of four dif ferent beams were modelled with 10 ft long posts and dif ferent eccentricities. Th e longer beams and posts

were considered more typical of those in bridge falsework. The calculated normalized failure load of the beams is plotted with respect to eccentricity, where the eccentricity is given in terms of a multiple of the web thickness, in Figure 3-14. Two of beams were smaller than typically used in falsework but were studied in order to determine the effect of eccentricities on beams with more slender webs where lateral web buckling is the critical failure mode. The figure shows that for cases which failed though lateral buckling or flange bending, there was around a 17 to 25% reduction in the capacity at an eccentricity of 6 times the web thickness. To ensure that the capacity is reduced by no more than 10%, the eccentricity should be limited to 3 times the web thickness. This is considered an appropriate maximum limit to be used in design. The reductions in failure load observed in this figure are consistent with those observed in the experiments.

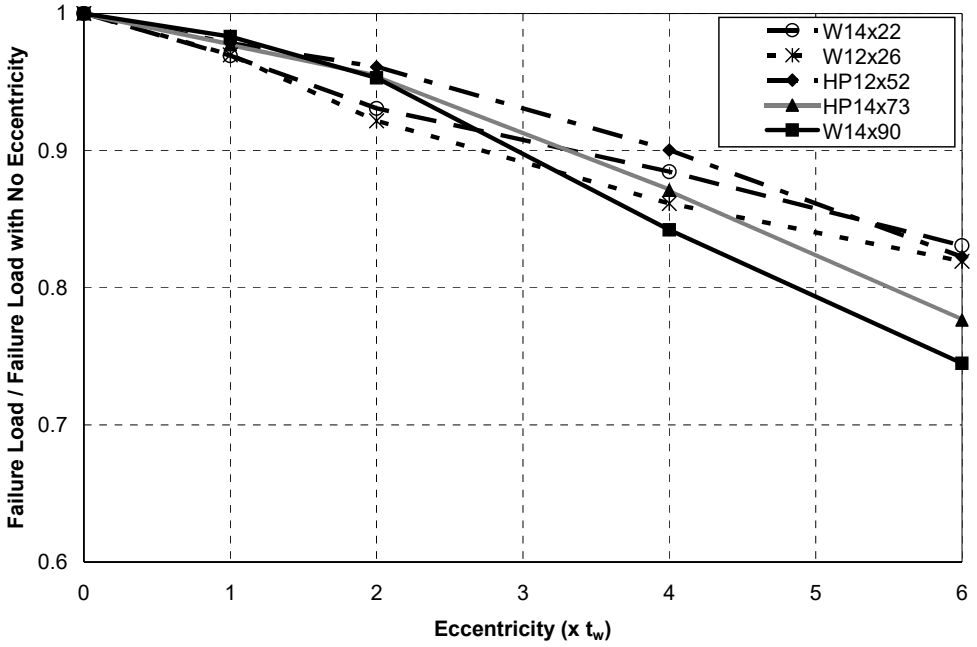

FIGURE 3-14 Failure load of beams with different eccentricities between the beam and post

SECTION 4
PREDICTION OF THE FLANGE BENDING, POST AND CORBEL CAPACITIES

4.1 Overview

The experimental and finite element models showed that either a combination of flange bending and post deformation or corbel-flange bending and corbel crushing (for sill beams) is likely to govern the design of cap and sill beams in falsework. Formulations are developed in this chapter to determine appropriate methodologies for predicting the flange-post joint capacity, with a timber or steel post, and flange-corbel capacity.

4.2 Post-flange Bending Limit State

From a yield line solution by Graham et al. (1959), the ultimate load that can be carried by a column flange, R_n, due to a tensile line load from an adjoining beam flange carrying a tension or compression force is given by (AISC 2005):

$$R_n = 6.25 t_f^2 F_{yf} \qquad ...4.1$$

where: t_f is the thickness of the flange and F_{yf} is the minimum specified yield stress of the flange. Another form of this equation was developed using yield line analysis by Tserry and Easterling (2000) for corbel-flange bending from bearing of perpendicular beams directly on the flange of a main beam in buildings. That equation used an appropriate yield line pattern for the new application, resulting in good agreement with experimental results. An adapted mechanism can be used to calculate the ultimate load for flange bending from a post patch load on a falsework sill or cap beam. The resulting ultimate load for beam flange bending, R_{fl}, is given by:

$$R_{fl} = \beta_1 t_f^2 F_{yf} \qquad ...4.2$$

where: β_1 is determined from a yield line analysis. For post loading, assuming a patch load with dimensions, b_p and d_p, as well as the yield line pattern and a uniform pressure, as shown in Figure 4-1, equating the internal and external virtual work for the patch load gives an expression for β_1 equal to:

$$\beta_1 = \frac{b_p b_{feff}}{2 b_{peff}^2}\left(\frac{d_p}{b_{feff}} + \frac{4}{\sin 2\theta} + \frac{2}{\tan\theta}\right) \qquad ...4.3$$

where: α is the angle of the yield line shown in Figure 4-1, b_{feff} is the effective width of the flange (shown in Fig. 4-1) given by:

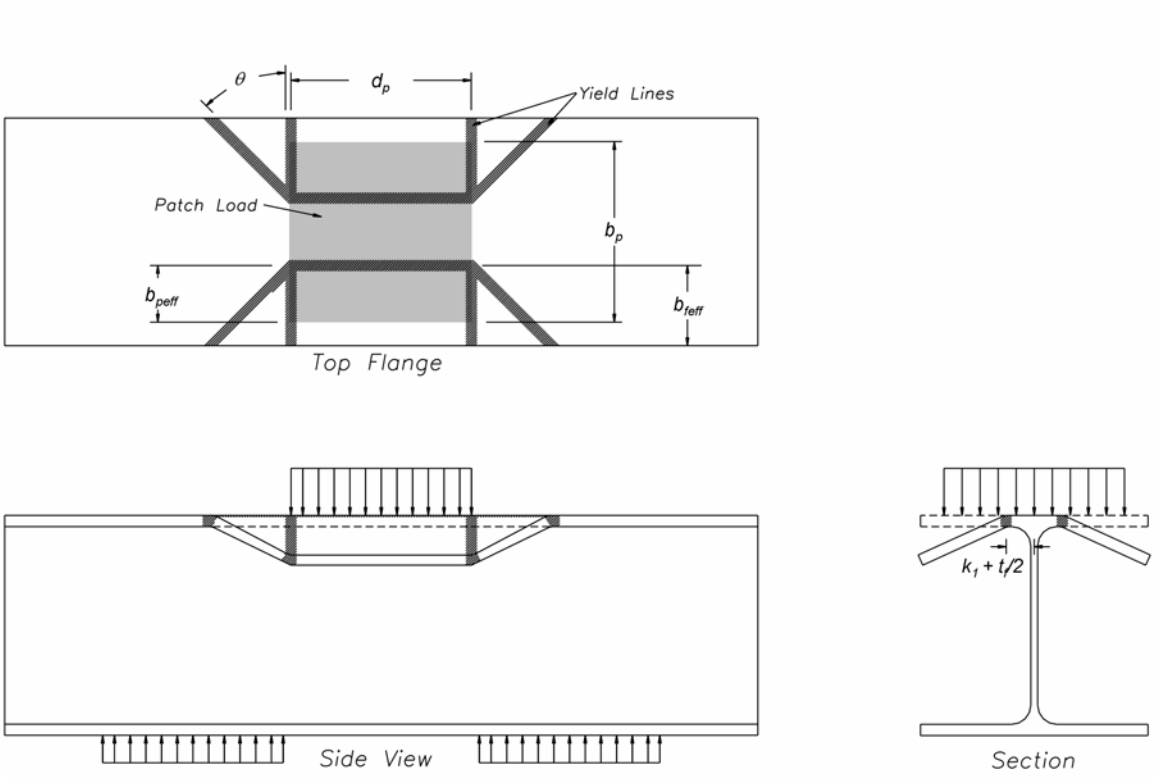

FIGURE 4-1 Yield line pattern on beams for a post patch load assuming a uniform stress distribution in the post

$$b_{feff} = \frac{b_f}{2} - k_1 - \frac{t_f}{2} \qquad ...4.4$$

where: k_1 is the distance from the center of the web to the edge of the fillet and b_f is the width of the flange. The effective width of the post, b_{peff}, is given by:

$$b_{peff} = \frac{b_p}{2} - k_1 - \frac{t_f}{2} \qquad ...4.5$$

The expression for β_1 can be minimized with respect to θ giving a minimum value at angle of 55 degrees. However, assuming an angle of 45 degrees gives a result for the last two terms of Equation 4.3 that is within 6% of the minimum value, therefore θ is assumed to equal 45 degrees, allowing Equation 4.3 to simplify to:

$$\beta_1 = \frac{b_p b_{feff}}{2 b_{peff}} \left(\frac{d_p}{b_{feff}} + 6 \right). \qquad ...4.6$$

Note that if d_p tends to zero, as for a line load, b_p is equal to b_f and therefore b_{peff} is equal to b_{feff}, and b_{feff} is assumed to be 0.96 $b_f/2$, then β_1 simplifies to 6.25 as in Equation 4.1. For typical falsework applications, where nominal 12 x 12 in. posts are used with actual dimensions, b_p and t_p, equal to 11.5 in., the values of β_1, for different typical beam sizes used in bridge falsework, are given in Table 4-1. The values of β_1 range from 10.9 to 18.1 for the different beam sizes considered. These are all greater than 6.25, which is to be expected. In order to simplify the calculation of flange bending capacity, a constant value of $\beta_1 = 11$ would be generally conservative for all cases considered.

TABLE 4-1 β_1 values for beams assuming uniform and triangular stress distributions and 11.5 in. square patch load

Section	HP12x53	HP14x73	HP14x89	W14x90	HP14x117	W14x120
Uniform	10.9	13.1	13.6	16.2	14.9	18.1
Triangular	20.1	24.4	26.1	35.3	29.9	41.9

Analyses show that, before crushing of the post occurs, a uniform stress distribution in the post is conservative for many beams, particular those with smaller flanges, as post stresses are concentrated around the web of the beam. Therefore, a new expression is developed assuming a triangular stress distribution (Fig. 4-2) instead of the uniform stress distribution. The resulting expression for β_1 is:

$$\beta_1 = \frac{3 b_p^2 b_{feff}}{8 b_{peff}^3} \left(\frac{d_p}{b_{feff}} + 6 \right) \qquad ...4.7$$

The value of β_1 for the different beam sizes assuming the triangular stress distribution is given in Table 4-1. The values range from 20.1 to 41.9, indicating an ultimate load that is approximately twice that for the assumed uniform distribution. It is noted that the value for the heaviest section considered based on the uniform stress distribution (18.1) is close to the β_1 value for the lightest section considered based on the triangular stress distribution (20.1). Before the timber post starts to fail locally, it is expected that the for the heavier sections a uniform distribution is most appropriate as the flanges will deflect a relatively small amount allowing the stresses to be uniformly distributed in the post, while for the lighter sections the flanges will deflect a greater amount making the triangular stress distribution more appropriate. Thus β_1 converges to a value of between 18 and 20. Different values for β_1 used in determining flange bending capacity are compared with the

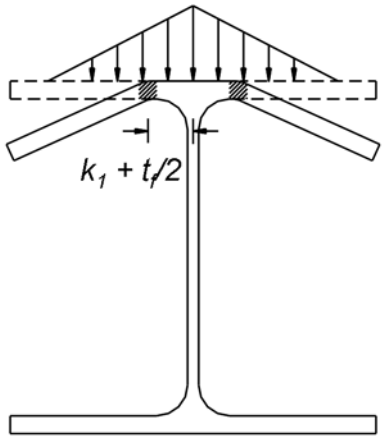

FIGURE 4-2 Cross section of a beam for a patch load assuming a triangular stress distribution in the post

experimental data and finite element analysis in Section 4.9. Once the timber post starts to crush the stress distribution changes, therefore if a higher β_1 value is considered it should only be used when the interaction with post crushing is also considered.

4.3 Post Compression Strength in the Flange-Post Connection Region

The strength of a timber post in compression is defined based on NDS specifications. To be consistent with the other limit states the NDS LRFD specifications (AFPA 1996) are used, although, the ASD specifications (AFPA 2001) are equivalent. In the flange-post connection region the compressive strength, R_p, is considered over a short length of the post and is given by:

$$R_p = F_c' A_p \qquad ...4.8$$

where: A_p is the nominal cross sectional area of the post and F_c' is the nominal stress in the post after modification factors are applied for moisture content, temperature, size, preservative treatment, fire-retardant treatment and column stability (AFPA 1996). As the compression capacity in the flange-post joint region is considered over a short length of post the column stability factor in this calculation is assumed to equal 1.0. Note that in the ASD specifications this is equivalent to the bearing strength of the column, although in the LRFD specifications the bearing strength is distinct from the compression strength. For consistency between the two specifications the compression strength based on a short column length is assumed. Stability of the full length of the column should be considered as a separate limit state in the design of the column.

As a steel post is axially much more rigid than a timber post, it does not result in an approximately even distribution of stresses in the end of the post when bearing against a beam with a flexible flange. Consequently, it is recommended that the localized axial capacity is calculated using the effective post bearing area described in Section 4.5.

4.4 Interaction between Flange Bending and Post Compression Limit States

The force at which bending occurs in the beam flange is related to that for crushing of the post where in contact with the beam. The flange will not bend unless the post deforms to accommodate the bending and, conversely, the compression strength of the post will be reduced, if flange bending occurs. Therefore, it is helpful to consider an interaction between the flange bending and post crushing limit states. A number of interaction equations have been proposed for different applications, such as for interaction between axial loads and bending moments in the design of columns, or for interaction between bending and torsional moments in members (AISC 2005). For the interaction between post crushing and flange bending an elliptical relationship is assumed, such that:

$$\left(\frac{R_u}{R_{fl}}\right)^2 + \left(\frac{R_u}{R_p}\right)^2 \leq 1 \qquad ...4.9$$

where: R_u is the applied axial load in the post. The application of this equation and comparisons to experimental data and finite element models is demonstrated later in the report.

4.5 Effective Post Bearing Area for Calculating Flange-Post Capacity

An alternative to the interaction equation is considered which focuses on the post crushing of yielding in determining the flange-post capacity. For this model an effective cross sectional area of the post is considered to carry the axial load, as shown in Figure 4-3, calculated using similar assumptions to those used for the web yielding equation in the AISC specifications (AISC 2005). The effective area of the post is determined by the width of the post effective in carrying the load multiplied by the thickness of the post within this width. An equation for the capacity of a timber post, R_p, is subsequently given by:

$$R_p = (\alpha t_f + 2k_1) d_p F_c' \qquad ...4.10$$

where: α is constant which depends on the slope of the stress gradient assumed through the flange, which will be determined using the experimental data and finite element

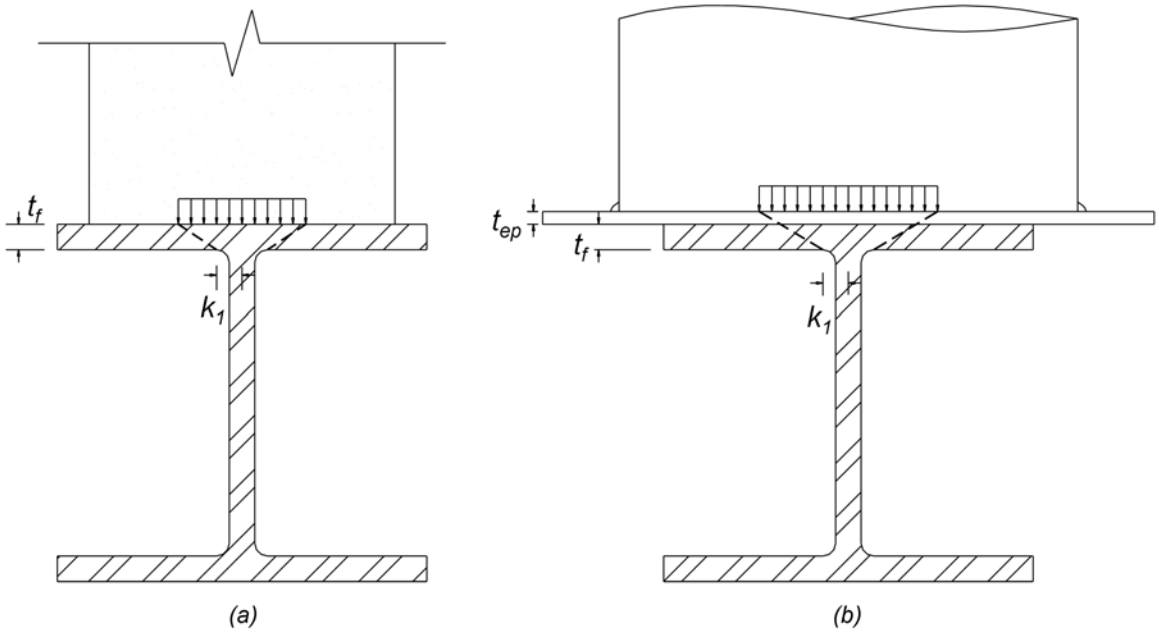

FIGURE 4-3 Effective area of a) timber post and b) steel post for calculation of ultimate post load

analysis, F_c' is the nominal compressive stress perpendicular to the grain for a short length of post and the other variables are as previously defined. A similar equation for the capacity of a steel post is given by:

$$R_p = (\alpha(t_f + t_{ep}) + 2k_1)2t_pF_{yp} \quad ...4.11$$

where: t_{ep} is the thickness of the end plate of the post, t_p is the wall thickness of the round hollow steel section and F_{yp} is the minimum specified yield stress of the post. The $2t_p$ allows for the transfer of axial load on two sides of the round hollow steel section.

4.6 Corbel-flange Bending Limit State

Similar to the relationship between the capacity of the post-flange and post, the capacity of the corbel-flange and corbels are also related. In the experiments and finite element analysis corbel-flange bending was observed in the beams as the corbels started to crush. However, the experiments were not representative of typical falsework as there are usually blocks, wedges and sand jacks between the sill beam and timber corbel. With these components it is difficult to predict the stress distribution that would result on the corbel-flange of the beam and interaction between the beam and corbels would be minimal. Thus, the best approach is to treat the two as independent and use conservative

assumptions with respect to corb el-flange bending and corbel crus hing, then check for both cas es. Th is assumes that any elements between the beam and corbel have the required capacity for a continuous transfer of load.

A similar methodology to that used in developing the flange bending equation for the post-flange can also be used for the corbel-flange where the beams bear onto the co rbels through sand jacks, blocks and wedges. Th e yield line pattern s hown in Figure 4-4 is assumed along with a uni form stress distribution on the fl ange from the corbels. The resulting ultimate load for beam flange bending, R_{f2}, is given by:

$$R_{f2} = \beta_2 t_f^2 F_{yf} \qquad ...4.12$$

where: β_2 is determined from a yield line anal ysis. Assuming a uniform loading in the shaded area and y ield lin e pattern, as show n in Figure 4-4, equating the internal and external virtual work for the patch load gives an expression for β_2 equal to:

$$\beta_2 = \frac{b_f}{2b_{feff}}\left(\frac{b_c + s_c}{b_{feff}} + \frac{4}{\sin 2\theta} + \frac{2}{\tan\theta}\right) \qquad ...4.13$$

where: θ is the angle of the yield line shown in Figure 4-4, b_{feff} is the ef fective width of the flange (shown in Fig. 4-4) given by equation 4.4, b_c is the width of each corbel and s_c is the spacing of the outermo st corbels in a group associat ed with each post. The expression for β_2 can be minimized with respect to θ, although as with the post-flange an angle of 45 degrees gives a result for the last two terms of Equation 4.13 that is within 6% of the minimum value, therefore θ is assumed to equal 45 degrees, allowing Equation 4.13 to simplify to:

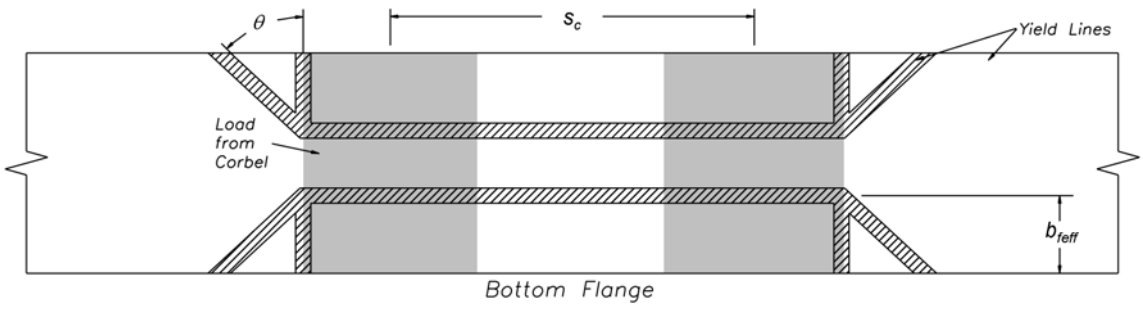

FIGURE 4-4 Yield line pattern on corbel-flange of sill beam due to reaction from the corbels

TABLE 4-2 β_2 values for beams assuming uniform stress distributions, 11.5 in. wide corbels and a spacing between corbels of 24 in.

Section	HP12x53	HP14x73	HP14x89	W14x90	HP14x117	W14x120
Uniform Stress	16.2	13.9	14.2	16.6	14.9	17.5

$$\beta_2 = \frac{b_f}{2b_{feff}}\left(\frac{b_c + s_c}{b_{feff}} + 6\right) \qquad ...4.14$$

For typical falsework applications, where nominal 12 x 12 in. corbels are used with the actual dimension, b_c, equal to 11.5 in., and the spacing of the corbels is 24 in. the value of β_2 for different typical beam sizes used in bridge falsework are given in Table 4-2. The values of β_2 range from 13.9 to 17.5 for the different beam sizes considered. A constant value of 14 could be assumed and would be within 20% for all values while at the lower end of the range. This would be conservative for all beams where the spacing of the outmost corbels is 24 in. or greater. Where other corbel spacings are used, and greater accuracy is desired, Equation 4.14 could be used to calculate an alternative value for β_2. Unlike for the post-flange, a triangular stress distribution is not considered for the corbel as the uniform stress distribution is conservative and there is more uncertainty in the properties of the applied load due to the elements including the sand jacks, wedges and blocks located between the corbel and the sill beam, as is further explained in Section 4.9.3.

4.7 Corbel Strength

The strength of a corbel in compression is defined based on the strength of timber perpendicular to the grain and the bearing area between the beam and corbel. Thus the capacity, R_c, is given by:

$$R_c = F_{c\perp}'A_{bg} \qquad ...4.15$$

where: A_{bg} is the bearing area and $F_{c\perp}'$ is the nominal stress after modification factors are for moisture content and other conditions (AFPA 1996).

4.8 Strength of Blocking

Generally timber blocks sized between 4 x 4 in. are 6 x 8 in. are used to increase the beam-post joint in falsework if deemed necessary. The capacity of these members can be calculated based on the axial compression capacity of a short timber member. However, comparison with experimental and analytical studies to follow show that the full capacity of the blocking is generally not effective, particularly for a steel post, thus the capacity of the timber blocking, P_b, can be given by:

$$P_b = \gamma F_c' A_b \qquad ...4.16$$

where: γ is the blocking effectiveness factor, F_c' is the nominal stress in the block after modification factors are applied (AFPA 1996) and A_b is the combined cross sectional area of the blocking on both sides of the web.

4.9 Comparison of Calculated Strengths with Finite Element Analysis

4.9.1 Capacity of Post-flange and Post for the Concentrically Loaded Unblocked Beams

The failure loads from the finite element models, described in Section 3, were compared with the calculated capacity using the different equations described above. Firstly, just the concentrically loaded, unblocked beams are considered. In calculating the capacity of the beams and posts, expected strengths based on 55 ksi yield stress for the steel beams, 46 ksi yield for the steel posts, and strengths based on component experiments for the timber posts (2.7 ksi) and blocking (4.0 ksi). The calculated flange bending capacity (Eq. 4.2), as a ratio of the capacity calculated from the finite element analysis for the different size concentrically loaded beams, is plotted in Figure 4-5. The flange bending capacity was calculated using three different methods for calculating β, 1) using Equation 4.6 assuming a uniform stress distribution from the patch load, 2) using Equation 4.7 assuming a triangular stress distribution, 3) assuming a constant value of $\beta = 11$ as a conservative estimate for an assumed uniform stress distribution and 4) assuming a constant value of $\beta = 18$, based on convergence of β from the uniform stress distribution for the largest beam and the triangular stress distribution for the smallest beam. In Figure 4-5, HP12x53, HP14x73, HP12x89 and W14x90 beams are modeled with timber posts and W14x90, HP14x117 and W14x120 beams are modeled with steel posts. In calculating the flange bending capacity with the steel post, the post was assumed to have an effective depth, d_p, (Fig. 4-1) equal to the diameter of the post (18 in.) and effective width, b_p, equal to the width of the flange. The capacity of the beams with timber posts are shown with the shaded markers, while the beams with steel posts are shown with unshaded markers.

Figure 4-5 shows that the calculated capacity of the flanges for the smallest beams is conservative compared to the failure load calculated from the finite element analysis, while for the larger beams the calculated capacity is unconservative, regardless of the

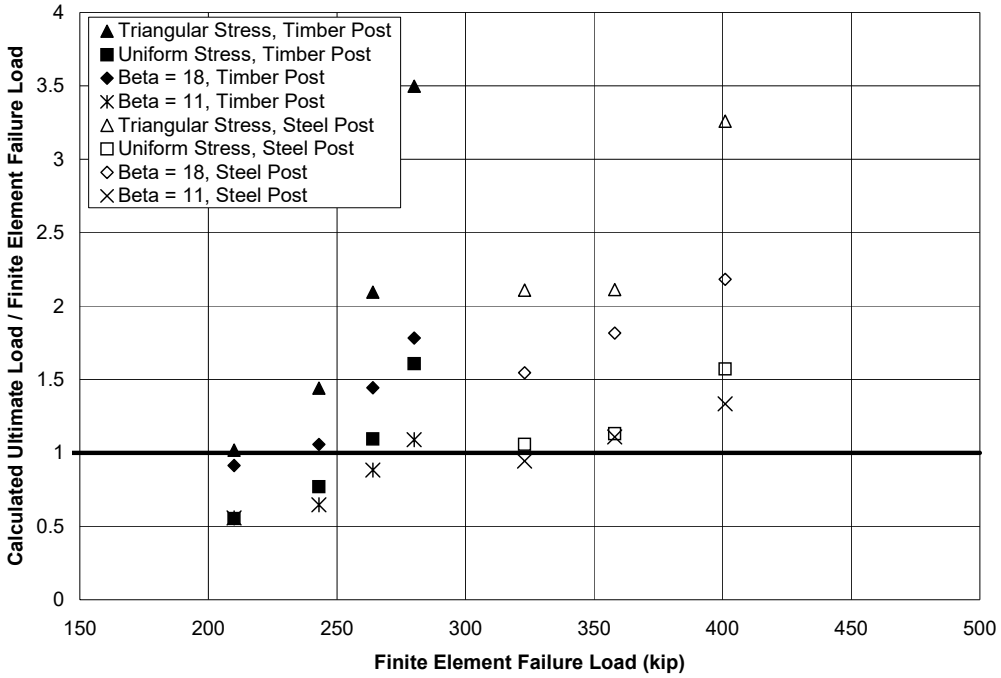

FIGURE 4-5 Comparison of flange bending capacity with failure load from the finite element models for different beams

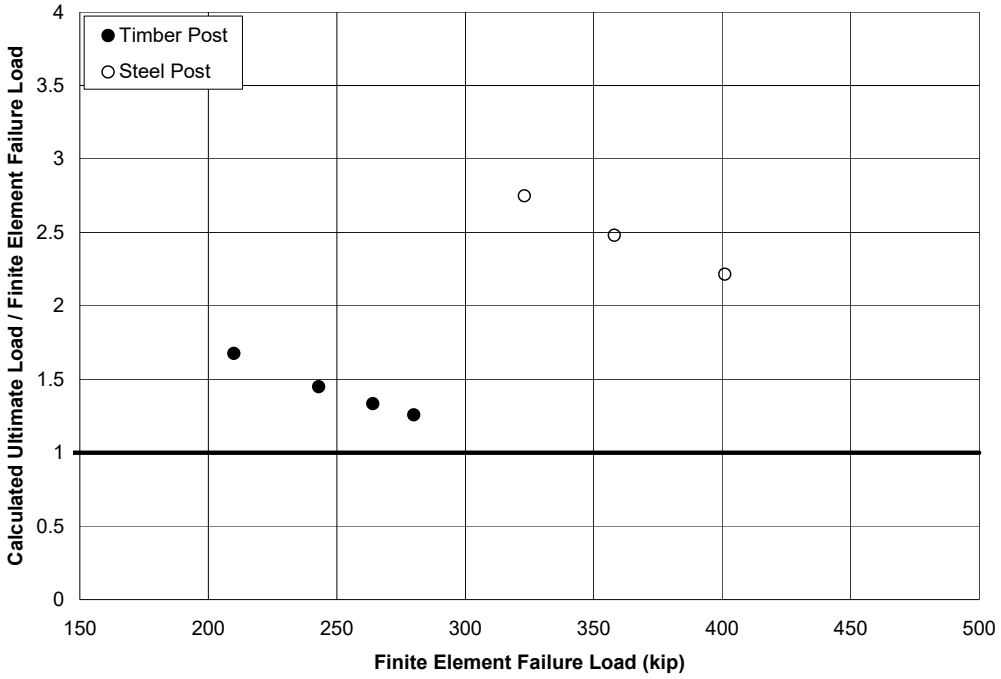

FIGURE 4-6 Comparison of post capacity for a short length of post with failure load from the finite element models for different beams

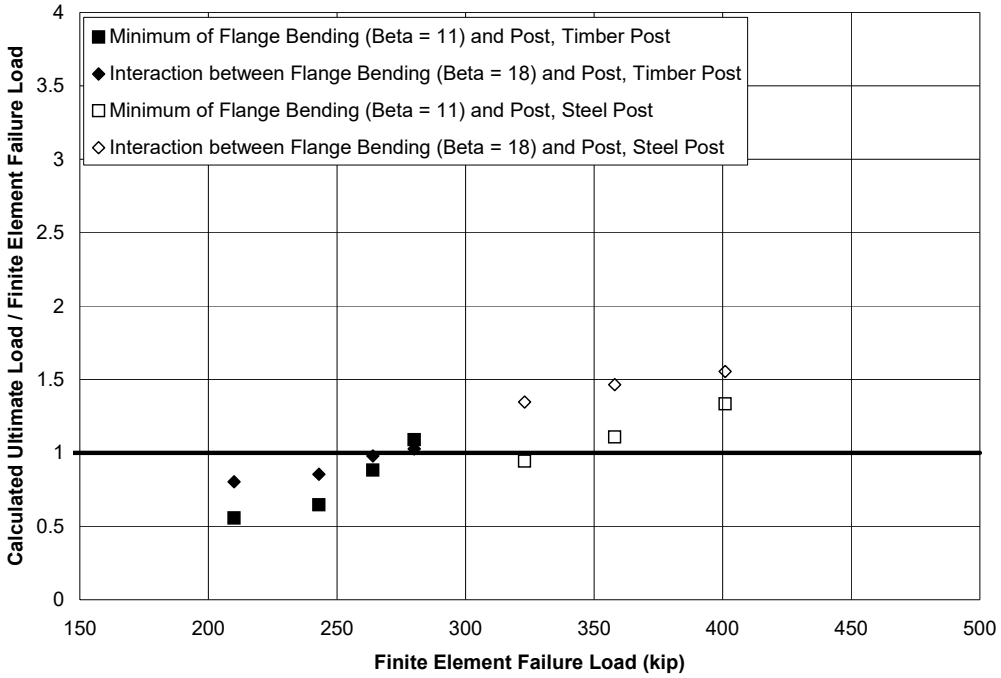

FIGURE 4-7 Calculated flange-post capacity a) using the minimum of the flange bending strength with β=11 and post strength and b) using the interaction equation between flange bending strength with β=18 and post strength, compared to failure load from the finite element models for different beams

method for calculating β. Therefore, the flange bending capacity calculations alone did not give a good estimate of the capacity of the flange-post connection region as the post strength also needs to be considered.

The nominal axial capacity for a short length of post (Eq. 4.8) is shown in Figure 4-6, as a ratio of the capacity of the beam-post connection region for the different beams from finite element analysis. The figure shows that the calculated capacity of the post in all cases is greater than the capacity of the beam-post connection region indicating that the post strength alone also does not give a good estimate of the flange-post connection region capacity.

When Equation 4.9 is used to model the interaction between the post capacity and flange capacity, with the flange capacity calculated assuming a constant value for β equal to 18, Figure 4-7 shows that estimated capacity of the beams is much closer to the failure load from the finite element analysis, particularly for the timber post. The estimate was between 80% and 103% of the ultimate capacity from the finite element analysis for the timber post. When this is compared to the minimum of the flange strength assuming a value of b equal to 11 (conservative value assuming a uniform stress distribution) and post strength, the interaction equation is shown to be more accurate with the timber post.

However, the minimum of the flange and post strength is generally conservative and only unconservative by 9% in the worst case with the timber post. Therefore the use of this more simplified method may be justified and is further investigated in following sections.

Neither of the above methods were conservative or accurate with the steel post. This is attributed to the high axial stiffness of the steel post which does not allow the end of the post to deform as for the timber post.

As an alternative to the interaction equation, the ultimate capacity of the beam-post joint region is calculated using the effective bearing area formulation (Eqs. 4.10 and 4.11). A value of $\alpha = 5$ is assumed, based on the 2.5:1 stress gradient assumed for web yielding in beam column connections by the AISC specifications (AISC 2005), with the resulting capacities compared to the finite element analysis given in Figure 4-8 for the different beam-post regions. This figure shows that with the timber post the method is excessively conservative with an estimated capacity of between 54% and 70% of the capacity from the finite element analysis. While it may be possible to adjust the α value to increase the accuracy in calculating the capacity of the beam-post joint region with a timber post using this method, it is uncertain how different ratios of beam and post stiffness and strength will affect this value. Therefore, the flange bending models are considered more appropriate than the bearing area model when using a timber post. For the steel post, the bearing area method is more accurate but still conservative, with capacities between 84% and 95% of the capacity from the finite element analysis. The effective bearing area method is therefore more effective than the flange bending methods with the steel post.

4.9.2 Effect of Eccentricity and Blocking on the Capacity of the Post-flange and Post

As the previous section showed two possible methods, were most suitable for calculating the capacity of the concentrically loaded, unblocked beam with a timber post, these are considered for calculating the capacity of beams with blocking and eccentricities between the centroids of the beam and post. Where blocking is used, the blocking capacity from Equation 4.16, assuming the blocking is fully effective ($\gamma = 1.0$), is added to be flange capacity to give the blocked flange capacity which was substituted for the flange capacity in the interaction equation. It is assumed that an eccentricity has little effect and thus the same methodology is used when an eccentricity of up to $^1/_6$th of the flange thickness is present.

A comparison of the calculated capacity of the flange-post joint region based on the interaction equation (Eq. 4.9) with the failure load from finite element analyses is shown in Figure 4-9 for beams with timber posts. The same four beam sections as those used previously with timber posts are assumed. The figure shows good correlation between the calculated capacity and the finite element models, with a calculated capacity of between 80% and 105% of the capacity calculated from the finite element model, with just two exceptions. These exceptions are for the larger beams with a large eccentricity, where the calculated capacity is up to 119% of that from the finite element model. This level of

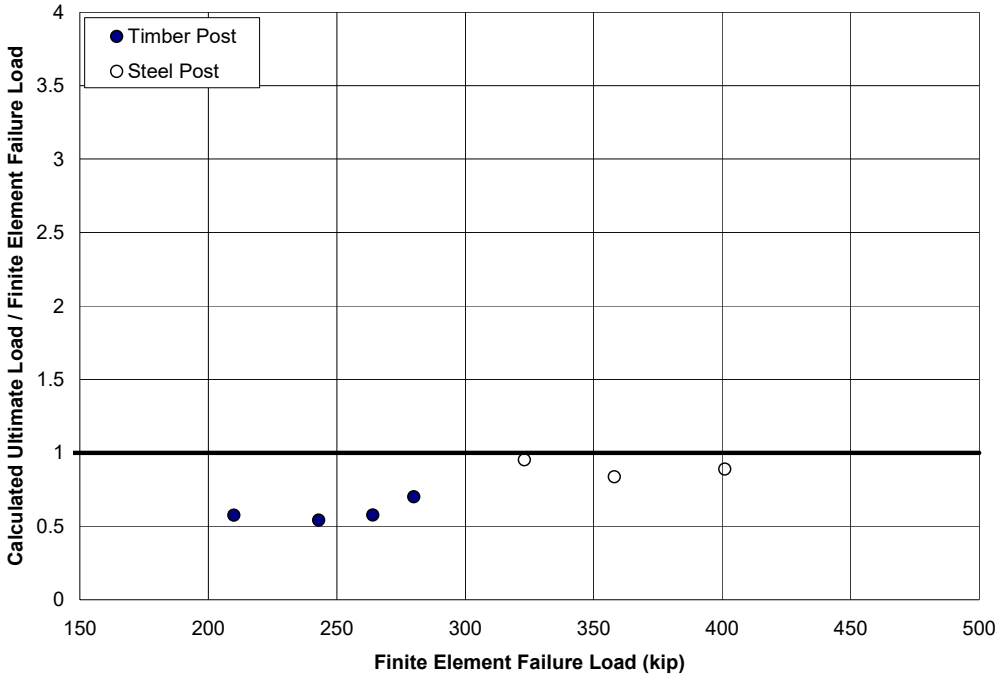

FIGURE 4-8 Comparison of calculated flange-post capacity using effective post bearing area with failure load from the finite element models for different beams

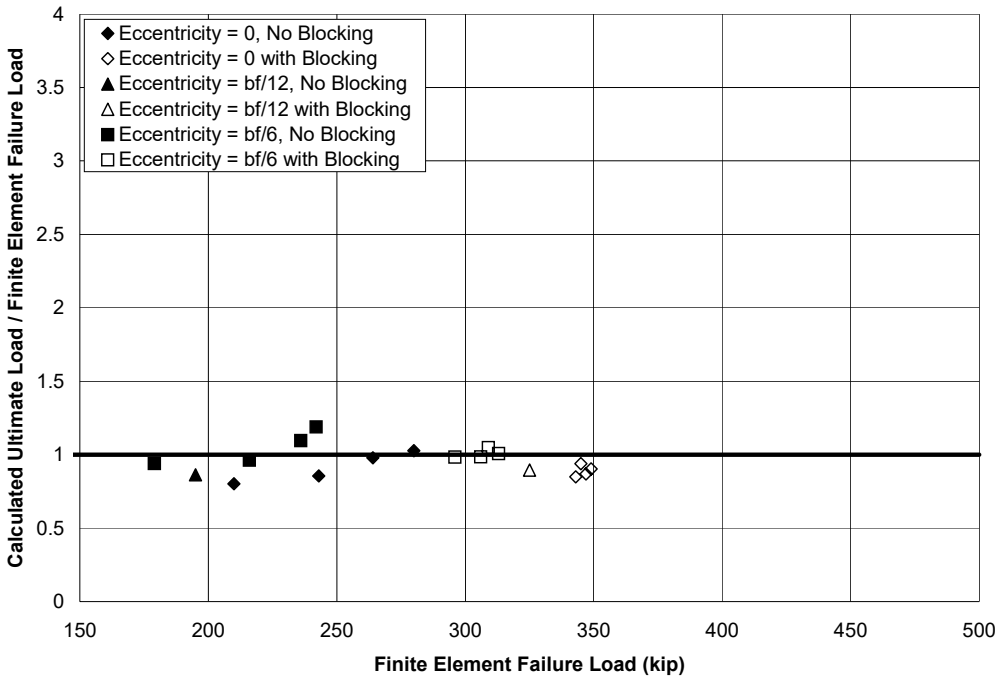

FIGURE 4-9 Comparison of calculated flange-timber post capacity using interaction equation with finite element failure load for beams with blocking and eccentricities

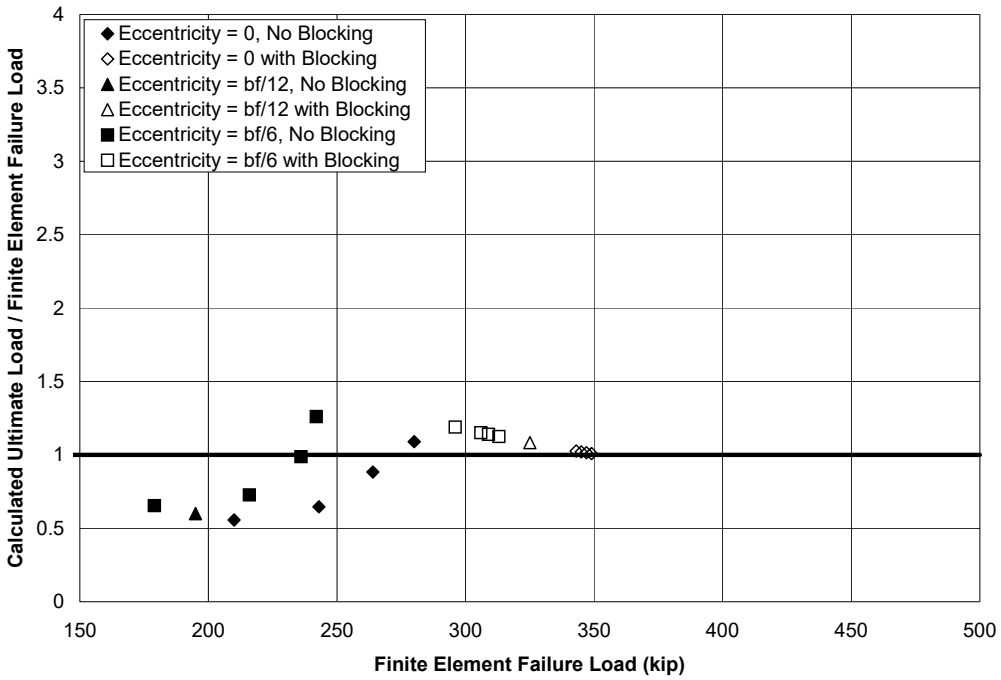

FIGURE 4-10 Comparison of calculated flange-timber post capacity using minimum of flange (β=11) and post strength with finite element failure load for beams with blocking and eccentricities

eccentricity is unlikely to occur in a real situation, therefore these cases are not of particular concern. Furthermore, when appropriate factors and nominal strengths are used in design instead of expected strengths, then even these cas es will be conservative. In practice the eccentricity should be minimized, but at worse limited to 3 times the web thickness as discussed in Section 3. This corresponds to an eccen tricity of typically around one half of the maximu m eccentricity assumed in th ese analyses. Thus, the calculated capacity based on the interaction equation appears to be relatively accurate and generally conservative for all cases including those with timber blocking.

As an alternative, the maximum of the flange capacity , assuming β = 1 1 for a uniform stress distribution, and the post capacity was calculate d for cases with blocking and eccentricities as given in Figur e 4-10. This figure showed a slightly gr eater variability in the es timated capacities co mpared to the finite element model, however the es timated capacities are generally conservative and acceptable. As with the interaction equation, the configurations with the lar gest eccentricities were most unconservative, although these eccentricities are un likely in practice and lim ited based on web limi t states d escribed in the following section. Therefore this si mplified method is considered acceptable, although the interaction method is considered to give greater accuracy.

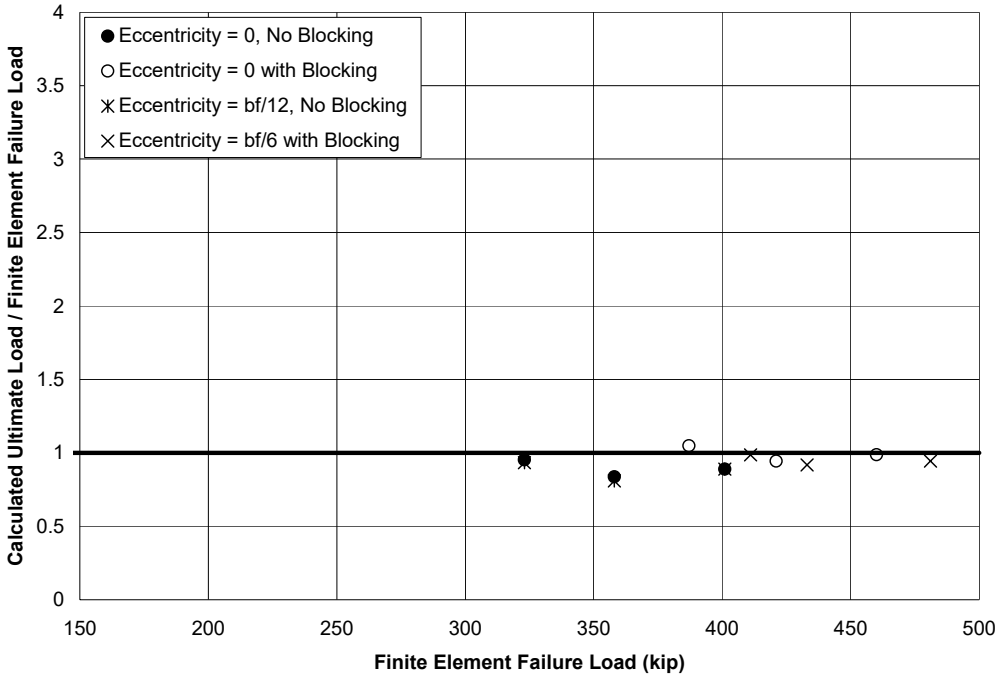

FIGURE 4-11 Comparison of calculated steel post capacity using effective yielding area with finite element failure load for beams with blocking and eccentricities

With the steel posts the ultimate capacity of the flange-post joint region is calculated using the effective bearing area method (Eq. 4.11). As the stiffness of the post is greater than the stiffness of the blocking, the effectiveness of the blocking is reduced to an assumed 30% ($\gamma = 0.3$). While the blocking could be loaded further and the force carried by the joint would continue to increase, significant flange bending and post yielding would occur resulting in significant permanent deformations in both. Thus, the effectiveness of timber blocking with a steel post is limited. Comparisons between the calculated capacity using the effective post bearing area and effective blocking capacity (Eqs. 4 and 5) and the finite element analyses are shown in Figure 4-11. The method is shown to be accurate and generally conservative, with calculated capacities between 81% and 105% of the those from the finite element model. The use of a 30% effectiveness for the timber blocking gives a ratio of calculated to finite element capacity with the timber blocking similar to that without the timber blocking. Any more and the calculated capacity with blocking capacity would tend to be unconservative.

4.9.3 Capacity of the Corbel-flange and Corbels

The strength of the corbel-flange and corbels is considered to be the lesser of Equation 4.12 and 4.15. From the component experiment on the timber corbel at the failure load and using the bearing area between the patch load and corbel (11.5 x 15 in.), results in a bearing stress equal to 0.54 ksi. Using this value, the calculated bearing capacity of the

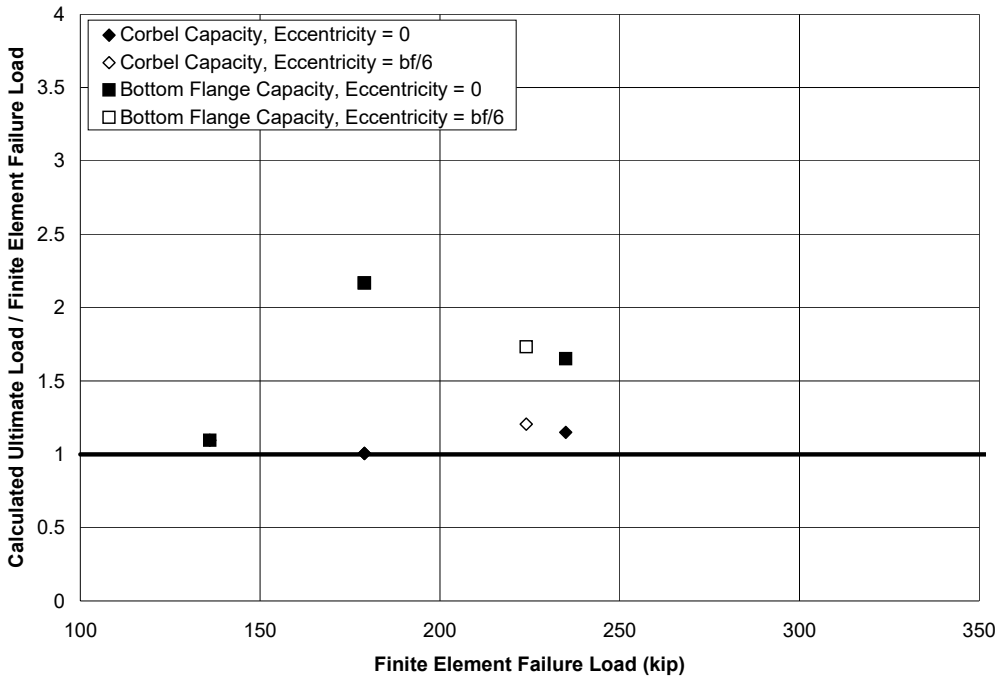

FIGURE 4-12 Comparison of calculated corbel capacity with finite element failure load for beams with corbel failures

corbels, using Equation 4.15 for different size beams, is compared to the failure load from the finite element models where corbel failure was observed in Figure 4-12. The calculated ultimate load due to corbel-flange bending, using Equation 4.12 and assuming $\beta_2 = 14$, is also compared to the finite element failure loads in this figure. It shows that the corbel-flange capacity is greater than the failure load from the finite element analysis while the corbel capacity is close to the finite element failure load. Even the corbel capacity is slightly unconservatively predicted by the equation, with calculated strengths between 101% and 121% of the finite element failure load. This is attributed to the interaction between corbel and corbel-flange. In reality, due to the sand jacks and other components between the corbels this interaction is expected to be less than observed in the finite element models, therefore the calculated capacity would become more conservative. In addition as the failure mechanism exhibits a high level of inelastic behavior, some overload, if it were to occur, will not result in catastrophic collapse. Therefore the equations for calculating the failure load are considered appropriate.

While not considered in finite element analysis or experiments, where the corbel-flange capacity is weaker than the capacity of the corbels, blocking located at the location of the corbels could be used to increase the effective corbel-flange capacity. The strength of the blocking can be directly added to the strength of the flange, in the same manner as for the post-flange.

4.10 Comparison of Calculated Limit States with Experimental Results

For the beams with timber posts, the capacity of the flange-post connection region was calculated using Equation 4.2 ($\beta = 18$) for the flange capacity, Equation 4.16 for the post capacity and Equation 4.9 for the interaction between the flange and post. When blocking was used this was added to the flange capacity assuming 100% effectiveness of the blocking. Expected strengths are again used to calculate the beam-post capacity. The resulting calculated capacity of the flange-post region for the different configurations is compared in Figure 4-13 to the estimated failure load from the experimental data. The estimated forces are approximately equal to or less than the observed forces, at between 71% and 105% of that observed, for all members. The variability is again largely attributed to the variability of material properties, particularly for the timber members, although the comparison shows that the calculated ultimate load is generally conservative even using expected strengths for the members. The lime flaking pattern observed in the beams after considerable inelastic flange bending was very similar to the yield pattern assumed in developing Equation 4.2. Therefore, this method is appropriate for predicting the capacity of the flange-post connection region with a timber post.

Alternatively, the simplified procedure using the lesser of the flange capacity (with $\beta = 11$) and the post capacity was compared to the experimental capacity of the beams. Figure 4-14 shows that there was a larger variability between the calculated and experimental capacities using this method, however, the capacities were generally conservative. The use of safety factors in design, such as allowable stresses or nominal strengths with load factors, would ensure that the capacity was not exceeded in the beam-post joint region. Therefore, based on the experimental data, as with the finite element analysis, the simplied method is acceptable but not as accurate as the interaction method.

The effective post bearing area method was used to estimate the capacity of the flange-post joint region with a steel post, based on Equation 4.11. The failure mode in the experiments with the steel post was consistent with the effective bearing area assumed for calculating the ultimate load, with yielding and crippling of the post around where it was bearing onto the beam in line with the web. Unfortunately the calculated ultimate load could not be directly compared to the experimental data as timber corbels were also used in experiments with the steel posts and these affected the ultimate load of the system.

The experimental failure load was also compared to the calculated ultimate load for the corbel-flange and timber corbels. As the corbel-flange was shown to have a greater capacity than the timber corbels for each configuration, only the corbel strength was considered for comparison with the experimental data. Figure 4-15 shows that the calculated ultimate load ranges between at between 76 and 104% of the experimental ultimate load. Therefore, the calculated ultimate load predicts the failure of the corbels relatively accurately and generally conservatively.

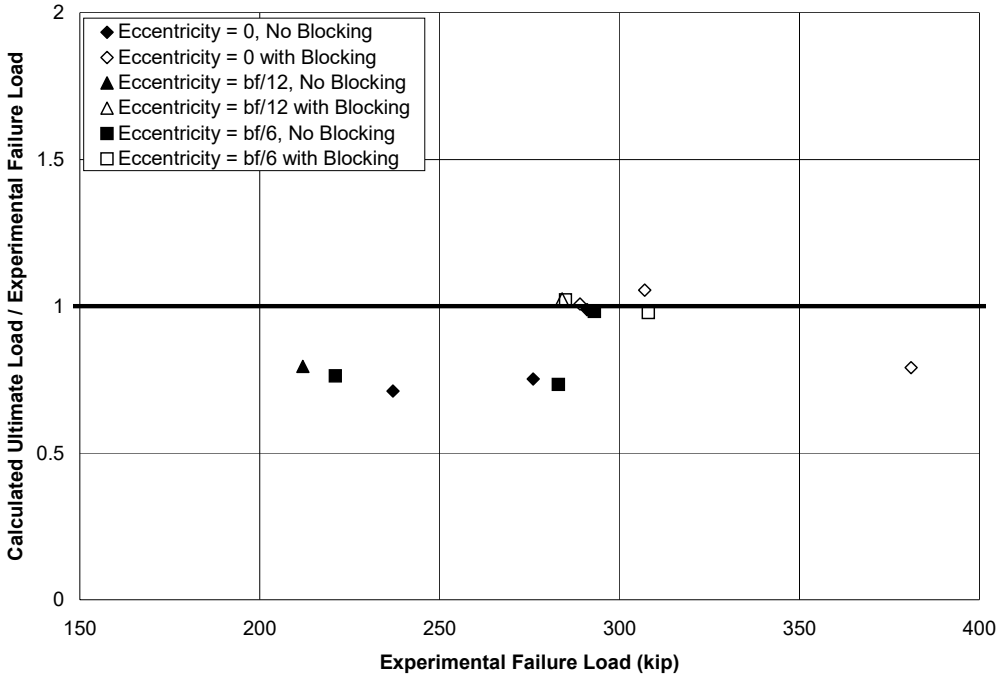

FIGURE 4-13 Comparison of calculated flange-timber post capacity using interaction equation with finite element failure load for beams with blocking and eccentricities

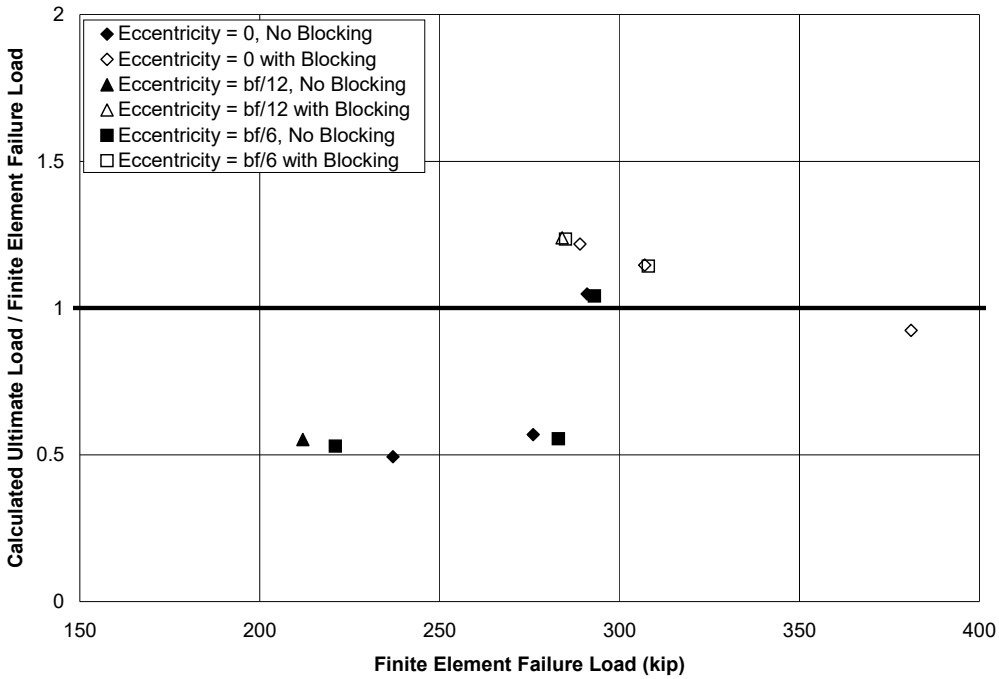

FIGURE 4-14 Comparison of calculated flange-timber post capacity using minimum of flange capacity (β=11) and post capacity with finite element failure load for beams with blocking and eccentricities

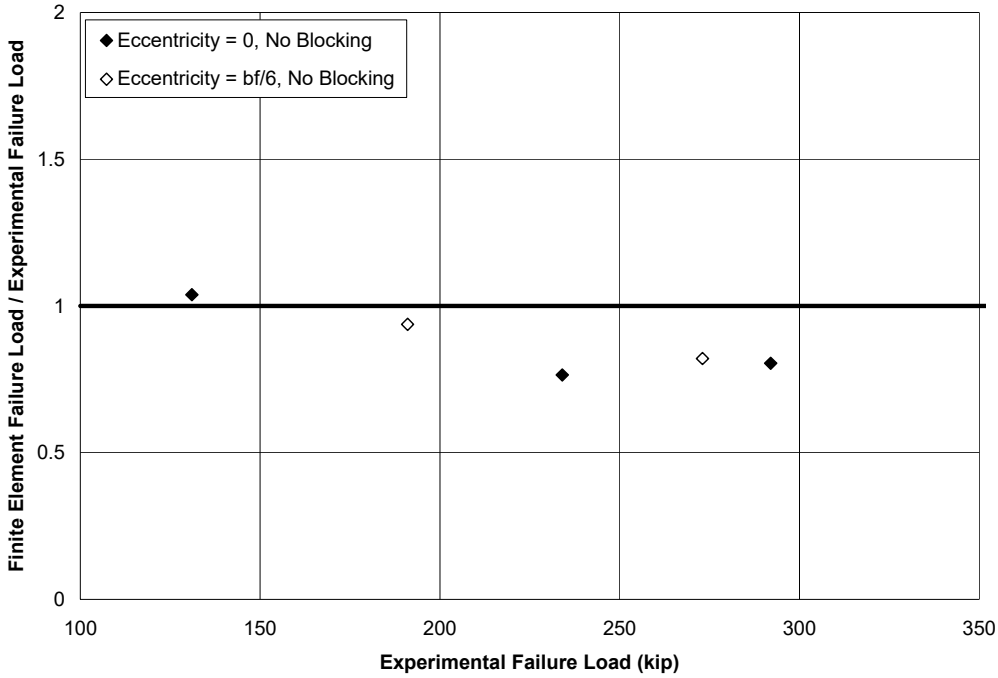

FIGURE 4-15 Comparison of calculated corbel capacity with experimental failure load for beams with and without eccentricities

SECTION 5
PREDICTION OF THE WEB YIELDING, CRIPPLING AND LATERAL BUCKLING CAPACITY

5.1 Overview

Finite element analysis and experimental data showed that there are two critical failure modes for the web of cap and sill beams in falsework. These are web yielding or crippling of the web, assuming that it is adequately stiffened or braced to prevent lateral deformation of the flanges, or lateral buckling of the web for inadequately braced beams. While in typical falsework beams, with relatively heavy webs, flange bending or post crushing is likely to govern the design of the beams, web yielding and buckling should be considered. Lateral web buckling becomes particularly critical for double stacked falsework beams.

5.2 Web Yielding and Crippling

The critical limit states for the web of beams in connection regions are web yielding and web crippling. The ultimate capacity of the web based on the web yielding limit state, R_w, loaded with a timber post can be given by:

$$R_w = (\alpha k + d_p)F_{yw}t_w \qquad ...5.1$$

where: α is a factor to allow for the stress gradient through the flange, k is the distance from the outer face of the flange to the toe of the web (Fig. 5-1), d_p is the depth of the post, F_{yw} is the yield stress in the web and t_w is the thickness of the web. Based on the Caltrans Falsework Manual (Caltrans 2001), α is equal to 2 for a 1:1 stress gradient. However, based on the AISC specifications, α is equal to 5 for an assumed 2.5:1 stress gradient through the flange and toe of the web. Appropriate stress gradients are investigated further in Section 5.5.

A similar equation can also be applied when using a steel post given by:

$$R_w = 2(\alpha(k + t_{ep}) + t_p)F_{yw}t_w \qquad ...5.2$$

where: t_{ep} is the thickness of the base plate of the steel post and t_p is the wall thickness of the round hollow steel section (Fig. 7b). This allows for yielding of the web in two locations, directly under each side of the post.

The web of these beams can also be checked for web crippling. Using the AISC specifications (AISC 2005) for web crippling, when the patch load is applied in at a

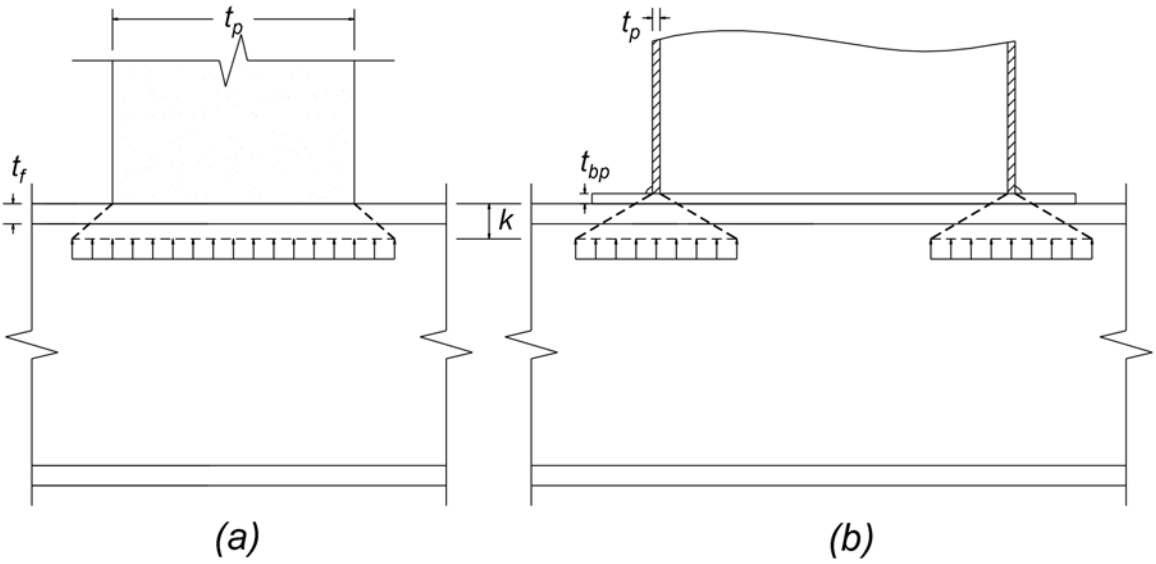

FIGURE 5-1 Effective web yielding region for a) timber post and b) steel post

distance from the end of the beam equal to at least one half of the depth of the beam, the ultimate load, R_w, is given by:

$$R_w = 0.80t_w^2\left[1 + 3\left(\frac{N}{d}\right)\left(\frac{t_w}{t_f}\right)\right]\sqrt{\frac{EF_{yw}t_f}{t_w}} \qquad ...5.3$$

where: d is the depth of the beam, t_f is the thickness of the flange and E is the elastic modulus of the steel beam.

5.3 Web Buckling

Buckling of an unbraced, unstiffened beam, where the flange is loaded with a timber or steel post is assumed to displace sideways through buckling of the web, is synonymous with column buckling. Unlike the other limit states where deformation is localized in the beam-post joint region, lateral web buckling occurs over a long length of the beam as the flexural stiffness of the flange prevents localized lateral buckling. To calculate the capacity for this limit state, the web of a beam can be treated like a column assuming that the effective length of the beam is equal to the tributary length associated with each post, which will often be equal to the spacing of the posts in a falsework bent. Based on the column buckling equations from the AISC specifications (AISC 2005), the nominal capacity of the web of a beam, R_w, can be given by:

$$R_w = t_w l_{eff} F_{cr} \quad ...5.4$$

where: l_{eff} is the effective tributary length of beam for a particular post and F_{cr} is equal to $0.877F_e$, where the Euler buckling load F_e is given by:

$$F_e = \frac{\pi^2 E}{\left(\frac{Kh}{r}\right)^2} \quad ...5.5$$

where: K is the effective length factor, h is the clear height of the web between the flanges less the fillet radius and r is the radius of gyration for the web. This assumes that the web will result in essentially elastic compression buckling, such that $F_e < 0.44F_{yw}$, which will be the case for the web of almost all beam sections. The effective length factor which will ideally range between 1.0 and 2.0 for a member that is free of deflect laterally at one end. From finite element analys es described previously for concen trically loaded beams, a K factor of 1.7 was found to be appropriate for different beams with a timber post, implying some but not full rotational restraint provided by the timber post. W ith a steel post the rotational restraint is higher, therefore assuming the s ame K value is conservative. The radius of gyration for the web alone is given by $t_w/\sqrt{12}$. If stiffeners are used to increase web buckling capacity then r will increase as calculated using conventional theory. When stiffeners are used, with a stif fener thickne ss similar to the web thic kness, la teral web buckling will not be a critical limit state in bridge falsework and need not be considered. Using the unstiffened radius of gyration and a K factor of 1.7, F_e can be simplified to:

$$F_e = \frac{\pi^2 E}{\left(\frac{6h}{t_w}\right)^2} \quad ...5.6$$

For typical beams used in bridge falsework with relatively thick webs, web buckling is unlikely to govern design. However , when b eams are stacked on top of each other , as is sometimes the case for sill beams in bridge falsework, the value of h in Equation 5.5 will become 2h and, as this is subsequently squared, F_e will be reduced by a factor of four. In this case even beams with relative thick w ebs will become susceptible to lateral web buckling.

5.4 Strength of Blocking

When used, experimental and analytical studies to follow show that the full capacity of the blocking may not be effective for increasing the web capacity. The capacity of the timber

blocking can be given by Equation 4.16 as used for calculating the additional capacity for flange bending. However, with web yielding and crippling the effectiveness factor, γ, will be reduced. Although experimental results suggested some increase in the lateral web buckling capacity for one size beam, the effectiveness of blocking is difficult to quantify with web buckling. Thus, it is recommended that either stiffeners or lateral bracing be used if necessary to increase the capacity of the web for lateral buckling.

5.5 Comparison of Calculated Strengths with Finite Element Analysis

5.5.1 Localized Capacity of Web for Braced Beams

The calculated web yielding and crippling capacity for a range of 12 and 14 in. deep beams, including: W12x26, W12x40, W12x53, W14x22, W14x30, W14x43, W14x61, W14x90, W14x132, HP12x53, HP14x73, HP14x89 and HP14x117 are compared to the failure load from finite element models in Figure 5-2. The finite element model assumed a rigid patch load applied to the beam, with lateral restraints to prevent lateral buckling. As the sections considered typical in bridge falsework, the heavier W and HP sections, all had relatively thick webs, a larger range of sections with thinner webs were considered to investigate potential web crippling. In Figure 5-2, only concentrically loaded unblocked beams are considered. In calculating the web yielding capacity two factors to account for different stress gradients were used. The first assumed a 1:1 stress gradient as in the Caltrans Falsework Manual (Caltrans 2001) thus had an α value of 2. The second assumed an α value of 5 for a 2.5:1 stress gradient as in the AISC specifications (AISC 2005). The calculated web crippling capacity was also compared to the finite element failure load. Figure 5-2 shows that web yielding assuming an α value of 2 conservatively and consistently predicts the ultimate web capacity of the beams, with calculated capacities between 85% and 91% of that from the finite element analyses. An α value of 5 typically over-predicts the web yielding capacity by up to 15% compared to the finite element model. Although, deformation of the web is observed indicative of web crippling, as shown in Figure 9c, Figure 5-2 shows that web crippling generally occurs at forces greater than the web yielding capacity for these beams.

Figure 5-3 compares the calculated web yielding capacity, assuming and α value of 2, for the different beams including those with eccentrically applied loads and with blocking for the larger beams typical of those in falsework. This figure shows that the calculated capacity was between 86 and 91% of the ultimate capacity from the finite element analysis, thus was consistently and conservatively estimated for each beam when eccentricities and blocking are considered. The blocking was assumed to be 50% effective, thus was modeled with a $\gamma = 0.5$. The cases with blocking resulted in a calculated ultimate load of between 90 and 102% of the ultimate load from the finite element analyses, therefore compared well. An equivalent transformed section, where the timber blocking is converted to an equivalent steel area, could be used instead of using the γ factor for reducing the blocking effectiveness. However, as the γ factor results in a

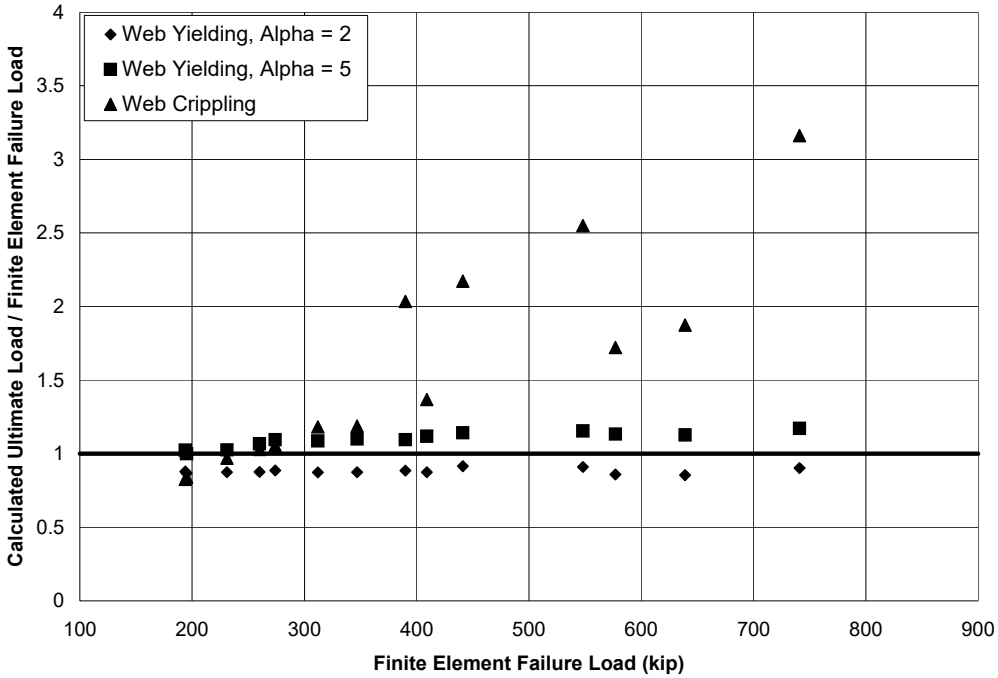

FIGURE 5-2 Calculated web yielding, and crippling capacity versus finite element failure load for concentrically load, unblocked beams

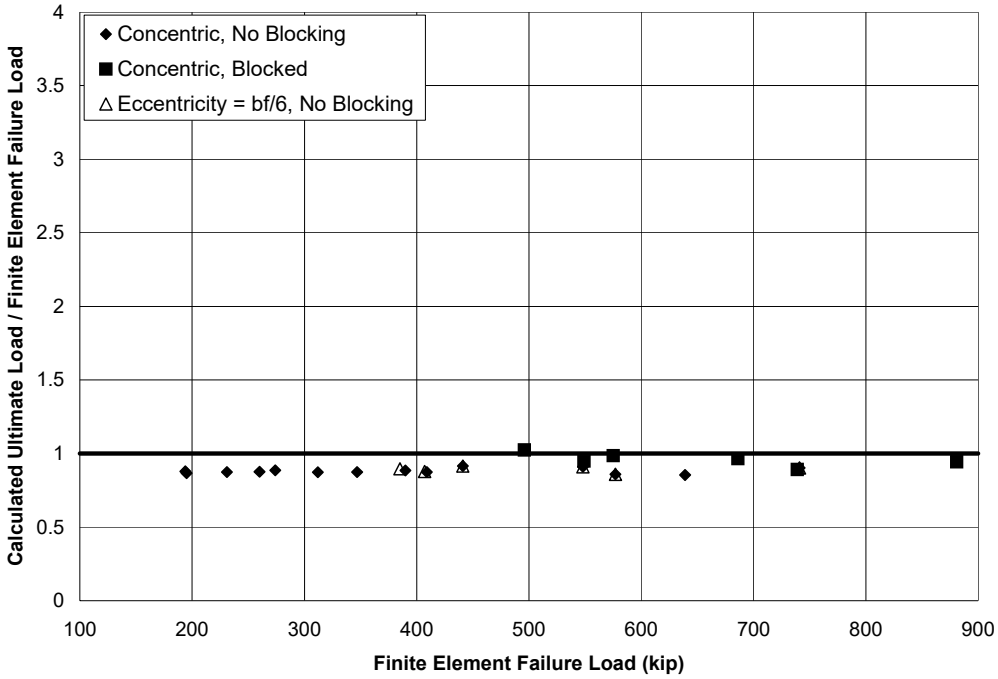

FIGURE 5-3 Calculated web yielding capacity (α=2) versus finite element failure load for different beams with blocking and eccentricities

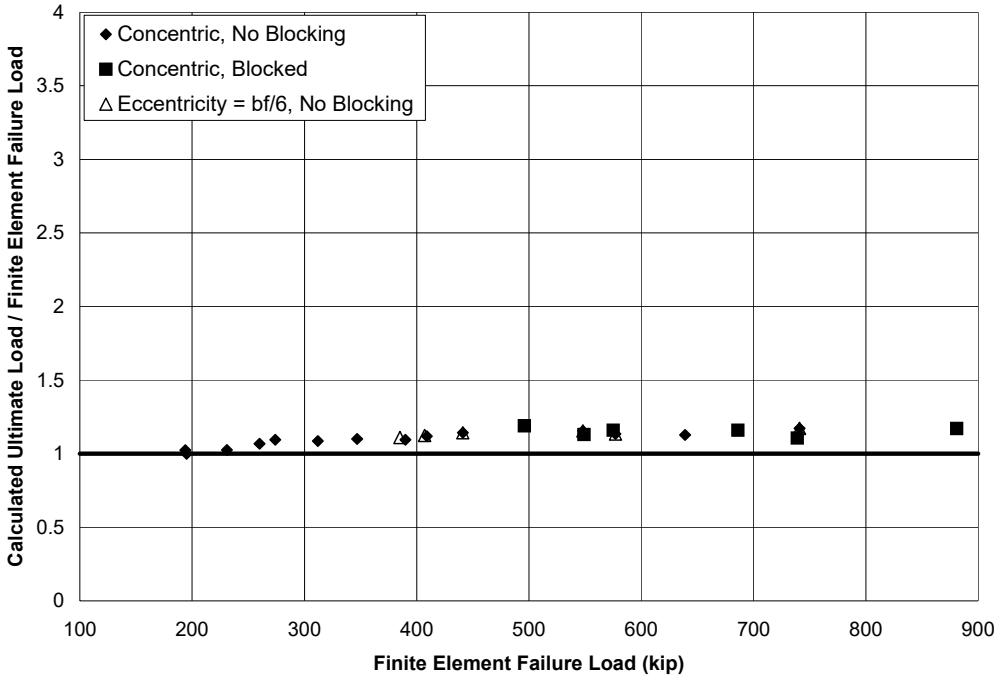

FIGURE 5-4 Calculated web yielding capacity (α=5) versus finite element failure load for different beams with blocking and eccentricities

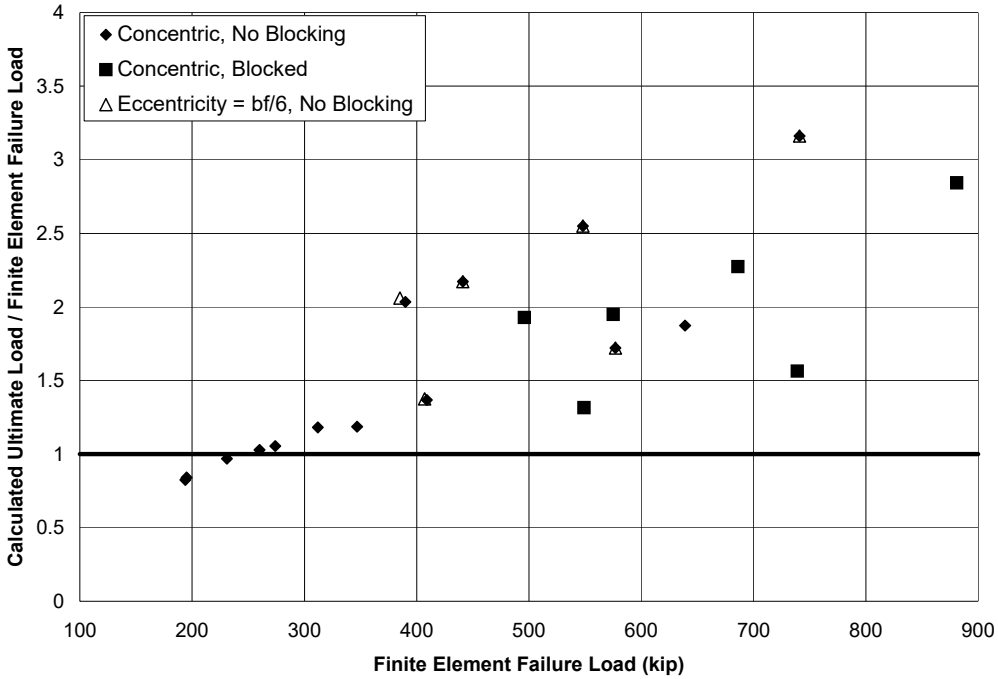

FIGURE 5-5 Calculated web crippling capacity versus finite element failure load for different beams with blocking and eccentricities

relatively accurate and consistent estimate of the ultimate capacity a transformed section is not considered necessary. The beam capacity from the eccentrically loaded cases were almost identical to the concentric cases, confirming that with a rigid patch load an eccentricity has no effect. A figure similar to Figure 5-3 compares the calculated web yielding capacity of the beams assuming an $\alpha = 5$ with the ultimate load from finite element analysis in Figure 5-4. The calculated capacity is again consistent compared to that from the finite element analysis, but unconservative by up to 19%, with this assumed α value. Therefore, an $\alpha = 2$ is considered more appropriate. If the ultimate load was defined differently, closer to the maximum load in the beam, then the α value of 5 will become less unconservative and the load would be tolerable. However, a larger amount of permanent deformation would be observed which is undesirable for reusing falsework beams.

The calculated web crippling capacity is compared to the ultimate load from finite element analysis of the beams in Figure 5-5. This figure shows that the calculated web crippling capacity is greater than the ultimate load governed by the web yielding limit state for all but the smallest W12x26 and W14x22 beams. Even for these beams, use of the web yielding formula for calculating the ultimate web capacity is conservative. In design the safety factor applied to the web crippling limit state is generally greater than for web yielding, thus it may govern for the lighter beams, although not for the heavier beams typically used in bridge falsework.

5.5.2 Lateral Web Buckling Capacity

The lateral web buckling capacity for the longer, 120in. long, beams with timber posts is compared to the calculated capacity in Figure 5-6. Lateral buckling was observed in the W12x26, W12x40, W14x22, W14x30 and W14x43 beams. When two beams were stacked on top of each other, for the larger beams like those typically used in bridge falsework, lateral buckling was observed in the HP12x53, HP14x73 and W14x90 beams. Figure 5-6 shows that assuming a K value equal to 1.7, the calculated capacity is conservative compared to the that from the finite element analyses by between 0 an 50%. The large variation is attributed to the sensitivity of the effective length factor, with a K value of 1.2 being appropriate for the beams with the largest discrepancy in the ultimate capacities. In general the K value of 1.7 is appropriate due to its conservatism.

The effect of post eccentricity was considered in Section 3 for the two beam sections most susceptible to buckling. It was found for both sections that for an eccentricity of 6 times the web thickness (1.4 in), the ultimate load dropped by around 18% of the ultimate load for the concentrically loaded beams. As the drop in load is approximately linear, this corresponds to a 3% reduction in load for each multiple of web thickness of eccentricity. The analyses show that eccentricity does have an effect on the buckling capacity of the web and large eccentricities should be avoided. Although, if accidental eccentricities are minimized and appropriate design safety factors are used, such eccentricities should not significantly affect the stability of a beam. For a reduction in strength of no more than

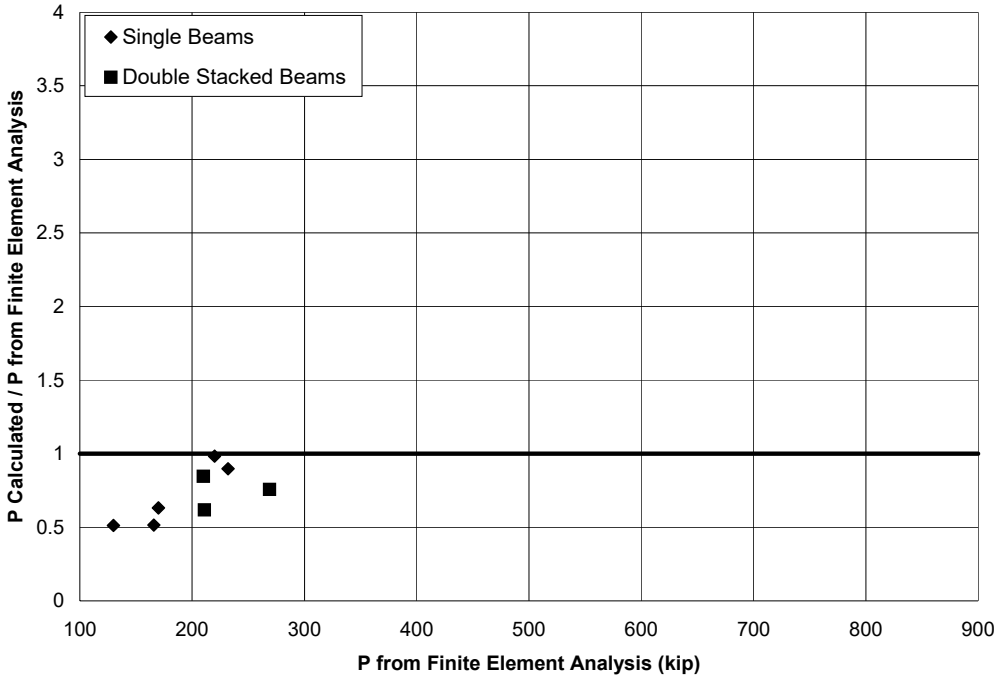

FIGURE 5-6 Calculated lateral web buckling capacity versus finite element failure load for 10 ft. long beams without blocking or eccentricities

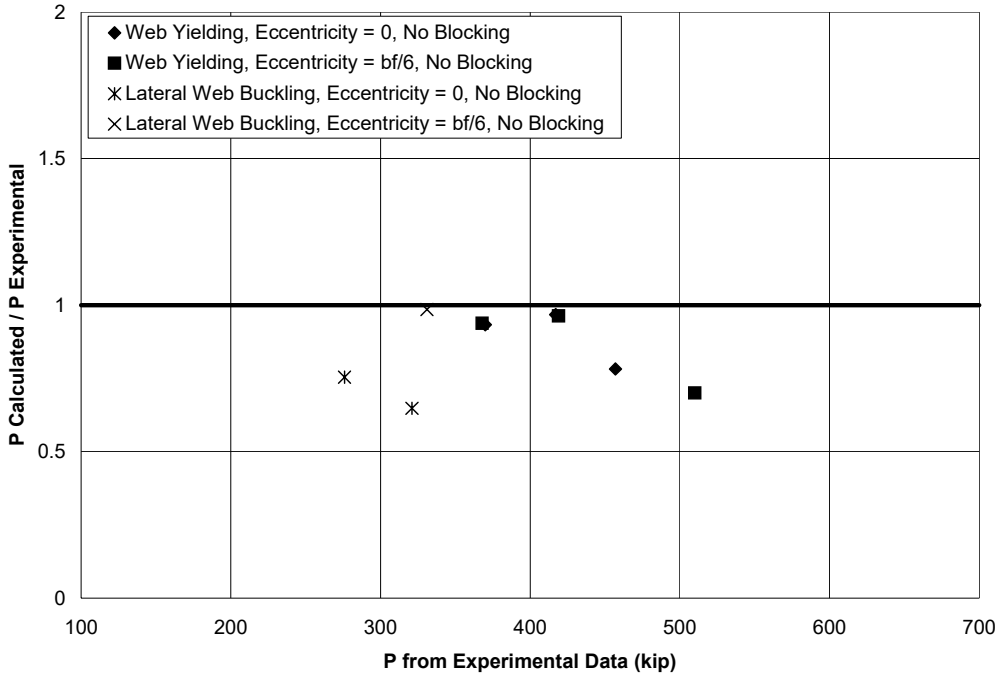

FIGURE 5-7 Comparison of calculated ultimate load using web yielding and lateral web buckling equations with the experimental failure load

10% of the concentric strengt h, the eccentricity should be limited to 3 times the web thickness.

5.6 Comparison of Calculated Strengths with Finite Element Analysis

The calculated web yielding capacity with an α value of 2 is compared to the experiment failure load for the different beams resulting in web yielding or crippling in Figure 5-7. For the beams resulting in lateral buckling, the calculated ultimate load assuming an effective length factor of 1.7 is also compared. Figure 5-7 shows that the calculated ultimate load in all cases is conservative compared to the observed failure load with the calculated load ranging between 65% and 98% of the observed load. For the HP12x53 and HP14x73 sections exhibiting web yielding the calculated load was within 7% of the observed load. For the W14x90 section the calculated ultimate load up to 30% less than the observed load. The larger difference is attributed to the thicker flange which provides some resistance to web yielding through flexure of the flange and is not considered in web yielding equation. However the calculated capacity is conservative. Using an α value of 5 as given in the AISC specifications would result in unconservatively calculated ultimate loads in each beam except the W14x90 beams. In reality a value of around 4 may be result in calculated loads on average closest to the observed failure loads, although the assumed value of 2 is conservative.

The calculated ultimate loads using the web buckling equation are conservative for the concentrically loaded (both W14x90) beams but accurate for the eccentrically loaded (HP14x73) beam that exhibited lateral buckling. The difference is again attributed to the response being very sensitive to the assumed effective length. Effective length factors of 1.48 and 1.37 respectively would result in calculated capacities identical to the observed ultimate load for the two concentrically loaded beams respectively. As the level of rotational fixity at the top of the beam is difficult to determine, assuming the more conservative value of 1.7 is appropriate.

SECTION 6
PROPOSED DESIGN OF FALSEWORK BEAMS AND POSTS FOR GRAVITY LOADS

6.1 Overview

In this section the design equations currently used for the critical limit states in falsework bents based on the Caltrans Falsework Manual (Caltrans 2001) and other predominant specifications, including the 2001 NDS specifications (AFPA 2001) for timber members, and the AISC Specifications (AISC 2005) for steel members, are examined. Equations from the different specifications are contrasted and compared with proposed equations from recent investigations. The various components of the falsework bents considered in this section are the cap beams, timber or steel posts, sill beams and corbels. It is assumed that the blocks, wedges and sand jacks between the sill beams and corbels are adequate to transfer load between the sill beams and corbels, with research on sand jacks currently being conducted at the University of California at San Diego. The stringer beams and elements above these are not considered. Foundation pads are also not considered. The equations in this section are presented in Allowable Stress Design (ASD) format, currently used in Caltrans falsework design, with equations in Load and Resistance Factor Design (LRFD) format presented in Appendix 1.

6.2 Design of Critical Members and Connections for Gravity Loads

6.2.1 Cap Beam Members for Flexure and Shear

The cap beams should be designed for the bending moments and shear forces due to the series of point loads from the reactions of the stringer beams. These limit states use conventional theory that is well established and is included in the Caltrans Falsework Manual.

6.2.2 Lateral Web Buckling in a Cap Beam

In addition to beam bending and shear, an unstiffened, unbraced cap beam should be checked for lateral web buckling based on Equations 5.4 and 5.5. There are currently no specifications for web buckling in the Caltrans Falsework Manual. The following equations are based on a modification of the column buckling formula in the AISC specifications. In ASD format the applied stress should be less than the critical buckling stress ($f_{cw} < F_{cr}$), where the applied stress, f_{cw}, is given by:

$$f_{cw} = \frac{R}{t_w l_{eff}} \qquad ...6.1$$

where: R is the reaction from a post, t_w is the thickness of the web and l_{eff} is the effective tributary length of the beam associated with a post. The critical buckling stress, F_{cr}, is given by:

$$F_{cr} = 0.525F_e \qquad ...6.2$$

where: the Euler load, F_e, is given by:

$$F_e = \frac{\pi^2 E}{\left(\frac{6h}{t_w}\right)^2} \qquad ...6.3$$

where: E is the elastic modulus, h is the clear height between the flanges less the fillet radius and r is the radius of gyration. This equation is based on elastic buckling of the web which will occur when $F_e < 0.44F_{yw}$. Most beam webs will fit into this category and where they do not, lateral web buckling need not be checked.

If the design of the beam is controlled by web buckling it is recommended that either stiffeners welded to the flanges and the web at the post location or bracing of the corbel-flange of the beam be used.

6.2.3 Web Yielding in a Cap Beam

The reaction of the cap beam from the post should be designed for web yielding such that the applied stress in the web is less than the allowable stress ($f_{cw} < F_{cwb}$). The applied stress, f_{cw}, in the beam for web yielding is given by:

$$f_{cw} = \frac{R}{(2k + d_p)t_w} \qquad ...6.4$$

where: k is the distance from the outer face of the flange to the toe of the web, d_p is the depth of the post in the longitudinal beam direction and t_w is the thickness of the web.

The allowable stress in a beam allowing for blocking, F_{cb}, is given by:

$$F_{cwb} = F_{cw}\left(1 + \frac{0.5F_{cb}'A_b}{F_{cw}(2k + d_p)t_w}\right) \qquad ...6.5$$

where: F_{cwb} is the allowable compressive stress in the web, F_{cb}' is the allowable stress in the timber blocking and A_b is the cross sectional area of the timber blocking. With no

blocking the term inside the brackets is equal to 1.0. The allowable stress in the web is 27 ksi for A36 steel based on the Caltrans S tandard Specifications (C altrans 1992) for web crippling, which are referred to by th e Falsework Manual. Based on the AISC specifications, the allowable stress would be 24 ksi for A36 steel or 33 ksi for A572 Gr50 or A992 steel.

Equation 6.4 is given in the Falsework Manual, although it is referred to as web crippling. The web crippling equation in the AISC specifications is qui te different. W eb yielding refers to loc alized ma terial y ielding in th e region of the appl ied load, whereas web crippling, based on the AISC spec ifications, refers to localized buckling of the web in the region of the applied load. For thinner webs web cri ppling may occur before web yielding, although the preceding analysis showed that web yi elding will govern for all typical falsework beams. T hus, crippling need not be c onsidered in the False work Manual. To align the Falsework Manual with current AISC specifications, Equation 3.4 should be considered web yielding.

6.2.4 Post-flange Bending in a Cap Beam with a Timber Post

6.2.4.1 Method 1 - Simplified Method

The flange-post capacity is based on flange bending assuming a uniform stress distribution from a timber post. This limit state is not currently included in the Falsework Manual. The allowable stress in the region between the fla nge of the cap beam and the post, F_{cf}, is given by:

$$F_{cf} = \frac{11 t_f^2 F_b + F_{cb}' A_b}{A_p} \qquad ...6.6$$

where: t_f is the thickness of the flange, F_b is the allowable bending stress in the flange of the beam, F_{cb}' is the allowable stress in the timber blocking, A_b is the cross sectional area of the timber blocking and A_p is the area of the post.

6.2.4.2 Method 2 - Interaction Method

For a more accurate estimate of the flange -post cap acity The conn ection between a sill beam and a timber post can be designed for the combination of flange bending and post crushing. The proposed equation for calculating the ca pacity of this connection is based on Equation 4.9, but rearranged based on and allowable stress in the post such that:

$$f_{cp} < \left(\frac{1}{F_{cf}^2} + \frac{1}{F_{cp}'^2} \right)^{-\frac{1}{2}} \qquad ...6.7$$

where: f_{cp} is the applied stress in the post from the reaction of the cap beam, F_{cp}' is the allowable stress in a short length of post (without modification by the stability factor) and F_{cf} is the allowable stress in the post-flange of the cap beam converted to an equivalent allowable post stress, given by:

$$F_{cf} = \frac{18t_f^2F_b + F_{cb}'A_b}{A_p} \qquad ...6.8$$

where: t_f is the thickness of the flange, F_b is the allowable bending stress in the flange of the beam and A_p is the area of the post.

The allowable stress in the beam flange is 22 ksi based on Caltrans Standard Specifications and AISC Specifications for A36 steel. For A572 Gr50 or A992 steel beams the allowable stress is 30 ksi. The allowable stress in a timber post or block loaded parallel to the grain based on Caltrans Standard Specifications is 1600 psi for a short length post or block. For Number 2 Douglas Fir timbers the allowable stress is 700 psi, therefore substantially less than the allowable stress in the Standard Specifications. This discrepancy is discussed in the following section. The above equation for flange bending is calibrated based on a 12 x 12 in. post. If two posts are used, this equation would conservatively predict the flange bending capacity. If smaller posts are used it would again be conservative as the width of the post relative to the width of the flange would be reduced.

6.2.5 Localized Yielding of a Steel Post from Bearing of the Cap Beam

The localized stresses in a post where a cap beam bears onto a post are designed to be less than the allowable stress ($f_{cp} < F_{cp}$). With the effective force in any blocking subtracted, the applied localized stress in the post, f_{cp}, is given by:

$$f_{cp} = \frac{R}{(5(t_f + t_{ep}) + 2k_1)2t_p} \qquad ...6.9$$

where: t_{ep} is the thickness of the end plate of the post, k_1 is the distance from the centroid of the beam web to the edge of the fillet and t_p is the thickness of the post wall.

The allowable stress in the steel post, allowing for blocking, F_{cpb}, is given by:

$$F_{cpb} = F_{cp}\left(1 + \frac{0.3F_{cb}'A_b}{F_{cp}(5(t_f + t_{bp}) + 2k_1)2t_p}\right) \qquad ...6.10$$

where F_{cp} is the allowable compression stress in the steel post. For an A500 GrB (42 ksi) round hollow steel section the allowable steel stress would be 28 ksi based on the AISC steel specifications. Conservatively, the same allowable stress to that used for web yielding could be used for an A36 steel beam could be used for the post.

6.2.6 Timber Post Design

The current equation for the design of a timber post for compressive forces in the Falsework Manual requires the applied stress to be less than the allowable stress in the post ($f_{cp} < F_{cp}'$), where F_{cp}' (in psi) is given by:

$$F_{cp}' = \frac{480000}{\left(\frac{L}{d_p}\right)^2} \leq 1600 \qquad ...6.11$$

where: L is the length of the post, d_p is the depth (or width, whichever is less) of the post. The NDS Specifications design for an applied stress less than the modified allowable stress ($f_{cp} < F_{cp}'$) where the modified allowable stress is given by:

$$F_{cp}' = C_p F_c^* \qquad ...6.12$$

where: F_c^* is the allowable compression stress multiplied by all applicable adjustment factors except the column stability factor and C_p is the column stability factor given by:

$$C_p = \frac{1 + \frac{F_{cE}}{F_c^*}}{2c} - \sqrt{\left[\frac{1 + \frac{F_{cE}}{F_c^*}}{2c}\right]^2 - \frac{F_{cE}}{cF_c^*}} \qquad ...6.13$$

where: $c = 0.8$ for sawn timber, F_{cE} is given by:

$$F_{cE} = \frac{K_{cE} E'}{\left(\frac{l_e}{d_p}\right)^2} \qquad ...6.14$$

where: K_{cE} is a constant equal to 0.3 for visually graded timber, E' is the allowable elastic modulus, l_e is the effective length of the column which can be assumed to equal L for falsework applications. This calculation of C_p is quite cumbersome, therefore for a 12 x 12 in. Number 2 Douglas Fir post with and allowable elastic modulus of 1300 ksi and other values as given above based on typical moisture content, temperature and other

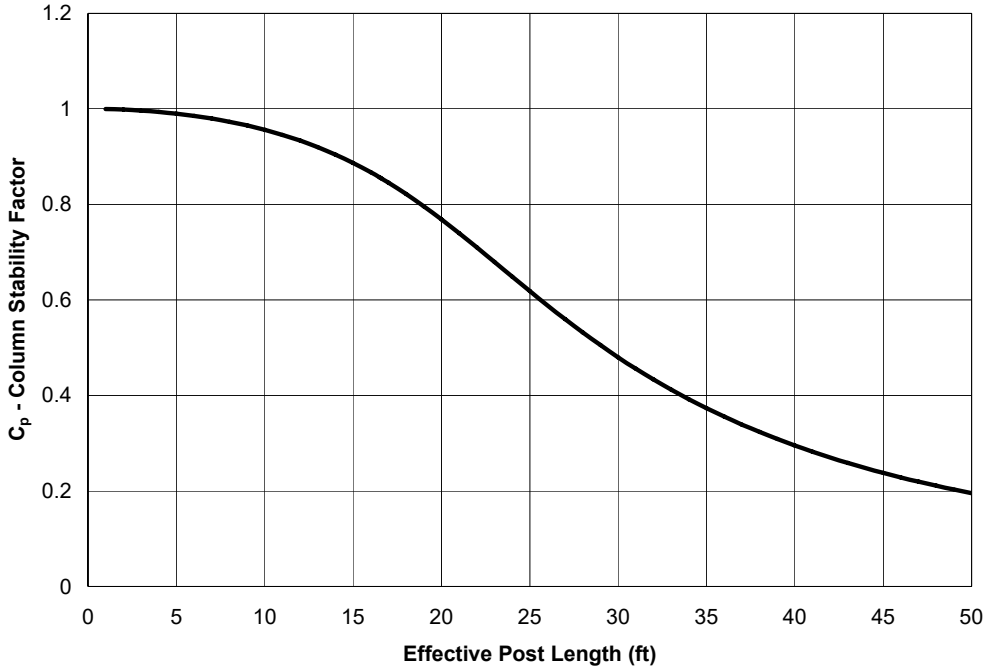

FIGURE 6-1 Column stability factor, C_p, for 12 x 12 in. Number 2 Douglas Fir posts of different lengths (AFPA 2001)

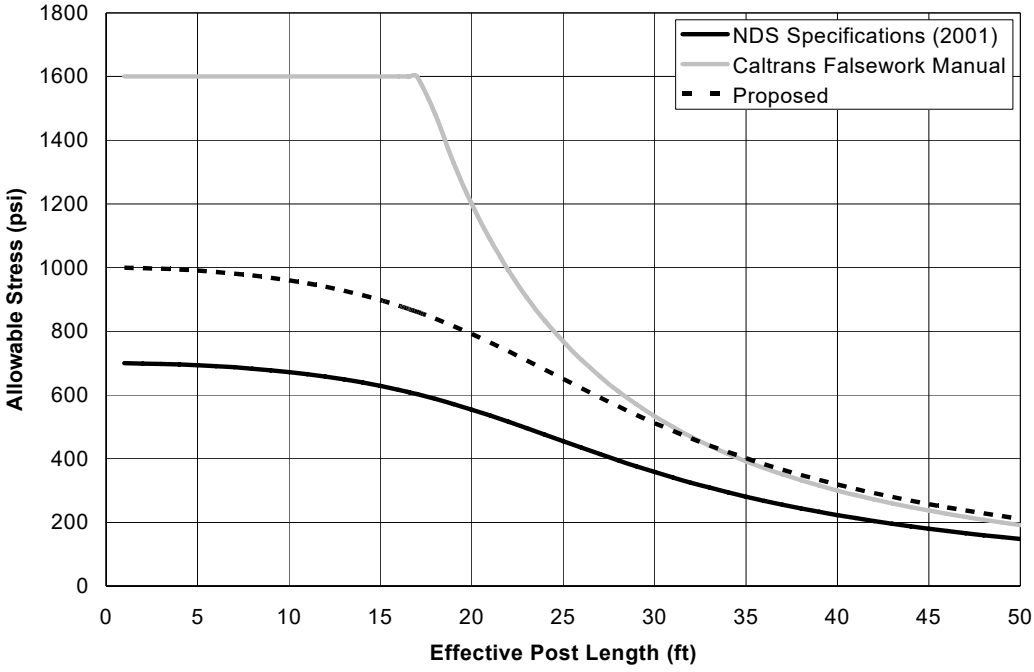

FIGURE 6-2 Allowable stress vs post length for 12 x 12 in. Number 2 Douglas Fir timber posts based on the NDS specifications and Caltrans Falsework Manual

conditions, C_p is plotted against column length in Figure 6-1. The slenderness of the post l_e/d_p should not exceed 50.

The maximum allowable stress parallel to the grain, F_c^*, is 700 psi for a Number 2 Douglas Fir member based on the NDS specifications. Thus the allowable stress in different length posts are given in Figure 6-2. This results in much lower allowable stresses than the Caltrans Falsework Manual, which has a maximum allowable stress of 1600 psi, with no reduction for posts up to 16.5 ft. long. Based on the component experiments using three short (4 ft. long) posts, the minimum failure load from the three posts was 221 kip, corresponding to a failure stress based on actual post dimensions is 1670 psi. This is very close almost equal to the allowable stress in the timber post based on the Caltrans specifications, thus with no safety factor, the Caltrans specifications are unconservative. However, given that the allowable stress found typical for the posts, used in the finite element model based on the other component experiments is 2660 psi, an allowable stress of 700 psi is excessively conservative. Thus, based on this limited data, an allowable stress of 1000 psi is considered appropriate. Using nominal post dimensions instead of the actual dimensions, a 1000 psi allowable stress has a safety factor of at least 1.5, with an average safety factor of 2.4. Figure 6-2 shows that assuming a maximum allowable stress of 1000 psi and using the C_p factor based on the NDS specifications results in reduced allowable stresses for shorter columns, but similar stresses for longer columns compared to the Caltrans specifications. Further research on the material properties would be beneficial.

6.2.7 Steel Post Design

The current equation for the design of a steel post in the Falsework Manual requires the applied stress to be less than the allowable stress in the post ($f_{cp} < F_{cp}$), where F_{cp} (in psi) is given by:

$$F_{cp} = 16000 - 0.38\left(\frac{L}{r}\right)^2 \qquad ...6.15$$

where: r is radius of gyration of the post. Based on the AISC specifications the allowable stress is given by:

$$F_{cp} = 0.525F_e \text{ for } (F_e < 0.44F_{yp}) \qquad ...6.16$$

or

$$F_{cp} = 0.658^{\frac{F_y}{F_e}}(0.6F_{yp}) \text{ for } (F_e > 0.44F_{yp}) \qquad ...6.17$$

where F_{yp} is the minimum yield stress of the post and F_e is given by:

$$F_e = \frac{\pi^2 E}{\left(\frac{KL}{r}\right)^2} \qquad ...6.18$$

where: K is the effective length factor assumed to equal 1.0 and E is the elastic modulus of the steel. For a A500 GrB (42 ksi) post the maximum allowable stress from the AISC specifications would be 25 ksi. The maximum stress based on the Caltrans equation is equal to 16 ksi, therefore is much more conservative than the AISC specifications. This conservatism continues for longer posts, as shown by Figure 6-3 for an 18 in. dia., $^3/_8$ in. thick, round steel hollow post, up to a length of 60 ft. For posts longer than 60 ft the capacity is similar. While there is no experimental data to suggest a preference of either method, the AISC equation has been developed more recently based on a larger base of experimental data.

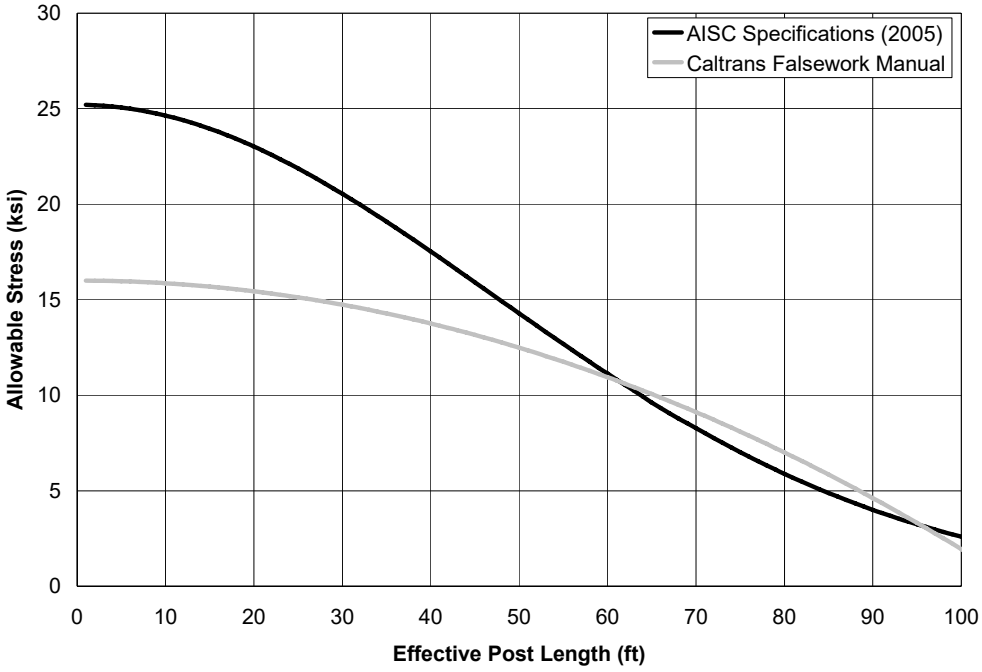

FIGURE 6-3 Allowable stress vs post length for 18 in. diameter 3/8 in. thick round hollow steel post based on the AISC specifications and Caltrans Falsework Manual

6.2.8 Localized Yielding of a Steel Post due to Bearing onto a Sill Beam

As at the top of a post where the cap beam b ears onto the post, the base of a steel post should be designed for localized yielding wh ere it bears on to a sill beam. The same formulation as that for the top of the post can be used (Eqs. 6.9 and 6.10).

6.2.9 Flange Bending-Post Crushing in a Sill Beam with a Timber Post

The design of the flange-post bearing region for a timber post bearing onto a sill beam should be consider ed in the same way as that for a cap beam bearing onto a post using either of the two methods described in Section 6.2.4 (Eqs. 6.6 to 6.8).

6.2.10 Web Yielding in a Sill Beam

The web of the sill beam should be checked for localiz ed stresses using the same equations as that for the cap beam (Eqs. 6.4 and 6.5).

6.2.11 Lateral Web Buckling in a Sill Beam

Lateral buckling of the web of a sill beam should be checked using Equations 6.1 through 6.3 as for the cap beam. Where double stacked sill beams are used, the height of the web in Equation 6.3 is considered to be the comb ination of heights of the two beams. For double stacked beams this limit state may b ecome critical, in which case fully welded stiffeners should be used beneath the post or the post-flange should be laterally braced.

6.2.12 Corbel-flange Bending in a Sill Beam

The corbel-flange of the sill beam, where it bears onto the wedges, sand jacks, blocks and corbels, should be checked for adequate beam flange capacity . This check is made by ensuring that the applied stress between the beam and supports above the corbels is less than the allowable bearing st ress due to flange bending ($f_{bg} < F_{gf}$). The applied bearing stress, f_{bg}, is given by:

$$f_{bg} = \frac{R}{A_{bg}} \qquad ...6.19$$

where: R is the applied load from a post and A_{bg} is the bearing area between the beam and its supports above the corbels. The allo wable bearing stress based on corbel-flange capacity and capacity of any blocks between the flanges, F_{gf}, is given by:

$$F_{gf} = \frac{14 t_f F_b + F_{cb}' A_b}{A_{bg}} \qquad ...6.20$$

where: t_f is the thickness of the corbel-flange, F_b is the allowable bending stress in the flange, F_{cb}' is the allowable compression stress in the blocking (1000 psi as for post), A_b is the cross-sectional area of the blocking and A_{bg} is the overlap (bearing) area between the flange and corbels. This equation assumes that at least two corbels are used beneath each post with a spacing between the corbels of at least 24 in. If only a single corbel is used then the equation need not be checked as corbel crushing will govern the response for all practical beam sizes. If blocking is required to increase the flange-corbel interaction strength, it can be placed directly under the post, unless there are corbels located more than 24 in. from the center of the post, in which case blocking should be also be placed directly above these corbels.

6.2.13 Corbel Capacity

The applied stress between the supports of the sill beams and the corbels should be compared to the allowable stress perpendicular to the grain in the corbels ($f_{bg} < F_{c\perp}$). The applied stress is given by:

$$f_{bg} = \frac{R}{A_{bg}} \qquad ...6.21$$

where: R is the applied post load and A_{bg} is the bearing area onto the corbels. The allowable stress in a Number 2 Douglas Fir member loaded perpendicular to the grain based on NDS specifications is 625 psi. The allowable stress in the Caltrans Standard Specifications is 450 psi. The calculated failure stress of the corbels from the component experiment, which was also found to be reasonable for the other experiments, was 540 ksi. Therefore, the allowable stress from the NDS specifications is very unconservative, as the allowable stress is greater than the observed failure stress. Even the allowable stress from the Caltrans specifications only has a factor of safety of 1.2. As the failure mechanism for a corbel is very stable, large deformations possible and an increasing load observed after failure, a relatively low factor of safety is acceptable. However, it is evident that no increase in the allowable stress of 450 psi should be made to compare with the NDS specifications.

6.3 Comparison of Different Limit States in Beams and Posts

6.3.1 Comparison using Actual Strengths

The critical limit states in cap and sill beams, posts and corbels are compared using the actual strengths based on the experimental data in Table 6-1. It is assumed that the beam

TABLE 6-1 Comparison of calculated ultimate beam, post and corbel loads based on actual strengths from experiments (kip)

Section	HP12x53	HP14x73	HP14x89	W14x90	W14x90	HP14x117	W14x120
Post Type	**Timber**	**Timber**	**Timber**	**Timber**	**Steel**	**Steel**	**Steel**
Flange - Post Interation[1,2]	168	208	258	288	308	299	356
Bottom Flange Bending[3]	149	200	296	388	388	505	680
Corbel Crushing[4]	149	182	182	180	270	277	274
Web Yielding[5]	333	389	481	345	473	924	716
Lateral Web Buckling[6]	711	814	1460	521	521	[7]	1260
Lateral Web Buckling for a Double Stacked Beam[6]	178	204	364	130	130	817	315
Post Strength - 4 ft long	352	352	352	352	888	888	888

Notes: 1. Top flange bending capacity is based on beta = 18.

2. Interaction equation used for timber post, effective post bearing area with alpha = 5 used for steel post.
3. Beta = 14 for bottom flange bending.
4. Two corbels spaced 24 in. apart o.c. assumed with timber post, three corbels with outer corbe spaced 24 in. apart o.c. assumed with steel post
5. Alpha = 2 for timber post and 5 for steel post
6. Assumed effective length of 10 ft
7. $P_{cr} > 0.44\ F_y$ and will not govern

represents a sill beam with a post bearing on the post-flange and corbels below the beam, although the flange-post behavior is equally applicable for a cap beam. The different limit states considered are: an interaction be tween flange bending (using the more accu rate interaction method) and post compression stre ngth with a timber post; Localized post yielding for the steel post; co rbel-flange bending; corbel crushing; web yielding; web crippling, and; lateral web buckling assumi ng 10 ft. long beams. Table 6-1 shows that corbel crushing typically govern s the response of all cases with single stacked beams. This is followed by post-flange bending a nd post crushing or localized yielding. The flange-post capacity is smaller than the web capacity for all but the double stacked beams where lateral buckling can govern the capacity. It shows that for b eams with thick webs, like those typically used in bridge falsework, web limit s tates are unlikely to control the capacity of the beam-post re gions. However, for double stacked beams lateral bracing of the beams should be used to pr event lateral web buckling if it is calculated to govern the capacity.

TABLE 6-2 Comparison of calculated allowable beam, post and corbel loads based on original Caltrans allowable stresses (kip)

Section	HP12x53	HP14x73	HP14x89	W14x90	W14x90	HP14x117	W14x120
Post Type	**Timber**	**Timber**	**Timber**	**Timber**	**Steel**	**Steel**	**Steel**
Flange - Post Interation[1]	N/A						
Bottom Flange Bending[1]	N/A						
Corbel Crushing	130	158	159	156	235	241	238
Web Yielding	163	189	232	177	232	454	351
Lateral Web Buckling[2]	N/A						
Lateral Web Buckling for a Double Stacked Beam[2]	N/A						
Post Strength - 4 ft long	230	230	230	230	307	307	307
Post Strength - 15 ft long	230	230	230	230	304	304	304
Post Strength - 30 ft long	77	77	77	77	286	286	286

Notes: 1. No current procedure for flange bending

2. No current procedure for web buckling

6.3.2 Comparison using Allowable Stresses based Current Caltrans Provisions

Table 6-2 shows the calculated load in each of the components based on allowable stresses currently used in Caltrans falsework design. The beams are assumed to be A36, with an allowable stress of 27 ksi for web yielding (termed crippling in the Falsework Manual). Post compression strength is added to the comparison, with the timber posts assumed to have an allowable maximum compression capacity of 1600 psi, modified for the appropriate length based on Equation 6.11. The timber corbels have an allowable stress of 450 psi with the bearing area assumed to be equal to the width of the beam flange multiplied by the combined width of the corbels. Nominal dimensions of 12 in. are used for the posts and corbels instead of the actual dimension of 11.5 used in generating Table 6-1, as this is typical of design practice. As there are no provisions for flange bending and web buckling, these are not included in Table 6-2.

Post compression strength is shown to govern for the longer timber post, and corbel crushing governs when shorter timber posts and steel posts are used. Although, the allowable post strength for the shorter post is less than that observed in typical experiments, it is greater than observed in the weakest post component experiment (221 kip), therefore the allowable post strength is not always conservative. Table 6-1 showed that web yielding is unlikely to govern, although when allowable stresses and A36 steel is considered, Table 6-2 shows that it becomes more likely.

TABLE 6-3 Comparison of calculated allowable beam-post loads based on recommended strengths from experiments (kip)

Section	HP12x53	HP14x73	HP14x89	W14x90	W14x90	HP14x117	W14x120
Post Type	**Timber**	**Timber**	**Timber**	**Timber**	**Steel**	**Steel**	**Steel**
Flange Bending -Simplif.[1]	47	63	93	122			
Flange - Post Interaction[2]	68	84	105	117			
Localized Post Yielding[3]					157	152	181
Bottom Flange Bending[4]	60	80	118	155	155	202	272
Corbel Crushing[5]	130	158	159	156	235	241	238
Web Yielding[6]	145	168	206	157	206	403	312
Lateral Web Buckling[7]	427	488	875	313	313	[8]	756
Lateral Web Buckling for a Double Stacked Beam[7]	107	122	219	78	78	490	189
Post Strength - 4 ft long	143	143	143	143	480	480	480
Post Strength - 15 ft long	129	129	129	129	463	463	463
Post Strength - 30 ft long	74	74	74	74	398	398	398

Notes: 1. Flange bending capacity is based on beta = 11

2. Flange bending capacity when using interaction equation is based on beta = 18.
3. Effective post bearing area defined with alpha = 5 for steel post.
4. Beta = 14 for corbel flange bending.
5. Two corbels spaced 24 in. apart o.c. assumed with timber post, three corbels with outer corbels spaced 24 in. apart o.c. assumed with steel post
6. Alpha = 2 for timber post and 5 for steel post
7. Assumed effective length of 10 ft
8. $P_{cr} > 0.44\ F_y$ and will not govern

6.3.3 Comparison using Allowable Stresses based Recommended Provisions

Based on the allowable stresses recommended in this report for the beams, posts and corbels, a comparison of the different critical limit states is made in Table 6-3. The beams are assumed to be A36, with allowable stresses of 22 ksi for flange bending and 24 ksi for web yielding. F_{cr} was reduced to 60% of the nominal value based on the allowable stresses for web buckling. The timber posts are assumed to have an allowable compression capacity of 1000 psi and the timber corbels have an allowable stress of 450 psi with nominal (12 in.) post and corbel dimensions used.

The resulting comparison is quite different from Table 6-1, as the strength of the beams are reduced from 55 ksi, the actual strength of an A572 Gr50 or A992 beam, compared to the 22 to 24 ksi allowable stresses. In addition, the safety factors for allowable stresses on the corbels are smaller than those for the beams and posts, thus the relative strength of the

corbels increased. This is justified as corbel crushing will not cause immediate collapse, while post crushing or web buckling is more likely to cause collapse. Table 6-3 shows that post compression strength is still likely to govern for longer posts and even for a shorter post the allowable load is reduced significantly compared to the current Caltrans procedure (Table 6-2). If the posts are short enough, flange bending-post crushing is shown to govern the response with the timber posts and smaller beams. Lateral web buckling of double stacked beams may also be critical. Therefore, compared to Table 6-2, potentially critical limit states, such as flange-post interaction and lateral buckling, are not considered by the current Caltrans Falsework Manual. Where flange bending becomes critical, blocking can be used to increase the capacity of both the post-flange and corbel-flange.

SECTION 7
DESIGN EXAMPLES

7.1 Overview

Two design examples are considered where the cap beam, post, sill beam and corbels are designed. The bridge in the first example has a relatively low height and the loads are relatively low thus timber posts are chosen. In the second example, the bridge is assumed to be higher with falsework bents and posts spaced further apart, thus steel posts are chosen. The critical steps are described for the gravity load design. Lateral loads are not considered.

7.2 Design of Falsework with Timber Posts

7.2.1 Loads

The critical limit states in a falsework bent with a timber post are illustrated in Figure 7-1. Based on falsework plans for the Arch Road Stage 4 Bridge (J. Lammers, Caltrans, Personal communication), with a general falsework layout and typical cross sections shown in Appendix 2, it is assumed that the applied load from the superstructure of the bridge, and including the joists and stringer beams is:

$$p_{D+L} = 450 \text{ psf}$$

For falsework bents spaced 20 ft apart, the line load on the cap beam of the falsework bent is:

$$w = 9000 \text{ lb/ft} = 9.00 \text{ kip/ft}$$

7.2.2 Cap Beam Bending

Try an A36, HP12x53 section for the cap beam, with a weight of 53 lb/ft, giving a total weight on the cap beam of:

$$w = 9.05 \text{ kip/ft}$$

If the posts are spaced 10 ft apart in the bent then the maximum bending moment in the bent can be conservatively calculated by:

$$M = \frac{wL^2}{8} = \frac{9.05(10^2)}{8} = 113 \text{ kip-ft} = 1360 \text{ kip-in}$$

and the applied stress is:

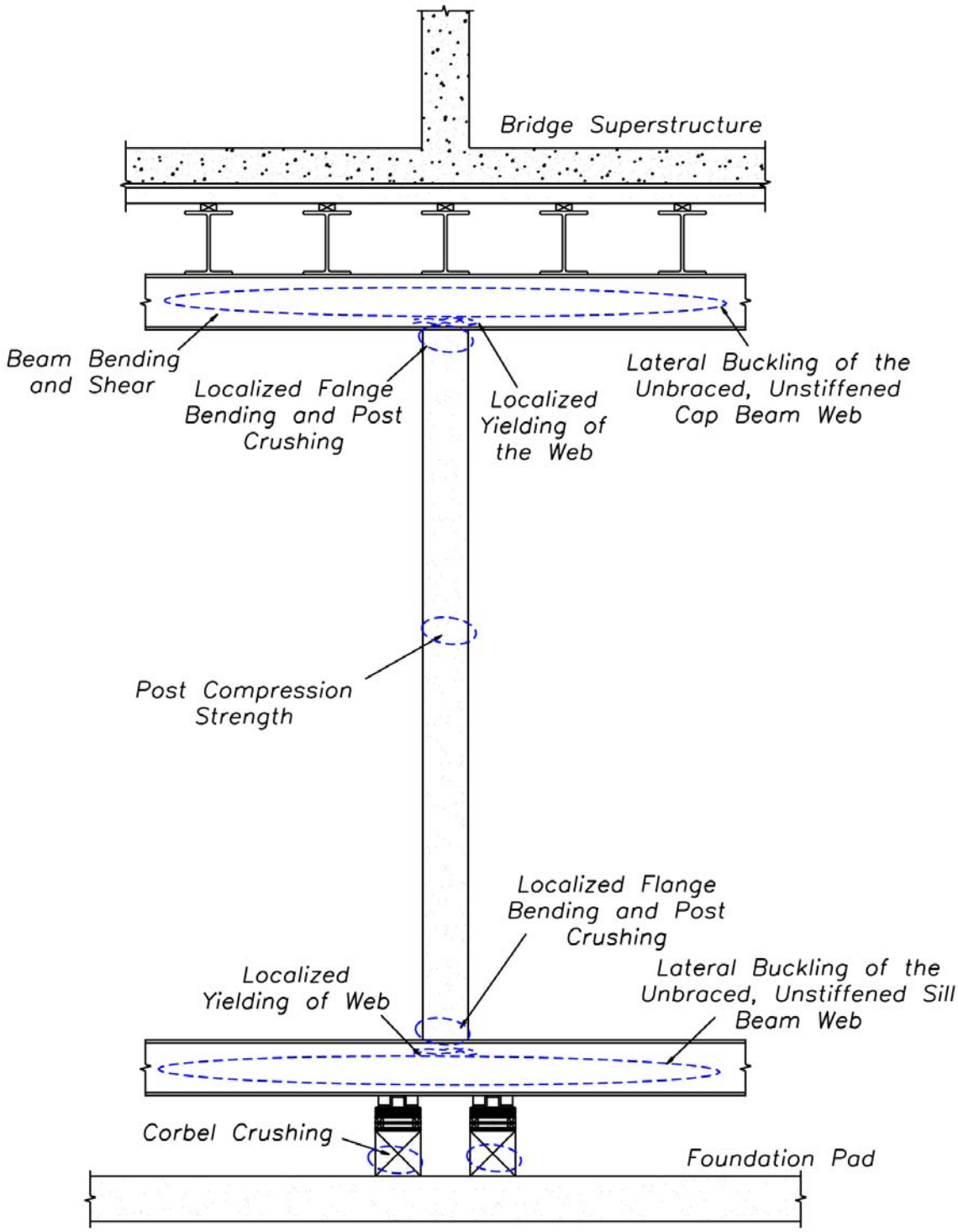

FIGURE 7-1 Portion of a falsework bent with timber post identifying critical limits states

$$f_b = \frac{M}{Z} = \frac{1370}{74} = 18.3 \text{ ksi}$$

compared to the allowable stress of:

$$F_b = 22 \text{ ksi}$$

which is greater than f_b, therefore the beam is adequate for bending.

7.2.3 Cap Beam Shear

The applied shear is:

$$V = \frac{wL}{2} = \frac{9.05(10)}{2} = 45.3 \text{ kip}$$

giving an applied shear stress:

$$f_v = \frac{V}{A_w} = \frac{45.3}{12(0.44)} = 8.57 \text{ ksi}$$

compared to the allowable stress:

$$F_v = 14.5 \text{ ksi}$$

which is greater than f_v, therefore the beam is adequate for shear.

7.2.4 Lateral Web Buckling in the Cap Beam

The reaction in the beam is:

$$R = wL = 9.05(10) = 90.5 \text{ kip}$$

thus, the average applied stress in the web for an effective length in the web of 10 ft is:

$$f_{cw} = \frac{V}{t_w l_{eff}} = \frac{90.5}{0.44(10)(12)} = 1.71 \text{ ksi}$$

The Euler buckling load for the web is given by:

$$F_e = \frac{\pi^2 E}{\left(\frac{6h}{t_w}\right)^2} = \frac{\pi^2(29000)}{\left(\frac{6(10.21)}{0.44}\right)^2} = 14.8 \text{ ksi}$$

Check: $F_e < 0.44\ F_y < 0.44(36) < 15.8$ ksi - Yes, therefore check of critical load should be made. Note that if $F_e > 0.44\ F_y$ then web is non slender as a equivalent column and check would not be necessary.

The critical load is given by:

$$F_{cr} = 0.525\ F_e = 0.525(14.8) = 7.77 \text{ ksi}$$

which is greater than f_{cw}, therefore the beam is easily adequate for web buckling (this limit state is only likely to become critical for double stacked beams).

7.2.5 Web Yielding in the Cap Beam

The applied localized stress in the web from the 12 x 12 in timber post is:

$$f_{cw} = \frac{R}{(2k + d_p)t_w} = \frac{90.5}{(2(1.13) + 12)(0.44)} = 14.4 \text{ ksi}$$

which, assuming no blocking, is compared to:

$$F_{cw} = 24(1 + 0) = 24 \text{ ksi}$$

which is greater than f_{cw}, therefore the beam is adequate for web yielding.

7.2.6 Localized Flange Bending in the Flange-Post Joint Region in the Cap Beam

The applied stress at the top of the post is given by:

$$f_{cp} = \frac{R}{A_p} = \frac{90.5}{12^2} = 0.628 \text{ ksi}$$

Assuming that the beam is unblocked, using the simplified method, the allowable stress in the post due to prevent bending in the flange is given by:

$$F_{cf} = \frac{11t^2F_b + F_{cb}'A_b}{A_p} = \frac{11(0.44^2)(22) + 0}{12^2} = 0.325 \text{ ksi}$$

which is less than f_{cp}, therefore blocking should be used to increase flange bending capacity. With blocking the effective flange strength is:

$$F_{cf} = \frac{11t^2F_b + F_{cb}'A_b}{A_p} = \frac{11(0.44^2)(22) + 1.00(8)(6)(2)}{12^2} = 0.992 \text{ ksi}$$

which is greater than f_{cp}, therefore the beam is adequate for flange bending. Note that the design could attempt to use the slightly more elaborate interaction method (See Section 6.2.4), particularly if the unblocked allowable stress is close to the applied stress, which may eliminate the need for blocking. Although, in this case, blocking would still be required.

7.2.7 Post Compression Strength

The maximum applied load in the post, including the weight of the post, is:

$$P = R + W_{post} = 90.5 + 1^2(15)(0.05) = 91.3 \text{ kip}$$

giving an applied stress in the post of:

$$f_{cp} = \frac{P}{A_p} = \frac{91.3}{12^2} = 0.634 \text{ ksi}$$

C_p is estimated at 0.90 from Figure 6-1 for the 15 ft long post, giving an allowable post stress of:

$$F_{cp} = C_pF_c^* = 0.9(1.00) = 0.900 \text{ ksi}$$

which is approximately equal to f_{cp}, therefore the post is adequate.

7.2.8 Flange-post Interaction, Web Yielding and Web Buckling in the Sill Beam

An HP12x53 can be assumed for the sill beam also. Therefore the capacity for flange-post interaction, web yielding and web buckling are the same as for the cap beam. As the applied loads are also almost identical, there is no need to check the design of the blocked sill beam for these limit states.

7.2.9 Corbel-flange Bending in Sill Beam

The reaction from the corbels is given by:

$$R = P + W_{beam} = 91.3 + 10(0.053) = 91.8 \text{ kip}$$

giving an applied stress:

$$f_{bg} = \frac{R}{A_{bg}} = \frac{91.8}{2(12)(12.0)} = 0.318 \text{ ksi}$$

With blocking used to increase the post-flange from bearing from the post, the corbel-flange is also considered to be blocked, thus the effective allowable bearing stress for the corbel-flange is given by:

$$F_{gf} = \frac{14t^2F_b + F_{cb}'A_b}{A_p} = \frac{14(0.44^2)(22) + 1.00(6)(8)(2)}{2(12)(12.0)} = 0.540 \text{ ksi}$$

which is greater than f_{bg}, therefore the corbel-flange is adequate

7.2.10 Corbels

The applied bearing stress in the corbels is equal to that given above for the bearing of the corbel-flange. The allowable stress in the corbels is:

$$F_{c\perp}' = 0.45 \text{ ksi}$$

which is greater than f_{bg}, therefore the corbels are adequate.

7.3 Design of Falsework with Steel Posts

7.3.1 Loads

The critical limit states in a falsework bent with a timber post are illustrated in Figure 7-2. It is assumed that the applied load from the superstructure of the bridge and including the joists and stringer beams is 450 psf as in the previous example. However in this example the falsework bents are assumed to have tributary loads from a 35 ft length of the bridge. Thus, the line load on a the cap beam of the falsework bent is:

$$w = 15750 \text{ lb/ft} = 15.8 \text{ kip/ft}$$

7.3.2 Cap Beam Bending

Try an A992, W14x120 section for the cap beam, with a weight of 120 lb/ft, giving a total weight on the cap beam of:

$$w = 15.9 \text{ kip/ft}$$

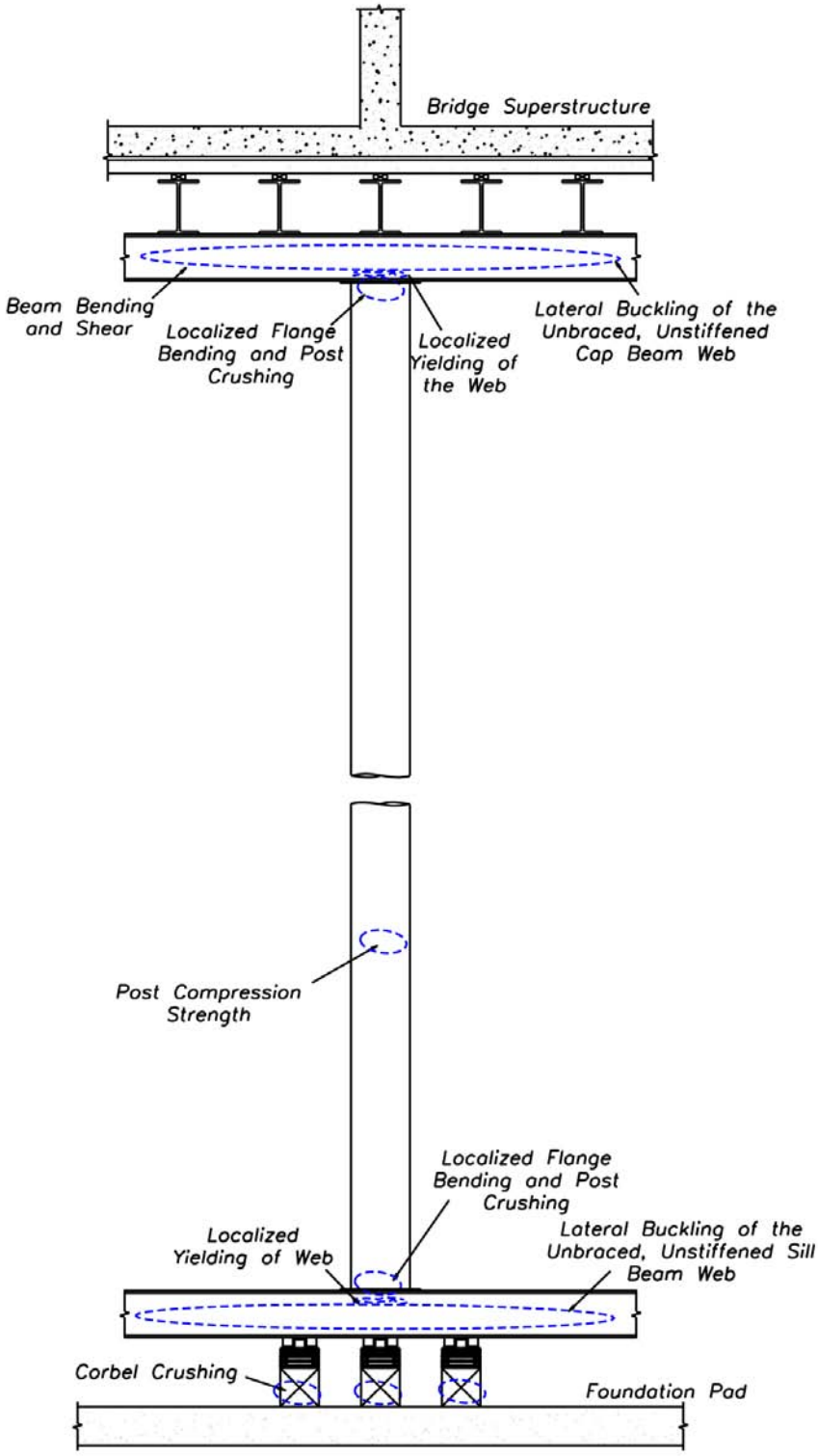

FIGURE 7-2 Portion of a falsework bent with steel post identifying critical limits states

If the posts are s paced 15 ft apart in the be nt then the maximum bending moment in the bent can be conservatively calculated by:

$$M = \frac{wL^2}{8} = \frac{15.9(15^2)}{8} = 447 \text{ kip-ft} = 5370 \text{ kip-in}$$

and the applied stress is:

$$f_b = \frac{M}{Z} = \frac{5370}{212} = 25.3 \text{ ksi}$$

compared to the allowable stress of:

$$F_b = 30 \text{ ksi}$$

which is greater than f_b, therefore the beam is adequate for bending.

7.3.3 Cap Beam Shear

The applied shear is:

$$V = \frac{wL}{2} = \frac{15.9(15)}{2} = 119 \text{ kip}$$

giving an applied shear stress:

$$f_v = \frac{V}{A_w} = \frac{119}{14.5(0.590)} = 13.9 \text{ ksi}$$

compared to the allowable stress:

$$F_v = 20 \text{ ksi}$$

which is greater than f_v, therefore the beam is adequate for shear.

7.3.4 Lateral Web Buckling in the Cap Beam

The reaction in the beam is:

$$R = wL = 15.9(15) = 239 \text{ kip}$$

thus, the average applied stress in the web for an effect length in the web of 15 ft is:

$$f_c = \frac{V}{t_w l_{eff}} = \frac{239}{0.59(15)(12)} = 2.25 \text{ ksi}$$

The euler buckling load for the web is given by:

$$F_e = \frac{\pi^2 E}{\left(\frac{6h}{t_w}\right)^2} = \frac{\pi^2(29000)}{\left(\frac{6(11.91)}{(0.59)}\right)^2} = 19.5 \text{ ksi}$$

Check: $F_e < 0.44\ F_y < 0.44(50) < 22.0$ ksi - Yes, therefore should check critical load.

The critical load is given by:

$$F_{cr} = 0.525\ F_e = 0.525(19.5) = 10.2 \text{ ksi}$$

which is greater than f_c, therefore the beam is adequate for web buckling.

7.3.5 Web Yielding in the Cap Beam

This need not be checked as the post has a thinner wall and lower yield stress than the beam web, therefore localized yielding in the post will occur before localized yielding in the web.

7.3.6 Localized Post Yielding in the Cap Beam

Assume an 18 in diameter, $^3/_8$ in thick, A500 GrB (42 ksi yield stress) post section. The applied stress in the critical region of the post, when the beam is unblocked, is given by:

$$f_{cp} = \frac{R}{(5(t_f + t_{ep}) + 2k_1)2t_p} = \frac{239}{(5(0.94 + 0.5) + 2(1.5))2(0.375)} = 31.2 \text{ ksi}$$

and the allowable stress in the post is:

$$F_{cpb} = F_{cp}\left(1 + \frac{0.3F_{cb}'A_b}{F_c(5(t_f + t_{bp}) + 2k_1)2t_p}\right) = 28(1 + 0) = 28 \text{ ksi}$$

The allowable stress is less than the applied stress, therefore will try using blocking to take a part of the post load. The resulting applied stress in the web is given by:

$$F_{cpb} = F_{cp}\left(1 + \frac{0.3F_{cb}'A_b}{F_c(5(t_f + t_{bp}) + 2k_1)2t_p}\right)$$

$$= 28\left(1 + \frac{0.3(1.0)(6)(8)(2)}{28(5(0.94+0.5)+2(1.5))2(0.375)}\right) = 31.7 \text{ ksi}$$

which is greater than f_c, therefore the blocked beam is adequate. Alternatively a larger end plate could be attached to the post. If a $^3/_4$ in end plate is used the applied stress is:

$$f_{cp} = \frac{R}{(5(t_f + t_{ep}) + 2k_1)2t_p} = \frac{239}{(5(0.94+0.75)+2(1.5))2(0.375)} = 27.8 \text{ ksi}$$

which is less than F_{cb}, therefore adequate without the use of blocking.

7.3.7 Post Compression Strength

The maximum applied load in the 25 ft long posts, including the weight of the post, is:

$$P = R + W_{post} = 239 + \frac{19.4(25)(0.490)}{144} = 241 \text{ kip}$$

giving an applied stress in the post of:

$$f_{cp} = \frac{P}{A_p} = \frac{241}{19.4} = 12.4 \text{ ksi}$$

The euler stress is given by:

$$F_e = \frac{\pi^2 E}{\left(\frac{KL}{r}\right)^2} = \frac{\pi^2(29000)}{\left(\frac{1.0(25)(12)}{6.24}\right)^2} = 124 \text{ ksi}$$

and as $F_e > 0.44F_y$

$$F_{cp} = 0.658^{\frac{F_y}{F_e}}(0.6F_y) = 0.658^{\frac{42}{124}}(0.6)(42) = 21.9 \text{ ksi}$$

which is greater than f_c, therefore column is adequate.

7.3.8 Flange-post Interaction, Web Yielding and Web Buckling in the Sill Beam

A W14x120 can also be assumed for the sill beam, therefore the capacity for flange-post interaction, web yielding and web buckling are the same as for the cap beam. As the

applied loads are also almost identical, there is no need to check the design of the blocked sill beam for these limit states.

7.3.9 Corbel-flange Bending in Sill Beam

The reaction from the corbels is given by:

$$R = P + W_{beam} = 241 + 15(0.120) = 243 \text{ kip}$$

giving an applied stress, assuming three corbels, of:

$$f_{bg} = \frac{R}{A_{bg}} = \frac{243}{3(12)(14.7)} = 0.459 \text{ ksi}$$

Assuming no blocking to simply the calcula tion (although blocking is required for local post yielding) the effective allowable bearing stress for the corbel-flange is given by:

$$F_{gf} = \frac{14t_f^2 F_b + F_{cb}' A_b}{A_p} = \frac{14(0.94^2)(22) + 0}{2(12)(14.0)} = 0.810 \text{ ksi}$$

which is greater than f_{bg}, therefore the corbel-flange is adequate.

7.3.10 Corbels

The applied bearing stress in the corbels is equal to that given above for the bearing of the corbel-flange. The allowable stress in the corbels is:

$$F_{c\perp}' = 0.45 \text{ ksi}$$

which is approximately equal to f_{bg}, therefore three corbels are adequate.

SECTION 8
SUMMARY, CONCLUSIONS AND RECOMMENDATIONS

8.1 Summary and Conclusions

A series of experimental a nd finite element studies we re performed on post and beam connections, typical of those found in bridge falsework, to identify the causes of observed failures in the field and identify the crit ical limit states for design. Configurations investigated included: steel still and cap b eams with timber posts, beams w ith steel posts, rigid patch loads on beams, and beams wit hout any lateral restraint. Using these configurations various limit states, including: flange bending, post crushing, post yielding web yielding and post-elastic crippling, lateral web buckli ng and corbel crushing were identified.

The conclusions from experimental and finite element studies are:

- The axial compression fail ure stresses of three 4 ft. long, 12 x 12 in. Number 2 Douglas Fir timber posts ranged between 1670 and 2770 psi.

- The axial bearing strength perpendicular to the grain for a 12 x 12 in Number 2 Douglas Fir timber corbel is 540 psi.

- The axial compression failure stresses of three 12 to 14 in. long, 12 x 12 in. Number 2 Douglas Fir timber blocks ranged between 3220 and 4820 psi.

- The steel sections had mate rial strengths around 0 to 12% percent greater than the minimum specified yield stress.

- Sill beams and short timber posts with ti mber corbels typically fail through crushing of the corbels and possible bending of the flange adjacent to the corbel.

- W ithout timber corbels, sill and cap b eams and timber posts t ypically fail through bending of the flange and localized crushing of the post.

- S teel post joint regions t ypically fail though lo calized yielding of the post in the region where the post is bearing onto the beam flange near the web.

- If the post applying the patch loading has sufficient capacity and rigidity , a beam with a relative thick web is likely to fail by web yielding, with post-elastic crippling occurring after the yielding. W eb yieldi ng is most likely to govern over web crippling for typical “stocky” falsework beams.

- Unbraced , unstif fened beams may fail through lateral buckling of the web, particularly double stacked beams.

- Blocks placed between the flanges and web may increase the flange bending and web yielding capacity of the beam, although their effect in increasing lateral buckling capacity is inconclusive.

- An eccentricity between the flange and post of around 3 times the web thickness reduces the flange bending, yielding and buckling capacity by around 10%.

8.2 Recommendations

From the experimental and finite element results, a series of design equations were developed to calculate the capacity of the critical limit states. Recommendations for the design of a falsework bent are as follows:

- Cap and sill beams should be designed for lateral buckling using the equation proposed based on a column buckling equation. If double stacked sill beams are used, the web height should be taken as the summation of the heights for the two beams. Bracing or fully welded stiffeners should be used in the cap and sill beams at the post locations if necessary to increase the lateral web buckling capacity. The radius of gyration in the equation can be increased accordingly with stiffeners.

- Cap and sill beams should be designed for web yielding using a 1:1 stress gradient through the flange. This uses the same equation as currently in the falsework manual, although the name "web crippling" should be changed to "web yielding" to be consistent with AISC specifications.

- The cap and sill beams should be designed for localized flange bending when a timber post is used. Two equations have been proposed for this purpose. The simplified equation is adequate but typically conservative, resulting in an increased need for blocking. The more elaborate interaction equation (for the interaction between flange bending and post crushing) could be used if additional accuracy is desired. The inclusion of the more elaborate equation in the specifications is left to the descretion of the falsework committee.

- A steel post should be designed for localized yielding where the ends of the post bearing onto the adjacent beams using a similar expression to that for web yielding except with a 2.5:1 stress gradient assumed.

- The timber and steel posts need to be designed for axial loads based on their length as ordinary columns. For the timber post, equations based on the NDS specifications are more conservative than the Caltrans Falsework specifications and are recommended based on the limited post experimental data. A plot showing the C_P factor (Figure 6-1) could be included in the design guidelines to simplify the calculation. An allowable stress of 1000 psi is tentatively recommended for Number 2 Douglas Fir posts. For the steel post the AISC design equations would allow for smaller posts than the Caltrans specifications and are also recommended.

- The bottom flange of a sill beam should be checked for flange bending where bearing on the sand jacks, blocks wedges and corbels based on the proposed equation.

- The timber corbels should be designed for bearing using the current Caltrans allowable stress for timber members. The allowable stress perpendicular to the grain for Number 2 Douglas Fir members in the NDS specifications is unconservative compared to the experimental data.

- Blocking can be used to increase flange bending and web yielding capacity if necessary and is considered 100% effective for increase flange bending capacity with a timber post, but only 30% effective for increasing flange bending/post bearing capacity with a steel post. It is considered 50% effective for increasing web yielding capacity.

- Any eccentricity between the centroid of the beam and post should be minimized, but at most it should be no more than 3 times the beam web thickness, for a reduction in flange bending and web buckling capacity of no more than 10%.

REFERENCES

American Forest and Paper Association (AFPA) (1996). *Load and Resistance Factor Design - Manual for Engineered Wood Construction.* AFPA, Washington, DC.

American Forest and Paper Association (AFPA) (2001). *National Design Specification for Wood Construction.* AFPA, Washington, DC.

American Institute of Steel Construction (AISC) (2005). *Specification for Structural Steel Buildings*. AISC, Chicago, IL.

California Department of Transportation (Caltrans) (2001). *Falsework Manual (updated November 2001)*. Caltrans Structure Construction, Sacramento, CA.

Chen, W.F., and Newlin, D.E. (1973). "Column Web Strength in Beam-to-Column Connections." *J. Struct. Div.*, 99(ST9), 1978-1984.

Elgaaly, M.(1983). "Web Design Under Compressive Edge Loads." *Engrg. J.*, Fourth Quarter, 153-171.

Galambos, T.V.(1976). *Proposed Criteria for Load and Resistance Factor Design of Steel Building Structures.* Research Report No. 45, Civil Engineering Department, Washington University, St Louis, MO.

Graciano, C., and Edlund, B. (2003). "Failure Mechanism of Slender Girder Webs with a Longitudinal Stiffener under Patch Loading." *J. of Const. Steel Research*, 59, 27-45.

Graham, J.D., Sherbourne, A.N., and Khabbaz, R.N. (1959). *Welded Interior Beam-to-Column Connections*. American Iron and Steel Institute, Inc., Chicago, IL.

Hadipriono, F.C. and Wang, H-K. (1986) Analysis of Causes of Falsework Failures in Concrete Structures." *J. of Construction Eng. and Management*, 112(1), 112-121.

Hibbett, Karlson & Sorensen, Inc. (2003). *ABAQUS - Finite Element Program*. Hibbett, Karlson & Sorensen, Inc., Fremont, CA.

Roberts, T.M., and Rockey, K.C. (1979). "A Mechanism Solution for Predicting the Collapse Loads for Slender Plate Girders when Subjected to In-Plane Patch Loading." Proc. Instn. Civ.Engrs., 67(2), 155-175.

Roberts, T.M., and Markovic, N. (1983), "Stocky Plate Girders Subjected to Edge Loading." *Proc. Instn. Civ.Engrs.*, 75(2), 539-550.

Roberts, T.M., and Newark, A.C.B. (1997). "Strength of Webs Subjected to Compressive Edge Loading." *J. of Struct. Engrg.,* 123(2), 176-183.

Terry, A.S., and Easterling, W.S. (2000). "Behavior of Bottom Flange Bending Beam-to-Girder Connections." *Proceedings of the Fourth International Workshop on Connections in Steel Structures*, Roanoke, VA, October 22-25.

Timoshenko S.P and Gere J.M., 1961. *Theory of Elastic Stability*. McGraw Hill Book Co. York, PA. 348-389.

APPENDIX 1
PREDICTION OF THE FLANGE BENDING, POST AND CORBEL CAPACITIES USING LOAD AND RESISTANCE FACTOR DESIGN

Overview

Equations for designing the critical components in a falsework bend are given below using the Load and Resistance Factor Design (LRFD) format.

Cap Beam Members for Flexure and Shear

Use conventional theory for flexure and shear.

Lateral Web Buckling in a Cap and Sill Beam

$$\phi_c R_n = \phi_c t_w l_{eff} F_{cr}$$

$$F_{cr} = 0.877 F_e$$

$$F_e = \frac{\pi^2 E}{\left(\frac{6h}{t_w}\right)^2}$$

Assuming $F_c < 0.44 F_y$

Web Yielding in a Cap and Sill Beam

$$\phi_c R_n = \phi_c (2k + d_p) F_{yw} t_w$$

Flange Bending-Post Crushing in a Cap and Sill Beam with a Timber Post

Method 1 - Simplified Method

$$\phi R_{nf} = \phi_b 11 t_f^2 F_{yf} + \lambda \phi_c F_c' A_b$$

Method 2 - Interaction Method

$$P_u < \left(\frac{1}{\phi R_{nf}^2} + \frac{1}{\lambda \phi R_{np}^2} \right)^{-\frac{1}{2}}$$

$$\phi R_{nf} = \phi_b 18 t_f^2 F_{yf} + \lambda \phi_c F_c' A_b$$

$$\lambda \phi R_{np} = \lambda \phi_c F_c' A_p$$

Localized Post Yielding of a Steel Post from Bearing of the Cap and Sill Beam

$$\phi R_{np} = \phi_c (5(t_f + t_{ep}) + 2k_1) F_{yp} 2t_p + \phi_c 0.3 F_c' A_b$$

Timber Post Design

$$\lambda \phi_c P_n = \lambda \phi_c F_c' A_p$$

Steel Post Design

$$\phi_c P_n = \phi_c A_p F_{cr}$$

$$F_{cr} = 0.877 F_e \text{ when } F_c < 0.44 F_y$$

$$F_{cr} = \left(0.658^{\frac{F_y}{F_e}}\right) F_y \text{ when } F_c > 0.44 F_y$$

$$F_e = \frac{\pi^2 E}{\left(\frac{KL}{r}\right)^2}$$

Corbel-flange Bending in a Sill Beam

$$\phi R_{nf} = \phi_b 14 t_f^2 F_{yf} + \lambda \phi_c F_c' A_b$$

Corbel Capacity

$$\lambda \phi_c R_n = \lambda \phi_c F_{c\perp}' A_{bg}$$

APPENDIX 2
GENERAL LAYOUT AND TYPICAL CROSS SECTIONS OF BRIDGE FALSEWORK FOR THE ARCH ROAD STAGE 4 BRIDGE

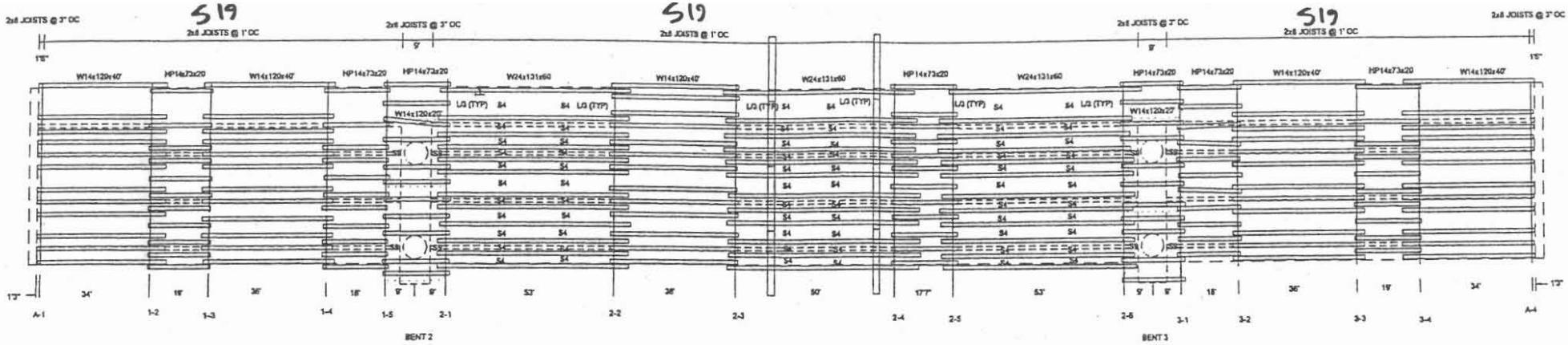

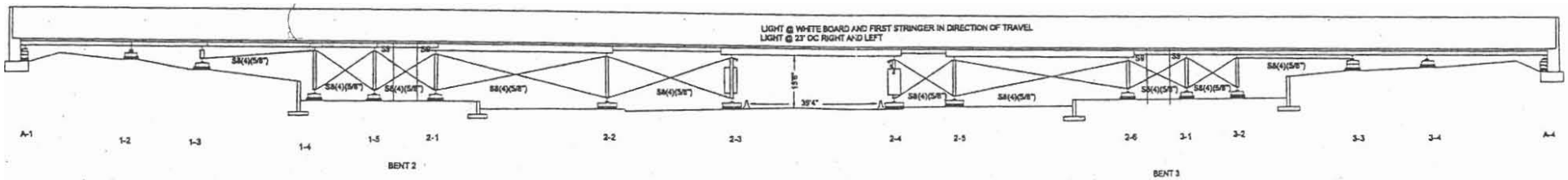

Notes

1. MAXIMUM SOIL BEARING PRESSURE: 4500 PSF DIRT; 6000 PSF PCC PAVEMENT
2. ANTICIPATED SETTLEMENT: BENTS ON SOIL 1 INCH; BENTS SUPPORTED ON PCC PAVEMENT 5/8 INCH
3. POUR SEQUENCE:
   A STEM & SOFFIT. THIS POUR INCLUDES CLOSURE POURS @ BENT CAPS
   B DECK
   POUR SEQUENCE: ABUTMENT 1 TO ABUTMENT 4
4. 2x8 JOISTS ON EDGE, +/- PARALLEL TO BENTS.
5. 5/8" SOFFIT PLYWOOD. PLACE 1" JOINTS BETWEEN SOFFIT PANELS W/ 5/8" PLY
6. HANDRAIL PER CAL-OSHA.
7. STEEL STRINGERS A36 EXCEPT AS FOLLOWS:
   W24x131 GRADE 50
8. ALL LUMBER MEETS OR EXCEEDS THE REQUIREMENTS OF S1-1.06B
9. VIKING WILL INSPECT THE FALSEWORK FOR CONFORMANCE WITH THE FALSEWORK PLANS PRIOR TO PLACEMENT OF CONCRETE.
10. DECK TO BE PLACED WITH BIDWELL 2 1/2" SCHEDULE 80 PIPE SCREED RAIL

EQUIPMENT

CRANES AS NEEDED TO PICK AND SET LOADS.
FORKLIFTS AS NEEDED TO PICK AND SET LOADS.
JACKS AS NEEDED TO ADJUST BENTS TO GRADE.
HAND TOOLS, CHAINSAWS, COME-A-LONGS AS NEEDED.

ERECTION PLAN

1 PLACE K-RAIL FOR TRAFFIC OPENING
2 CONSTRUCT PADS, CORBELS AND BOTTOM CAPS.
GRADE BOTTOM CAPS LEVEL TO CORRECT ELEVATIONS.
3 CONSTRUCT AND STAND BENTS. FLAG TRAFFIC DURING ERECTION OF 2-3 & 2-4.
4 PLACE FALSEWORK LIGHTING AT 2-3 AND 2-4.
5 BRACE BENTS EITHER WITH TEMPORARY AND/OR PLANNED LONGITUDINAL AND TRANSVERSE CABLES.
6 LAND STRINGERS. LAND STRINGERS AT SPAN 2-3 TO 2-4 WITH TRAFFIC CLOSURE PER PLANS.
7 FLY SOFFIT PANELS.
8 COMPLETE SUPERSTRUCTURE.

REMOVAL PLAN

1 REMOVE WEDGES/BLOW OUT SAND JACKS. HOLD TRAFFIC WHILE BLOWING JACKS AT 2-3 & 2-4. REPLACE ANY REQUIRED TEMPORARY BRACING BEFORE LOWERING.
2 REMOVE SOFFIT PANELS. REMOVE PANELS AT SPAN 2-3 TO 2-4 WITH TRAFFIC CLOSURE PER PLANS.
3 REMOVE STRINGERS. REMOVE STRINGERS AT SPAN 2-3 TO 2-4 WITH TRAFFIC CLOSURE PER PLANS.
4 REMOVE BENTS. HOLD TRAFFIC DURING REMOVAL OF BENTS AT 2-3 AND 2-4.
5 REMOVE REMAINING FALSEWORK.

ERECTION SEQUENCE
ABUTMENT 4 TO ABUTMENT 1

REMOVAL SEQUENCE
ABUTMENT 4 TO ABUTMENT 1

APPROVED
Pursuant to Section 5-1.02
of the Standard Specifications
State of California
DEPARTMENT OF TRANSPORTATION
Director of Public Works & Construction
Signed _____
Structure Representative
Reg. Civil Engr. No. 65926
12-16-04
Date

* Minor Correction:
See Attached Sheet
For Location of
Mechanical Connectors.

REGISTERED PROFESSIONAL ENGINEER
JAMES [illegible]
No. 57554
EXP 12-05
STATE OF CALIFORNIA
10/25/04

RECEIVED
DEC 16 2004
DEPT. OF TRANSPORTATION

ARCH ROAD STAGE 4 10-1A7004 BR 29-316		
REV		DATE
1	NOTES	10-25-04
JOB NO. 42		
DRAWN BY J. LORENZEN	DATE 10-11-04	SHEET 1 OF 7

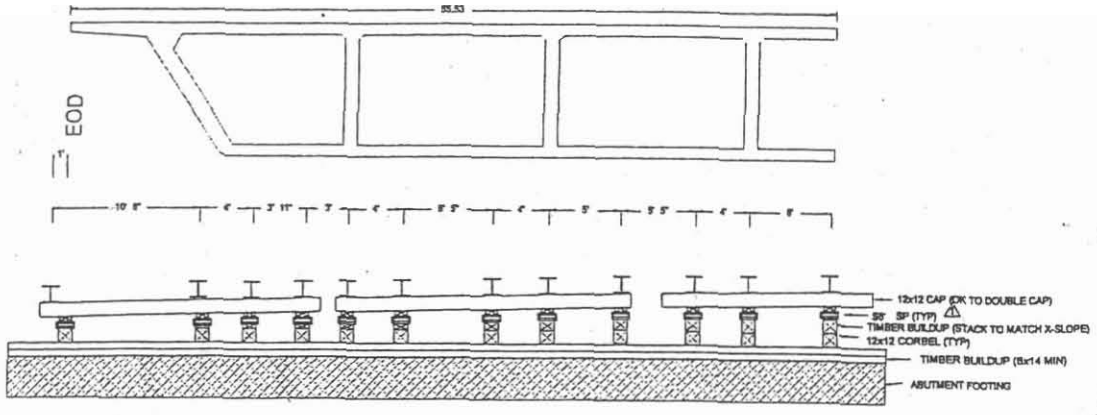

A-1

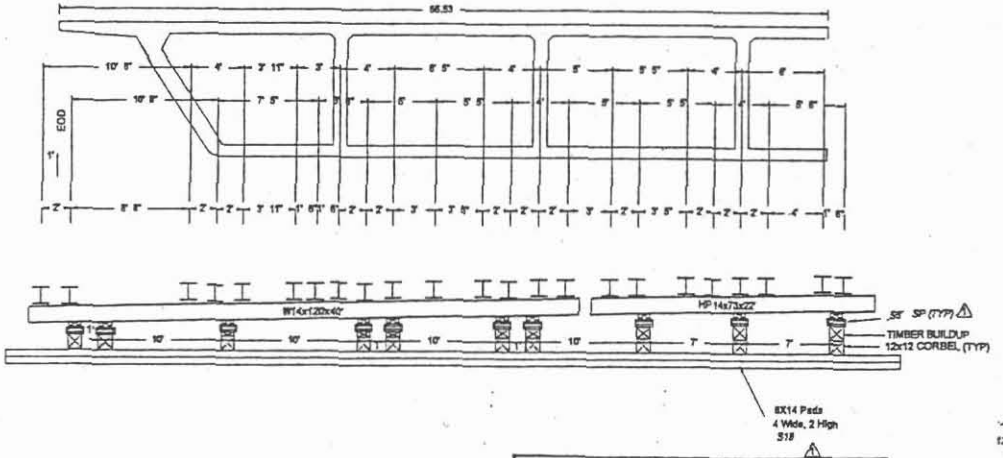

1-2

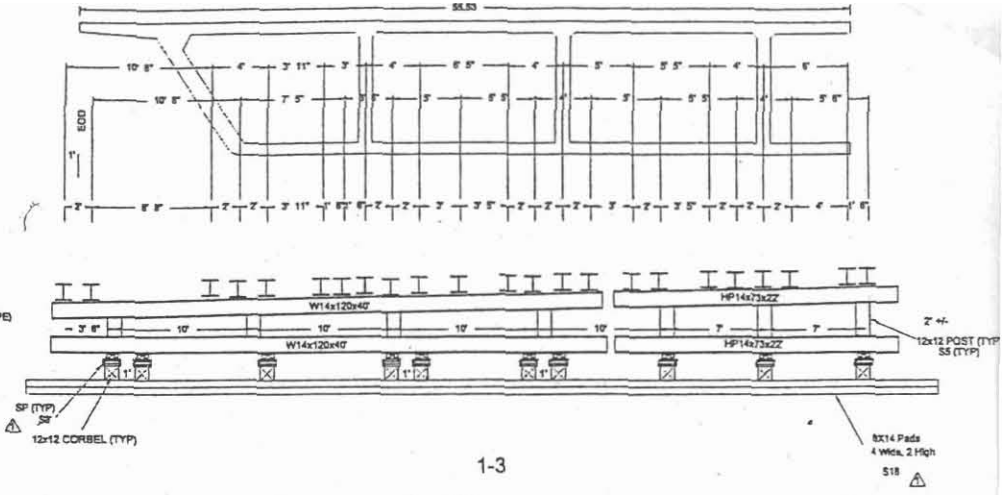

1-3

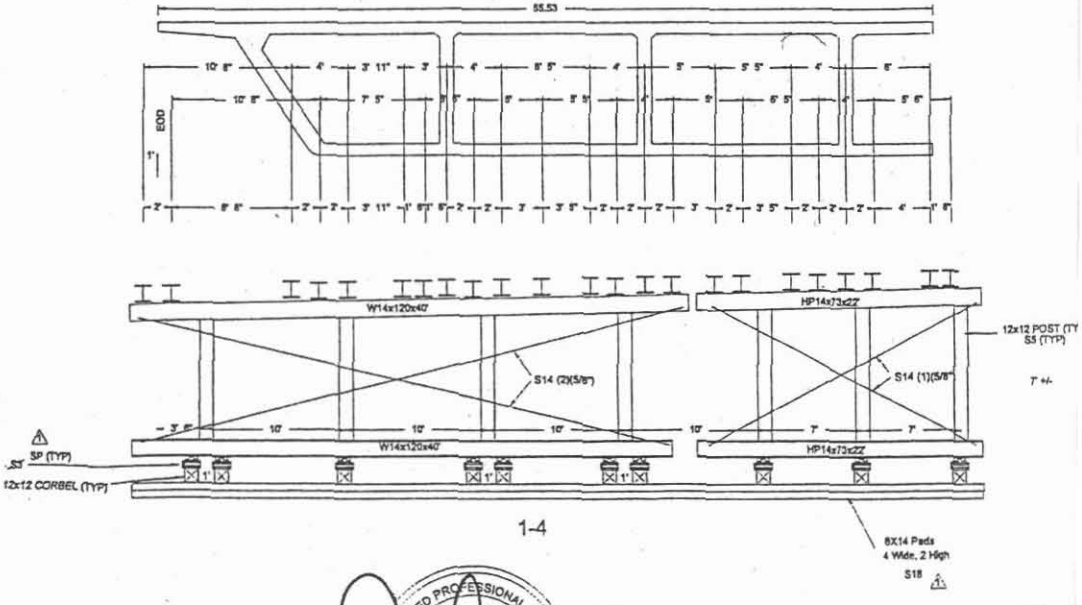

1-4

APPROVED
Pursuant to Section 5-1.02
of the Standard Specifications
State of California
DEPARTMENT OF TRANSPORTATION
Engineering Service Center
Division of Structure Construction
Signed _____
Structure Representative
Reg. Civil Engr. No. 63926
Date 12-16-04

REGISTERED PROFESSIONAL ENGINEER
JAMES J. LORENZEN
No. 47554
EXP 12-05
STATE OF CALIFORNIA
10/25/04

ARCH ROAD STAGE 4 10-1A7004 BR 29-316

REV		DATE
1	REFERENCE STD DETAIL, SP SANDJACK	10-25-04

JOB NO. 42
DRAWN BY J. LORENZEN DATE 10-6-04 SHEET 2 OF

LIST OF CCEER PUBLICATIONS

Report No.	Publication
CCEER-84-1	Saiidi, M., and R. Lawver, "User's Manual for LZAK-C64, A Computer Program to Implement the Q-Model on Commodore 64," Civil Engineering Department, Report No. CCEER-84-1, University of Nevada, Reno, January 1984.
CCEER-84-2	Douglas, B. and T. Iwasaki, "Proceedings of the First USA-Japan Bridge Engineering Workshop," held at the Public Works Research Institute, Tsukuba, Japan, Civil Engineering Department, Report No. CCEER-84-2, University of Nevada, Reno, April 1984.
CCEER-84-3	Saiidi, M., J. Hart, and B. Douglas, "Inelastic Static and Dynamic Analysis of Short R/C Bridges Subjected to Lateral Loads," Civil Engineering Department, Report No. CCEER-84-3, University of Nevada, Reno, July 1984.
CCEER-84-4	Douglas, B., "A Proposed Plan for a National Bridge Engineering Laboratory," Civil Engineering Department, Report No. CCEER-84-4, University of Nevada, Reno, December 1984.
CCEER-85-1	Norris, G. and P. Abdollaholiaee, "Laterally Loaded Pile Response: Studies with the Strain Wedge Model," Civil Engineering Department, Report No. CCEER-85-1, University of Nevada, Reno, April 1985.
CCEER-86-1	Ghusn, G. and M. Saiidi, "A Simple Hysteretic Element for Biaxial Bending of R/C in NEABS-86," Civil Engineering Department, Report No. CCEER-86-1, University of Nevada, Reno, July 1986.
CCEER-86-2	Saiidi, M., R. Lawver, and J. Hart, "User's Manual of ISADAB and SIBA, Computer Programs for Nonlinear Transverse Analysis of Highway Bridges Subjected to Static and Dynamic Lateral Loads," Civil Engineering Department, Report No. CCEER-86-2, University of Nevada, Reno, September 1986.
CCEER-87-1	Siddha rthan, R., "Dynamic Effective Stress Response of Surface and Embedded Footings in Sand," Civil engineering Department, Report No. CCEER-86-2, University of Nevada, Reno, June 1987.
CCEER-87-2	Norris, G. and R. Sack, "Lateral and Rotational Stiffness of Pile Groups for Seismic Analysis of Highway Bridges," Civil Engineering Department, Report No. CCEER-87-2, University of Nevada, Reno, June 1987.
CCEER-88-1	Orie, J. and M. Saiidi, "A Preliminary Study of One-Way Reinforced Concrete Pier Hinges Subjected to Shear and Flexure," Civil Engineering Department, Report No. CCEER-88-1, University of Nevada, Reno, January 1988.
CCEER-88-2	Orie, D., M. Saiidi, and B. Douglas, "A Micro-CAD System for Seismic Design of Regular Highway Bridges," Civil Engineering Department, Report No. CCEER-88-2, University of Nevada, Reno, June 1988.
CCEER-88-3	Orie, D. and M. Saiidi, "User's Manual for Micro-SARB, a Microcomputer Program for Seismic Analysis of Regular Highway Bridges," Civil Engineering Department, Report No. CCEER-88-3, University of Nevada, Reno, October 1988.
CCEER-89-1	Douglas, B., M. Saiidi, R. Hayes, and G. Holcomb, "A Comprehensive Study of the Loads and Pressures Exerted on Wall Forms by the Placement of Concrete," Civil Engineering Department, Report No. CCEER-89-1, University of Nevada, Reno, February 1989.

CCEER-89-2 Richardson, J. and B. Douglas, "Dynamic Response Analysis of the Dominion Road Bridge Test Data," Civil Engineering Department, Report No. CCEER-89-2, University of Nevada, Reno, March 1989.

CCEER-89-2 Vrontinos, S., M. Saiidi, and B. Douglas, "A Simple Model to Predict the Ultimate Response of R/C Beams with Concrete Overlays," Civil Engineering Department, Report NO. CCEER-89-2, University of Nevada, Reno, June 1989.

CCEER-89-3 Ebrahimpour, A. and P. Jagadish, "Statistical Modeling of Bridge Traffic Loads - A Case Study," Civil Engineering Department, Report No. CCEER-89-3, University of Nevada, Reno, December 1989.

CCEER-89-4 Shields, J. and M. Saiidi, "Direct Field Measurement of Prestress Losses in Box Girder Bridges," Civil Engineering Department, Report No. CCEER-89-4, University of Nevada, Reno, December 1989.

CCEER-90-1 Saiidi, M., E. Maragakis, G. Ghusn, Y. Jiang, and D. Schwartz, "Survey and Evaluation of Nevada's Transportation Infrastructure, Task 7.2 - Highway Bridges, Final Report," Civil Engineering Department, Report No. CCEER 90-1, University of Nevada, Reno, October 1990.

CCEER-90-2 Abdel-Ghaffar, S., E. Maragakis, and M. Saiidi, "Analysis of the Response of Reinforced Concrete Structures During the Whittier Earthquake 1987," Civil Engineering Department, Report No. CCEER 90-2, University of Nevada, Reno, October 1990.

CCEER-91-1 Saiidi, M., E. Hwang, E. Maragakis, and B. Douglas, "Dynamic Testing and the Analysis of the Flamingo Road Interchange," Civil Engineering Department, Report No. CCEER-91-1, University of Nevada, Reno, February 1991.

CCEER-91-2 Norris, G., R. Siddharthan, Z. Zafir, S. Abdel-Ghaffar, and P. Gowda, "Soil-Foundation-Structure Behavior at the Oakland Outer Harbor Wharf," Civil Engineering Department, Report No. CCEER-91-2, University of Nevada, Reno, July 1991.

CCEER-91-3 Norris, G., "Seismic Lateral and Rotational Pile Foundation Stiffnesses at Cypress," Civil Engineering Department, Report No. CCEER-91-3, University of Nevada, Reno, August 1991.

CCEER-91-4 O'Connor, D. and M. Saiidi, "A Study of Protective Overlays for Highway Bridge Decks in Nevada, with Emphasis on Polyester-Styrene Polymer Concrete," Civil Engineering Department, Report No. CCEER-91-4, University of Nevada, Reno, October 1991.

CCEER-91-5 O'Connor, D.N. and M. Saiidi, "Laboratory Studies of Polyester-Styrene Polymer Concrete Engineering Properties," Civil Engineering Department, Report No. CCEER-91-5, University of Nevada, Reno, November 1991.

CCEER-92-1 Straw, D.L. and M. Saiidi, "Scale Model Testing of One-Way Reinforced Concrete Pier Hinges Subject to Combined Axial Force, Shear and Flexure," edited by D.N. O'Connor, Civil Engineering Department, Report No. CCEER-92-1, University of Nevada, Reno, March 1992.

CCEER-92-2 Wehbe, N., M. Saiidi, and F. Gordaninejad, "Basic Behavior of Composite Sections Made of Concrete Slabs and Graphite Epoxy Beams," Civil Engineering Department, Report No. CCEER-92-2, University of Nevada, Reno, August 1992.

CCEER-92-3 Saiidi, M. and E. Hutchens, "A Study of Prestress Changes in A Post-Tensioned Bridge During the First 30 Months," Civil Engineering Department, Report No. CCEER-92-3, University of Nevada, Reno, April 1992.

CCEER-92-4 Saiidi, M., B. Douglas, S. Feng, E. Hwang, and E. Maragakis, "Effects of Axial Force on Frequency of Prestressed Concrete Bridges," Civil Engineering Department, Report No. CCEER-92-4, University of Nevada, Reno, August 1992.

CCEER-92-5 Siddharthan, R., and Z. Zafir, "Response of Layered Deposits to Traveling Surface Pressure Waves," Civil Engineering Department, Report No. CCEER-92-5, University of Nevada, Reno, September 1992.

CCEER-92-6 Norris, G., and Z. Zafir, "Liquefaction and Residual Strength of Loose Sands from Drained Triaxial Tests," Civil Engineering Department, Report No. CCEER-92-6, University of Nevada, Reno, September 1992.

CCEER-92-7 Douglas, B., "Some Thoughts Regarding the Improvement of the University of Nevada, Reno's National Academic Standing," Civil Engineering Department, Report No. CCEER-92-7, University of Nevada, Reno, September 1992.

CCEER-92-8 Saiidi, M., E. Maragakis, and S. Feng, "An Evaluation of the Current Caltrans Seismic Restrainer Design Method," Civil Engineering Department, Report No. CCEER-92-8, University of Nevada, Reno, October 1992.

CCEER-92-9 O'Connor, D., M. Saiidi, and E. Maragakis, "Effect of Hinge Restrainers on the Response of the Madrone Drive Undercrossing During the Loma Prieta Earthquake," Civil Engineering Department, Report No. CCEER-92-9, University of Nevada, Reno, February 1993.

CCEER-92-10 O'Connor, D., and M. Saiidi, "Laboratory Studies of Polyester Concrete: Compressive Strength at Elevated Temperatures and Following Temperature Cycling, Bond Strength to Portland Cement Concrete, and Modulus of Elasticity," Civil Engineering Department, Report No. CCEER-92-10, University of Nevada, Reno, February 1993.

CCEER-92-11 Wehbe, N., M. Saiidi, and D. O'Connor, "Economic Impact of Passage of Spent Fuel Traffic on Two Bridges in Northeast Nevada," Civil Engineering Department, Report No. CCEER-92-11, University of Nevada, Reno, December 1992.

CCEER-93-1 Jiang, Y., and M. Saiidi, "Behavior, Design, and Retrofit of Reinforced Concrete One-way Bridge Column Hinges," edited by D. O'Connor, Civil Engineering Department, Report No. CCEER-93-1, University of Nevada, Reno, March 1993.

CCEER-93-2 Abdel-Ghaffar, S., E. Maragakis, and M. Saiidi, "Evaluation of the Response of the Aptos Creek Bridge During the 1989 Loma Prieta Earthquake," Civil Engineering Department, Report No. CCEER-93-2, University of Nevada, Reno, June 1993.

CCEER-93-3 Sanders, D.H., B.M. Douglas, and T.L. Martin, "Seismic Retrofit Prioritization of Nevada Bridges," Civil Engineering Department, Report No. CCEER-93-3, University of Nevada, Reno, July 1993.

CCEER-93-4 Abdel-Ghaffar, S., E. Maragakis, and M. Saiidi, "Performance of Hinge Restrainers in the Huntington Avenue Overhead During the 1989 Loma Prieta Earthquake," Civil Engineering Department, Report No. CCEER-93-4, University of Nevada, Reno, June 1993 (in final preparation).

CCEER-93-5 Maragakis, E., M. Saiidi, S. Feng, and L. Flournoy, "Effects of Hinge Restrainers on the Response of the San Gregorio Bridge During the Loma Prieta Earthquake," (in final preparation) Civil Engineering Department, Report No. CCEER-93-5, University of Nevada, Reno.

CCEER-93-6 Saiidi, M., E. Maragakis, S. Abdel-Ghaffar, S. Feng, and D. O'Connor, "Response of

Bridge Hinge Restrainers During Earthquakes -Field Performance, Analysis, and Design," Civil Engineering Department, Report No. CCEER-93-6, University of Nevada, Reno, May 1993.

CCEER-93-7 Wehbe, N., Saiidi, M., Maragakis, E., and Sanders, D., "Adequacy of Three Highway Structures in Southern Nevada for Spent Fuel Transportion, Civil Engineering Department, Report No. CCEER-93-7, University of Nevada, Reno, August 1993.

CCEER-93-8 Roybal, J., Sanders, D.H., and Maragakis, E., "Vulnerability Assessment of Masonry in the Reno-Carson City Urban Corridor," Civil Engineering Department, Report No. CCEER-93-8, University of Nevada, Reno, May 1993.

CCEER-93-9 Zafir, Z. and Siddharthan, R., "MOVLOAD: A Program to Determine the Behavior of Nonlinear Horizontally Layered Medium Under Moving Load," Civil Engineering Department, Report No. CCEER-93-9, University of Nevada, Reno, August 1993.

CCEER-93-10 O'Connor, D.N., Saiidi, M., and Maragakis, E.A., "A Study of Bridge Column Seismic Damage Susceptibility at the Interstate 80/U.S. 395 Interchange in Reno, Nevada," Civil Engineering Department, Report No. CCEER-93-10, University of Nevada, Reno, October 1993.

CCEER-94-1 Maragakis, E., B. Douglas, and E. Abdelwahed, "Preliminary Dynamic Analysis of a Railroad Bridge," Report CCEER-94-1, January 1994.

CCEER-94-2 Douglas, B.M., Maragakis, E.A., and Feng, S., "Stiffness Evaluation of Pile Foundation of Cazenovia Creek Overpass," Civil Engineering Department, Report No. CCEER-94-2, University of Nevada, Reno, March 1994.

CCEER-94-3 Douglas, B.M., Maragakis, E.A., and Feng, S., "Summary of Pretest Analysis of Cazenovia Creek Bridge," Civil Engineering Department, Report No. CCEER-94-3, University of Nevada, Reno, April 1994.

CCEER-94-4 Norris, G.M. and Madhu, R., "Liquefaction and Residual Strength of Sands from Drained Triaxial Tests, Report 2," Civil Engineering Department, CCEER-94-4, University of Nevada, Reno, August 1994.

CCEER-94-5 Saiidi, M., Hutchens, E., and Gardella, D., "Prestress Losses in a Post-Tensioned R/C Box Girder Bridge in Southern Nevada," Civil Engineering Department, CCEER-94-5, University of Nevada, Reno, August 1994.

CCEER-95-1 Siddharthan, R., El-Gamal, M., and Maragakis, E.A., "Nonlinear Bridge Abutment , Verification, and Design Curves," Civil Engineering Department, CCEER-95-1, University of Nevada, Reno, January 1995.

CCEER-95-2 Norris, G.M., Madhu, R., Valceschini, R., and Ashour, M., "Liquefaction and Residual Strength of Loose Sands from Drained Triaxial Tests," Report 2, Civil Engineering Department, Report No. CCEER-95-2, University of Nevada, Reno, February 1995.

CCEER-95-3 Wehbe, N., Saiidi, M., Sanders, D., and Douglas, B., "Ductility of Rectangular Reinforced Concrete Bridge Columns with Moderate Confinement,"Civil Engineering Department, Report No. CCEER-95-3, University of Nevada, Reno, July 1995.

CCEER-95-4 Martin, T., Saiidi, M., and Sanders, D., “Seismic Retrofit of Column-Pier Cap Connections in Bridges in Northern Nevada,” Civil Engineering Department, Report No. CCEER-95-4, University of Nevada, Reno, August 1995.

CCEER-95-5 Darwish, I., Saiidi, M., and Sanders, D., “Experimental Study of Seismic Susceptibility

Column-Footing Connections," Civil Engineering Department, Report No. CCEER-95-5, University of Nevada, Reno, September 1995.

CCEER-95-6 Griffin, G., Saiidi, M., and Maragakis, E., "Nonlinear Seismic Response of Isolated Bridges and Effects of Pier Ductility Demand," Civil Engineering Department, Report No. CCEER-95-6, University of Nevada, Reno, November 1995.

CCEER-95-7 Acharya, S., Saiidi, M., and Sanders, D., "Seismic Retrofit of Bridge Footings and Column-Footing Connections," Report for the Nevada Department of Transportation, Civil Engineering Department, Report No. CCEER-95-7, University of Nevada, Reno, November 1995.

CCEER-95-8 Maragakis, E., Douglas, B., and Sandirasegaram, U., "Full-Scale Field Resonance Tests of a Railway Bridge," A Report to the Association of American Railroads, Civil Engineering Department, Report No. CCEER-95-8, University of Nevada, Reno, December 1995.

CCEER-95-9 Douglas, B., Maragakis, E., and Feng, S., "System Identification Studies on Cazenovia Creek Overpass," Report for the National Center for Earthquake Engineering Research, Civil Engineering Department, Report No. CCEER-95-9, University of Nevada, Reno, October 1995.

CCEER-96-1 El-Gamal, M.E. and Siddharthan, R.V., "Programs to Computer Translational Stiffness of Seat-Type Bridge Abutment," Civil Engineering Department, Report No. CCEER-96-1, University of Nevada, Reno, March 1996.

CCEER-96-2 Labia, Y., Saiidi, M., and Douglas, B., "Evaluation and Repair of Full-Scale Prestressed Concrete Box Girders," A Report to the National Science Foundation, Research Grant CMS-9201908, Civil Engineering Department, Report No. CCEER-96-2, University of Nevada, Reno, May 1996.

CCEER-96-3 Darwish, I., Saiidi, M., and Sanders, D., "Seismic Retrofit of R/C Oblong Tapered Bridge Columns with Inadequate Bar Anchorage in Columns and Footings," A Report to the Nevada Department of Transportation, Civil Engineering Department, Report No. CCEER-96-3, University of Nevada, Reno, May 1996.

CCEER-96-4 Ashour, M., Pilling, P., Norris, G., and Perez, H., "The Prediction of Lateral Load Behavior of Single Piles and Pile Groups Using the Strain Wedge Model," A Report to the California Department of Transportation, Civil Engineering Department, Report No. CCEER-96-4, University of Nevada, Reno, June, 1996.

CCEER-97-1-A Rimal, P. and Itani, A. "Sensitivity Analysis of Fatigue Evaluations of Steel Bridges", Center for Earthquake Research, Department of Civil Engineering, University of Nevada, Reno, Nevada Report No. CCEER-97-1-A, September, 1997.

CCEER-97-1-B Maragakis, E., Douglas, B., and Sandirasegaram, U. "Full-Scale Field Resonance Tests of a Railway Bridge," A Report to the Association of American Railroads, Civil Engineering Department, University of Nevada, Reno, May, 1996.

CCEER-97-2 Wehbe, N., Saiidi, M., and D. Sanders, "Effect of Confinement and Flares on the Seismic Performance of Reinforced Concrete Bridge Columns," Civil Engineering Department, Report No. CCEER-97-2, University of Nevada, Reno, September 1997.

CCEER-97-3 Darwish, I., M. Saiidi, G. Norris, and E. Maragakis, "Determination of In-Situ Footing Stiffness Using Full-Scale Dynamic Field Testing," A Report to the Nevada Department of Transportation, Structural Design Division, Carson City, Nevada, Report No. CCEER-97-3, University of Nevada, Reno, October 1997.

CCEER-97-4 Wehbe, N., and M. Saiidi, “User’s manual for RCMC v. 1.2 : A Computer Program for Moment-Curvature Analysis of Confined and Unconfined Reinforced Concrete Sections,” Center for Civil Engineering Earthquake Research, Department of Civil Engineering, University of Nevada, Reno, Nevada, Report No. CCEER-97-4, November, 1997.

CCEER-97-5 Isakovic, T., M. Saiidi, and A. Itani, “Influence of new Bridge Configurations on Seismic Performance,” Department of Civil Engineering, University of Nevada, Reno, Report No. CCEER-97-5, September, 1997.

CCEER-98-1 Itani, A., Vesco, T. and Dietrich, A., “Cyclic Behavior of “as Built” Laced Members With End Gusset Plates on the San Francisco Bay Bridge” Center for Civil Engineering Earthquake Research, Department of Civil Engineering, University of Nevada, Reno, Nevada Report No. CCEER-98-1, March, 1998.

CCEER-98-2 G. Norris and M. Ashour, “Liqueficiation and Undraned response evaluation of Sands from Drained Formulation.” Center for Civil Engineering Earthquake Research, Department of Civil Engineering, University of Nevada, Reno, Nevada, Report No. CCEER-98-2, May, 1998.

CCEER-98-3 Qingbin, Chen, B. M. Douglas, E. Maragakis, and I. G. Buckle, "Extraction of Nonlinear Hysteretic Properties of Seismically Isolated Bridges from Quick-Release Field Tests", Center for Civil Engineering Earthquake Research, Department of Civil Engineering, University of Nevada, Reno, Nevada, Report No. CCEER-98-3, June, 1998.

CCEER-98-4 Maragakis, E., B. M. Douglas, and C. Qingbin, "Full-Scale Field Capacity Tests of a Railway Bridge", Center for Civil Engineering Earthquake Research, Department of Civil Engineering, University of Nevada, Reno, Nevada, Report No. CCEER-98-4, June, 1998.

CCEER-98-5 Itani, A., Douglas, B., and Woodgate, J., “Cyclic Behavior of Richmond-San Rafael Retrofitted Tower Leg”. Center for Civil Engineering Earthquake Research, Department of Civil Engineering, University of Nevada, Reno. Report No. CCEER-98-5, June 1998

CCEER-98-6 Moore, R., Saiidi, M., and Itani, A., “Seismic Behavior of New Bridges with Skew and Curvature”. Center for Civil Engineering Earthquake Research, Department of Civil Engineering, University of Nevada, Reno. Report No. CCEER-98-6, October, 1998.

CCEER-98-7 Itani, A and Dietrich, A, “Cyclic Behavior of Double Gusset Plate Connections”, Center for Civil Engineering Earthquake Research, Department of Civil Engineering, University of Nevada, Reno, Nevada, Report No. CCEER-98-5, December, 1998.

CCEER-99-1 Caywood, C., M. Saiidi, and D. Sanders, “ Seismic Retrofit of Flared Bridge Columns With Steel Jackets,” Civil Engineering Department, University of Nevada, Reno, Report No. CCEER-99-1, February 1999.

CCEER-99-2 Mangoba, N., M. Mayberry, and M. Saiidi, “Prestress Loss in Four Box Girder Bridges in Northern Nevada,” Civil Engineering Department, University of Nevada, Reno, Report No. CCEER-99-2, March 1999.

CCEER-99-3 Abo-Shadi, N., M. Saiidi, and D. Sanders, "Seismic Response of Bridge Pier Walls in the Weak Direction", Civil Engineering Department, University of Nevada, Reno, Report No. CCEER-99-3, April 1999.

CCEER-99-4 Buzick, A., and M. Saiidi, "Shear Strength and Shear Fatigue Behavior of Full-Scale Prestressed Concrete Box Girders", Civil Engineering Department, University of Nevada, Reno, Report No. CCEER-99-4, April 1999.

CCEER-99-5 Randall, M., M. Saiidi, E. Maragakis and T. Isakovic, "Restrainer Design Procedures For Multi-Span Simply-Supported Bridges", Civil Engineering Department, University of Nevada, Reno, Report No. CCEER-99-5, April 1999.

CCEER-99-6 Wehbe, N. and M. Saiidi, "User's Manual for RCMC v. 1.2, A Computer Program for Moment-Curvature Analysis of Confined and Unconfined Reinforced Concrete Sections", Civil Engineering Department, University of Nevada, Reno, Report No. CCEER-99-6, May 1999.

CCEER-99-7 Burda, J. and A. Itani, "Studies of Seismic Behavior of Steel Base Plates," Civil Engineering Department, University of Nevada, Reno, Report No. CCEER-99-7, May 1999.

CCEER-99-8 Ashour, M., and G. Norris, "Refinement of the Strain Wedge Model Program," Civil Engineering Department, University of Nevada, Reno, Report No. CCEER-99-8, March 1999.

CCEER-99-9 Dietrich, A., and A. Itani, "Cyclic Behavior of Laced and Perforated Steel Members on the San Francisco-Oakland Bay Bridge," Civil Engineering Department, University, Reno. December 1999.

CCEER 99-10 Itani, A., A. Dietrich, "Cyclic Behavior of Built Up Steel Members and their Connections," Civil Engineering Department, University of Nevada, Reno. December 1999.

CCEER 99-11 Itani, A., J. Woodgate, "Axial and Rotational Ductility of BuiltUp Structural Steel Members," Civil Engineering Department, University of Nevada, Reno December 1999.

CCEER-99-12 Sgambelluri, M., Sanders, D.H., and Saiidi, M.S., Behavior of One-Way Reinforced Concrete Bridge Column Hinges in the Weak Direction, Report No. Department of Civil Engineering, University of Nevada, Reno, December 1999.

CCEER-99-13 Laplace, P., Sanders, D.H., Douglas, B, and Saiidi, M, Shake Table Testing of Flexure Dominated Reinforced Concrete Bridge Columns, Report No. Department of Civil Engineering, University of Nevada, Reno, December 1999.

CCEER-99-14 Ahmad M. Itani, Jose A. Zepeda, and Elizabeth A. Ware "Cyclic Behavior of Steel Moment Frame Connections for the Moscone Center Expansion," December 1999.

CCEER 00-1 Ashour, M., and Norris, G. "Undrained Lateral Pile and Pile Group Response in Saturated Sand", Civil Engineering Department, University of Nevada, Reno, Report No. CCEER-00-1, May 1999. January 2000.

CCEER 00-2 Saiidi, M. and Wehbe, N., "A Comparison of Confinement Requirements in Different Codes for Rectangular, Circular, and Double-Spiral RC Bridge Columns," Civil Engineering Department, University of Nevada, Reno, Report No. CCEER-00-2, January 2000.

CCEER 00-3 McElhaney, B., M. Saiidi, and D. Sanders, "Shake Table Testing of Flared Bridge Columns With Steel Jacket Retrofit," Civil Engineering Department, University of Nevada, Reno, Report No. CCEER-00-3, January 2000.

CCEER 00-4 Martinovic, F., M. Saiidi, D. Sanders, and F. Gordaninejad, "Dynamic Testing of Non-Prismatic Reinforced Concrete Bridge Columns Retrofitted with FRP Jackets," Civil Engineering Department, University of Nevada, Reno, Report No. CCEER-00-4, January 2000.

CCEER 00-5 Itani, A., and M. Saiidi, "Seismic Evaluation of Steel Joints for UCLA Center for Health Science Westwood Replacement Hospital," Civil Engineering Department, University of Nevada, Reno, Report No. CCEER-00-5, February 2000.

CCEER 00-6 Will, J. and D. Sanders, "High Performance Concrete Using Nevada Aggregates," Civil Engineering Department, University of Nevada, Reno, Report No. CCEER-00-6, May 2000.

CCEER 00-7 French, C., and M. Saiidi, "A Comparison of Static and Dynamic Performance of Models of Flared Bridge Columns ," Civil Engineering Department, University of Nevada, Reno, Report No. CCEER-00-7, October 2000.

CCEER 00-8 Itani, A., H. Sedarat, "Seismic Analysis of the AISI LRFD Design Example of Steel Highway Bridges," Civil Engineering Department, University of Nevada, Reno, Report No. CCEER 00-08, November 2000.

CCEER 00-9 Moore, J., D. Sanders, and M. Saiidi, "Shake Table Testing of 1960's Two Column Bent with Hinges Bases," Civil Engineering Department, University of Nevada, Reno, Report No. CCEER 00-09, December 2000.

CCEER 00-10 Asthana, M., D. Sanders, and M. Saiidi, "One-Way Reinforced Concrete Bridge Column Hinges in the Weak Direction," Civil Engineering Department, University of Nevada, Reno, Report No. CCEER 00-10, April 2001.

CCEER 01-1 Ah Sha, H., D. Sanders, M. Saiidi, "Early Age Shrinkage and Cracking of Nevada Concrete Bridge Decks, "Civil Engineering Department, University of Nevada, Reno, Report No. CCEER 01-01, May 2001.

CCEER 01-2 Ashour, M. and G. Norris, "Pile Group program for Full Material Modeling an Progressive Failure." Civil Engineering Department, University of Nevada, Reno, Report No. CCEER 01-02, July 2001.

CCEER 01-3 Itani, A., C. Lanaud, and P. Dusicka, "Non-Linear Finite Element Analysis of Built-Up Shear Links." Civil Engineering Department, University of Nevada, Reno, Report No. CCEER 01-03, July 2001.

CCEER 01-4 Saiidi, M., J. Mortensen, and F. Martinovic, "Analysis and Retrofit of Fixed Flared Columns with Glass Fiber-Reinforced Plastic Jacketing," Civil Engineering Department, University of Nevada, Reno, Report No. CCEER 01-4, August 2001

CCEER 01-5 Saiidi, M., A. Itani, I. Buckle, and Z. Cheng," Performance of A Full-Scale Two-Story Wood Frame Structure Supported on Ever-Level Isolators," Civil Engineering Department, University of Nevada, Reno, Report No. CCEER 01-5, October 2001

CCEER 01-6 Laplace, P., D. Sanders, and M. Saiidi, "Experimental Study and Analysis of Retrofitted Flexure and Shear Dominated Circular Reinforced Concrete Bridge Columns Subjected to Shake Table Excitation, "Civil Engineering Department, University of Nevada, Reno, Report No. CCEER 01-6, June 2001.

CCEER 01-7 Reppi, F., and D. Sanders, "Removal and Replacement of Cast-in-Place, Post-tensioned, Box Girder Bridge," Civil Engineering Department, University of Nevada, Reno, Report No. CCEER 01-7, December 2001.

CCEER 02-1 Pulido, C., M. Saiidi, D. Sanders, and A. Itani, "Seismic Performance and Retrofitting of Reinforced Concrete Bridge Bents," Civil Engineering Department, University of Nevada, Reno, Report No. CCEER 02-1, January 2002.

CCEER 02-2 Yang, Q., M. Saiidi, H. Wang, and A. Itani, "Influence of Ground Motion Incoherency on Earthquake Response of Multi-Support Structures," Civil Engineering Department, University of Nevada, Reno, Report No. CCEER 02-2, May 2002.

CCEER 02-3 M. Saiidi, B. Gopalakrishnan, E. Reinhardt, and R. Siddharthan, A Preliminary Study of Shake Table Response of A Two-Column Bridge Bent on Flexible Footings Civil Engineering Department, University of Nevada, Reno, Report No. CCEER 02-03, June 2002.

CCEER 02-4 Not Published

CCEER 02-5 Banghart, A., Sanders, D., Saiidi, M., "Evaluation of Concrete Mixes for Filling the Steel Arches in the Galena Creek Bridge," Civil Engineering Department, University of Nevada, Reno, Report No. CCEER 02-05, June 2002.

CCEER 02-6 Dusicka, P., Itani, A., Buckle, I. G., "Cyclic Behavior of Shear Links and Tower Shaft Assembley of San Francisco – Oakland Bay Bridge Tower" Civil Engineering Department, University of Nevada, Reno, Report No. CCEER 02-06, July 2002.

CCEER 02-7 Mortensen, J., and M. Saiidi, " A Performance-Based Design Method for Confinement in Circular Columns," Civil Engineering Department, University of Nevada, Reno, Report No. CCEER 02-07, November 2002.

CCEER 03-1 Wehbe, N., and M. Saiidi, "User's manual for SPMC v. 1.0 : A Computer Program for Moment-Curvature Analysis of Reinforced Concrete Sections with Interlocking Spirals," Center for Civil Engineering Earthquake Research, Department of Civil Engineering, University of Nevada, Reno, Nevada, Report No. CCEER-03-1, May, 2003.

CCEER 03-2 Wehbe, N., and M. Saiidi, "User's manual for RCMC v. 2.0 : A Computer Program for Moment-Curvature Analysis of Confined and Unconfined Reinforced Concrete Sections," Center for Civil Engineering Earthquake Research, Department of Civil Engineering, University of Nevada, Reno, Nevada, Report No. CCEER-03-2, June, 2003.

CCEER 03-3 Nada, H., D. Sanders, and M. Saiidi, " Seismic Performance of RC Bridge Frames with Architectural-Flared Columns," Civil Engineering Department, University of Nevada, Reno, Report No. CCEER 03-3, January 2003.

CCEER 03-4 Reinhardt, E., M. Saiidi, and R. Siddharthan, " Seismic Performance of a CFRP/ Concrete Bridge Bent on Flexible Footings." Civil Engineering Department, University of Nevada, Reno. Report No. CCEER 03-4, August 2003.

CCEER 03-5 Johnson, N., M. Saiidi, A. Itani, and S. Ladkany, "Seismic Retrofit of Octagonal Columns with Pedestal and One-Way Hinge at the Base," Center for Civil Engineering Earthquake Research, Department of Civil Engineering, University of Nevada, Reno, Nevada, Report No. CCEER-03-5, August 2003.

CCEER 03-6 Mortensen, C., M. Saiidi, and S. Ladkany, "Creep and Shrinkage Losses in Highly Variable Climates," Center for Civil Engineering Earthquake Research, Department of Civil Engineering, University of Nevada, Reno, Nevada, Report No. CCEER-03-6, September 2003.

CCEER 03- 7 Ayoub, C., M. Saiidi, and A. Itani, "A Study of Shape-Memory-Alloy-Reinforced Beams and Cubes," Center for Civil Engineering Earthquake Research, Department of Civil Engineering, University of Nevada, Reno, Nevada, Report No. CCEER-03-7, October 2003.

CCEER 03-8 Chandane, S., D. Sanders, and M. Saiidi, "Static and Dynamic Performance of RC Bridge Bents with Architectural-Flared Columns," Center for Civil Engineering Earthquake Research, Department of Civil Engineering, University of Nevada, Reno, Nevada, Report No. CCEER-03-8, November 2003.

CCEER 04-1 Olaegbe, C., and Saiidi, M., "Effect of Loading History on Shake Table Performance of A Two-Column Bent with Infill Wall," Center for Civil Engineering Earthquake Research, Department of Civil Engineering, University of Nevada, Reno, Nevada, Report No. CCEER-04-1, January 2004.

CCEER 04-2 Johnson, R., Maragakis, E., Saiidi, M., and DesRoches, R., "Experimental Evaluation of Seismic Performance of SMA Bridge Restrainers," Center for Civil Engineering Earthquake Research, Department of Civil Engineering, University of Nevada, Reno, Nevada, Report No. CCEER-04-2, February 2004.

CCEER 04-3 Moustafa, K., Sanders, D., and Saiidi, M., "Impact of Aspect Ratio on Two-Column Bent Seismic Performance," Center for Civil Engineering Earthquake Research, Department of Civil Engineering, University of Nevada, Reno, Nevada, Report No. CCEER-04-3, February 2004.

CCEER 04-4 Maragakis, E., Saiidi, M., Sanchez-Camargo, F., and Elfass, S., "Seismic Performance of Bridge Restrainers At In-Span Hinges," Center for Civil Engineering Earthquake Research, Department of Civil Engineering, University of Nevada, Reno, Nevada, Report No. CCEER-04-4, March 2004.

CCEER 04-5 Ashour, M., Norris, G. and Elfass, S., "Analysis of Laterally Loaded Long or Intermediate Drilled Shafts of Small or Large Diameter in Layered Soil," Center for Civil Engineering Earthquake Research, Department of Civil Engineering, University of Nevada, Reno, Nevada, Report No. CCEER-04-5, June 2004.

CCEER 04-6 Correal, J., Saiidi, M. and Sanders, D., "Seismic Performance of RC Bridge Columns Reinforced with Two Interlocking Spirals," Center for Civil Engineering Earthquake Research, Department of Civil Engineering, University of Nevada, Reno, Nevada, Report No. CCEER-04-6, August 2004.

CCEER 04-7 Dusicka, P., Itani, A. and Buckle, I., "Cyclic Response and Low Cycle Fatigue Characteristics of Plate Steels," Center for Civil Engineering Earthquake Research, Department of Civil Engineering, University of Nevada, Reno, Nevada, Report No. CCEER-04-7, November 2004.

CCEER 04-8 Dusicka, P., Itani, A. and Buckle, I., " Built-up Shear Links as Energy Dissipaters for Seismic Protection of Bridges," Center for Civil Engineering Earthquake Research, Department of Civil Engineering, University of Nevada, Reno, Nevada, Report No. CCEER-04-8, November 2004.

CCEER 04-9 Sureshkumar, K., Saiidi, S., Itani, A. and Ladkany, S., "Seismic Retrofit of Two-Column Bents with Diamond Shape Columns," Center for Civil Engineering Earthquake Research, Department of Civil Engineering, University of Nevada, Reno, Nevada, Report No. CCEER-04-9, November 2004.

CCEER 05-1 Wang, H. and Saiidi, S., "A Study of RC Columns with Shape Memory Alloy and Engineered Cementitious Composites," Center for Civil Engineering Earthquake Research, Department of Civil Engineering, University of Nevada, Reno, Nevada, Report No. CCEER-05-1, January 2005.

CCEER 05-2 Johnson, R., Saiidi, S. and Maragakis, E., "A Study of Fiber Reinforced Plastics for Seismic Bridge Restrainers," Center for Civil Engineering Earthquake Research, Department of Civil Engineering, University of Nevada, Reno, Nevada, Report No. CCEER-05-2, January 2005.

CCEER 05-3 Carden, L.P., Itani, A.M., Buckle, I.G, "Seismic Load Path in Steel Girder Bridge Superstructures," Center for Civil Engineering Earthquake Research, Department of Civil Engineering, University of Nevada, Reno, Nevada, Report No. CCEER-05-3, January 2005.

CCEER 05-4 Carden, L.P., Itani, A.M., Buckle, I.G, "Seismic Performance of Steel Girder Bridge Superstructures with Ductile End Cross Frames and Seismic Isolation," Center for Civil Engineering Earthquake Research, Department of Civil Engineering, University of Nevada, Reno, Nevada, Report No. CCEER-05-4, January 2005.

CCEER 05-5 Goodwin, E., Maragakis, M., Itani, A. and Luo, S., "Experimental Evaluation of the Seismic Performance of Hospital Piping Subassemblies," Center for Civil Engineering Earthquake Research, Department of Civil Engineering, University of Nevada, Reno, Nevada, Report No. CCEER-05-5, February 2005.

CCEER 05-6 Zadeh M. S., Saiidi, S, Itani, A. and Ladkany, S., "Seismic Vulnerability Evaluation and Retrofit Design of Las Vegas Downtown Viaduct," Center for Civil Engineering Earthquake Research, Department of Civil Engineering, University of Nevada, Reno, Nevada, Report No. CCEER-05-6, February 2005.

CCEER 05-7 Phan, V., Saiidi, S. and Anderson, J., "Near Fault (Near Field) Ground Motion Effects on Reinforced Concrete Bridge Columns" Center for Civil Engineering Earthquake Research, Department of Civil Engineering, University of Nevada, Reno, Nevada, Report No. CCEER-05-7, August 2005.

CCEER 05-8 Carden, L., Itani, A. and Laplace, P., "Performance of Steel Props at the UNR Fire Science Academy subjected to Repeated Fire" Center for Civil Engineering Earthquake Research, Department of Civil Engineering, University of Nevada, Reno, Nevada, Report No. CCEER-05-8, August 2005.

CCEER 05-9 Yamashita, R. and Sanders, D., "Shake Table Testing and an Analytical Study of Unbonded Prestressed Hollow Concrete Column Constructed with Precast Segments" Center for Civil Engineering Earthquake Research, Department of Civil Engineering, University of Nevada, Reno, Nevada, Report No. CCEER-05-9, August 2005.

CCEER 05-10 Moustafa, K. D. Sanders, and M. Saiidi, "Seismic Behavior of R/C Bridge Bents with Architectural-Flared Columns Including both Horizontal and Vertical Gaps," Center for Civil Engineering Earthquake Research, Department of Civil Engineering, University of Nevada, Reno, Nevada, Report No. CCEER-05-10, February 2005.

CCEER 05-11 Carden, L. P., Itani, A., and Pekcan, G., "Recommendations for the Design of Beams and Posts in Bridge Falsework," Center for Civil Engineering Earthquake Research, Department of Civil Engineering, University of Nevada, Reno, Nevada, Report No. CCEER-05-11, January 2006.